

STATUS OF THESIS

Title of thesis

Hydroformylation of Higher Olefins Using Rodium Phosphite Complex Catalyst

I, MAIZATUL SHIMA SHAHARUN

hereby allow my thesis to be placed at the Information Resource Center (IRC) of Universiti Teknologi PETRONAS (UTP) with the following conditions:

1. The thesis becomes the property of UTP
2. The IRC of UTP may make copies of the thesis for academic purposes only.
3. This thesis is classified as

Confidential

Non-confidential

If this thesis is confidential, please state the reason:

The contents of the thesis will remain confidential for _____ years.

Remarks on disclosure:



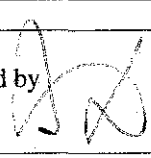
Signature of Author

Permanent address:

29, Persiaran Perdana 13,
Taman Pinji Perdana,
31500 Lahat, Perak

Date : 7/8/09

Endorsed by


Signature of Supervisor

Name of Supervisor

Prof. Binay K. Dutta

Date : 7/8/09

UNIVERSITI TEKNOLOGI PETRONAS

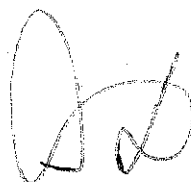
HYDROFORMYLATION OF HIGHER OLEFINS USING RHODIUM PHOSPHITE
COMPLEX CATALYST

by

MAIZATUL SHIMA SHAHARUN

The undersigned certify that they have read, and recommend to the Postgraduate Studies Programme for acceptance this thesis for the fulfilment of the requirements for the degree stated.

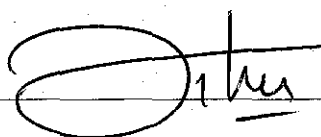
Signature:



Main Supervisor:

Prof. Brijay K. Dutta

Signature:



Co-Supervisor:

AP DR HILMI MURTAZAR

UNIVERSITI TEKNOLOGI PETRONAS

HYDROFORMYLATION OF HIGHER OLEFINS USING RHODIUM PHOSPHITE
COMPLEX CATALYST

by

MAIZATUL SHIMA SHAHARUN

A Thesis

Submitted to the Postgraduate Studies Programme

as a Requirement for the Degree of

DOCTOR OF PHILOSOPHY IN

CHEMICAL ENGINEERING

UNIVERSITI TEKNOLOGI PETRONAS

BANDAR SERI ISKANDAR,

PERAK

AUGUST 2009

DECLARATION OF THESIS

Title of thesis

Hydroformylation of Higher Olefins Using Rodium Phosphite Complex Catalyst

I, MAIZATUL SHIMA SHAHARUN

hereby declare that the thesis is based on my original work except for quotations and citations which have been duly acknowledged. I also declare that it has not been previously or concurrently submitted for any other degree at UTP or other institutions.

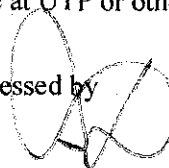


Signature of Author

Permanent address: 29, Persiaran Perdana 13,
Taman Pinji Perdana,
31500 Lahat,
Perak

Date : 7/8/09

Witnessed by



Signature of Supervisor

Name of Supervisor

Prof. Binay K. Dutta

Date : 7/8/09

Incompliance the terms of the Copyright Act 1987 and the IP Policy of the university, the copyright of this thesis has been reassigned by the author to the legal entity of the university,

Institute of Technology PETRONAS Sdn Bhd.

Due acknowledgement shall always be made of the use of any material contained in, or derived from, this thesis.

© Name of candidate, Year of Thesis submission
Institute of Technology PETRONAS Sdn Bhd
All rights reserved

ACKNOWLEDGEMENT

Praise and gratitude to the almighty, Allah, the creator and governor of the universe and his prophet Mohammed, peace upon him.

I wish to express my deepest gratitude and appreciation to my respectful supervisor, Prof. Dr. Binay K Dutta for his invaluable guidance, patience, support and enthusiasm throughout this research work. It was a great pleasure to conduct this research under his constructive comments. I would like to express my sincere appreciation to Assoc. Prof. Dr. Hilmi Mukhtar who provided an inspiration, motivating and critical atmosphere during the course of my study. The merit also goes to Mr. Bobby Ho of Hisco (Malaysia) Sdn. Bhd., AP Dr Suzana Yusup and Prof. Duvvuri Subarao for their warm cooperation and assistance in providing me the technical guidance to operate the high pressure reactor. I am also grateful to Prof. Dr. Subash Bhatia and AP Dr Saikat Maitra, for their criticism, suggestions and stimulating discussions in the improvement of my journal papers.

My special acknowledgement to Universiti Teknologi PETRONAS and Ministry of Science, Technology and Innovation, under the Research Project No.03-02-02-SF0019: *Development of a green process for the production of higher aldehydes from olefins by hydroformylation* for the financial support that made this work possible. A special thank you also goes to the technicians, Mr. Jailani Kasim, Mr. Fauzi Abu Bakar and Mr. Yusoff Mohd for their assistance and useful discussions, in the use of the instrumentation of GC-FID, GC-MS and AAS respectively. Finally but definitely not the least, I also wish to express my appreciation to all technicians, colleagues and countless individuals who have contributed directly or indirectly towards accomplishment of my research work.

Dedication of this thesis is given with deepest appreciation to my late father, Shaharun bin Ashaari and my beloved family for their endless love, understanding, prayers, trust, encouragement and continued support morally, for which I'm forever indebted.

“.....it was Your light that raised me,”
for my beloved children, husband, father and mother.

ABSTRACT

Hydroformylation of olefins with CO and H₂ at total pressure of 15 to 50 bar and temperature of 80 to 120°C, in presence of rhodium (Rh)-based homogeneous catalysts for production of aldehydes has demonstrated high yields and selectivity. Rh-based catalysts are expensive and the commercial viability of a process that uses such catalysts substantially depends on the efficiency of catalyst recovery and product separation. In this work, a novel temperature dependent multi-component solvent (TMS) or 'thermomorphic solvent' system has been used as the reaction medium to investigate hydroformylation of two higher olefins – 1-octene and 1-dodecene – to synthesize the corresponding aldehydes at a lower pressure of 15-25 bar and temperature of 80 to 100°C. Such a solvent mixture changes thermally from biphasic to monophasic with distribution of the products and of the catalyst in the non-polar and polar phases thus simplifying the process of separation and recycling of the catalyst.

A TMS- system consisting of three components – propylene carbonate (PC), *n*-dodecane and 1,4-dioxane was used in this study. The presence of 1,4-dioxane imparts the thermomorphic character to the solvent mixture. For a gas-liquid reaction, the solubility of the reactant gas in the liquid medium is an important parameter required for the interpretation of reaction kinetics. Therefore experimental measurement of solubility of the gaseous reactants – CO and H₂ – in the individual components of the solvent as well as in their mixtures was performed up to a pressure of 1.5 MPa and temperature range of 298-343 K. The effects of solvent composition, partial pressures of the gaseous reactants – CO and H₂, reaction temperature and catalyst loading on the rate, yield and selectivity of the linear aldehydes were also investigated. At a reaction temperature of 363 K and total pressure of 1.5 MPa and 0.68 mM HRh(CO)(PPh₃)₃, the conversion of 1-octene and the yield of aldehyde were 97 % and 95 %, respectively. The aldehyde product was recovered in the non polar phase whereas the catalyst remained in the polar phase with low catalyst loss of 3 %. With a reaction-time of 2 h and a selectivity of 89 %, this catalytic system can be considered as highly reactive and selective. The rate was found to be first order with respect to catalyst, 1-octene and P_{H_2} . The rate vs. P_{CO} resembled a typical case of substrate inhibited kinetics.

The solubility data have been correlated using three models – an empirical model based on the Henry's law, the regular solution theory with Yen and McKetta modification and the modified UNIFAC model. The accuracy of prediction with the second model without any adjustable constant was within 11.0 % whereas the UNIFAC model offered a better accuracy of 8.5 %. In the kinetic study a mechanistic rate model for the hydroformylation of higher olefins using Rh-based catalyst in a homogeneous system was developed by using *ab initio* technique of quantum chemical computation to identify the rate-controlling steps in the reaction pathways. Computations were done for three olefins – 1-decene, 1-dodecene and styrene - by the restricted Hartree-Fock method at the second order Moller-Plesset level of perturbation theory and basis set of 6-31++G(d,p) using the GAMESS Pro 11.0 program package. Three generalized mechanistic rate models were developed on the basis of the reaction path analysis and experimental findings available in the literature. The rate model with oxidative H₂-addition as the controlling step predicted the conversion of the three alkenes quite satisfactorily with an average deviation of ± 7.6 %. The UNIQUAC and UNIFAC models were used to model the catalyst and product recovery (at 298 K) of the hydroformylation of 1-octene. The average deviation of the calculated mole fractions from the experimental values for the UNIQUAC and UNIFAC method was ± 6.5 % and ± 8.2 %, respectively.

The work done has established the potential of the thermomorphic solvent system and the rhodium phosphite complex catalyst for the hydroformylation of 1-octene and 1-dodecene. In the range of conditions employed, the rate and selectivity calculated using the developed mechanistic rate model and selectivity model were in good agreement with experimental result. The work also concluded that the novel TMS system can be used to produce valuable fine chemicals from syngas and olefin at a lower operating cost.

ABSTRAK

Hidroformilasi olefin dengan tindakbalas karbon monoksida dan hidrogen pada tekanan 15-50 bar dan suhu pada 353-393 K dengan kehadiran mangkin homogen berasaskan rodium (Rh) untuk pengeluaran alkanal telah menunjukkan hasil dan selektiviti yang tinggi. Mangkin berasaskan rodium (Rh) berharga tinggi dan daya hidup komersial sesuatu proses yang menggunakan mangkin tersebut bergantung kepada kecekapan pemulihan mangkin dan pengasingan produk. Di dalam penyelidikan ini, sistem multikomponen pelarut yang bergantung pada suhu (TMS) ataupun pelarut termomorfik telah digunakan sebagai media tindak balas untuk mengkaji tindak balas hidroformilasi menggunakan dua olefin berat – 1-oktena dan 1-dodekana – untuk menghasilkan alkanal pada tekanan yang lebih rendah 15-25 bar dan suhu pada 353-373 K. Bergantung kepada suhu, campuran pelarut tersebut berubah daripada dua fasa kepada satu fasa, dan pengasingan produk serta mangkin berlaku dalam fasa tidak-polar dan polar. Keadaan ini memudahkan proses pengasingan dan kitar semula mangkin.

Sistem TMS yang mengandungi tiga komponen – propenakarbonat (PC), *n*-dodekana dan 1,4-dioksana telah digunakan di dalam penyelidikan ini. Kehadiran 1,4-dioksana memberi sifat termomorfik kepada campuran pelarut tersebut. Untuk tindak balas gas-cecair, keterlarutan gas reaktan di dalam media cecair adalah salah satu parameter penting yang diperlukan untuk mentafsirkan tindakbalas kinetik. Oleh itu sukatan kelarutan gas reaktan – CO dan H₂ – di dalam setiap komponen pelarut termasuk juga campuran pelarut telah diperolehi melalui eksperimen sehingga ke tekanan 1.5 MPa dan suhu dalam lingkungan 298-343 K. Kesan parameter proses seperti komposisi pelarut, tekanan reaktan gas – CO and H₂, suhu tindak balas dan pengisian mangkin terhadap kadar tindak balas, hasil tindak balas dan selektiviti *n*-alkanal juga telah dikaji. Pada suhu tindak balas 363 K, tekanan 1.5 MPa dan 0.68 mM HRh(CO)(PPh₃)₃, penukaran 1-oktena dan hasil alkanal masing-masing adalah 97% dan 95%. Produk alkanal telah dipulihkan dalam fasa tidak-polar manakala, mangkin terkumpul dalam fasa polar bersama kehilangan mangkin yang rendah iaitu sebanyak 3%. Dalam tindak balas selama 2 jam hasil eksperimen menunjukkan selektiviti sebanyak 89% dan sistem pemangkin ini boleh dianggap sebagai reaktif dan selektif. Kadar tindak balas didapati bertertib satu

terhadap mangkin, 1-oktena dan tekanan hidrogen. Kadar tindak balas terhadap tekanan karbon monoksida menyamai kinetik perencatan substrat.

Data keterlarutan telah dihubungkan menggunakan tiga models – model empirikal berdasarkan hukum Henry, teori larutan biasa bersama ubahsuai Yen dan McKetta dan model ubahsuai UNIFAC. Dengan menggunakan model kedua tanpa penyelarasan konstan, ketepatan penganggaran adalah sekitar lingkungan $\pm 11\%$, manakala model UNIFAC memberi ketepatan yang lebih baik iaitu sekitar $\pm 8.5\%$. Di dalam kajian kinetik, model kadar mekanistik untuk hidroformilasi olefin berat menggunakan mangkin berasaskan-Rh di dalam sistem homogen telah dihasilkan menggunakan teknik ab initio secara pengiraan kuantum kimia bagi mengenalpasti langkah penentu kadar di dalam mekanisme tindak balas. Komputasi dijalankan untuk tiga olefin - 1-dekena, 1-dodekena dan stirena – menggunakan kaedah Hartree-Fock pada tahap Moller-Plesset tertib kedua daripada teori pertubasi dan set asas 6-31++G(d,p) menggunakan pakej program GAMESS Pro 11.0. Tiga model kadar mekanistik dihasilkan berasaskan analisa mekanisme tindak balas dan penemuan eksperimen yang tercatat dalam penerbitan. Model kinetik berasaskan oksidatif H₂-tambahan sebagai langkah penentu kadar manggangarkan perubahan ketiga-tiga olefin agak memuaskan dengan purata perbezaan $\pm 7.6\%$. Model UNIQUAC dan UNIFAC telah digunakan untuk mentafsirkan proses pengasingan mangkin dan produk untuk hidroformilasi 1-oktena menggunakan sistem TMS. Dengan menggunakan model UNIFAC, ketepatan penganggaran adalah sekitar lingkungan $\pm 8.2\%$, manakala model UNIQUAC memberi ketepatan yang lebih baik iaitu $\pm 6.5\%$.

Hasil kerja ini telah membuktikan bahawa sistem TMS bersama kompleks mangkin Rh-fosfit mempunyai potensi untuk tindak balas hidroformilasi 1-oktena dan 1-dodekana. Di dalam lingkungan keadaan yang digunakan, kiraan kadar tindakbalas dan selektiviti menggunakan model kadar mekanistik dan model selektiviti menyamai dengan keputusan eksperimen. Hasil kerja ini juga telah merumuskan bahawa sistem TMS boleh digunakan bagi menghasilkan produk kimia bernilai tinggi daripada tindak balas singas dan olefin dengan kos operasi yang rendah.

TABLE OF CONTENTS

	PAGE
STATUS OF THESIS	ii
APPROVAL PAGE	iii
DECLARATION OF THESIS	v
ACKNOWLEDGEMENT	vii
ABSTRACT	viii
ABSTRAK	x
TABLE OF CONTENTS	xii
LIST OF TABLES	xvi
LIST OF FIGURES	xviii
NOMENCLATURE	xx
CHAPTER 1: INTRODUCTION	1
1.1. Hydroformylation of Olefins	1
1.2. Recent Technological Developments	6
1.2.1. Aqueous Biphasic Catalysis	6
1.2.2. Non-aqueous Catalysis	7
1.3. Problem Statement	9
1.4. Objectives of the Study	10
1.5. Scope of the Study	11
1.5.1. Development of a novel temperature dependent multi-component solvent (TMS) system	11
1.5.2. Study on the Effect of Operating Conditions	12
1.5.3. Development of Kinetic Models	13
1.5.4. Liquid-liquid equilibrium (LLE) Behavior and Distribution	13
CHAPTER 2: LITERATURE REVIEW	14
2.1. Hydroformylation Catalyst	14
2.2. Mechanism of Hydroformylation	15
2.2.1. Unmodified Catalyst	16
2.2.2. Phosphine Modified Catalysts	17
2.3. Kinetic Study	20
2.4. Influence of Process Parameters	29
2.5. Solubility and Reaction Rate of Linear α -Olefin in Water.	30
2.6. Solubility Study and Thermodynamic Modeling	32
2.7. Liquid-liquid Equilibrium Study	33
2.8. Summary	36
CHAPTER 3: DEVELOPMENT OF THE MECHANISTIC RATE MODEL USING AB INITIO CALCULATION	37
3.1. Kinetic Models	37
3.1.1. Developing Empirical Models	37
3.1.2. Developing Mechanistic Models	38

3.1.3.	Empirical versus Mechanistic Models	38
3.2.	Approaches to Kinetic Modeling	39
3.3.	Molecular modeling	40
3.3.1.	Electron Correlation Methods	43
3.3.1.1.	Møller–Plesset Perturbation Theory	44
3.3.1.2.	Density Functional Theory	45
3.3.2.	Geometry Optimization	46
3.4.	The <i>ab Initio</i> Molecular Orbital Calculation	47
3.5.	The Reaction Pathways	50
3.6.	Computational Methodology	53
3.6.1.	Test Calculation	56
3.7	Results and Discussion	58
3.7.1.	Quantum Chemical Calculation	58
3.7.1.1.	Alkene Insertion	58
3.7.1.2.	Formation of Acyl Complex	59
3.7.1.3.	H ₂ Oxidative Addition	60
3.7.1.4.	The Potential Energy Profile	62
3.7.2.	Development of the Mechanistic Rate Equation	64
3.7.3	Determination of the Rate Parameters	67
CHAPTER 4:	MATERIAL AND METHOD	78
4.1.	Materials	78
4.2.	Development of the TMS-system	79
4.2.1.	Composition of the TMS- Systems	79
4.2.2.	Determination of the Gas Solubility	80
4.2.2.1.	Pressure Test	82
4.2.2.2.	Purging and Evacuation	82
4.2.2.3.	Solubility Experiment	82
4.3.	Parameteric Study of Reaction Variables and Kinetic Study	85
4.3.1.	Pressure Test	88
4.3.2.	Reaction and Kinetic Measurement	89
4.3.3.	Solubility Measurement	89
4.4.	Liquid-liquid Equilibria	90
4.4.1.	Distribution Coefficient	91
4.5.	Analytical Techniques	91
4.5.1.	Gas Chromatography	91
4.5.2.	Atomic Absorption Spectroscopy	92
CHAPTER 5:	RESULTS AND DISCUSSION	93
5.1.	Development of the TMS- System	93
5.1.1.	TMS-systems: PC+Dodecane+1,4-Dioxane	93
5.1.2.	Solubility Data	94
5.1.3.	Empirical Modeling	98
5.1.4.	Thermodynamic modeling	99
5.1.4.1.	Prediction of H ₂ and CO Solubility by the RST- based Model	100

5.1.4.2.	Prediction of H ₂ and CO Solubility by the Modified UNIFAC Group Contribution Model	102
5.1.4.3.	Results of the Thermodynamic Modeling	106
5.2.	Parametric Study of Reaction Variables	109
5.2.1.	Selection of Solvent Composition	109
5.2.2.	Effect of Reaction Parameters	112
5.2.2.1.	Effect of Catalyst Concentration	112
5.2.2.2.	Effect of Temperature	115
5.2.2.3.	Effect of the Total Pressure of Syngas	117
5.2.2.4.	Effect of CO/H ₂ Ratio	118
5.2.2.5.	Effect of Ligand to Catalyst Ratio	119
5.2.2.6.	Effect of 1-Octene Concentration	122
5.3.	Kinetic Study	123
5.3.1.	Solubility of CO and H ₂	123
5.3.2.	Kinetics	124
5.3.2.1.	Effect of Catalyst Concentration	125
5.3.2.2.	Effect of 1-Octene Concentration	126
5.3.2.3.	Effect of Hydrogen Partial Pressure	127
5.3.2.4.	Effect of Carbon Monoxide Partial Pressure	128
5.3.3.	Kinetic Modeling	129
5.3.3.1.	Empirical model	129
5.3.3.2.	Mechanistic model	134
5.4.	Liquid-liquid Equilibrium Study	143
5.4.1.	Liquid-liquid equilibrium data	144
5.4.2.	Thermodynamic modeling	150
5.4.2.1.	UNIQUAC (UNIversal QUAsi-Chemical) model	151
5.4.2.2.	The UNIFAC (UNIQUAC Functional Group Activity Coefficients) model	152
5.5.	Additional Validation of UNIQUAC and UNIFAC Model	161
CHAPTER 6: CONCLUSION AND RECOMMENDATIONS		162
6.1.	Conclusion	162
6.2.	Recommendations for Future Work	164
REFERENCES		166
APPENDIX A	Key Structures Involved in the Catalytic Cycle of Hydroformylation of 1-Decene and Selected Parameters	181
APPENDIX B	Key Structures Involved in the Catalytic Cycle of Hydroformylation of 1-Dodecene and Selected Parameters	185
APPENDIX C	Key Structures Involved in the Catalytic Cycle of Hydroformylation of Styrene and Selected Parameters	188
APPENDIX D	Kinetic Data for Hydroformylation of Higher Alkenes in Homogeneous System	191

APPENDIX E	Estimated Rate Parameters	199
APPENDIX F	Derivation of the Rate Equation	201
APPENDIX G	Solubility of CO and H ₂ at Different Pressure and Temperature	202
APPENDIX H	Effect of Reaction Conditions on the Conversion and Selectivity	210
APPENDIX J	Kinetic Data	212
APPENDIX K	AAS Standard Calibration Curve	221
APPENDIX L	Experimental Tie-Line Data	222
APPENDIX M	Papers Published/Presented	224

LIST OF TABLES

	PAGE
1.1. Commercial application of hydroformylation of olefins.	2
2.1. A summary of kinetic studies involving hydroformylation reaction.	21
2.2. Variation of α -alkenes.	31
3.1. Description of the catalytic cycle in Figure 3.1.	52
3.2. Optimized parameters for the μ -acyl complex A'(Mo) at the RHF/6-31G(d,p) level.	57
3.3. Activation energies calculated at MP2 level of theory.	62
3.4. Range of experimental conditions used for development of the mechanistic rate equation.	68
3.5. Estimated M1 kinetic model parameters with 95% confidence limits.	71
4.1. Physical properties of the pure components.	79
4.2. Critical properties and acentric factors used in the PR EoS.	85
4.3. Range of variables studied in the present work.	86
5.1. Parameters in Eq (5.1) for hydrogen and carbon monoxide solubilities at a partial pressure and temperature of 101.3 kPa and 298-343 K, respectively.	99
5.2. Parameters for modeling with RST model.	102
5.3. UNIFAC parameters r and q of the components.	105
5.4. Modified UNIFAC group interaction parameters.	106
5.5. Effect of the composition of TMS-systems.	111
5.6. Typical results on conversion of 1-octene, selectivity and yields.	118
5.7. Solubility of H ₂ and CO in TMS-system of PC/dodecane/1,4-dioxane.	123
5.8. Constants in polynomial fitting nonanal concentration vs. time.	130
5.9. Estimated kinetic model parameters with 95% confidence limit.	131
5.10. Estimated A1 kinetic model parameters with 95% confidence limits.	142
5.11. Distribution coefficients of species in TMS- system.	149
5.12. UNIFAC parameters r and q of the components.	155
5.13. Binary interaction parameters of UNIQUAC equation.	156
5.14. Interaction parameter a_{jk} of the UNIFAC equation.	157
5.15. The average deviation (%) of the experimental data from the calculated mole fractions using UNIQUAC and UNIFAC model.	157
5.16. Experimental and predicted distribution of 1-octene, nonanal and HRh(CO)(PPh ₃) ₃ .	160

LIST OF FIGURES

	PAGE
1.1. Two phase catalysis in the presence of water soluble rhodium complex.	4
1.2. Biphasic thermomorphic hydroformylation system	8
2.1. Catalytic cycle of hydroformylation for unmodified cobalt catalysts.	17
2.2. Initial equilibria forming the active species, L = PPh ₃ or TPPTS.	18
2.3. Catalytic cycle of hydroformylation for phosphine modified rhodium catalysts.	19
2.4. Effect of phosphine/rhodium (PPh ₃ /HRh(CO)(PPh ₃) ₃) ratio on reaction rate and selectivity	30
2.5. Dependence of reaction rate on chain length of alkenes	32
3.1. Plausible steps for rhodium catalyzed hydroformylation in the presence of low concentration of phosphine ligand.	51
3.2. Flowchart illustrating the steps involved in quantum chemical calculations of molecular structures.	55
3.3. Optimized structure of the the μ -acyl complex A'(Mo) as an intermediate in hydroformylation using a hetero-bimetallic complex catalyst.	57
3.4a Selected geometrical parameters of optimized structures (Å) of the transition state TS-1 (E1/F1) for the 1-dodecene insertion at RHF level.	59
3.4b Optimized Bond lengths (Å) of transition state TS-2 (H1/J1) for the CO insertion at the RHF level (1-octene)	60
3.4c Optimized structures (Å) of the transition state TS-3 (J1/N1) for the H ₂ oxidative addition at the RHF level (1-dodecene).	61
3.5a. The potential energy profile of 1-decene hydroformylation reaction.	63
3.5b. The potential energy profile of 1-dodecene hydroformylation reaction	63
3.5c. The potential energy profile of styrene hydroformylation reaction	64
3.6. Flowchart illustrating the steps involved in kinetic modeling	70
3.7. Experimental and predicted initial reaction rates vs. concentration of olefin, at temperature of 323 K.	72
3.8. Experimental and predicted initial reaction rates vs. concentration of olefin, at temperature of 333 K.	72
3.9. Experimental and predicted initial reaction rates vs. concentration of olefin, at temperature of 343 K.	73
3.10. Experimental and predicted concentration of 1-dodecene and CO or H ₂ as a function of contact time at temperature of 323, 333 and 343 K.	74
3.11. Parity plots of the model predictions of the rate of hydroformylation of styrene, 1-octene, 1-decene and 1-dodecene in homogeneous system.	74
4.1. Schematic of the high pressure solubility cell unit	81
4.2. Photograph of the high pressure solubility cell unit	81
4.3. Reaction products of hydroformylation of 1-octene	86
4.4. Schematic of the experimental setup	87
4.5. Photograph of the Parr high pressure reactor	88
4.6. GC signal for hydroformylation of 1-octene	92
4.7. GC signal for hydroformylation of 1-dodecene	92
5.1. Phase diagram of the solvent system PC+dodecane+1,4 dioxane	94

5.2.	Experimental solubility of gases in PC, biphasic PC+dodecane mixture (1:1) and TMS-systems of PC/dodecane/1,4-dioxane	95
5.3.	Experimental and predicted solubility of gases in PC, biphasic PC+dodecane mixture and TMS- systems of PC/dodecane/1,4-dioxane	96
5.4.	Experimental solubilities of H ₂ at partial pressure of 101.3 kPa as a function of temperature.	96
5.5.	Experimental solubilities of CO at partial pressure of 101.3 kPa as a function of temperature.	97
5.6.	Solubility of CO and H ₂ in TMS-systems PC/dodecane/1,4-dioxane at partial pressure of 101.3 kPa.	107
5.7.	Solubility of CO and H ₂ in biphasic PC/dodecane mixture at partial pressure of 101.3 kPa.	107
5.8.	Solubility of CO and H ₂ in propylene carbonate at partial pressure of 101.3 kPa.	108
5.9.	Parity plots of the model predictions of the solubility of CO and H ₂ .	109
5.10.	Phase diagram of the solvent system PC/dodecane/1,4 dioxane	110
5.11.	An organic solvent mixture composed of PC/dodecane/1,4-dioxane (0.3/0.1/0.6) formed the biphasic system at 298 K.	112
5.12.	A: Time evolution of the yield of total aldehyde at different concentration of HRh(CO)(PPh ₃) ₃ catalyst; B: Effect of HRh(CO)(PPh ₃) ₃ concentration.	113
5.13.	Expanded GC signal for the formation for C ₉ -aldehyde isomers	114
5.14.	Expanded GC signal for the octene isomers and octane	115
5.15.	A: Time evolution of the yield of total aldehyde at different reaction temperatures; B: Effect of temperature.	116
5.16.	A: Yield of total aldehyde as a function of reaction time at different total syngas pressure; B: Effect of total pressure	117
5.17.	A: Yield of total aldehyde as a function of reaction time at different CO/H ₂ pressure ratio; B: Effect of CO/H ₂ ratio	119
5.18.	A: Yields of total aldehyde as a function of reaction time at different ratio of ligand to catalyst concentration. B: Effect of P(OPh) ₃ /HRh(CO)(PPh ₃) ₃ ratio.	120
5.19.	HRh(CO)(PPh ₃) ₃ dissociation equilibrium	121
5.20.	A: Yield of total aldehyde as a function of reaction time at different 1-octene concentrations; B: Effect of 1-octene concentration.	122
5.21.	Effect of partial pressure of H ₂ and CO on solubility	123
5.22.	Effect of agitation speed on the rate of reaction in hydroformylation of 1-octene and 1-dodecene.	124
5.23.	Effect of catalyst concentration on the rate of reaction.	125
5.24.	Effect of 1-octene concentration on the rate of reaction.	126
5.25.	Effect of partial pressure of H ₂ on the rate of reaction.	127
5.26.	Effect of partial pressure of CO on the rate of reaction.	128
5.27.	Typical plot of concentrations of 1-otene, nonanal and 2-methyloctanal versus reaction time.	130
5.28.	Parity plot of the experimental and calculated reaction rates.	133

5.29.	Parity plot of the experimental and calculated selectivity (<i>n/iso</i>).	134
5.30.	Plausible steps for rhodium catalyzed hydroformylation in the presence of excess concentration of P(OPh) ₃ ligand.	135
5.31.	Effect of partial pressure of CO on the rate of hydroformylation of 1-octene (A) and 1-dodecene (B).	139
5.32.	Effect of partial pressure of H ₂ on the rate of hydroformylation of 1-octene (A) and 1-dodecene (B).	140
5.33.	Effect of concentration of 1-olefin on the rate of hydroformylation of 1-octene (A) and 1-dodecene (B).	140
5.34.	Effect of concentration of catalyst on the rate of reaction: 1-octene (A) and 1-dodecene (B).	141
5.35.	Parity plot of the model predictions of the rate of hydroformylation of 1-octene and 1-dodecene in TMS-systems of PC/dodecane/1,4-dioxane.	141
5.36.	LLE ternary diagram for PC+dodecane+1,4-dioxane at 298.15 K.	144
5.37.	LLE ternary diagram for PC+dodecane+1,4-dioxane at 313.15 K.	145
5.38.	LLE ternary diagram for PC+dodecane+1,4-dioxane at 333.15 K;	145
5.39.	LLE ternary diagram for PC+dodecane+1,4-dioxane at 353.15 K;	146
5.40.	Distribution coefficient <i>D</i> of nonanal as a function of the mass fraction <i>x</i> of nonanal in non polar phase.	147
5.41.	Distribution coefficient <i>D</i> of HRh(CO)(PPh ₃) ₃ catalyst as a function of the mass fraction <i>x</i> of HRh(CO)(PPh ₃) ₃ in non polar phase.	148
5.42.	Distribution coefficient <i>D</i> of 1-octene as a function of the mass fraction <i>x</i> of 1-octene in non polar phase.	148
5.43.	LLE ternary diagram for ternary (TMS+nonanal+1-octene) systems at 298.15 K.	159
5.44.	LLE ternary diagram for ternary (TMS+nonanal+1-octene) systems at 308.15 K.	159
5.45.	Parity plots of the model predictions of the LLE data of TMS+1-octene+nonanal+triphenylphosphite+HRh(CO)(PPh ₃) ₃ system at temperature of 298 K.	161

NOMENCLATURE

		UNIT
A	pre-exponential factor, units will be identical to the rate constant	-
a	attraction parameter	-
a_{nm}	modified UNIFAC interaction parameter between groups m and n , Eq. (5.14)	-
A_{nm}, B_{nm}	parameters in Eq. (5.14)	-
A, B, C	parameters in Eq. (5.1)	-
[alkene]	concentration of alkene in the reaction mixture	$\text{kmol}\cdot\text{m}^{-3}$
b	van der Waals covolume	-
B_i	interaction potential	-
$C_{L,1}$	solute concentration in liquid at the interface	$\text{kmol}\cdot\text{m}^{-3}$
$C_{L,2}$	solute concentration in bulk liquid	$\text{kmol}\cdot\text{m}^{-3}$
[C_{ald}]	concentration of aldehyde	$\text{kmol}\cdot\text{m}^{-3}$
[catalyst]	concentration of $\text{HRh}(\text{CO})(\text{PPh}_3)_3$ in the reaction mixture	$\text{kmol}\cdot\text{m}^{-3}$
[CO]	concentration of carbon monoxide in the reaction mixture	$\text{kmol}\cdot\text{m}^{-3}$
D	distribution coefficients	-
E_a	activation energy for rate constant	$\text{kJ}\cdot\text{mol}^{-1}$
E_{ne}	electron-nuclear attraction functional	-
E_{xc}	exchange correlation functional	-
ea	one ligand in equatorial and the other in apical positions	-
ee	coordinating groups (L, CO) are in equatorial positions	-
f_2^G	fugacity of pure gas at atmospheric pressure	MPa
f_2^0	fugacity of a hypothetical pure liquid	MPa
f_2^L	fugacity of hypothetical liquid solute at atmospheric pressure	MPa
F	Fock operator	-
g	number of various groups in the mixture	-
H	Henry's law constant	$\text{MPa}\cdot\text{m}^3\cdot\text{kmol}^{-3}$
\hat{H}	Hamiltonian operator	-
ΔH	heat of reaction	$\text{kJ}\cdot\text{mol}^{-1}$
ΔH_v	heat of vaporization	$\text{J}\cdot\text{mol}^{-1}$
[H_2]	concentration of hydrogen in the reaction mixture	$\text{kmol}\cdot\text{m}^{-3}$
\hbar	Planck's constant	J·s
i, j, k	component identifications	-
J	Coulomb integral which reflects the average interaction potential of electron i due to all other electrons	-
K	equilibrium constants for the elementary steps in the catalytic cycle	-
K	exchange integral	-
K	characteristic constant in Eq. (4.9)	-
k	reaction rate constant, units will be specific to the form of	-

	the rate expression	
MRSS	mean residual sum of squares	-
n	number of moles	mol
n/iso	linear to branched	-
N	number of components	-
NX 795	2,2,4-trimethyl-1,3-pentanediolmono(2-methylpropanoate)	-
[octene]	concentration of 1-octene in the reaction mixture	$\text{kmol}\cdot\text{m}^{-3}$
P	total pressure	MPa
p^v	vapour pressure of pure solvent	MPa
PC	propylene carbonate	-
P_{CO}	partial pressure of CO	MPa
P_{H_2}	partial pressure of H_2	MPa
P_0	initial partial pressure	MPa
ω	acentric factor	-
q_i	van der Waals surface area of component i	-
R	gas constant: $0.08206 \text{ dm}^3\cdot\text{atm}\cdot\text{K}^{-1}\cdot\text{mol}^{-1}$; $8.314 \text{ J}\cdot\text{mol}^{-1}\cdot\text{K}^{-1}$	
r_i	van der Waals volume of component i	m^3
r	distance from the nucleus to the electron	pm
SEE	average standard error of estimation	%
ΔS	entropy of reaction	$\text{J}\cdot\text{mol}^{-1}\cdot\text{K}^{-1}$
sc	supercritical	-
t	time	s
T	absolute temperature	K
T_b	normal boiling temperature	K
T_c	critical temperature	K
T_S	kinetic energy functional	-
TS	transition state	-
TMS	temperature dependent multi-component solvent	-
TON	turnover number	-
TOF	turnover frequency	h^{-1}
v	molar volume	$\text{m}^3\cdot\text{mol}^{-1}$
v_{ki}	content of the group k in molecules of component i	-
V_{liq}	volume of liquid	m^3
V_{gas}	volume of gas	m^3
x_i	mole fraction of component i in the liquid phase	-
y_i	mole fraction of component i in the gas phase	-
Z	compressibility factor	-
Z	nuclear charge	-
	GREEK SYMBOL	
δ	solubility parameter	$\text{J}^{1/2}\cdot\text{m}^{-3/2}$
$\bar{\delta}$	average solubility parameter	$\text{J}^{1/2}\cdot\text{m}^{-3/2}$
ϕ	surface area fraction	-
ρ	density	$\text{g}\cdot\text{cm}^{-3}$
ρ_L	molar density	$\text{mol}\cdot\text{dm}^{-3}$

γ_2^∞	infinite dilution activity coefficient of the gas	-
γ_i	activity coefficient of component i	-
Φ	objective function	-
φ	segment fraction	-
θ	volume fraction	-
α	scaling factor defined by Eq. (4.5)	-
$\alpha, \beta, \gamma, \delta$	parameters in Eq. (5.21)	-
ω	acentric factor	-
Γ_m	activity coefficient of group m in the mixture	-
$\Gamma_m^{(i)}$	activity coefficient of group m in pure compound i	-
Γ_m	function of group fraction	-
ψ	interaction parameter	-
ξ	effective nuclear charge	-
ε_i	eigenvalues	-
$\Psi_{\text{mol}}(t)$	wave function	-
	Subscript and superscripts	
G	gas	-
L	liquid	-
c	critical property	-
exp	experimental	-
$calc$	calculated	-

CHAPTER 1

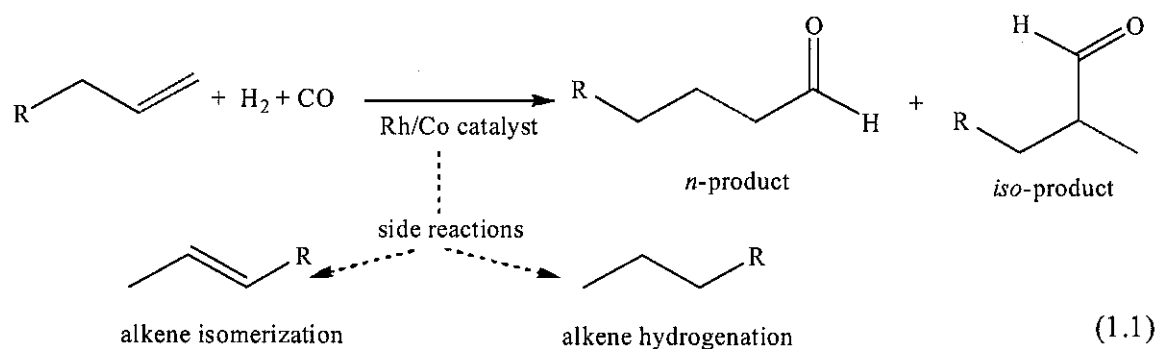
INTRODUCTION

Homogeneous catalysis has traditionally been exploited for reactions in a single phase system. It is now an area rich with opportunities for the implementation of commercial reactions and processes in multiphasic solvent systems as well with the unique advantage of catalyst recovery and product separation. One of the examples of such cases is the temperature dependent multi-component solvent (TMS) or thermomorphic solvent system. This chapter summarizes the available information on hydroformylation in general and the use of thermomorphic solvent system as the reaction medium in particular. The limitations of hydroformylation of higher olefins using current industrial processes are also highlighted. The material presented here is intended as a general review for the subsequent chapters. More details specific to the chapter topics are addressed therein.

1.1 Hydroformylation of Olefins

Hydroformylation or the oxo reaction has provided a versatile route for the synthesis of a vast array of bulk and specialty chemicals. The hydroformylation products prepared on the largest scale are butyraldehyde and ethylhexanol (Bohnen and Cornils, 2003). Both of these are produced from propylene which is derived from natural gas. Either rhodium or cobalt phosphine complexes are employed as the catalyst. The second largest industrial application of hydroformylation is the production of C₈-C₂₀ range alcohols which are the basic material of biodegradable detergents. This process starts with ethylene oligomerization, olefin isomerization and olefin metathesis, followed by hydroformylation. Collectively the olefin synthesis steps are referred to SHOP for Shell Higher Olefin Process (Weissermel and Arpe, 1997).

In hydroformylation, reactions occur at the olefinic double bond with synthesis gas (carbon monoxide and hydrogen) in the presence of transition metal catalyst (rhodium or cobalt) to form linear (*n*) and branched (*iso*) aldehydes containing an additional carbon atom as primary products. The overall reaction can be represented by Eq. (1.1).



The most important hydroformylation products are in the range C₃-C₁₉. The economic importance of hydroformylation synthesis is mainly based on butanal with a share of 73 % of overall hydroformylation capacity. The *n*-butanal is converted to 2-ethylhexanol which is used in the production of dioctyl phthalate (DOP), a plasticizer that is used in the polyvinylchloride (PVC) applications. Until the mid 1970s, cobalt was used as catalyst in commercial processes (e.g., by BASF, Ruhrchemie, Kuhlmann). Because of the instability of cobalt carbonyl (HCo(CO)₄) catalyst, the reaction conditions were significantly high with the pressure range of 20.0-35.0 MPa to avoid decomposition of the catalyst and deposition of the metallic cobalt. The ligand modification introduced by Shell researchers was a significant progress in hydroformylation (Johnson, 1985). The replacement of carbon monoxide with phosphines enhanced the selectivity towards linear aldehyde (*n/iso*) and the stability of cobalt carbonyl catalyst, leading to a reduction of the required carbon monoxide pressure. Table 1.1 shows the commercial hydroformylation catalyst systems.

Table 1.1: Commercial Hydroformylation Catalyst Systems (Master, 1977)

Company	Catalyst System	Temperature (K)	Pressure (MPa)	Selectivity (%)	<i>n/iso</i> (1-olefin)	Metal/olefin (%)	Typical olefin
Shell	Co ₂ (CO)(PBU ₃) ₂	433~473	5.0~30	80	6~8/1	0.5~1.0	C2~C12
Union Carbide	HRh(CO)(PPh ₃) ₃	353~393	1.5~2.5	96	10~14/1	0.01	C2~C4
Ruhrchemie	HRh(CO)(TPPTS) ₃	353~403	4.0~5.0	99	19	0.2	C2~C4

The $\text{HCo}(\text{CO})_3(\text{PR}_3)$ catalyst system is only used by Shell. It is tightly coupled to *Shell's Higher Olefins Process* (SHOP) that produces a C_4 through C_{20} blend of linear, internal alkenes for hydroformylation to detergent grade alcohols. The electronic effect of substituting an electron donating alkylated phosphine for one of the carbonyl ligands to produce $\text{HCo}(\text{CO})_3(\text{PR}_3)$, results in stronger Co-CO bonding. The use of $\text{HCo}(\text{CO})_3(\text{PR}_3)$ catalyst system operates at 5.0-10.0 MPa of pressure, and could be run at higher temperatures without any decomposition of catalyst to cobalt metal. Therefore, the catalyst and product are separated by distillation under reaction conditions. The electron-donating phosphine ligand also increases the hydridic nature of the hydride ligand and dramatically increases the hydrogenation capabilities of the $\text{HCo}(\text{CO})_3(\text{PR}_3)$ catalyst. Therefore the aldehydes produced are subsequently hydrogenated by $\text{HCo}(\text{CO})_3(\text{PR}_3)$ to produce alcohols. The better hydrogenation ability, however, also results in increased alkene hydrogenation side-reactions producing alkanes that can range from 10-20 % of the product distribution (depending on the phosphine and reaction conditions). Because of the aldehyde hydrogenation step, the syngas (H_2/CO) ratios of 2:1 (or slightly higher) are typically used. In addition, this catalyst is less active than $\text{HRh}(\text{CO})(\text{PPh}_3)_3$ and therefore higher reaction temperatures are used in conjunction with longer reaction times and larger reactor volumes. From a steric viewpoint the bulkier trialkylphosphine ligand favors formation of linear products with regioselectivities of 6-8:1. There is a phosphine cone angle cut-off at about 132° , after which the phosphine ligand's steric effects do not increase the product linear regioselectivity any further.

During 1974-1976 Union Carbide Corporation (UCC) and Celanese increase the product linear regioselectivity any further. Corporation, independently, introduced rhodium-based catalysts, specifically, $\text{HRh}(\text{CO})(\text{PPh}_3)_3$ on an industrial scale (Cornils and Herrmann, 2002). These processes combined the advantages of ligand modification with the use of rhodium as a catalyst metal. The rhodium catalyst is modified by ligands to form an active catalyst complex; phosphine ligands used in industry have been $\text{P}(\text{C}_6\text{H}_5)$ and $\text{P}(\text{C}_4\text{H}_9)$, and triphenylphosphine oxide (TPPO) for homogeneous systems. Since the reaction conditions were much milder, the process was called 'low-pressure oxo' (LPO) process. Then low-pressure oxo (LPO) processes took the leading role and despite the higher price of rhodium, cobalt catalysts for the hydroformylation of propene

$\text{P}(\text{Ph-}m\text{-SO}_3\text{Na}^+)_3$ (TPPTS), a highly water soluble catalyst is generated: $\text{HRh}(\text{CO})[\text{P}(\text{Ph-}m\text{-SO}_3\text{Na}^+)_3]_3$. In aqueous solution the catalyst essentially has a -9 charge, making it totally insoluble in all but the most polar organic solvents. The use of a water soluble catalyst system brings substantial advantages for industrial practice, because the catalyst can be considered to be heterogeneous. The separation of catalyst solution and reaction products, including high-boiling by-products, is achieved by phase separation technique. Separation relies upon the fact that the product is insoluble in the catalyst phase and the two phases can be easily separated without exposing the system to any unnecessary thermal stress, which may lead to catalyst decomposition. The drive for this development arose from the wish to implement Rh catalysed hydroformylation, which is well documented as having greater reactivity under milder conditions than the commonly used process using cobalt catalysts. The success of this plant and more plants that have been built since, is shown in the volume of their output, over 500 000 tons per year of C_4 products. The aqueous biphasic method shows low ligand and rhodium leaching from the aqueous phase; this along with the low cost of solvents made it an industrially attractive process.

The optimised process uses a P:Rh ratio of at least 60/1 and by continuous addition of fresh ligand, to replace any oxidised phosphane, the catalyst lifetime can be prolonged. Excess TPPTS ligand is required for good *n:iso* selectivities, as with conventional Rh/ PPh_3 catalysts. The only drawback of the aqueous biphasic process is the poor solubility of higher olefins in water, resulting in lower activities for these substrates and thereby limiting the RCH/RP process to C_3 and C_4 substrates (Beller et al, 1995). In order for the reaction to occur, the alkenes must have appreciable water solubility to migrate into the aqueous catalyst phase. Remigration of the aldehyde product back into the organic phase allows easy phase separation of product from catalyst. The reaction is never homogeneous even with C_3 and C_4 alkenes and it is unclear whether the reaction occurs on dissolved alkene within the water droplets or only at the interface. Good mixing merely increases the area of the liquid-liquid interface and improves the transport of the alkene into the aqueous phase. Rather high linear to branched regioselectivities of 16-19:1 for propylene can be obtained via this water soluble catalyst. Rates are slower than with conventional Rh/ PPh_3 catalysts due to lower alkene concentrations in the water

phase. The process is limited to the shorter chain alkenes (C₂-C₄). Alkenes higher than 1-pentene are not soluble enough in water. Celanese-Ruhrchemie currently operates several hydroformylation plants based on this water soluble rhodium catalyst technology.

In its present form, the RCH/RP process is unsuitable for the hydroformylation of alkenes greater than C₄, due to the limited solubility of such molecules in the aqueous catalyst phase. Some attempts have been made to adjust this process for the hydroformylation of higher olefins, in order to overcome their low solubility. Additives can be included in the reaction, such as alcohols and glycols (Purwanto and Delmas, 1995). However, these only add to the cost of the process, as an extra separation step is required to remove them from the product. Alternatively increasing the organic solubility of the catalyst may increase the hydroformylation rates, but it is also likely to increase the loss of Rh and ligand to the organic phase. It seems more probable that a different solvent system or immobilisation (heterogenisation) of the catalyst would provide the desired results.

1.2 Recent Technological Developments

1.2.1. Aqueous Biphasic Catalysis

Several techniques have been proposed to overcome the solubility and mass transport limitations that are typical in the conventional aqueous biphasic system for the hydroformylation of higher alkenes. Concerning two phase hydroformylation of higher olefins in an aqueous-organic reaction system, the different approaches can be categorized as follows:

- i. The use of water-soluble ligands with amphiphilic properties which will either improve the solubility of the higher olefins via formation of micelles or increase the reaction rate by preferential concentration of the catalyst complex close to the interface of the aqueous and the organic phase (Chen et al., 1999; Karakhanov, 1996)
- ii. Modification of the Ruhrchemie/Rhone-Poulenc system with co-solvents such as polar, alcoholic solvents or by use of detergent cations, modified cyclodextrins and surfactants (Haumann et al., 2002; Zhang et al., 2002; Purwanto and Delmas

1995; Monteil et al. 1994) to enhance the mutual solubility and the mobility of the components across the boundary.

- iii. The principle of thermoregulated phase-transfer catalysis (TRPTC), originally developed by Bergbreiter et al. (1998), which has been applied to two-phase hydroformylation by Jin et al. (1997), Zheng et al. (1998) and Liu et al. (2003), which is based on a temperature-controlled switch of the catalyst system from the aqueous phase to the organic phase.
- iv. Immobilization of unmodified rhodium catalyst (i.e., without ligands) in the aqueous phase by using resin, polymeric, oligomeric water-soluble or mineral supports (Diwakar et al., 2005; Chen and Alper, 1997; Terreros et al., 1989).
- v. Supported aqueous-phase catalysis (SAPC) that involves absorption of an aqueous solution of a catalytic active organometallic complex onto a high surface area hydrophilic support material. (Riisager et al., 2003; Zhu et al., 2003; Jáuregui-Haza et al., 2001; Arhancet et al., 1990)

1.2.2. Non-aqueous Catalysis

Non-aqueous approaches toward biphasic hydroformylation have been demonstrated by Horváth and Rábai (1994) with the use of a fluorous biphasic system containing a rhodium catalyst having partially fluorinated “ponytail” ligands. The technique is based on the limited miscibility of fluorinated solvent and fluorinated ligand in hydrocarbon. A biphasic system is mixture which has two phases or distinct layer. For example, a biphasic hydroformylation catalyst system was developed to take advantage of the unusual solvent characteristics of perfluorocarbons combined with typical organic solvents. Fluorous mixtures such as perfluoromethylcyclohexane (PFMCH/toluene) are immiscible at ambient temperature but become a single phase solution at an elevated temperature (Scott, 1948; Hildebrand and Cochran, 1949; Dorset, 1990). However, it is doubtful whether the fluorous biphasic would achieve any breakthrough in the large-scale industry, because of the toxicity of perfluorous solvents and ligands and risks related to ozone depletion (Liu et al., 2002; Kollhofer and Plenio, 2003). Bianchini (1995) describe an alternative to fluorous biphasic systems using new ligand $\text{NaO}_3\text{S}(\text{C}_6\text{H}_4)\text{CH}_2\text{C}(\text{CH}_2\text{-PPh}_2)_3$ (sulphos) dissolved in light alcohols (methanol, ethanol). The hydroformylation

reaction of 1-hexene gives C_7 alcohols in an alcohol/hydrocarbon system and C_7 aldehydes in an alcohol-water/hydrocarbon system. All rhodium is recovered in the polar phase at the end of the catalytic reactions.

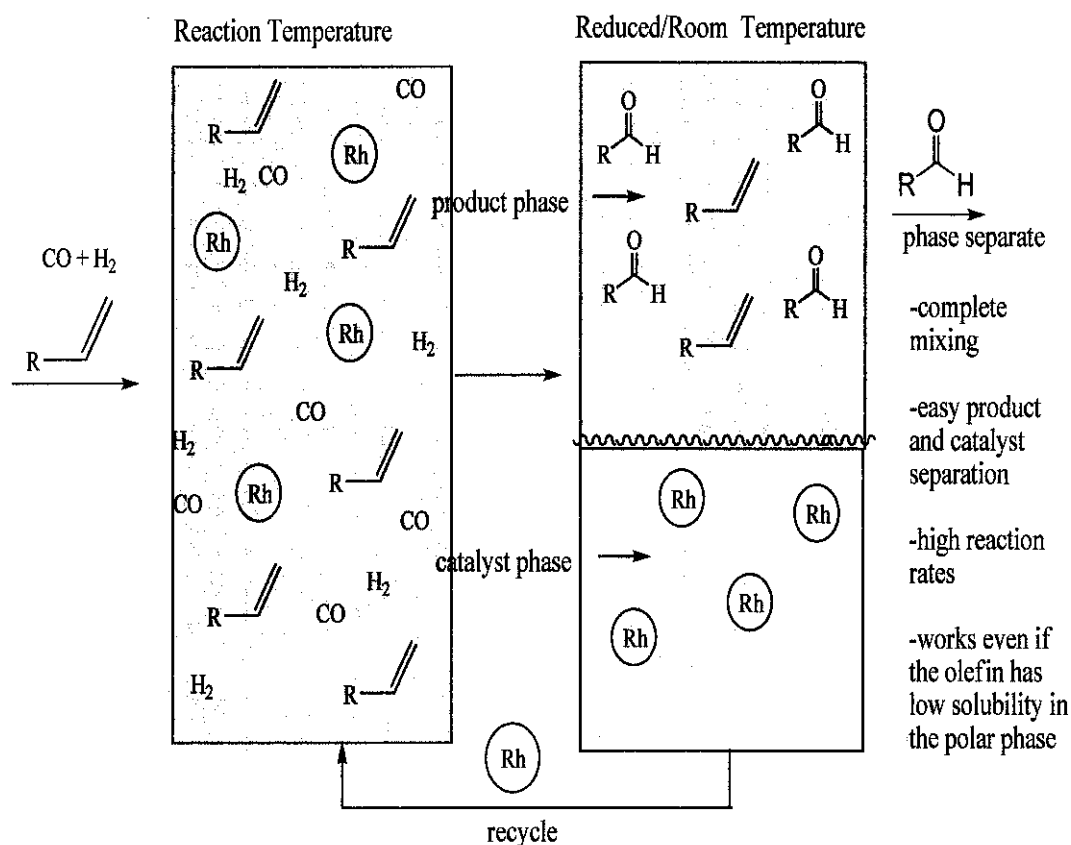


Figure 1.2: Biphasic thermomorphic hydroformylation system

In the recent time, a novel solvent system that itself reversibly changes from biphasic to monophasic as a function of temperature and known as a thermomorphic biphasic or temperature-depending multicomponent solvent (TMS) system has gained interest as the reaction medium. The use of TMS system allows performing a reaction in a single-phase at a high reaction temperature followed by a phase split at a lower temperature. The TMS systems consist of a polar solvent (s_1) and nonpolar solvent (s_2). In one of these components the catalyst is dissolved and the other one acts as extraction agent for the

reaction products. A semi-polar solvent (s3) operates as mediator for the two other solvents. Dependent on the composition and the temperature a mixture of s1, s2, and s3 is either homogeneous or heterogeneous (Behr et al., 2005a, 2005b; Behr and Roll, 2005; Behr and Fagenswisch, 2003). This new concept is especially suitable for reactions which have to be operated in single phase because of low solubilities of the reactants in the phase containing the catalyst. As illustrated in Figure 1.2, in these TMS-systems the reaction takes place in a single phase at an elevated reaction temperature, while lower temperatures (room temperature for example) cause the liquid to split up in two separate phases again. The catalyst remains in one of two phases and can be reused by simple phase separation. This concept combines the advantages of a reaction in a single phase system with the advantages of the catalyst recycling of a two-phase system. The TMS-system was applied to a liquid phase peptide synthesis by using a cyclohexane-soluble platform in cyclohexane and typical organic solvents in a temperature range of 288 to 338 K (Chiba et al., 2002). Behr and Miao (2004) used TMS- system for the rhodium-catalyzed co-oligomerization of sunflower fatty acid methyl ester (SFAME) and ethylene with PC/SFAME/dioxane solvents system and in the absence of any tagged ligand. Similarly, the TMS- system was used in the hydroaminomethylation of 1-octene using PC/dodecane/morpholine solvent system (Behr and Roll, 2005). The isomerizing hydroformylation of trans-4-octene in the TMS-system of PC/dodecane/*p*-xylene has been carried out producing a very high conversion (about 99%) of the trans-4-octene and offering very attractive selectivities of *n*-nonanal ranging from 79 to 90% (Behr et al. 2005b), but a strong rhodium leaching as high as 47% was reported. On the other hand, Tijani and Ali (2006) has developed a thermomorphic biphasic rhodium system using an inexpensive and conventional ligand such as P(OPh)₃ to catalyze the hydroformylation of higher olefins (>C6). However, neither kinetic nor thermodynamic data on the hydroformylation of higher olefins in the TMS-system are available in the literature.

1.3 Problem Statement

The catalytic hydroformylation of higher olefin faces several challenges. In the homogeneous process, the rhodium catalyst tends to undergo decomposition at the temperatures required for product separation through distillation. On the other hand, in

the biphasic process, the low solubility of the olefin reactant in the aqueous phase renders the reaction rates too low for commercialization purposes. In addition, both processes are limited by syngas solubility in the reaction phase (Master, 1977). Consequently, higher olefin hydroformylation is typically carried out in homogeneous organic solvents with inexpensive Co-based catalysts, whose activities are three-orders of magnitude lower than the Rh-based catalysts. In practice, as shown in Table 1.2, more severe conditions particularly high operating pressure and temperature are required to activate the cobalt catalysts and intensify the reaction. This leads to the high capital and maintenance costs. Further, the recovery and regeneration of cobalt catalysts during higher olefin hydroformylation are rather expensive and tedious due to large quantities of acid and alkaline solutions are involved in the demetalization step to recover the catalyst (Cornils and Hermann, 2002; Garton et al, 2003). Therefore, the energy- and material-intensive nature of these processes poses both economical and environmental concerns.

For this reason a biphasic process for the hydroformylation of higher olefins with more selective rhodium catalysts, which allows for a catalyst recycling by phase separation, would be highly desirable with lower operating pressure up to 20 bars. In addition the use of Rh catalyst offers significant reduction of capital, operating and maintenance cost. Since the Rh catalyst is an expensive material, the recovery and recycling of the catalyst would be a better option to reduce the operating cost. However, no catalytic system has been found which yields sufficiently high conversion rates and yet brings about a complete catalyst separation by decantation. Hence it is our hope that the desired process will contain features such as high catalyst activity, facile catalyst recovery, enhanced mass transfer, relatively mild operating conditions, and, above all, economic viability.

1.4 Objectives of the Study

The objectives of this research work are given as follows:

- i. To develop a novel temperature dependent multi-component solvent (TMS) system for the hydroformylation of higher olefins using Rh-phosphite catalyst.
- ii. To study the effect of reaction conditions for the hydroformylation of 1-octene using Rh-phosphite catalyst in a TMS-system of propylene

carbonate/dodecane/1,4-dioxane by investigating the effect of total pressure, partial pressure of CO and H₂, temperature and concentration of 1-octene, phosphite ligand and catalyst on the total conversion of 1-octene and selectivity (*n/i*).

- iii. To determine the optimum process condition for the hydroformylation reaction of 1-octene using Rh-phosphite catalyst in a TMS-system of PC/dodecane/1,4-dioxane by evaluating the formation of total yield of aldehyde and selectivity to linear aldehyde (*n*).
- iv. To develop the mechanistic and empirical rate model for the hydroformylation of higher olefins using Rh-based catalyst in a homogeneous system and fitting of the available experimental data.
- v. To study the liquid-liquid equilibrium (LLE) behavior and distribution of 1-octene, nonanal, HRh(CO)(PPh₃)₃ catalyst and P(OPh)₃ in TMS-system of PC/dodecane/1,4-dioxane.

1.5 Scope of the Study

The scope of this research is divided into the following section:

1.5.1. Development of a novel TMS-system

The TMS-systems consist of a polar and a non-polar solvent. The third solvent which is semi-polar acts as a mediator between the polar and the non-polar solvent. Dependent on the composition and temperature, a mixture of the polar, non-polar and semi-polar solvent is either homogeneous or heterogeneous. In this work, PC was chosen as the polar solvent because of the low solubility of alkenes in PC. Furthermore, PC was found to increase the activity of the Rh-catalyst to conversions of 95% as well as the selectivity to the linear aldehyde up to 95 % (Behr et al., 2005b). In addition, we have chosen long-chain hydrocarbon, dodecane as the non-polar solvent as it poorly dissolves the catalyst but perfectly the reaction products. The TMS-system of PC/dodecane/*p*-xylene has proved to provide very high conversions (99%) of the *trans*-4-octene and a very attractive selectivities of *n*-nonanal ranging from 79 to 90% (Behr et al., 2005b). However, via ICP-investigations, a strong rhodium leaching of 47% was observed. The more *p*-xylene is

used, the more rhodium is transferred into the nonpolar dodecane phase. With this basis, 1,4-dioxane was chosen as the solvent mediator, because it has a greater polarity compared to *p*-xylene and we anticipated that it might reduce the effect of the catalyst leaching. In addition these solvents are preferred because of high boiling point, thermal stability, and inert nature with respect to the homogeneous catalyst, olefin, hydrogen, carbon monoxide and the hydroformylation products (Tijani and Ali, 2006; Behr et al., 2005; Behr and Miao, 2004). The phase behaviour of the TMS-system (PC/dodecane/1,4-dioxane) at different temperatures and composition was determined by the cloud point method at 298, 353 and 373 K. The big miscibility gap of this solvent system facilitates a good operating range for the hydroformylation.

Solubilities of H₂ and CO in pure solvent and solvent mixtures relevant to the hydroformylation process were also studied in this work, particularly in the TMS-systems involving propylene carbonate, dodecane and 1,4-dioxane. Isothermal gas solubility data (*P*-*x* data) for H₂ and CO in propylene carbonate (PC), biphasic PC+dodecane mixtures, 1:1 (v/v), and temperature dependent multi-component solvent (TMS)- system (PC/dodecane/1,4-dioxane) were determined over the temperature and pressure range of 298-343 K and 0.1-1.5 MPa, respectively. The measured solubilities were tested against activity coefficient models based on the regular solution theory (RST) with Yen and McKetta extension for polar solvents and with UNIFAC group contribution method.

1.5.2. Parametric Study of Reaction Variables

Synthesis of *n*-nonanal, a commercially important fine chemical, by the hydroformylation reaction of 1-octene using a homogeneous catalyst consisting of HRh(PPh₃)₃(CO) catalyst precursor and P(OPh)₃ in a TMS- system containing propylene carbonate (PC), dodecane and 1,4-dioxane was investigated. HRh(PPh₃)₃(CO) and P(OPh)₃ were chosen as the complex catalyst because polar phosphite ligands will favourably partition in the polar phase and therefore facilitating the catalyst recovery process. The easy availability of such phosphite ligands also provided a valuable and straightforward route to rhodium complexes. In addition, by using phosphite-modified catalyst, less reactive olefins such as 1-octene and 2,3-dihydrofuran, are hydroformylated at much higher rates compared to those achieved with phosphine-modified catalysts Beller et al., (1995). In determining the

optimum process condition, the effect of total pressure, partial pressure of CO and H₂, temperature, concentration of 1-octene, catalyst loading, catalyst to ligand ratio on the selectivity (*n/i*), total conversion and yield of total aldehyde were identified. The detailed kinetics of hydroformylation of two higher olefins (1-octene and 1-dodecene) using the above catalyst and reaction medium were also studied. The effect of concentration of the olefins, catalyst loading, partial pressure of CO and H₂ and temperature on the rates of both reactions have been studied at three temperature- 353, 363 and 373 K.

1.5.3. Development of Kinetic Models

The present work uses *ab initio* quantum chemical computations to determine the energetics and reaction pathways of hydroformylation of higher alkenes using a rhodium complex homogeneous catalyst. The *ab initio* calculations of fragments of the potential energy surfaces of the HRh(CO)(PPh₃)₃-catalyzed hydroformylation of 1-octene, 1-decene, 1-dodecene and styrene were performed by the restricted Hartree-Fock method, at the second-order Møller-Plesset (MP2) level of perturbation theory, and basis set of 6-31++G(d,p). Generalized rate models were developed on the basis of above reaction path analysis and experimental findings available in the literature. The kinetic and equilibrium parameters of the models were estimated by nonlinear least square regression of available literature data. This forms to basis of application of the rate models for the experimental hydroformylation rate data in a TMS- system.

1.5.4. Liquid-liquid equilibrium (LLE) Behavior and Distribution

Four different temperatures (298, 313, 333 and 353 K) at atmospheric pressure were selected to study the ternary equilibrium system of the TMS- system (PC+1,4-dioxane+dodecane) in order to observe the binodal (solubility) curves and tie-lines. Understanding how the TMS- system affects the distribution of catalyst, reactants and products in terms of phase equilibrium thermodynamics is of utmost importance. Therefore, the distribution of 1-octene, nonanal, and HRh(CO)(PPh₃)₃ catalyst in this system was measured at atmospheric pressure and two different temperatures (298 and 308 K) to model the extraction efficiency for a typical reaction, the hydroformylation of 1-octene.

CHAPTER 2

LITERATURE REVIEW

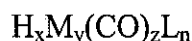
A review of the kinetic study of hydroformylation reaction is presented in this chapter. An overview of the mechanism of reaction and solubility of the gaseous reactant – CO and H₂ - illustrates the development of the mechanistic rate equation and factors that influence solvent selection. Following that, a review of liquid-liquid equilibrium and solute distribution studies highlights the considerations necessary for the hydroformylation reaction in the selected TMS- system. The material presented here is intended as a general reference for the subsequent chapters. More details specific to the chapter topics are addressed therein.

2.1. Hydroformylation Catalyst

Compounds of several transition metals catalyze hydroformylation to some extent, but the major interest lies in catalysis by cobalt or rhodium compounds. On the other hand, platinum and ruthenium catalysts are mainly subjects of academic interest, not thoroughly investigated by industrial researchers. The generally accepted order of hydroformylation activity for unmodified monometallic catalysis is as follow (Cornils and Herrmann, 2002):



A typical hydroformylation catalyst can be represented by the formula



where M and L are metal atom and ligand, respectively. When $n = 0$, the catalyst is called unmodified. Coordination of the metal center by ligands other than CO or hydrogen are designated modified. For a modified catalyst, n is an integer of from 1 to 3. Huge number of ligand applications appear in the area of hydroformylation, however the only classes of ligands used in industrial hydroformylation plants are substituted phosphines PR_3 ($\text{R} = \text{C}_6\text{H}_5, n\text{-C}_4\text{H}_9$), triphenylphosphine oxide (TPPO) and phosphites, $\text{P}(\text{OR})_3$ (Cornils and Herrmann, 2002). Nitrogen substituted ligands have attracted some interest in oxo

research. Shell has patented the rhodium catalyzed hydroformylation of 2-propen-1-ol and 3-buten-2-ol using phosphinoamines (Drent and Jager, 1995). However, in general nitrogen containing ligands such as amines, amides, or iso-nitriles showed low reaction rates due to their strong coordination to the metal center. Rhodium-triphenylphosphine oxide (TPPO) is used in the production of iso-nonanol by hydroformylation of octenes (Onada, 1993). This is the only example known of an oxidized phosphine ligand for an industrial application. Rhodium catalysts with phosphites are used in the hydroformylation of long-chain olefins due to their high catalytic activity (van Leeuwen et al., 1991).

In the mid-1960s, Wilkinson and co-workers discovered that phosphine modified rhodium catalysts gave better selectivities to the desired linear aldehyde product and activities for alkene hydroformylation under lower temperatures and pressures than the common cobalt catalysts (Osborn et al., 1965). They also produced fewer by-products such as isomerised alkenes, alcohols esters and acetals than are produced with a cobalt catalyst. Generally, the industrial process operates with a high concentration of triphenylphosphine, for instance, the Union Carbide process for hydroformylation of propene operates with a P/Rh ratio of 106 (Foster et al, 2002). This high loading of phosphine leads to increase selectivity to the linear aldehyde product as the increased amount of PPh₃ leads to more heavily substituted Rh complexes and increases the steric hindrance to the formation of branched products.

In the triphenylphosphine modified rhodium catalysed hydroformylation, low phosphine concentration results in a low linear to branched ratio (approximately 3:1), similar to that of unmodified cobalt reaction and so industrial processes which utilize this catalytic system operate under a very high concentration of phosphine (Cornils and Herrmann, 2002; Cotton and Wilkinson, 1988). However, with the perfluorinated triaryl phosphine ligand, high selectivity can be achieved (6.3: 1) at relatively low ligand concentrations (Rh: P(C₆H₄C₆F₁₃)₃ = 1: 10).

2.2. Mechanism of Hydroformylation

Mechanism of the hydroformylation reaction is still poorly established and has not been clarified in every detail (Matsubara, 1997). Several differences in hydroformylation

mechanism are observed between modified and unmodified catalyst systems. Therefore it will be useful to discuss them separately.

2.2.1. Unmodified Catalysts

The mechanism for cobalt catalyzed hydroformylation was developed by Heck and Breslow in the early 1960s (van Leeuwen and Roobek, 1983). The mechanism can also be applied to unmodified rhodium complexes as well. Catalytic cycle of hydroformylation with unmodified cobalt catalyst is shown in Figure 2.1. The hydroformylation cycle consists of six elementary steps:

Step 1: $\text{Co}_2(\text{CO})_8$ react with hydrogen to form two equivalents of the hydridometal carbonyl species $\text{HCo}(\text{CO})_4$.

Step 2: Dissociation of CO to generate the unsaturated species $\text{HCo}(\text{CO})_3$ and coordination of an alkene.

Step 3: Coordination of CO and hydride migration results in the formation of alkyl metal carbonyl species

Step 4: Insertion of CO to give the Co(I)-acyl complex

Step 5: Addition of hydrogen to the unsaturated Co(I)-acyl complex

Step 6: Hydride migration results in the formation of aldehyde and the catalytic cycle is completed with the regeneration of active species $\text{HCo}(\text{CO})_3$.

Kinetic studies support the $\text{HCo}(\text{CO})_4$ mechanism with a general rate expression given in Eq. (2.1).

$$\frac{d(\text{aldehyde})}{dt} = k[\text{alkene}][\text{catalyst}][\text{H}_2][\text{CO}]^{-1} \quad (2.1)$$

The rate determining step was H_2 addition to the Co(I)-acyl species, step 5. The inverse dependence on CO pressure is consistent with the mechanistic requirement for CO dissociation from the various saturated 18e species to open up a coordination site for alkene or H_2 binding (Natta et al., 1954). When using a 1:1 ratio of H_2/CO , the reaction rate is essentially independent of pressure due to the opposing orders of H_2 and CO.

Increasing the H_2/CO ratio is of limited use for increasing the overall reaction rate because $HCo(CO)_4$ is only stable under certain minimum CO partial pressures at a given temperature.

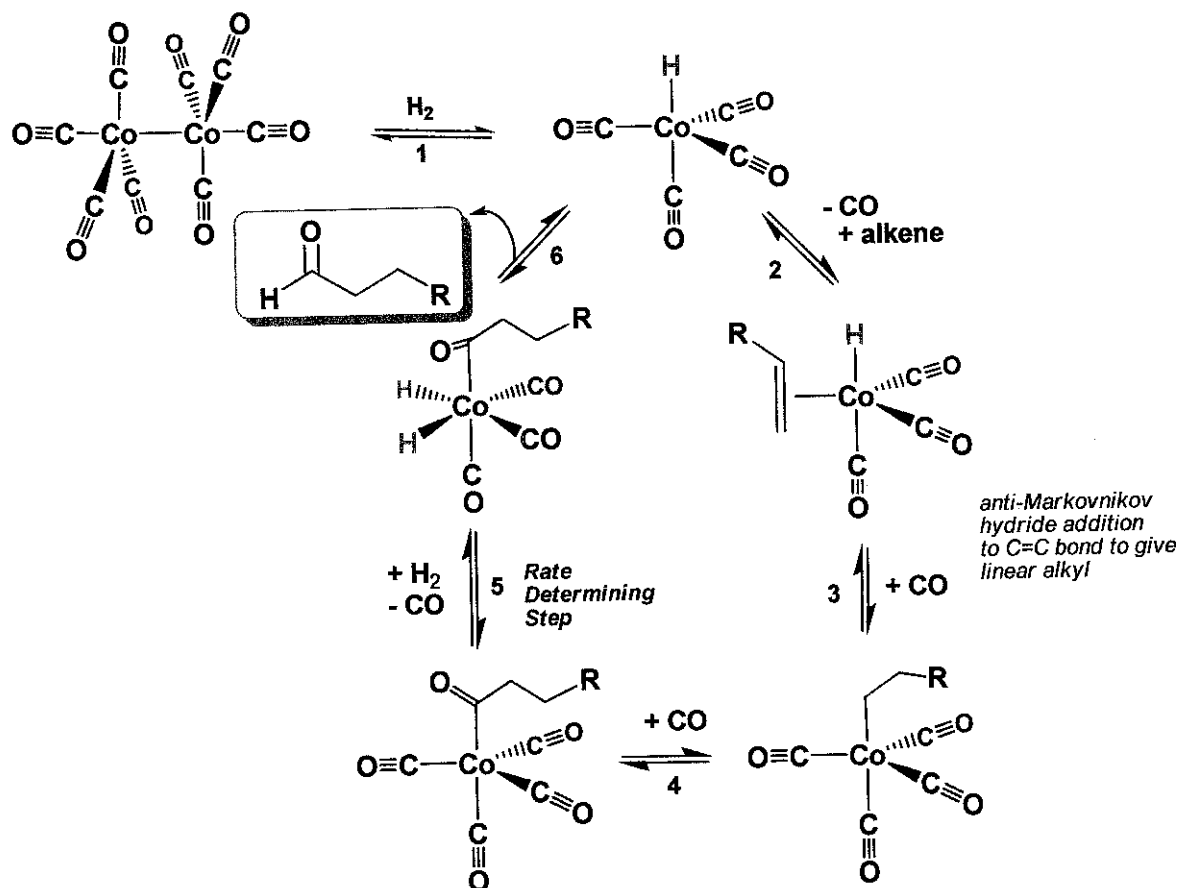


Figure 2.1: Catalytic cycle of hydroformylation for unmodified cobalt catalysts (van Leeuwen and Roobek, 1983).

2.2.2. Phosphine Modified Catalysts

Introduction of phosphine ligand into catalytic system brings some critical changes. $HRh(CO)(PPh_3)_3$ is believed to be the precursor of the active hydroformylation species. Model studies with this hydride complex provide explanation for different reaction behavior and indicated extensive dissociation of this complex. This means equilibrium exists between various substituted rhodium complexes before the catalytic cycle occurs as shown in Figure 2.2. Each catalytic species is assigned an individual reaction rate and

a characteristic product distribution. For example high phosphorus rhodium ratio and low partial pressure of carbon monoxide favor $\text{HRh}(\text{CO})(\text{L})_2$ complex which is assumed to give high linear aldehyde ratio (*n/iso*) as a result of steric effects. The mechanism for hydroformylation developed by Heck and Breslow (1961) for unmodified cobalt catalyst is valid with minor modification for phosphine modified rhodium catalysts. The catalytic cycle for phosphine modified rhodium catalysts was established by Wilkinson with two possible pathways - the associative and the dissociative mechanisms (Brown and Wilkinson, 1970). Both mechanisms start with five coordinated bisphosphine complex $\text{HRh}(\text{CO})_2(\text{PPh}_3)_2$, but differ as regards to the primary reaction step, coordination of olefin to the rhodium center as shown in Figure 2.3. In associative mechanism (route A), olefins attach directly to the bisphosphine species, and after hydride migration step, alkylrhodium complex is obtained which is an intermediate of dissociative mechanism as well.

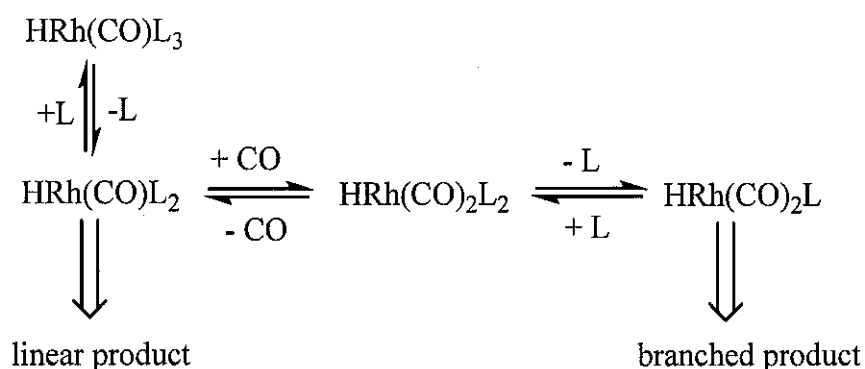


Figure 2.2: Initial equilibria forming the active species, $\text{L} = \text{PPh}_3$ or TPPTS.

In dissociative mechanism (route D) two different coordinatively unsaturated complexes $\text{HRh}(\text{CO})(\text{PPh}_3)_2$ and $\text{HRh}(\text{CO})_2(\text{PPh}_3)$ can be formed by dissociation of CO or phosphine. Addition of alkene to this unsaturated complex (step 1) is followed by hydride migration (step 2). After coordination of CO (step 3), insertion of CO (step 4) occurs to give a rhodium acyl complex. The unsaturated rhodium acyl complex undergoes hydrogenolysis (step 5) and completes the catalytic cycle with the regeneration of active species and the production of either the linear or the branched aldehyde.

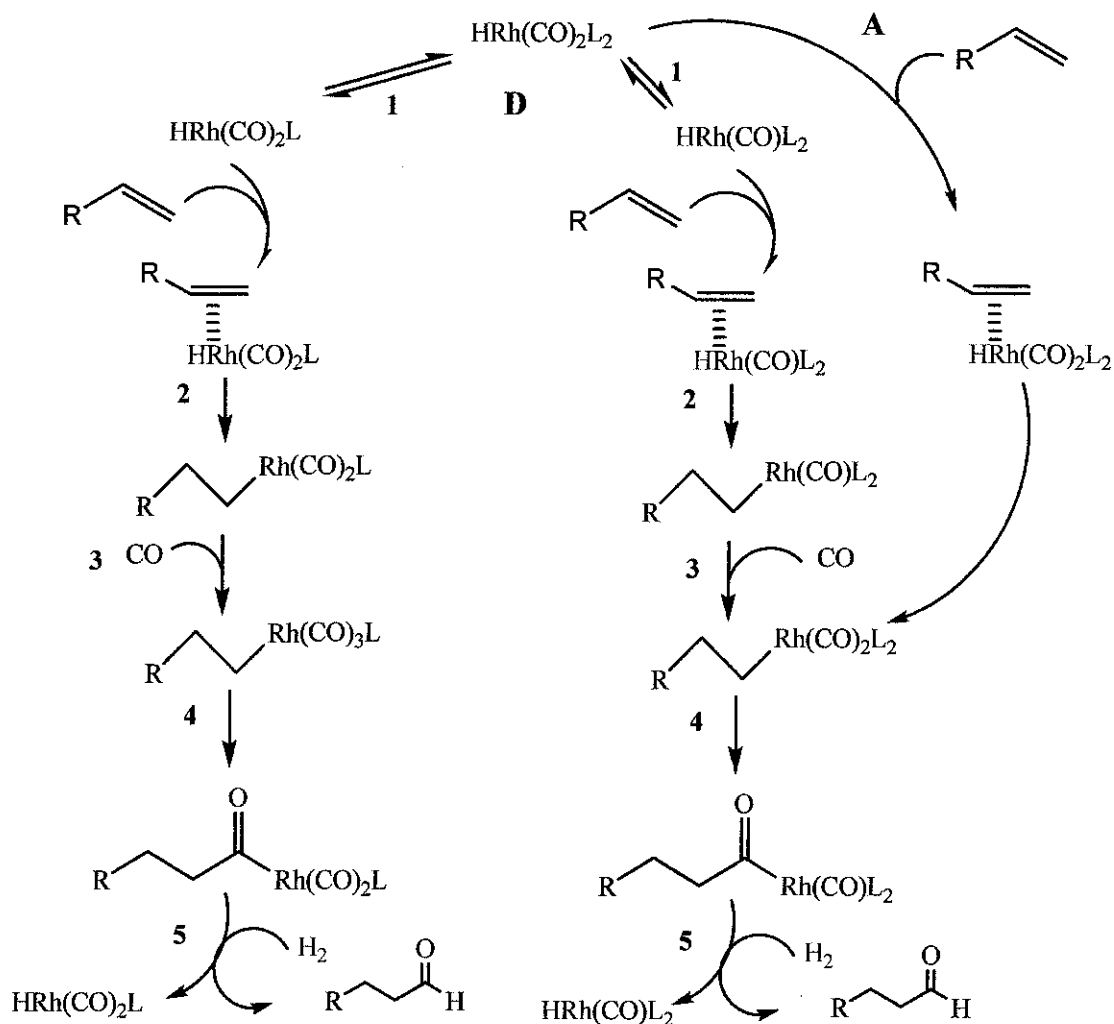


Figure 2.3: Catalytic cycle of hydroformylation for phosphine modified rhodium catalysts (Brown and Wilkinson, 1970).

Dissociative mechanism is generally accepted under industrial operating conditions (Evans et al., 1968). The active species in this mechanism are unsaturated rhodium complexes containing one or two coordinated phosphine ($\text{HRh}(\text{CO})_2(\text{PPh}_3)$ or $\text{HRh}(\text{CO})(\text{PPh}_3)_2$) formed by dissociation of phosphine or CO. It is widely believed that the *n/iso* ratio of the reaction is largely controlled by the competitive reaction of olefin with these unsaturated complexes. As a result of steric effect the species $\text{HRh}(\text{CO})_2(\text{PPh}_3)$ would be responsible for the formation of the branched aldehyde whereas $\text{HRh}(\text{CO})(\text{PPh}_3)_2$ would be responsible for the formation of linear aldehyde. However, remarkable differences were observed between the catalytic activity and the

selectivity of the water soluble catalyst $\text{HRh}(\text{CO})(\text{TPPTS})_3$ and organic soluble one (Horvath 1991). In the hydroformylation of propene, the latter shows much lower activity with an increased selectivity to linear products. This is explained by the high dissociation energy (30 kcal mol^{-1}) of TPPTS from $\text{HRh}(\text{CO})(\text{TPPTS})_3$ (Horvath 1991). This energy is about 10 kcal mol^{-1} higher than that necessary for dissociation of PPh_3 . The lower catalytic activity might be due to higher dissociation energy. On the other hand because of high dissociation of TPPTS, the equilibrium between active species shifts towards unsaturated complex with two phosphine ligand, thus leading higher linear to branched aldehyde ratio (*n/iso*).

2.3. Kinetic Study

The kinetics of the hydroformylation reactions is often represented by non-linear rate equations, some purely empirical and some are based on proposed mechanisms. A summary of kinetic studies in hydroformylation reaction is presented in Table 2.1. Kinetic modeling of hydroformylation of propylene and cyclohexene was studied by Natta et al. (1954) using Co-carbonyl catalyst. The reaction was found to be first order with olefin, catalyst and hydrogen but negative order dependent with CO. At constant P_{H_2} , the rate increases with increasing P_{CO} up to about 10 atm but decreases with higher P_{CO} . Gholap et al. (1992) reported rate equations to represent kinetics of formation of both *n*- and *iso*-butyraldehyde in Co-carbonyl catalyzed hydroformylation of propylene. Deshpande and Chaudari (1988) investigated detailed kinetics of hydroformylation of 1-hexene using $\text{HRh}(\text{CO})(\text{PPh}_3)_3$ catalyst. The important observations were a strong substrate inhibition with respect to CO and a mild substrate inhibition with respect to olefins and requirement of a critical catalyst concentration. A similar kinetic model was also developed by Bhanage et al. (1997) to describe the kinetics of the $\text{HRh}(\text{CO})(\text{PPh}_3)_3$ catalyzed hydroformylation of 1-dodecene. The reaction is first order with respect to concentration of catalyst and partial pressure of hydrogen. However the partial pressure of CO inhibits the reaction above a threshold value. The kinetic order for 1-dodecene is one in the lower concentration range while at higher concentration range, a zero order dependence was reported. In all these cases, the rate models proposed were empirical in spite of a reasonably well-understood mechanism for hydroformylation.

Table 2.1: A summary of kinetic studies involving hydroformylation reaction

Reference	Substrate	Catalyst	Rate Equation	Remarks
Natta et al. (1954)	propylene	HCo(CO) ₄	$r = \frac{k[\text{substrate}][\text{catalyst}][H_2]}{[CO]}$	<ul style="list-style-type: none"> Reaction condition: $T = 383\text{--}388\text{ K}$; $P_{CO} = 0.3\text{--}5.4\text{ MPa}$; $P_{H_2} = 2.7\text{--}11\text{ MPa}$; in toluene.
Deshpande and Chaudari (1988)	1-hexene	HRh(CO)(PPh ₃) ₃	$r = \frac{k[H_2][CO][\text{catalyst}][\text{substrate}]}{(1 + K_1[\text{substrate}])^{2.1}(1 + K_2[CO])^{2.5}}$	<ul style="list-style-type: none"> Reaction condition: $T = 303\text{--}323\text{ K}$; $P_{CO} = 0.074\text{--}1.693\text{ MPa}$; $P_{H_2} = 0.611\text{--}1.693\text{ MPa}$; in ethanol. The E_a was higher compared to the homogeneous system using toluene as solvent and as well as in biphasic system, $117.3\text{ kJ}\cdot\text{mol}^{-1}$. Existence of a critical concentration of catalyst
Gholap et al. (1992)	propylene	Co ₂ (CO) ₈	$r = \frac{k[H_2]^{0.55}[CO][\text{catalyst}]^{0.75}[\text{substrate}]^{0.87}}{(1 + K_1[CO])^2}$	<ul style="list-style-type: none"> Reaction condition: $T = 383\text{--}423\text{ K}$; $P = 3.5\text{--}10.0\text{ MPa}$; $P_{CO} = 1\text{--}7.5\text{ MPa}$; $P_{H_2} = 2.5\text{--}7.5\text{ MPa}$; in toluene. The <i>n/iso</i> ratio was found to increase with increases in catalyst concentration and in the P_{CO} and P_{H_2}, but decreased with increase in propylene concentration. The E_a: <i>n</i>-butyraldehyde = $54\text{ kJ}\cdot\text{mol}^{-1}$; isobutyraldehyde = $82\text{ kJ}\cdot\text{mol}^{-1}$.
Divekar et al. (1993)	1-decene	HRh(CO)(PPh ₃) ₃	$r = \frac{k[H_2]^{1.5}[CO][\text{catalyst}]^{1.2}[\text{substrate}]}{(1 + K_1[CO])^3(1 + K_2[\text{substrate}])}$ and Equation (2.2)	<ul style="list-style-type: none"> Temperature range: $323\text{--}343\text{ K}$ The E_a was found to be $49.3\text{ kJ}\cdot\text{mol}^{-1}$.

Table 2.1 (Continue)

Reference	Substrate	Catalyst	Rate Equation	Remarks
Purwanto and Delmas (1995)	1-octene	[RhCl(1,5-COD)] ₂ with TPPTS ligand	$r = \frac{k[H_2][CO][catalyst][substrate]}{(1 + K_1[CO])^2(1 + K_2[H_2])}$	<ul style="list-style-type: none"> • Used biphasic system; aqueous phase: 2.0×10^{-4} m³; organic phase: 0.5×10^{-4} m³ (octene/octane = 3/7). • Reaction condition: $T = 333-343$ K; $P = 1.5-2.5$ MPa; $C_L/C_{Rh} = 8$ in presence of ethanol as a cosolvent. • Selectivity to linear aldehyde = ~ 80%.
Deshpande et al. (1996)	1-octene	[RhCl(1,5-COD)] ₂ with TPPTS ligand	$r = \frac{k[H_2][CO][catalyst][substrate]}{1 + K_1[CO]^2 + K_2[H_2] + K_3[H_2][CO]}$	<ul style="list-style-type: none"> • Reaction condition: $P_{CO} = 0.5-1.5$ MPa; $P_{H_2} = 0.5-1.5$ MPa; [1-octene] = 0.0055 to 0.0278 kmolm⁻³; $T = 323-343$ K; $C_L/C_{Rh} = 8$, in the presence of ethanol as co-solvent • E_a was found to be 65.8 kJ·mol⁻¹
Bhanage et al. (1997)	1-dodecene	HRhCO(PPh ₃) ₃	$r = \frac{k[H_2][CO][catalyst][substrate]}{(1 + K_1[CO])^2(1 + K_2[substrate])}$	<ul style="list-style-type: none"> • Reaction condition: $P_{CO} = 0.17-2.04$ MPa; $P_{H_2} = 0.68-1.7$ MPa; [1-dodecene] = 0.18 to 2.2 kmolm⁻³; $T = 323-343$ K in toluene. • E_a was found to be 57.12 kJ·mol⁻¹.
Nair et al. (1999)	styrene	HRhCO(PPh ₃) ₃	Equation (2.2)	<ul style="list-style-type: none"> • Reaction condition: $P_{CO} = 0.3-4.12$ MPa; $P_{H_2} = 1.03-4.12$ MPa; [styrene] = 0.92 to 6.89 kmolm⁻³; $T = 333-353$ K in toluene. • Rate was independent of [styrene] because of the higher concentration of styrene used. • E_a was found to be 68.802 kJ·mol⁻¹
Palo and Erkey (1999)	1-octene (scCO ₂)	HRh(CO)[P(<i>p</i> -CF ₃ C ₆ H ₄) ₃] ₃	$r = \frac{k[H_2]^{0.48}[catalyst]^{0.84}[octene]^{0.5}}{1 + K_1[CO]^{2.2}}$	<ul style="list-style-type: none"> • Reaction condition: $T = 333$ K; $P = 27.3$ MPa

Table 2.1 (Continue)

Reference	Substrate	Catalyst	Rate Equation	Remarks
Kiss et al. (1999)	ethylene	Rh(acac)(CO) ₂ /PPh ₃	TOF= $\frac{k_1(P_{C_2H_4} / [PPh_3])}{1 + K_1(P_{CO} / [PPh_3]) + K_2([PPh_3] / P_{CO})}$	<ul style="list-style-type: none"> • Reaction conditions: $P_{CO} = 0.0081-0.56$ MPa; $P_{H_2} = 0.29-0.75$ MPa; $T = 353-383$ K, $p_{ethylene} = 0.072-0.38$ MPa, $C_L/C_{Rh} = 3-50$. • Ethane selectivity increases with increasing T, indicating that the E_a for olefin hydrogenation is higher than hydroformylation. • The aldehyde hydrogenation selectivity is very low. • The E_a was found to be in the range of $76.3-80.0$ kJ·mol⁻¹.
Zhang et al. (2002)	1-dodecene	RhCl(CO) (TPPTS) ₂ (with CTAB)	Equation (2.3)	<ul style="list-style-type: none"> • Reaction condition: $T = 353-373$ K, $P = 0.9-1.3$ MPa. • A semi-empirical rate equation was developed, combining mechanisms of homogeneous reaction with interfacial reaction of biphasic hydroformylation. • The E_a was found to be 72.8 kJ·mol⁻¹.
Yang et al. (2002a)	1-dodecene	RhCl(CO)(TPPTS) ₂ (with CTAB)	$r = A_0 N^{k_1} [CTAB]^{k_2} [substrate]^{k_3} \left(\frac{V_0}{V_w} \right)^{k_4}$	<ul style="list-style-type: none"> • Reaction condition: $T = 373$ K; $P = 1.1$ MPa • CTAB was used to enhance the reaction rate of long chain olefin and the ratio of n/iso. • The extent of emulsification had a positive effect on conversion and a negative effect on regioselectivity, and consequently on the separation of the aqueous catalyst phase from the organic phase.

Table 2.1 (Continue)

Yang et al. (2002b)	propylene	RhCl(CO)(TPPTS) ₂ (with CTAB)	Equation (2.4) and (2.5)	<ul style="list-style-type: none"> • Reaction conditions: $T = 363\text{--}383\text{ K}$, $p = 3.1\text{ MPa}$, $p_{\text{Propylene}} = 0.7\text{ MPa}$, $C_I/C_{\text{Rh}} = 60\text{--}30$. • The E_a was found to be in the range of 75 to $85\text{ kJ}\cdot\text{mol}^{-1}$. • Molar ratio of normal/isomeric aldehyde varied from 3.9 to 56.1. • Plausible reaction pathway was proposed.
Diwakar et al. (2005)	1-hexene	Rh-TPPTS (SAPC)	$r = \frac{kP_{H_2} P_{CO} [\text{substrate}]}{\left(1 + K_b P_{CO}^2\right)}$	<ul style="list-style-type: none"> • Reaction condition: $P_{\text{CO}} = 0.34\text{--}5.52\text{ MPa}$; $P_{\text{H}_2} = 0.69\text{--}3.45\text{ MPa}$; $[1\text{-hexene}] = 0.25$ to 1.0 kmolm^{-3}; $T = 353\text{--}373\text{ K}$. • The E_a was found to be higher compared to homogeneous system, $84.37\text{ kJ}\cdot\text{mol}^{-1}$.
Rosales et al. (2007a)	1-hexene	Rh(acac)(CO) ₂ (dppe)	$r = \frac{K_1 K_2 K_3 [\text{Rh}][\text{substrate}][\text{CO}]}{[\text{CO}] + K_1 K_2 [\text{substrate}]}$	<ul style="list-style-type: none"> • Reaction condition: 353 K, $0.1\text{--}0.7\text{ MPa H}_2$ and $0.1\text{--}0.7\text{ MPa CO}$ in toluene. • Linear to branched ratios were in the range $2\text{--}2.6$ and independent of the reaction conditions, except when the syngas and CO pressure were increased, where a slight reduction of the <i>n/iso</i> ratio was observed.
Rosales et al. (2007b)	1-hexene	[Rh(COD)(PPh ₃) ₂] ₂ PF ₆	$r = \frac{K_1 K_2 K_3 k_4 [\text{Rh}][\text{substrate}][\text{H}_2]}{[\text{CO}] + K_1 [\text{H}_2]}$	<ul style="list-style-type: none"> • Reaction condition: $P = 0.2\text{--}0.5\text{ MPa}$ and $T = 333\text{ K}$ for Rh and 373 K for Ir in toluene. • <i>n/iso</i> = 3.0 and 3.7 for Rh and ~ 2 for Ir. • Plausible reaction pathways were proposed. Although similar in the main features, the two systems display notable differences in the values of the constants of the equilibria involved.

Nair et al. (1999) and Divekar et al. (1993) derived a rate equation of Equation 2.2 considering the mechanism proposed by Evans et al. (1968) for HRh(CO)(PPh₃)₃ catalyzed hydroformylation of styrene and 1-decene, respectively. In deriving the mechanistic model, the elementary steps involve in the catalytic cycle were simplified. The rate models, derived assuming oxidative addition of hydrogen to Rh-acyl species as the rate determining step, were:

$$r = \frac{kK_1K_2[H_2][CO][catalyst][substrate]}{1 + K_2[CO] + K_1K_2[CO][substrate] + K_1K_2K_3[CO]^2[substrate] + K_1K_2K_3K_4[CO]^3[substrate]} \quad (2.2)$$

This model predicted the negative order dependence with CO, a unique feature of kinetics of olefin hydroformylation. However, the physical meanings of the rate coefficients in the denominator were not discussed. Kiss et al. (1999) also reported a mechanistic model for kinetics of ethylene hydroformylation using Rh(acac)(CO)₂/PPh₃ catalyst with unusual observations of first order with ethylene at higher PPh₃ concentration. The complex kinetics and change in reaction orders have been explained as a result of shift in rate-determining step under different conditions.

The kinetics of biphasic hydroformylation of 1-dodecene catalyzed by RhCl(CO)(TPPTS)₂ has been investigated in the presence of cationic surfactant, cetyltrimethyl ammonium bromide (CTAB) by Zhang et al, (2002). The molar ratio of linear to branched aldehydes in the reaction product is rather high (up to 20) and the reaction rate was also significantly enhanced by the surfactant. In contrast to the earlier reports using homogeneous catalysts, in this case, substrate inhibition with CO was not observed. This is due to the lower range of dissolved CO concentrations as a result of its lower solubility in aqueous catalyst phase. An orthogonal experimental design was performed for analyzing the effects of catalyst, 1-dodecene and surfactant, ligand concentration as well as the volume ratio of organic phase to aqueous phase and temperature on the reaction rate and regioselectivity. The optimal reaction conditions are suggested by the margin and variance analyses of experimental data according to the reaction rate with suitable compromise of the ratio of normal/isomeric aldehydes and hydroformylation selectivity to aldehyde. A semi-empirical rate equation was developed,

combining the mechanism of homogeneous hydroformylation with interfacial reaction of biphasic hydroformylation:

$$r = \frac{3.806 \times 10^{18} \exp(-8755/T) p_{H_2} p_{CO} [catalyst] [substrate] W_{CTAB}^2 (V_0/V_w)^{-1.44} / (1 + 0.03423([P]/[Rh]))}{(1 + 2657 \exp(-2558/T) p_{H_2}) (1 + 1.672 p_{CO}) (1 + 3307 [catalyst]) (1 + 1.646 [substrate]) (1 - 44.26 W_{CTAB})} \quad (2.3)$$

This model indicates that the exponents of reactants (H₂, CO, 1-dodecene) are fractional for the initial reaction rate. The surfactant has important influence on the mechanism, hence on the reaction rate. Furthermore, the liquid–liquid dispersion and interfacial area are also greatly influenced by the surfactant and impose effects on reaction rate. The effect of co-solvent on kinetics of biphasic hydroformylation of 1-octene has been reported by Deshpande et al. (1996) and by Purwanto and Delmas (1995) for a catalyst prepared from a precursor [Rh(COD)Cl]₂ and TPPTS ligand. Due to enhancement of solubility of CO in presence of the co-solvent, ethanol, a substrate inhibition with CO was observed as expected. However, ethanol reacts with nonanal to form acetals during the reaction. The formation of acetals were avoided by adding a buffer solution of sodium carbonate and bicarbonate (pH = 10). A mechanistic rate equation derived assuming the addition of olefin to the active catalyst as a rate-determining step was found to fit the data satisfactorily. A thermodynamic analysis concerning the solubilities of octane and gases in the reaction medium was studied by Purwanto and Delmas (1995) and a semiempirical kinetic model was used to describe the rate of reaction.

Yang et al. (2002a) investigated the effect of reaction engineering factors on biphasic hydroformylation of 1-dodecene. Novel agitator configurations have been reported to be effective in promoting interphase mass transfer rate in the gas-liquid-liquid hydroformylation system, thus increasing the initial rate and improving the *n/iso* ratio of products. High initial rate and regioselectivity were achieved with increase in olefin and CTAB concentrations, and that high agitation speed or organic/aqueous phase volume ratio increased the initial reaction rate but inhibited linear aldehyde formation. An empirical macro-kinetic equation for the initial rate and the correlation of normal/isomeric aldehyde ratio was proposed to represent the kinetics.

Yang et al. (2002b) studied the kinetics of $\text{RhCl}(\text{CO})(\text{TPPTS})_2/\text{TPPTS}$ catalyzed hydroformylation of propylene using an orthogonal experimental design method. The effects of several process variables on the initial rate of reaction were determined by margin and variance analysis. The rate was found to be in positive order with respect to hydrogen partial pressure and rhodium catalyst concentration, while higher CO, propylene partial pressure and TPPTS concentration showed substrate-inhibited kinetics. A power rate equation and a semi-empirical rate equation were presented:

$$r = 1.286 \times 10^8 \exp\left(\frac{-76.78}{RT}\right) P_{H_2}^{0.2515} P_{CO}^{-0.6403} P_p^{-0.9808} C_{Rh}^{0.9789} C_L^{-1.188} \quad (2.4)$$

$$r = \frac{A_0 \exp(-E/R_G T) P_{H_2} P_{CO} P_p C_{Rh}}{(1 + k_1 P_{H_2})(1 + k_2 P_{CO})^2 (1 + k_3 P_p)^2 (1 + k_5 C_L)^3} \quad (2.5)$$

Further verification was performed on the applicability of the empirical models. Eqs. (2.4) and (2.5) were used to predict the pressure drop in the autoclave during hydroformylation runs. Both models represent well at the initial period of hydroformylation only and were not directly applicable to the circumstances with decreased total pressure in the autoclave.

Palo and Erkey (1999) reported kinetics of hydroformylation of 1-octene in supercritical CO_2 with $\text{HRh}(\text{CO})[p\text{-CF}_3\text{C}_6\text{H}_4)_3]_3$ as a catalyst at 323 K and 27.3 MPa pressure. The reaction order was found to be 0.5 with both H_2 and 1-octene, 0.84 with catalyst and a negative order with CO. The catalyst solubility in supercritical CO_2 is reported to be higher than that in organic solvents and the critical catalyst concentration was not observed as in the conventional homogeneous catalyst. The main advantage of supercritical CO_2 is the higher solubility of H_2 , CO and catalyst, but for hydroformylation, the higher CO concentration is not desirable due to rate inhibition with CO and hence it is necessary to optimize the H_2/CO ratio for achieving higher rates in supercritical medium.

Diwakar et al. (2005) studied the kinetics of hydroformylation of 1-hexene using Rh/TPPTS complex exchanged on anion exchange resin to Amberlite IRA-93. The rate was found to be first order dependent on catalyst, 1-hexene concentrations and hydrogen

partial pressure. The inhibition in rate with enhanced CO pressure was observed. However, the inhibition is not as strong as that observed in other homogeneously catalyzed reaction, particularly in ethanolic solvent. A reasonable explanation for this behaviour was not provided. The hydroformylation of the isomerized hexenes was not favored over this catalyst, which was due to hindered access for 2-methylheptanal. The catalyst was also stable and could be recycled with no loss in activity or selectivity for five recycles.

A mechanistic model representing the kinetics of the homogeneous hydroformylation of 1-hexene using rhodium catalyst formed by addition of 1 equiv. bidentate ligand of 1,2-bis(diphenylphosphino)ethane (dppe) to Rh(acac)(CO)₂ under mild reaction conditions (353 K, 0.1–0.7 MPa H₂ and 0.1–0.7 MPa CO) in toluene was developed (Rosales et al., 2007a). The reaction rate was found to be first-order in dissolved hydrogen concentration at pressures below 3 atm, but independent of this parameter at higher pressures. In both regimes (low and high H₂ pressure), the initial rate was first-order with respect to the concentration of Rh and fractional order with respect to 1-hexene concentration. Increasing CO pressure had a positive effect on the rate up to a threshold value above which inhibition of the reaction was observed; the range of positive order on CO concentration is smaller when the total pressure is increased. The kinetic data and related coordination chemistry are consistent with a mechanism involving RhH(CO)(dppe) as the active species initiating the cycle, hydrogenolysis of the acyl intermediate as the rate-determining step of the catalytic cycle at low hydrogen pressure, and migratory insertion of the olefin into the metal-hydride bond as rate limiting at high hydrogen pressure. This catalytic cycle is similar to the one commonly accepted for HRh(CO)(PPh₃)₃. Rosales et al (2007b) performed kinetic and mechanistic studies using rhodium and iridium complexes of the type [M(COD)(PPh₃)₂]PF₆ (M = Rh, Ir) as catalyst precursors for the hydroformylation of 1-hexene under mild pressures (0.2–0.5 MPa) and temperatures (333 K for Rh and 373 K for Ir) in toluene solution. For both complexes, the reaction proceeds according to the rate law

$$r = \frac{K_1 K_2 K_3 k_4 [M][\text{substrate}][H_2][CO]}{[CO]^2 + K_1 [H_2][CO] + K_1 K_2 K_3 [\text{substrate}][H_2]} \quad (2.6)$$

The experimental data are consistent with the proposed general mechanism in which the transfer of the hydride to a coordinated olefin promoted by an entering CO molecule is the rate-determining step of the catalytic cycle. The kinetics of 1-hexene hydroformylation catalyzed by the iridium precursor are first order with respect to the catalyst and substrate concentrations and fractional order with respect to dissolved CO concentration, which tends to a highly negative order at high CO pressure. However, in contrast to the Rh pre-catalyst, the reaction rate varies in accord with a saturation curve with respect to hydrogen concentration, that is, a first order kinetics at low hydrogen concentration, which tends to zero order at high H₂ concentration ($P > 0.3$ MPa).

2.4. Influence of Process Parameters

The effects of the major process parameters – namely, the olefin concentration, catalyst concentration, ligand concentration, total pressure, gas composition and temperature on the rate and selectivity have been reported (Bhaduri and Mukesh, 2000; van Leeuwen and Claver, 2000). Effect of temperature is almost similar for all type of catalysts (unmodified and modified cobalt and rhodium). The rate of the oxo synthesis increases with temperature. The *n/iso* ratio decreases for almost all olefins toward higher temperatures. The decrease of the *n/iso* ratio is more pronounced with modified rhodium catalysts. This tendency is inversed for α -olefins bearing a functional group which is directing the regioselectivity toward linear products (van Leeuwen and Claver, 2000).

Raising the hydrogen partial pressure increases the reaction velocity and to some extent the *n/iso* ratio. However, hydrogen partial pressure has no significant effect on the *n/iso* ratio at high P_{H_2} (>60 bar). Increasing the carbon monoxide partial pressure has negative effect on the reaction rate at high P_{CO} whereas positive effect at low P_{CO} (Bianchi et al., 1977). These are true for both unmodified and modified catalysts. Following equilibrium may be proposed for ligand modified catalyst:



The equilibrium shifts to the right handside at low P_{CO} and formation of linear aldehyde is favored. The n/iso ratio decreases with increasing P_{CO} . At higher partial pressures the species $HM(CO)_4$ becomes dominant, thus favoring the linear product again (Piacenti et al., 1970). The increasing ligand/metal ratio increases the n/iso ratio in general whereas the catalytic activity varies in a nonlinear fashion as a function of phosphine concentration (Figure 2.4). Reactivity reaches a maximum at a point where the selectivity of the reaction remains constant.

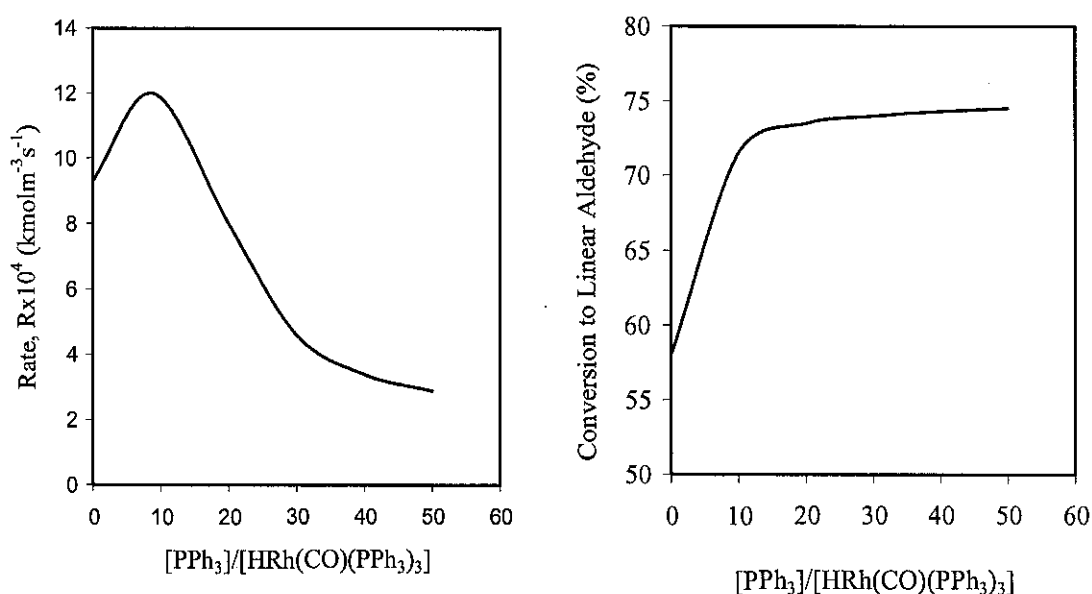


Figure 2.4: Effect of phosphine/rhodium ($PPh_3/HRh(CO)(PPh_3)_3$) ratio on reaction rate and selectivity (Cornils and Herrmann, 1996).

2.5. Solubility and Reaction Rate of Linear α -Olefin in Water.

Under the conditions of the Ruhrchemie/Rhone-Poulenc process, the space-time yield of the hydroformylation reaction decreases with increasing chain length of the substrate. Table 2.2 summarizes the results of the batchwise hydroformylation of different α -olefin at 30-80 bar syngas pressure (Bahrmann et al., 2004). Generally all substrate provide high selectivity toward linear products whereby the n/iso ratio ranging from 94:6 to 100:0. However, the rate decreases by two orders of magnitude with the increasing chain length of the substrate from C_5 to C_{12} .

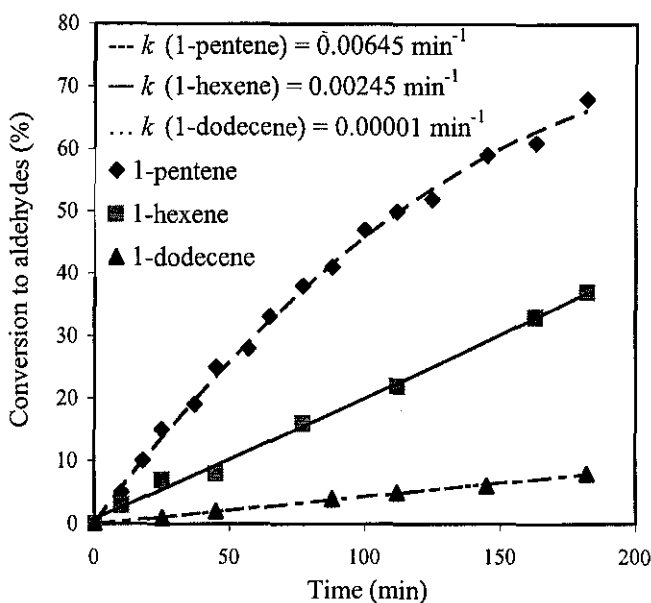


Figure 2.5: Dependence of reaction rate on chain length of alkenes (Brady et al. 1982)

2.6. Solubility Study and Thermodynamic Modeling

For a gas-liquid reaction, the solubility of the reactant gas in the liquid medium is an important parameter required for the interpretation of reaction kinetics and for reactor design. The simplest method of estimation of gas solubility is to use the Henry's law if the Henry's law constant is known or can be found out by fitting experimental solubility data. In the absence of sufficient and reliable data, thermodynamic models or techniques have proved to be useful for estimation of gas solubility. So far as the solubility of syngas (H_2/CO) in a hydroformylation solvent is concerned, all the above techniques have been used with varying degree of success. The regular solution theory (RST) has been used by several workers to interpret the solubilities of H_2 and CO in different hydroformylation solvents (Still et al., 2006; Jauregui-Haza et al., 2004; Breman and Beenackers, 1996; Purwanto et al., 1996; Radhakrishnan et al., 1983). The average error of prediction has been less than 10% in most cases. Fredenslund et al. (1977) proposed the UNIFAC group contribution method to predict the solubility of a gas in liquid. Antunes and Tassios (1983) used a modified Universal Functional Activity Coefficient (UNIFAC) model for prediction of Henry's constant for methane, nitrogen, and oxygen in alkane solvents and in water. Sander et al. (1983) presented the UNIFAC thermodynamic parameters and results for the promising method developed by Mathias

and O-Connel to predict the solubility of methane, ethane, ethylene, acetylene, hydrogen, oxygen, nitrogen, hydrogen sulphide, carbon monoxide and carbon dioxide in pure solvent and solvent mixtures. The method was found to be applicable at low pressures and temperature ranging from 210-475 K and to both polar and nonpolar solvents. Fahim and Elkilani (1991) predicted the solubility of hydrogen in naphtha reformat over a temperature range of 423 to 473 K by the UNIFAC method with an accuracy of $\pm 10\%$. However, one of the principal limitations of the UNIFAC method is that group interaction parameters needed for solubility estimation may not always be available.

Solubilities of H_2 and CO in pure solvent and solvent mixtures relevant to the hydroformylation process are studied in this work, particularly in the temperature-dependent multi-component solvent (TMS)-systems involving propylene carbonate, dodecane and 1,4-dioxane. These solvents are preferred because of high boiling point, thermal stability, and inert nature with respect to the homogeneous catalyst, olefin, hydrogen, carbon monoxide and the hydroformylation products (Tijani and Ali, 2006, Behr et al., 2005, Behr and Miao, 2004). However, neither experimental data nor any theoretical model on solubilities for CO and H_2 in the TMS-system are available in the literature.

2.7. Liquid-liquid Equilibrium (LLE) Study

The issue of solvent selection for extraction or for use as a reaction medium has received increase interest in the recent time (Palo and Erkey, 1999; Behr et al., 2005). Multicomponent solvent systems have been explored in order to achieve desired extraction properties while eliminating hazardous components making it relatively benign. Besides, a solvent system should be inexpensive, and easily recoverable, a good solvent should be relatively immiscible with feed components other than solute and have a different density from the feed to facilitate phase separation. Also, it must have a very high affinity for the solute, from which it should be easily separated by distillation or other simple separation processes. For instance, propylene carbonate (PC) is widely used as an extractant of aromatic hydrocarbons, in the petrochemical industries (Zaretskii, et al., 2008). Therefore, we anticipate that PC will enable an effective extraction of the $HRh(CO)(PPh_3)_3$ catalyst and $P(OPh)_3$ ligand due to the presence of the aromatic or

phenyl groups. Several models are available to correlate the LLE experimental data. Some are empirical such as those proposed by Margules and Van Laar (Novak et al., 1987); others, use the local composition concept, such as Wilson (1964) and NRTL (Renon and Prausnitz, 1968); still some others, such as UNIQUAC (Abrams and Prausnitz, 1975), have a more rational theoretical basis; and finally, a few such as ASOG (Kojima and Tochigi, 1979); and UNIFAC (Fredenslund 1989), use the group contribution method, in which the activity coefficients are calculated from the contributions of the various groups making up the molecules of the solution.

A few LLE studies on the PC, dodecane and 1,4-dioxane have been reported and the more relevant ones are presented herein. In order to simulate the extraction of aromatics from reformat, Annesini et al., (1985), studied the liquid-liquid equilibria for ternary systems paraffin-aromatic hydrocarbon-propylene carbonate at 20°C. The experimental data were correlated by means of the Non-Random Two Liquid (NRTL) and Universal Quasi-Chemical Activity Coefficients (UNIQUAC) models. Generally the NRTL equation gives root mean square values slightly lower than those of the UNIQUAC equation but the difference is not significant. Liquid-liquid equilibria for the ternary systems (octane+toluene+propylene carbonate), (2,2,4-trimethylpentane+ethylbenzene+propylene carbonate), (methylcyclohexane+benzene+propylene carbonate), and (1-decene+toluene+propylene carbonate) were measured by Fahim and Merchant (1998) over a temperature range of 293 K to 348 K. The results were used to estimate the interaction parameters between each of the three compounds present in each system for the NRTL and the UNIQUAC equations and between each of the main groups of hydrocarbons (CH₂, C=C, ACH, and ACCH₂) and propylene carbonate for the UNIFAC model as a function of temperature. Among the three methods NRTL and UNIQUAC gave the best fit with root-mean-square deviation (rmsd) of 1.3%. Recently, Chernyak (2008) studied the liquid-liquid equilibria of water/PC and water/butylene carbonate systems at atmospheric pressure and *T* of 280.65 to 293.15 K using analytical sampling techniques. The main method of composition analysis employed in this study was based on the samples' density measurements using vibrating tube densimeter. The experimental data were correlated with a NRTL model and the deviations between experimental and predicted values, were less than 0.15 %.

Liquid-liquid equilibria involving 1,4-dioxane was reported by Katayama (1999). The ternary systems methanol–cyclohexane and 1,3-dioxolane or 1,4-dioxane of cyclic ether compounds were measured in the range of 277.79–308.64 K. His results indicate that the expanses of the two-liquid phase were related to the magnitude of the solubility parameters of the ethers. The results were well correlated by the UNIQUAC equation through minimizing the objective function with weighting factors. As for dodecane, the LLE data for the ternary mixtures of (methanol + aniline + *n*-octane) and (methanol + aniline + *n*-dodecane) at $T = 298.15$ K and ambient pressure were reported to study the extraction efficiency of methanol or ethanol to recover aromatic hydrocarbons from refinery process streams (Mohsen-Nia et al., 2008). The UNIQUAC and NRTL activity coefficient models satisfactorily correlated the LLE experimental data of the studied systems. It was found that the efficiency of methanol for the extraction of aniline from (aniline + *n*-dodecane) mixtures is higher than that for the extraction of aniline from (aniline + *n*-octane) mixtures.

Robbins et al (2007) presented the liquid-liquid equilibrium data that relates to the hydroformylation reaction. The LLE of the aqueous biphasic solvent system and the distribution of 1-octene and nonanal in four ternary systems: the *n*-hexane + THF + water, *n*-hexane + acetonitrile + water, *n*-hexane + 1,4-dioxane + water, and ethyl ether + 1,4-dioxane + water were studied. The LLE and distribution were modeled using both the UNIQUAC and NRTL g^E models. The ternary LLE results were accurately predicted for each system with both equations while only the UNIQUAC model was successful in predicting the product distribution coefficients. Lee and Peters (2004) used UNIFAC method to predict equilibrium phase partitioning behavior of a cosolvent in a two-phase nonaqueous phase liquid (NAPL)–water system. The work demonstrated how the UNIFAC model could be used to predict cosolvent-enhanced NAPL solubilization as well as co-solvent partitioning into the NAPL phase that could lead to alterations in volume, density, and viscosity of the phase. Although a number of research papers have appeared on the LLE of a multi-component solvent system, the experimental LLE data and thermodynamic modeling related to the TMS- system are not available in the literature.

2.8. Summary

The most important applications of higher hydroformylation products are plasticizer alcohols in the C₈-C₁₁ range and synthetic detergent alcohols in the C₁₂-C₁₈ range, with a worldwide consumption of 1.5 million tons and 1.2 million tons in 1995, respectively (Cornils and Herrmann, 2004). Compared with cobalt, rhodium as catalyst metal is favorable with respect to the raw material economy and the energy balance in the hydroformylation of higher olefins. Since the use of a temperature-dependent multi-component solvent (TMS) process, in which a catalyst is designed as a residue in one of the liquid phases and the product in the other liquid phase, can be an enabling approach for a commercial application of the hydroformylation process with high selectivity, efficiency, and ease of product recovery (Behr et al., 2005), it was proposed to perform experimental studies to develop the process of hydroformylation in TMS- systems involving the use of commercially available Rh-based catalyst, phosphite ligands and solvents. The challenge is to identify the appropriate solvent mediator since a correlation between the amount of the solvent mediator and the amount of catalyst leaching has been reported (Behr et al., 2005). The complex multistep mechanism also represents a challenge in the development of the mechanistic model. As a proof of concept, studies on the solubilities of the gaseous reactants, kinetics and distribution of solutes in the TMS-system involving hydroformylation of higher olefins have been performed.

CHAPTER 3

DEVELOPMENT OF THE MECHANISTIC RATE MODEL USING AB INITIO CALCULATIONS

Molecular simulation is a very powerful toolbox in modern molecular modeling, and enables us to follow and understand structure and dynamics with minute detail – literally on scales where motion of individual atoms can be tracked. This chapter highlights the *ab initio* quantum chemical computations on the intermediates formed at different steps of a hydroformylation reaction pathway in a homogeneous solvent system using rhodium phosphite catalyst. The *ab initio* computational methodology is found to be a reliable tool for arriving at the reaction energetics and pathways for this class of reactions. These information together with experimental data proves to be effective in developing macroscopic practically useful rate models.

3.1. Kinetic Models

Kinetic model for a chemical reaction is an equation which links the reaction rate with concentrations or pressures of reactants and constant parameters (normally rate coefficients and partial reaction orders). They can be used in the design or modification of chemical reactors to optimize product yield, more efficiently separate products, and eliminate environmentally harmful by-products and process economics study. There are two main approaches to developing kinetic models which are empirical or data based modeling and mechanistic or building models based on the mechanism of the reaction. The following will discuss differences between the two approaches.

3.1.1. Developing Empirical Models

An empirical model can be described as a model where the fitting capacities are the only criterion used. The aim is to describe the observed data as well as possible, using a convenient mathematical relationship without any knowledge about chemical processes or underlying mechanism (Costa and Kristbergsson, 2009). Therefore, empirical modeling much depends on the availability of representative data for model building and

validation. Apart from cause-and-effect between variables, not much else is required in terms of process knowledge and a trial and error approach is adopted

3.1.2. Developing Mechanistic Models

The development of mechanistic models uses fundamental knowledge of the interactions between reaction variables to define the model structure. Mechanistic modeling therefore does not require much data for model development, and hence is not subject to the idiosyncrasies in data. However, it requires a fundamental understanding of the physics and chemistry governing the process and therefore can be very time consuming. Very often, a model can be a combination of some mechanistic and empirical components which is called semi-empirical. Most researchers agree that semi-empirical models are inherently superior to empirical models as they give a better understanding of the chemical reaction.

3.1.3. Empirical versus Mechanistic Models

When available, mechanistic models can provide more realistic predictions, and more can be done with it in terms of analyses. For example, the details contained within a mechanistic model offer the opportunity to test the sensitivities of the process to meaningful entities such as activation energies; substrate inhibition effect, catalyst poisoning, etc. With very few exceptions, the parameters of data based models are just numbers encapsulating combined effects. Therefore, it is very difficult to attach physical meaning to them, and hence such sensitivity studies cannot be performed. Another comparison that is always made between the two modelling approaches is that of cost. Due to the complexity of many processes, mechanistic modelling is indeed very expensive in terms of human effort and expertise. As the mechanistic modelling approach forces a detailed examination of fundamental process behaviour, some of the cost is recovered in terms of increased 'deep' knowledge of process behaviour. Such benefits are intangible though, and are often discounted. In practice, empirical modeling can be expensive as well. It requires large amounts of 'representative' data, and in many instances, these can only be acquired by perturbing the process via planned experiments. Inevitably production will be disrupted, and the lost revenue can exceed the cost of hiring

someone to develop a mechanistic model. The advantage with empirical modelling lies in the fact that empirical modelling will deliver some form of working model in a much shorter time.

3.2. Approaches to Kinetic Modeling

Kinetics of industrially important hydroformylation of higher olefins have been reported by several workers. The kinetics of homogeneous hydroformylation of higher olefins using Rh-based catalyst has been studied by Palo and Erkey (1999), Bhanage et al. (1997), Divekar et al. (1993) and Deshpande and Chaudari (1988). However, the rate equations proposed were essentially empirical. Palo and Erkey (1999) studied the kinetics of hydroformylation of 1-octene in supercritical carbon dioxide ($scCO_2$) with $HRh(CO)[P(p-CF_3C_6H_4)_3]_3$ at 50°C and 273 bar. The observed kinetic behaviour differs from the conventional systems using $HRh(CO)(PPh_3)_3$ in organic solvents. This may be due to several factors - $scCO_2$ solvent effects, the modified phosphine ligands, and the increased H_2 and CO concentrations relative to conventional systems. Chaudhari and co-workers developed kinetic rate expressions using several different substrates (1-hexene, 1-decene and 1-dodecene in organic solvent) and calculated the rate parameters and activation for each system (Bhanage et al. (1997), Divekar et al. (1993), Deshpande and Chaudari (1988)). A mechanistic model was also proposed for the hydroformylation of styrene by Nair et al. (1999) but was not used to develop a general kinetic equation for the hydroformylation of olefins. Details of the kinetic models are presented in Section 2.3. Summarizing the observations reported in literature, it can be stated that the kinetic rate of hydroformylation has been found to be influenced positively by increasing the concentration of catalyst and hydrogen, whereas increased carbon monoxide exerted a negative effect. The apparent activation energy required for aldehyde formation has been found to be in the range from 30 to 100 $kJmol^{-1}$.

In this work we make the first contribution to the study of the kinetics of hydroformylation of higher olefins, using a first principle method such as *ab initio*. The most widely used ligand in a homogeneous hydroformylation process is triphenylphosphine (PPh_3). In the rhodium- PPh_3 catalyzed hydroformylation, it has been established that hydridocarbonyl-tris(triphenylphosphine)rhodium (I) ($HRh(CO)(PPh_3)_3$)

is a direct catalyst precursor. In spite of the commercial importance of the rhodium-PPh₃ catalyst, only limited data have been published on the kinetics of the hydroformylation reaction under the industrial operating conditions ($T = 343\text{-}393\text{ K}$, CO partial pressure = 5-25 bar, H₂ partial pressure = 5-25 bar, Rh loading = 1 mM and olefin concentration = 0.1-2 M). The *ab initio* technique of quantum chemical computation was used to obtain the energetics and to identify the reaction pathways of Rh-catalyzed hydroformylation of higher olefins (1-octene, 1-decene, 1-dodecene and styrene) using low concentration of phosphine ligand. Since the available computational tools did not allow prediction of the kinetic parameters of the systems under study, the mechanistic model was developed based on the mechanism and pathways given by the *ab initio* calculation. Several simplifying assumptions were made to develop a generalized kinetic model based upon the well-documented mechanistic steps in homogeneous hydroformylation of olefins using Rh-based catalyst. It is assumed that

- i. the reaction has reached a steady-state,
- ii. all but one of the reaction steps are in equilibrium,
- iii. the starting intermediate species at the reaction interface is the complex $\text{HRh}(\text{CO})_2(\text{L})_2$, and
- iv. the total rhodium concentration remains constant and the catalyst is uniformly distributed over the cross section of the reactor,
- v. the concentration of dissolved CO and H₂ is constant in the reaction mixture - this assumption is justified because the syngas is continuously added to a well-mixed reaction mixture (Ollis and Turchi, 1990).

The kinetic constants were evaluated by fitting experimental hydroformylation data at different process conditions. The resulting activation energies matched remarkably well with that predicted by the quantum chemical method thereby validating its applicability to this class of homogeneous catalytic reactions.

3.3. Molecular modeling

Molecular modeling based on quantum mechanical computations is emerging as a useful and reliable strategy of predicting energetics and kinetics of chemical reactions (Saeys et al., 2005; Cavallotti et al., 2007). The strategy has three major ramifications – the *ab initio* electronic structure and molecular orbital (MO) calculations, semi-empirical methods and molecular mechanics. Of the three, *ab initio* molecular orbital methods are the most accurate and consistent because they provide the best mathematical approximation to the actual system (Le Bris and Defranceschi, 2000). The term *ab initio* implies that the computations are based on the laws of quantum mechanics, the masses and charges of the electrons and atomic nuclei, and the values of fundamental physical constants (Hehre et al., 1986). Virtually no conceptual approximations are involved. On the other hand, semi-empirical methods are based on the Hartree-Fock theory, using empirical corrections in order to improve performance (Streitwieser, 1961). The method is very important in computational chemistry for treating large molecules where the Hartree-Fock method without the approximations is too expensive. The use of empirical parameters appears to allow some inclusion of electron correlation effects into the methods. Within the framework of Hartree-Fock calculations, some pieces of information (such as two-electron integrals) are sometimes approximated or completely omitted. In order to correct for this loss, semi-empirical methods are parameterized, whereby results are fitted by a set of parameters, normally in such a way as to produce results that best agree with experimental data, but sometimes to agree with *ab initio* results. The term molecular mechanics refers to the use of Newtonian mechanics to model molecular systems. A group of molecules is treated as a collection of balls and springs rather than a quantum collection of electrons and nuclei. The potential energy functions and the parameters used in molecular mechanics are known as “force fields” (Roat-Malone, 2002). Molecular mechanics can be used to study small molecules as well as large biological systems or material assemblies with many thousands to millions of atoms.

Molecular orbital methods deal with solution of the Schrodinger’s equation

$$\hat{H}_{\text{mol}} \Psi_{\text{mol}}(t) = i\hbar \frac{\partial \Psi_{\text{mol}}(t)}{\partial t} \quad (3.1)$$

where \hat{H} is the Hamiltonian operator representing the sum of kinetic and potential energies, \hbar is Planck's constant, i is the imaginary unit, $\Psi_{\text{mol}}(t)$ is the wave function, which is the probability amplitude for different configurations of the system and t is time. For a chemical system a 'basis set' of functions is used that satisfy a series of rigorous mathematical approximations (Bell et al., 2007). Improvement in calculations is obtained by the use of triple-split-valence basis sets, of which the only important one is 6-311G. Here there are 6 Gaussians for the core basis functions and the valence functions are split into three sets, comprising three, one, and one Gaussians, respectively. In general electronic structure calculations are often improved by adding functions corresponding to orbitals with a higher angular momentum than those that are occupied. For example p functions may be added to hydrogen, d functions to C, N, O, and so forth, and f functions to transition metals. These are denoted by adding an asterisk to the basis set or specifying p , d functions, and so forth, for example,

6-31G* or 6-31G(d): Adds d functions to 2nd row elements (C, N, O, etc.).

6-31G** or 6-31G(d,p): Adds d functions to 2nd row elements (C, N, O, etc.) and p functions to H.

For anions and atoms with lone pairs it may be that there is some electron density far from the nuclei. This can be handled by the addition of diffuse functions, which are broad Gaussian functions (small α coefficient) that are not readily calculated for isolated atoms, but are chosen by well-established rules of thumb. These functions are represented in the basis set specification by a + or ++ sign. Experience shows that the addition of polarization and diffuse functions to H atoms is not usually necessary, for example,

6-31+G: Adds diffuse functions to 2nd row elements (C,N, O, etc.).

6-31++G: Adds diffuse functions to 2nd row elements and H.

Calculations involving the heavier atoms, for example, transition metals, can be very time-consuming owing to the large numbers of electrons involved and the fact that larger

basis sets are not available for heavier atoms. The problem can be reduced in size by restricting the full calculation to the valence electrons only and including the core electrons simply as an effective core potential (ECP). A number of these have been proposed, of which probably the most popular is the Los Alamos ECP (Bell et al., 2007). In combination with double-zeta functions for the valence electrons, the Los Alamos ECP is used in the “LanL2DZ” basis set, which is often employed in calculations on molecules involving transition metals.

Ab initio molecular orbital calculations are specified by ‘model chemistry’ (Hehre et al., 1986). The accuracy and computational time depend upon the choice of the method and the basis set, the general structure and electronic state of the molecular system under study (e.g., charge and spin states), and the treatment of electron spin. Reasonable accuracy in moderate computer time may be achieved for larger molecules ($n \sim 10-30$ atoms) only by using the basic theory with minimal basis sets (i.e., H-F or Hartree-Fock approximation), whereas calculations on chemical reactions between simple diatomic molecules can be performed with the state-of-the-art model chemistries. For very large systems ($n \sim 50$ atoms or more), an excessive computational time may be avoided with less sophisticated models, like semi-empirical methods and molecular mechanics (De Paz and Ciller, 1993). A brief review of the computational theories are given here.

3.3.1. Electron Correlation Methods

The major deficiency of the Hartree-Fock Self-Consistent Field (HF-SCF) method is that it treats each electron as moving under the influence of the average effect of all other electrons. A SCF approach to treating electron correlation was described in terms of an adjustable parameter, ξ , in place of the nuclear charge, Z , in the one-electron wavefunction:

$$\phi_{1s} = \left(\frac{1}{\sqrt{\pi}} \right) \xi^{2/3} \exp(-\xi r) \quad (3.2)$$

where ξ represents the effective nuclear charge interacting with one electron due to the presence of another and r , the distance from the nucleus to the electron (Shaik and

Hiberty, 2007). The Hamiltonian that describes this approximation (called the Fock operator) is given by:

$$F_i = -1/2\nabla^2 - \sum Z_j/r_{ji} + \sum (2J_i - K_i) \quad (3.3)$$

where F is the Fock operator, J (called Coulomb integral) reflects the average interaction potential of electron i due to all other electrons, K is a second integral (called the exchange integral) and Z , the nuclear charge. Finding the Hartree–Fock one-electron wavefunctions is now equivalent to solving the eigenfunction equation:

$$(h_i + B_i)\psi_i = \varepsilon_i\psi_i \quad (3.4)$$

Within this model, the interaction between solute and solvent is represented by an interaction potential, B_i , which is treated as a perturbation to the Hamiltonian h_i of the solute molecule in vacuum. The interaction potential and eigenvalues ε_i are called orbital energies. Since ψ_i is part of B , the solution is obtained iteratively whereby a set of ψ_i are initially guessed, from which B_i is computed. The Fock operator is then used to solve for a new ψ_i , which is used to compute a new B_i . This process is repeated until ψ_i becomes constant. However, this approach fails to account completely for Coulombic interactions between electrons causing them to repel each other. In other words motion of the electrons are said to be correlated, and electron correlation causes electrons to be further apart than as described by the HF-SCF approach. Electron correlation can be handled in quantum chemical calculations using Møller–Plesset perturbation theory or density functional theory.

3.3.1.1. Møller–Plesset Perturbation Theory

Perturbation theory is a well-established method in quantum mechanics for the solution of the Schrödinger equation, where the Hamiltonian can be represented by the addition of a small perturbation to one for which solutions are known. Simple examples of applications of perturbation theory are given in most introductory texts on quantum chemistry, where it is shown that improvements can be achieved by taking the

perturbation to successively higher orders. Electron correlation can be treated by a perturbation approach, since the problem that we are trying to solve is similar to the HF-SCF solution. Møller and Plesset used a perturbation theory method to determine the correlation energy correction, following an HF-SCF calculation (Bell et al., 2007). The perturbation can be truncated at second order (MP2), third order (MP3) or even higher orders (MP4 and MP5). This procedure is computationally intensive, especially for higher orders and even for small molecules can require several gigabytes of disk space for temporary storage of the integrals that are generated. Nevertheless, the effort is rewarded by results that give a much closer fit to experimental data than the HF-SCF method.

3.3.1.2. Density Functional Theory

Density functional theory (DFT) provides an alternative approach to electron correlation. The basis of this theory, developed by Hohenberg and Kohn in 1964, is the proof that the ground-state electronic energy is determined completely by the electron density, ρ . The aim of DFT methods is to design functionals connecting electron density with the energy. A functional equation is an equation where the unknown is a function itself. Thus although a wavefunction is a function, an energy depending on a wavefunction or electron density is a functional. A generalized DFT expression is (Bell et al., 2007)

$$E_{\text{DFT}}[\rho]=T_{\text{S}}[\rho]+E_{\text{ne}}[\rho]+J[\rho]+E_{\text{xc}}[\rho] \quad (3.5)$$

where T_{S} is the kinetic energy functional (S denotes that the kinetic energy is obtained from a Slater determinant), E_{ne} is the electron–nuclear attraction functional, J is the Coulomb part of the electron–electron repulsion functional, and E_{xc} represents the exchange correlation functional. The dependence of each of these terms on the electron density, ρ , is represented by ρ in brackets following each term. In practice, it is customary to use hybrid SCF-DFT methods in which the exchange energy is calculated by the HF method. A wide variety of hybrid methods are available, the one used most frequently is B3-LYP, which incorporates Becke’s three parameter exchange functional (B3) (Becke, 1993) with the Lee, Yang, and Parr correlation functional (LYP) (Lee et al., 1988).

Hybrid DFT-SCF methods, in general, are particularly attractive because they are only marginally more computationally intensive than HF-SCF, yet provide results that are comparable with those obtained using the much more demanding MP perturbation method.

3.3.2. Geometry Optimization

In any quantum chemical calculation the first step requires optimization of the molecular geometry. Model building may be done using molecular visualization software, such as the Gaussian graphical interface GaussView, or by the ChemBio3D. Even when experimental structures are available it is still necessary to optimize the geometry at the level of theory we are using before attempting calculations of molecular properties (Le Bris and Defranceschi, 2000). Geometry optimization involves the mathematical procedure called nonlinear optimization, for which several algorithms have been developed. The energy and wavefunctions are computed for the initial guess of the geometry which is then modified iteratively until (i) an energy minimum has been identified and (ii) forces within the molecule become zero. ChemBio3D uses the Eigenvector Following (EF) routine as the default geometry optimization routine for minimization calculations. The EF approach minimises a Rayleigh–Ritz ratio

$$\lambda(y) = \frac{y^t H y}{y^2} \quad (3.6)$$

with respect to the vector y , where superscript t denotes the transpose. Therefore, $\lambda(y)$ becomes the smallest eigenvalue of the Hessian H and y becomes the corresponding eigenvector. The numerical second derivative of the energy is used as an approximation to $\lambda(y)$, with $E(X_0)$ the energy at point X_0 in nuclear configuration space and $\xi \ll 1$:

$$\lambda(y) \approx \frac{E(X_0 + \xi y) + E(X_0 - \xi y) - 2E(X_0)}{(\xi y)^2} \quad (3.7)$$

Differentiating (Equation 3.7) gives

$$\frac{\partial \lambda}{\partial y} = \frac{\nabla E(X_0 + \xi y) - \nabla E(X_0 - \xi y)}{(\xi y)^2} - \frac{2\lambda y}{y^2}. \quad (3.8)$$

In the present EF approach, the eigenvector obtained by minimising the above Rayleigh–Ritz ratio was used as the direction of uphill search, and minimise in the tangent space using a gradient-based approach. The present calculations allowed a maximum of 10 iterations in the variational calculation of the smallest Hessian eigenvalue and the corresponding eigenvector. There is no need to converge the eigenvector accurately at the beginning of a search (convergence only becomes important close to the transition state). Therefore, since the previous eigenvector is used as the starting point after the first step, a small number of iterations are most efficient. No tangent space minimizations were performed until the smallest non-zero eigenvector became negative and converged in two iterations or less. The variational calculation was deemed to be converged when the root-mean-square gradient specified by Equation (3.5) fell below $0.15 \text{ eV } \text{Å}^{-3}$. The EF step size along the eigenvector obtained variationally was set to 0.16 Å until the corresponding eigenvalue became negative. Each stationary point optimization was deemed to be converged when the root-mean-square gradient fell below about $0.001 \text{ eV } \text{Å}^{-1}$.

This can often be difficult for non rigid molecules, where there may be several energy minima, and some effort may be required to find the global minimum. Since an optimized geometry should result in zero forces within the molecule, all principal force constants should be positive and therefore not result in any imaginary vibrational frequencies. If there are one or more imaginary frequencies, then the geometry optimization has ended in a transition state rather than an energy minimum (Schlegel and Yarkony, 1994). The eigenvectors of the imaginary frequencies will then help to point in the direction of the structure corresponding to an energy minimum. Finding transition states is, of course, a necessary part of using quantum chemical methods to model reactions.

3.4. The *ab Initio* Molecular Orbital Calculation

The quantum mechanical description of chemical bonds is given by a space and time dependent probability distribution: the molecular wavefunction, $\Psi_{mol}(t)$, defined by the Schrödinger equation (Eq. 3.1). For systems of more than two interacting particles, the Schrödinger equation cannot be solved exactly. Therefore, all *ab initio* calculations for molecules involve some level of approximation and indeed, some level of empirical

parameterisation. The standard MO treatment for most closed-shell molecules involves a spin-restricted Hartree-Fock self-consistent field (HF-SCF) calculation. HF-SCF calculations generally yield accurate molecular structures but are less successful at predicting molecular energies. The main source of error in HF calculations is neglect of electron correlation, which results in systematic overestimates of molecular energies. Different tools of varying complexities have been developed to enhance accuracy (Saeys et al., 2002; Zhang et al., 1999).

Ab initio MO studies require a basis set of mathematical functions to solve the wave equation. Standard *ab initio* software packages provide a choice of basis sets that vary both in size and in their description of the electrons in different orbitals. Quantitative accuracy improves with the size of basis sets, since larger basis sets contain more adjustable parameters and thus offer better approximations of the true molecular wave functions. In general, *ab initio* MO studies on complex systems should begin with calculations using small basis sets, to obtain a qualitative assessment of molecular properties. For general use, the smallest standard basis set is recommended in the Gaussian 98 is 6-31G(d) package. A number of quantities such as molecular orbital energies, total energy from electronic and nuclear repulsion, heat of formation, dipole moment are obtainable from molecular orbital calculations.

In exploring a potential energy surface for a reaction, normally the first step is to optimize the geometry of the relevant stationary points, i.e. the reactants, transition structure and products. To confirm a reaction mechanism, it may be necessary to prove that the particular transition structure found in the optimization connects the desired reactants and products. This can be done by following the path of steepest descent downhill from the transition structure toward the reactants and toward the products. Following the reaction path can also show whether the mechanism involves any intermediates between reactants and products. Although the path of steepest descent depends on the coordinate system, a change in the coordinate system does not change the nature of the stationary points and does not alter the fact that the energy decreases monotonically along the reaction path from the transition structure toward reactants or products. Thus any coordinate system can be used to explore the mechanism of a reaction. One system, the mass-weighted Cartesian coordinates, has special significance

for reaction dynamics, and the path of steepest descent in this coordinate system is called the intrinsic reaction coordinate (IRC) (Schlegel, 1994).

It will be pertinent at this point to refer to the reported applications of the methodology to the study of energetics and kinetics of non-catalytic and catalytic reactions, both homogeneous and heterogeneous. Saeys et al. (2005) developed a Langmuir-Hinshelwood-Hougen-Watson (LHHW) kinetic model for the hydrogenation of toluene based on the first-principles density functional theory calculations for the hydrogenation of benzene over Pt catalyst. The LHHW model is able to capture the main trends in the reaction pathways and rates. Rocha et al. (2001) has performed a theoretical study on the homogeneous catalysis of isomerization of β -pinene, a hydroformylation precursor. The isomerization was investigated at three different levels of theory, HF, MP2 and MP4(SDQ), using 4 different size of basis set, 6-31G, 6-31G(d), 6-31+G(d) and 6-311++G(d,p) provided in the computational package. It was reported that the use of different basis set and the inclusion of the electron correlation effects had little influence on the relative stability of the β -pinene isomers but the effect on the energy barrier for the process was significant. Another theoretical study on the mechanism of the isomerization of 1-butene catalyzed by Rh-complex has been reported by Luo et al. (2005). The quantum mechanical calculations were carried out in the density functional theory framework to evaluate the potential energy profile and the reaction mechanisms involved. Rocha (2004) studied the reaction mechanisms involved in the last step of the catalytic cycle of the hydroformylation of alkene promoted by Pt-Sn catalyst, which is the hydrogenolysis process. Very recently, Cavallotti et al. (2007) reported *ab initio* computational studies on cyclohexane oxidation leading to kinetic parameters of primary reactions. These results together with available experimental data were used to formulate and test a detailed kinetic model.

The quantum approach still assumes a reaction scheme and then *ab initio* calculates the potential energy of intermediates and transition states. In this way the outline of a kinetic model with a sound theoretical basis is built that can be used to predict the macroscopic parameters of the process and to compare directly with experiment (a kind of benchmarking). In some cases it may be possible to predict the outcome of new chemical processes.

3.5. The Reaction Pathways

The tentative reaction pathways for *ab initio* computation is shown in Figure 3.1 (computations are confined to the reactions within the box). Qualitative reasoning and some available experimental observations form the basis of the scheme. According to van Leeuwen and Claver (2000), hydroformylation reactions are quite sensitive to experimental conditions such as the concentrations of catalyst, carbon monoxide, hydrogen, olefin and added ligand. At low Rh concentration, using $\text{HRh}(\text{PPh}_3)_3\text{CO}$ as the catalyst precursor without addition of additional PPh_3 ligands, substantial dissociation can occur with the formation of mono-phosphine or phosphine-free catalysts. Therefore, it is anticipated that at a high CO pressure of 20-40 bar and low PPh_3 concentration, the PPh_3 ligand of the catalyst precursor of $\text{HRh}(\text{PPh}_3)_3\text{CO}$ (species **A**) can exchange with carbon monoxide to form **B** and **C** (Figure 3.1). The ^{31}P NMR magnetization transfer experiments described by Brown and Kent (1987) also indicated that PPh_3 dissociation from the RhL_2 [L = ligand] complex **B** could occur at a significantly slower rate than the corresponding PPh_3 dissociation from tris-triphenylphosphine complex, **A**. In addition, spectroscopic experiments have revealed that under hydroformylation conditions, rhodium tri(*o*-*t*-butylphenyl)phosphite complex is coordinated by only one phosphite, $\text{HRh}[\text{P}(\text{OAr})_3](\text{CO})_3$ (Jongsma et al., 1991). van der Veen et al. (2000) claimed that the rate of hydroformylation is two orders of magnitude slower than the rate of carbon monoxide exchange of isomers of type **B**. The relative concentrations of these intermediates are controlled by the PPh_3 and CO concentrations. Thus, we may conclude that the initiation of the catalytic cycle by dissociation of CO and PPh_3 should not be rate determining since it has been found to be fast on the time-scale of hydroformylation.

Wilkinson suggested that species **C**, formed at a low concentration of PPh_3 , leads to a lower selectivity for linear aldehyde (linear:branched = 4:1) compared to hydroformylation reaction with additional amount of PPh_3 (van Leeuwen, 2004). The overall steric hindrance at the rhodium metal of species **B** is low because two relatively small carbonyl ligands are coordinated next to two bulky triphenylphosphine, PPh_3 .

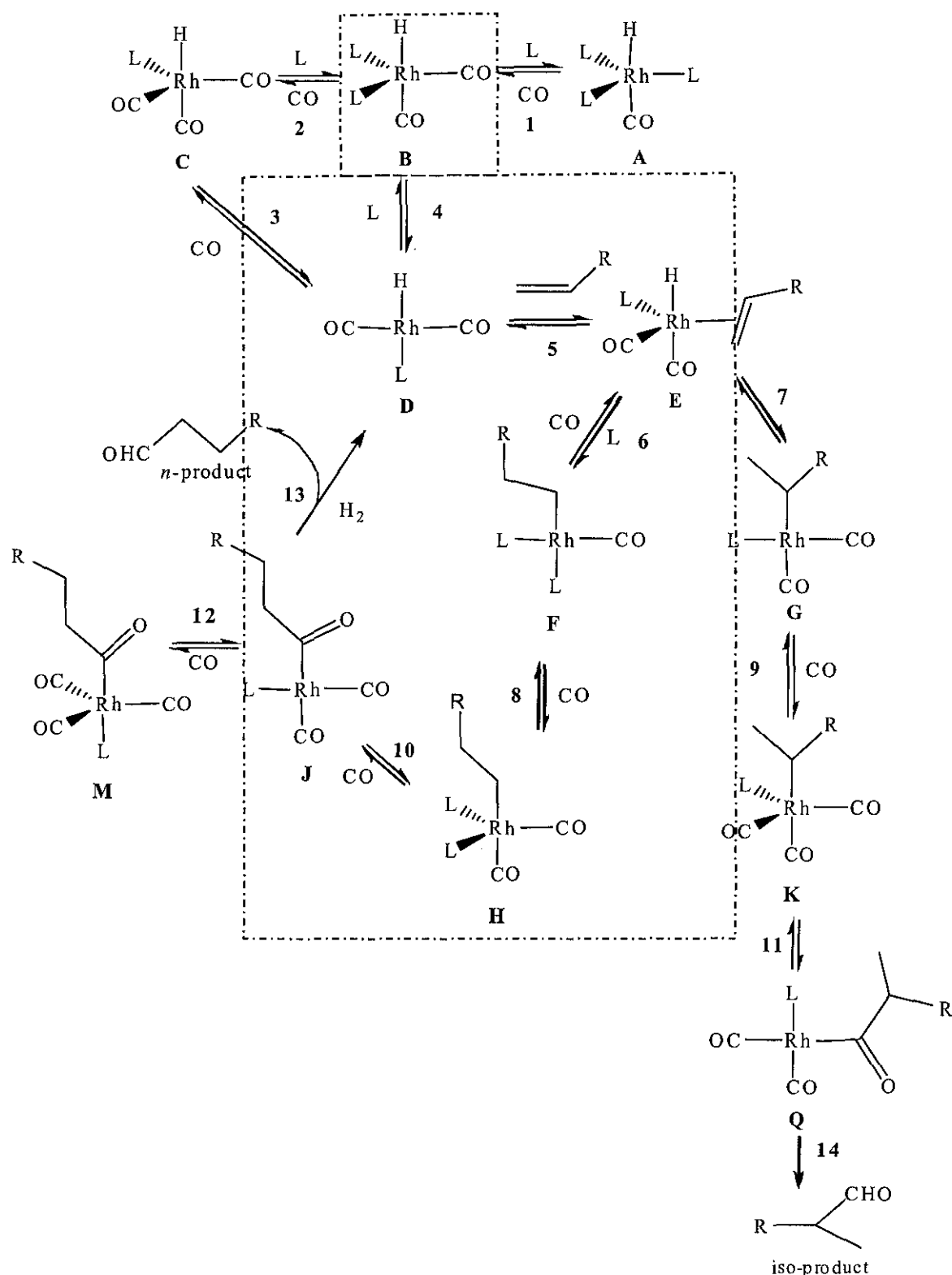


Figure 3.1: Plausible steps for rhodium catalyzed hydroformylation in the presence of low concentration of phosphine ligand.

Table 3.1: Description of the catalytic cycle in Figure 3.1.

Step	Description
1	For PPh ₃ as the ligand (L), the starting complex is HRh(CO)(PPh ₃) ₃ (complex A), which in the presence of carbon monoxide forms diphosphine intermediate, containing the phosphine ligands in equatorial positions (ee) or one in an apical position and the other ligand in an equatorial position (ae). Brown and Kent (1987) found a preference for the “ee” isomer (i.e., complex B). The other possible isomer (ae) of the complex is not shown.
2	At low Rh concentration, using HRh(CO)(PPh ₃) ₃ as the precursor without addition of PPh ₃ ligand, substantial dissociation will occur to form monophosphine catalyst, complex C (Evans et al., 1968). In addition, according to Jongsma et al. (1991), complex B may undergo exchange of ligand to form single coordinated PPh ₃ ligand, C , at high CO pressure.
3 and 4	Reversible addition/elimination of either L or CO from B or C leads to the square-planar intermediate D .
5	Complex D associate with olefin to give complex E which eventually gives rise to the product aldehyde (<i>n</i> - or <i>iso</i> -) through a number of steps that follow.
6 and 7	Complex E undergo a migratory insertion step to give square planar alkyl complexes F or G . Complex E can undergo β-hydride elimination, thus leading to isomerization especially when higher alkenes are used (step 7). Wilkinson suggested that formation of species F , lead to higher linear aldehyde selectivity (<i>n:iso</i> = 20: 1), and that species G , containing only one phosphine, lead to a lower selectivity for linear aldehyde (<i>n:iso</i> = 4: 1) (Evans et al., 1968).
8 and 9	Complex F (and also G) react further with CO to form trigonal bipyramidal complexes H (and also K).
10 and 11	Complex H (and also K) undergo the second migratory insertion of the alkyl ligand to form acyl complexes J (and also Q).
12	Complex J can react further with CO to give the saturated acyl intermediate M , which have been observed spectroscopically (Jongsma et al., 1991).
13 and 14	Complexes J (and Q) reacts with H ₂ to give the aldehyde product and gives back the unsaturated intermediate D . The reaction with H ₂ involves presumably oxidative addition and reductive elimination.

The rhodium center containing two weak phosphine donors and strongly electron withdrawing carbonyl ligands is predictably electron deficient. As a result, the carbonyl ligands are strongly bound and the fast dissociation of phosphine (structure **C**) and subsequent olefin addition results in high reaction rates. Hydride migration in a latter step results in the formation of the linear or branched rhodium alkyl complex, **F** and **G** (Figure 3.1). The isomerization reaction is often ignored in developing the rate equation. Under the reaction condition, the rhodium alkyl complexes **F** and **G** can undergo either migratory insertion forming the rhodium acyl complex or β -hydride elimination. As for the primary rhodium alkyl **F**, the β -hydride elimination will lead to the initial substrate. However the secondary rhodium alkyl complex, **G** can form the 1-alkene and a by-product, internal 2-alkenes, by β -hydride elimination. Since β -hydride elimination is faster for the secondary rhodium alkyl than for the primary rhodium alkyl complex, high isomerization rates will reduce the formation of the branched rhodium acyl to a larger extent than the linear rhodium acyl. Another possible side reaction is the formation of the inactive tricarbonyl rhodium species **M**, from the addition of CO to the unsaturated rhodium acyl complex, **J** (Nair et al., 1999; Musaev et al., 1995). Further details of the reaction pathways are given in Table 3.1. It is also to be noticed that species **N** and **P**, which are not included in Figure 3.3 are dihydride acyl species and aldehyde-coordinate intermediate, respectively. Since, the transition state which involve aldehyde reductive elimination step was not selected for detailed study in our work, species **N** and **P** are not included in the catalytic cycle in Figure 3.1. However, the X-Y-Z structures of the species are provided in Appendices A, B and C.

3.6. Computational Methodology

A tentative mechanism of the reaction pathways is a pre-requisite of the *ab initio* computation (Matsubara, 1997). The quantum-chemical calculations at the Restricted Hartree-Fock (RHF) level may then be performed with the GAMESS (General Atomic Molecular and Electronic Structure System) Pro 11.0 program package and ChemBio3D 11.0 as a frontend graphical user interface (GUI). ChemBio3D 11.0 allows building molecular species from atoms, and provides a means to generate or convert input files for the GAMESS program package. All geometries of transition states as well as

The rhodium center containing two weak phosphine donors and strongly electron withdrawing carbonyl ligands is predictably electron deficient. As a result, the carbonyl ligands are strongly bound and the fast dissociation of phosphine (structure **C**) and subsequent olefin addition results in high reaction rates. Hydride migration in a latter step results in the formation of the linear or branched rhodium alkyl complex, **F** and **G** (Figure 3.1). The isomerization reaction is often ignored in developing the rate equation. Under the reaction condition, the rhodium alkyl complexes **F** and **G** can undergo either migratory insertion forming the rhodium acyl complex or β -hydride elimination. As for the primary rhodium alkyl **F**, the β -hydride elimination will lead to the initial substrate. However the secondary rhodium alkyl complex, **G** can form the 1-alkene and a by-product, internal 2-alkenes, by β -hydride elimination. Since β -hydride elimination is faster for the secondary rhodium alkyl than for the primary rhodium alkyl complex, high isomerization rates will reduce the formation of the branched rhodium acyl to a larger extent than the linear rhodium acyl. Another possible side reaction is the formation of the inactive tricarbonyl rhodium species **M**, from the addition of CO to the unsaturated rhodium acyl complex, **J** (Nair et al., 1999; Musaev et al., 1995). Further details of the reaction pathways are given in Table 3.1. It is also to be noticed that species **N** and **P**, which are not included in Figure 3.3 are dihydride acyl species and aldehyde-coordinate intermediate, respectively. Since, the transition state which involve aldehyde reductive elimination step was not selected for detailed study in our work, species **N** and **P** are not included in the catalytic cycle in Figure 3.1. However, the X-Y-Z structures of the species are provided in Appendices A, B and C.

3.6. Computational Methodology

A tentative mechanism of the reaction pathways is a pre-requisite of the *ab initio* computation (Matsubara, 1997). The quantum-chemical calculations at the Restricted Hartree-Fock (RHF) level may then be performed with the GAMESS (General Atomic Molecular and Electronic Structure System) Pro 11.0 program package and ChemBio3D 11.0 as a frontend graphical user interface (GUI). ChemBio3D 11.0 allows building molecular species from atoms, and provides a means to generate or convert input files for the GAMESS program package. All geometries of transition states as well as

intermediates were optimized at the restricted Hartree-Fock (RHF)/6-31G(d,p) level. For the energetics, the electron correlation calculations were performed with the frozen-core second-order Møller-Plesset (MP2) perturbation method, using basis sets 6-31++G(d,p) (Luo et al., 2005). We used two basis sets, basis set I for the RHF geometrical optimization and basis set II for the MP2 energy calculation and higher level calculations. The vibrational analysis and internal reaction calculations (IRC) were also performed to verify the transition states. The path of a chemical reaction can be traced from the transition state to the product(s) and/or to the reactant(s) using the IRC technique. The IRC describes the path of steepest descent from the transition state down to the local energy minimum. The path is computed in small steps simultaneously optimizing all atomic coordinates orthogonal to it thus constituting a sequence of constrained optimization subproblems. Vibrational frequencies were also calculated at the RHF/6-31G(d,p) level. Calculation of the harmonic vibrational frequencies for the transition state (TS) species revealed that each contained the single imaginary frequency required to classify it as a true TS. In all cases, electronic correlation was taken into account at the second order Moller-Plesset level in the frozen core approximation. A scaling factor of 0.937 was used (Merrick et al., 2007). In addition, zero point energy (ZPE), which a quantum system possesses at 0 K in contrast to a classical system, was also calculated. The contribution of the ZPE that arises out of the residual vibration, to the reaction enthalpy and Gibbs free energy may sometimes be significant. Since *ab initio* ZPE calculations yield slightly higher values than actual, a scaling factor of 0.89 was used (Pople et al., 1981). The contribution of ZPE to the PE was around 5% for most of the species involved in this study. Possible formation of isomers was taken into account in potential energy calculations. The equilibrium geometries of each species were first determined by optimizing the structures by *ab initio* RHF method using a 6-31G(d,p) basis set.

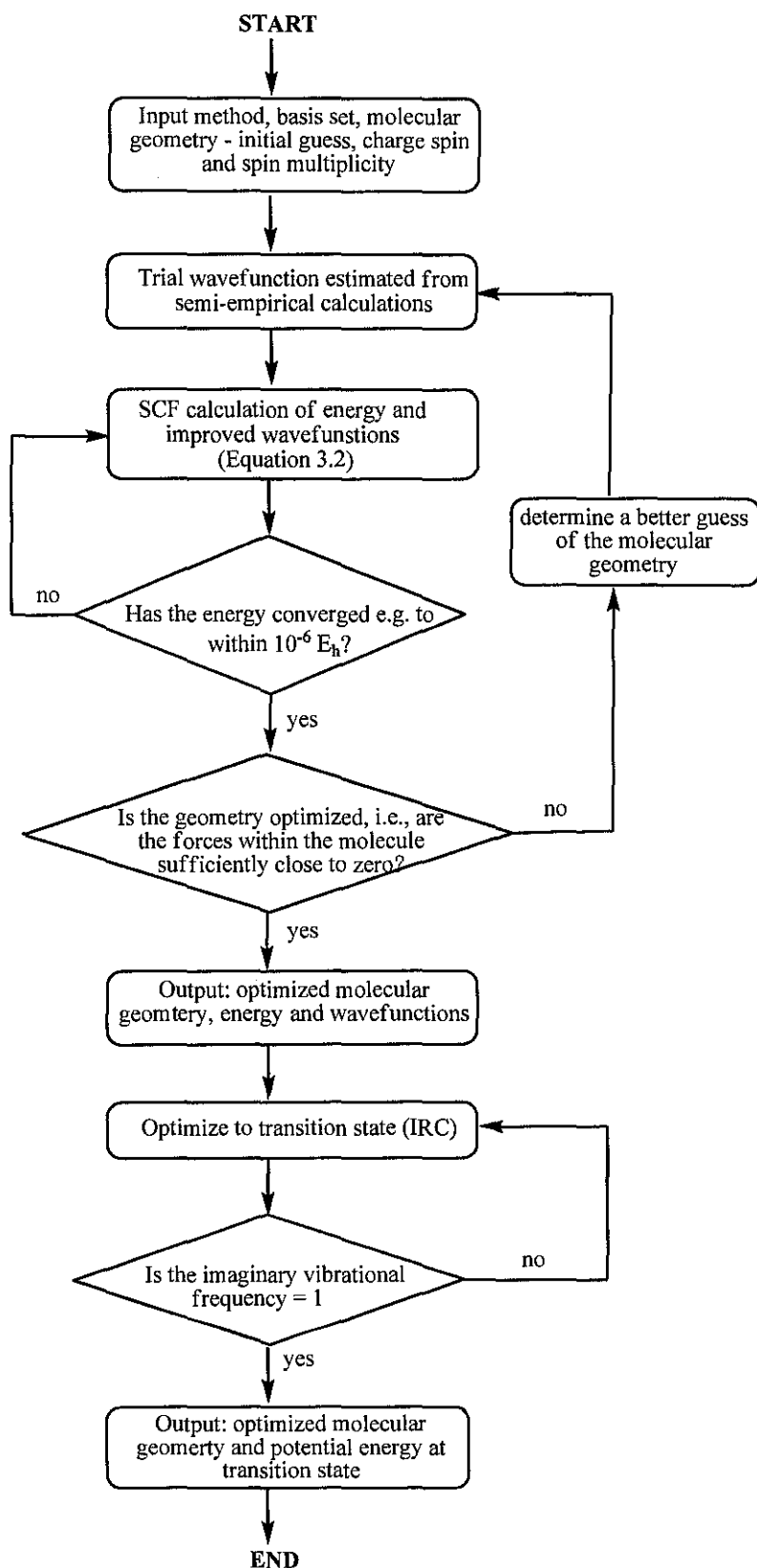


Figure 3.2: Flowchart illustrating the steps involved in quantum chemical calculations of molecular structures.

A conformational analysis was carried out on the optimized geometries (ae or ee geometric isomers) by rotating the torsional angles of the ligands in steps of 30°. The resulting conformers (a maximum of about 10,000) were further optimized by energy minimization. A conformer was retained if its energy varied by less than 2 kJmol⁻¹ from that of the most stable conformer. Thus, only the most stable conformers with lowest energy were selected. Figure 3.2 shows a flowchart for the steps involved in geometry optimization.

Activation energies were calculated for the five transition structures of Rh-catalyzed hydroformylation of ethylene identified by Matsubara et al. (1997) (alkene insertion, H-insertion onto alkene ligand, CO insertion, H₂ oxidative addition and aldehyde reductive elimination). However, only three transition states with the three highest energy barrier (alkene insertion, CO insertion and H₂ oxidative addition) were selected for detailed study. Structure of PH₃ is chosen to mimic the organic phosphorus ligand PPh₃ to avoid excessive computational time without appreciable loss of accuracy (Luo et al., 2005; Musaeu, et al., 1995).

3.6.1. Test Calculation

Coutinho et al. (1997) reported experimental studies on hydroformylation of phosphino-alkenes with hetero-bimetallic complex catalyst, (CO)₄M(μ-PPh₂)₂RhH(CO)(PPh₃), where M = Cr, Mo or W. They isolated a few intermediates in the reaction process and determined their structural parameters by spectroscopic and X-ray diffraction. Later on, Tang et al. (2007) reported a computational studies of the reaction steps and intermediates using Gaussian 03 package and compared some of their computed results with the experimental structural data of Coutinho et al (1997). Therefore in this work, the structural parameters (bond length and bond angle) of an μ-acyl intermediate [called A'(Mo) in Tang et al., 2007] at MP2/6-31G(d,p) level were computed and compared with the Tang's computed data and Coutinho's experimental data obtained by X-ray crystallography. The structure of the μ-acyl intermediate and the comparison of calculated and experimental values are shown in Figure 3.3 and Table 3.2, respectively. The above comparison validates the accuracy of the above computed results at RHF MP2/6-31(d,p) level.

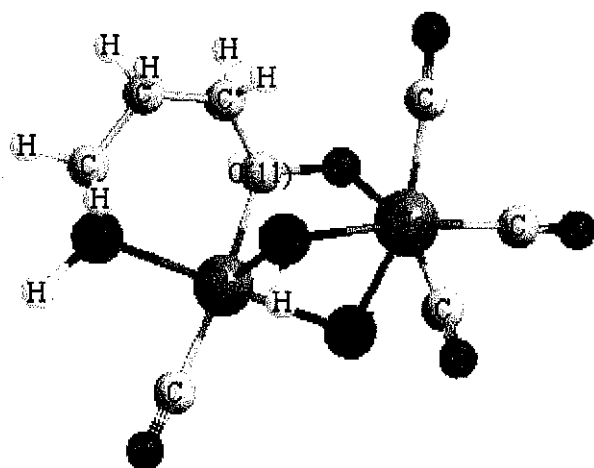


Figure 3.3: Optimized structure of the the μ -acyl complex A'(Mo) as an intermediate in hydroformylation using a hetero-bimetallic complex catalyst.

Table 3.2: Optimized parameters for the μ -acyl complex A'(Mo) at the RHF/6-31G(d,p) level (present work), computed results of Tang et al. (2007) and Coutinho's experimental data obtained by X-ray crystallography.

Bond length ($^{\circ}$ A)/ Bond angle (degree)	Calculated (Present work)	Calculated (Tang et al, 2007)	Experimental (Coutinho et al., 1997)
Rh-Mo	2.79	2.85	2.78
Rh-P(2)	2.34	2.40	2.32
Rh-P(3)	2.35	2.41	2.34
Rh-C(11)	2.05	2.06	2.05
Rh-P(5)	2.34	2.34	2.29
Mo-P(2)	2.49	2.52	2.47
Mo-P(3)	2.47	2.51	2.49
Mo-O	2.28	2.32	2.25
Rh-Mo-P(2)	52.2	52.8	52.1
Rh-Mo-P(3)	52.3	52.8	52.4
Rh-Mo-O	66.0	65.0	66.4
P(2)-Mo-P(3)	104.0	105.3	103.9
P(2)-Mo-O	78.8	78.5	78.7
Rh-Mo-C(11)	72.0	72.2	71.9

3.7. Results and Discussion

3.7.1. Quantum Chemical Calculation

As stated before, quantum chemical calculations are confined to the reactions within the dashed box in Figure 3.1. The main reaction mechanism involves eight elementary steps, three of which pass through transition states (TS): (i) alkene insertion (step **D** to **F**), (ii) formation of acyl complex (step **F** to **J**), (iii) H₂ oxidative addition (step **J** to **N**). These three reactions will be examined individually, and at the end the overall potential energy profile will be analyzed.

3.7.1.1. Alkene Insertion:

In this step, alkene ligand inserted into the Rh–H bond to generate an unsaturated Rh–alkyl complex **F** (or **G**). The MP2 optimized geometry of the alkene insertion transition states TS1 originating from H₂-alkene adducts **E1** was displayed in Figure 3.5a. In proceeding from the H₂-alkene adducts to insertion transition states, the alkene ligand must rotate out of the equatorial plane and shifted upward in order to favor its alkene group to align with the axial hydride. As seen in Figure 3.5a, the alkene ligand in the transition states oriented itself intermediary between a perpendicular and parallel alignment. Simultaneously, the axial hydride bent toward the incoming alkene ligand to expedite insertion. Alkene insertion transition states TS1(**E1/F1**) and TS1(**E2/F2**) were located at the MP2 level: TS1(**E1/F1**) originating from the *ee* H₂-alkene adduct, along with TS1(**E2/F2**) originating from *ea* H₂-alkene adduct. Vibrational frequency calculations confirmed that all two species are indeed transition states containing a single imaginary frequency. In each case animation of the normal mode for the single imaginary frequency displayed the desired nuclear displacements required for alkene insertion into the Rh–H bond. For evidence from the structures of the TS1(**E1/F1**) and TS1(**E2/F2**) confirmed by calculation of the IRC, TS1(**E1/F1**) generated the *trans* Rh–alkyl insertion product (**F1**), while TS1(**E2/F2**) leads to the *cis* Rh–alkyl insertion product (**F2**).

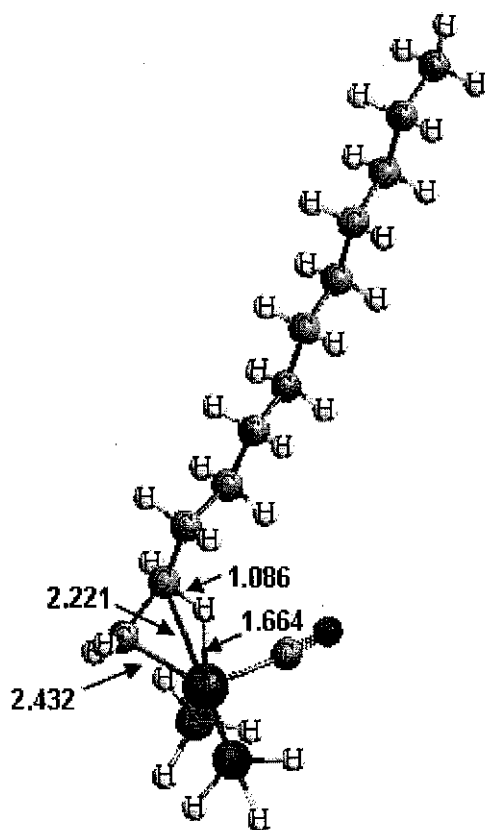


Figure 3.4a: Selected geometrical parameters of optimized structures (Å) of the transition state TS-1 (E1/F1) for the 1-dodecene insertion at RHF level.

3.7.1.2. Formation of Acyl Complex:

Along the reaction coordination, the axial alkyl ligand is bended toward the equatorial CO ligand before the three-member ringed, trigonal bipyrimidal-like transition structure was formed as shown in Figure 3.4b. This distortion was coupled with a bending of the oxygen atom of the CO ligand away from the incoming alkyl group in order to decrease the steric and electronic repulsion. The bond angle Rh–C–O changes from 178° in H₂ to 163° in TS 2(H2/J2) which indicated that the CO ligand also bent slightly to align with the incoming alkyl ligand. In the TS 2 structures the Rh–C(alkyl) bond was about 0.03 nm longer than its value in species H while the C(alkyl)–C(CO) distance became shorter by about 0.2 nm. On the other hand, analysis on the bond orders also illustrate that the Rh–C (alkyl) bond was weakened while C (alkyl)–C(CO) was strengthened in the process and this conclusion accorded with the change of bond length. Additional, Rh–C (CO

insertion) bond is shortened by about 0.014 nm along the process from H to TS2, which demonstrates bond strengthening. However, the length of Rh–C (CO insertion) bond was elongated by about 0.015 nm from TS2 to insertion product J according to the much more decrease of bond order along this proceeding. The product of CO insertion had two isomers, J1 and J2. Obviously, J2 is a more stable isomer by a preferred energy in the range of 6.7 to 7.5 kJ mol⁻¹ of I1 and these were confirmed by IRC calculations.

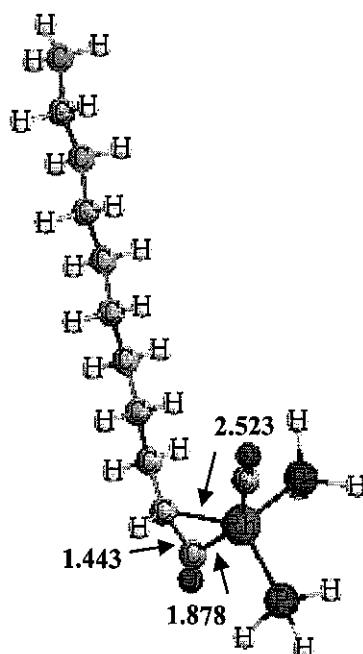


Figure 3.4b: Optimized Bond lengths (Å) of transition state TS-2 (H1/J1) for the CO insertion at the RHF level (1-octene).

3.7.1.3. H₂ Oxidative Addition:

The third transition state considered in this work was oxidative addition of H₂ to the unsaturated four-coordinated complexes **J** to give rise to a dihydride acyl species **N**. Calculated at the MP2 level, the H₂ addition step for all three substrates was predicted to be endothermic in the range of 21.0 to 37.5 kJ mol⁻¹. There were two possible attacking paths, one is when H₂ molecular closed to the center metal parallel to P–Rh–C(CO) in **J** forming transition state TS3(J1/N1), the other was H₂ molecular along with C(CO)–Rh–C(CO) moves up to rhodium to give rise to TS3(J2/N2). TS3(J1/N1) and TS3(J2/N2)

gave rise to oxidative addition products N1 and N2, respectively. The three-membered ring transition states TS3(J1/N1) and TS3(J2/N2) consisted of two hydrogen and rhodium, in which the H–H bond was elongated apparently than in free H₂ molecular but not broken is shown in Figure 3.4c. The bond order of it decreased from 0.78 in free H₂ molecular to 0.5 in TS3 that also indicated the H–H bond was sharply weakened. Calculated at MP2 level of theory, the energy barrier for TS 3(J2/N2) was a little lower than the other pathway through TS3 (J1/N1), therefore the reaction with H₂ attacking along the C(CO)–Rh–C(CO) was regarded as the better one of the two possible paths. Calculation using 1-octene, 1-dodecene and styrene as substrate, the energy barrier for the two paths was in the range of 52.9 to 66.2 kJmol⁻¹. Finally, H–H bond was broken completely along with the two Rh–H bond formations and six coordinated species N1 and N2 are formed. Accordingly, the bond order of H–H was close to zero while that of Rh–H bond increased from about 0.24 to 0.39 in the transition state TS3.

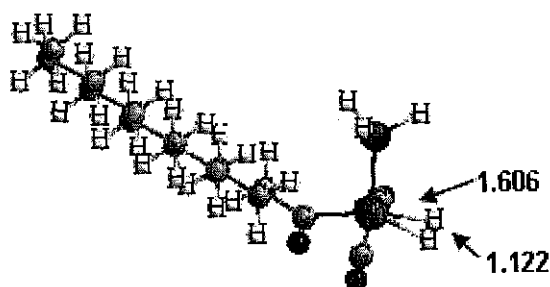


Figure 3.4c: Optimized structures (Å) of the transition state TS-3 (J1/N1) for the H₂ oxidative addition at the RHF level (1-dodecene).

The activation energies for the above three reaction steps of the alkenes were obtained from the potential energy values calculated by considering higher electron spin number (triplet). It may be mentioned that use of this higher spin number yielded more consistent values of the potential energy compared to those obtained by using the spin number 1 in our initial calculations. The tabulated values (Table 3.3) show that if both the coordinating groups (L, CO) are in equatorial positions (ee), the activation energy is generally less than that for the case of one ligand in equatorial and the other in apical (ea)

positions. The variations in the activation energies for the transition states of the three alkenes can be explained in terms of steric hindrance or steric crowding of the alkyl ligands (van Rooy et al., 1996). Styrene, which has a bulky phenyl group, has the highest activation energy among the three olefins for all the transition states. The activation energy of the reactions of 1-dodecene are higher than the corresponding values of 1-decene and can be explained on the same basis. X-Y-Z structures of the species at stationary points are provided in Appendices A, B and C.

Table 3.3: Activation energies calculated at MP2 level of theory

Substrate	Activation energy (kJ mol ⁻¹)					
	Olefin insertion		Acyl complex formation		H ₂ oxidative addition	
	ee (1)	ae (2)	ee (1)	ae (2)	ee (1)	ae (2)
1-Decene	39.0	41.4	39.4	40.3	52.9	59.6
1-Dodecene	41.6	42.5	43.5	41.0	57.7	62.3
Styrene	56.4	57.4	48.3	46.8	63.2	66.2

3.7.1.4. The Potential Energy Profile:

The potential energy profile of the hydroformylation of 1-decene, 1-dodecene and styrene are presented in Figures 3.5a, b and c, respectively. The reaction coordinate represents the progress along the reaction pathway. The active catalyst which mediates the catalytic cycle, is considered to be HRh(CO)₂(PPh₃) [**B** in Figure 3.1]. The transition state of the insertion of alkene into Rh-complex (TS-1), formation of acyl complex (TS-2) and oxidative addition of H₂ (TS-3) were optimized by the ab initio MO method to determine the potential energy surface of the intermediates. The H₂ oxidative addition (TS- 3) were found to be endothermic and the alkene insertion (TS- 1) and CO insertion reaction (TS- 2), are exothermic. Similar results were reported for the hydroformylation of ethene by Musaev, et al. (1995). The largest barrier is the H₂ oxidative addition step, in agreement with the experimental proposal that the H₂ oxidative addition is rate determining.

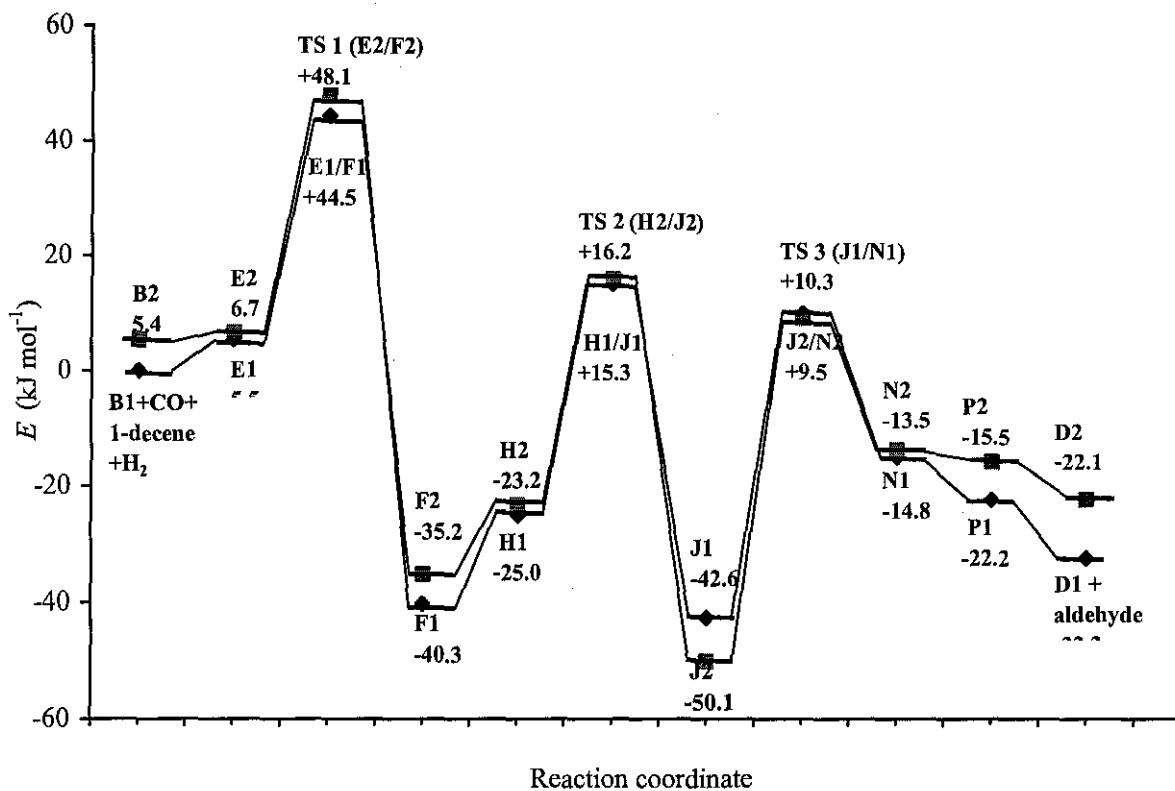


Figure 3.5a: The potential energy profile of 1-decene hydroformylation reaction

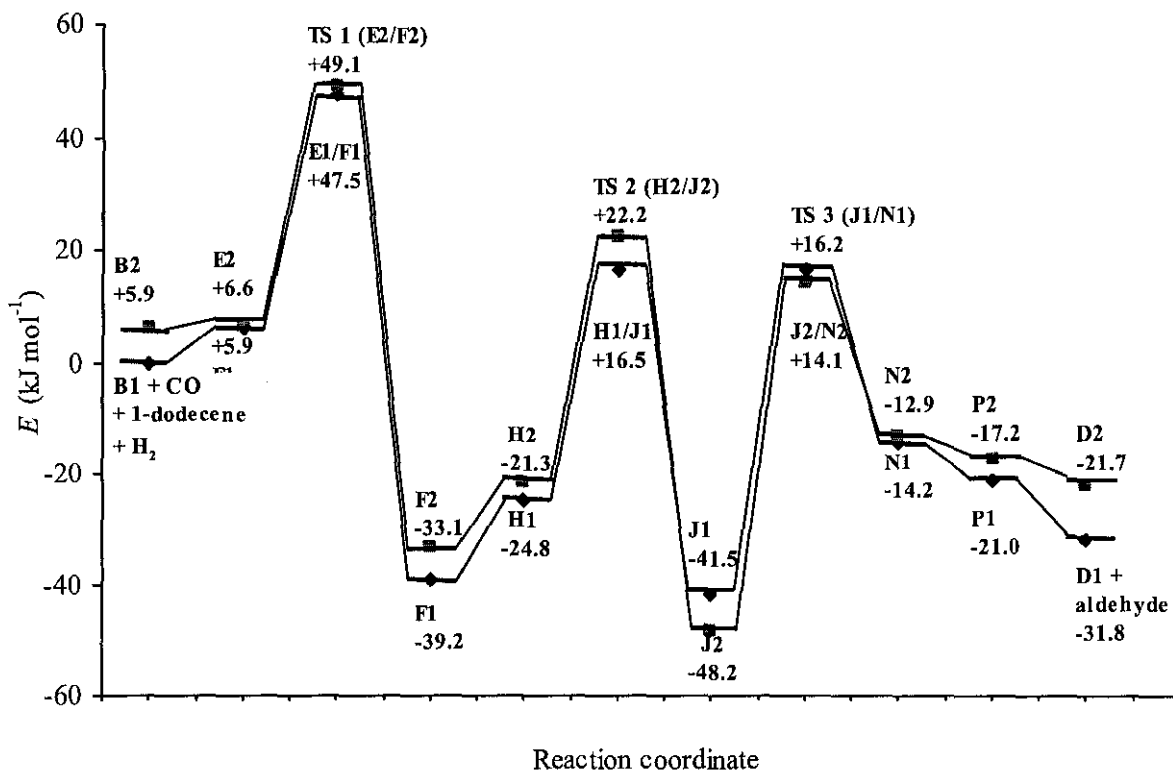


Figure 3.5b: The potential energy profile of 1-dodecene hydroformylation reaction

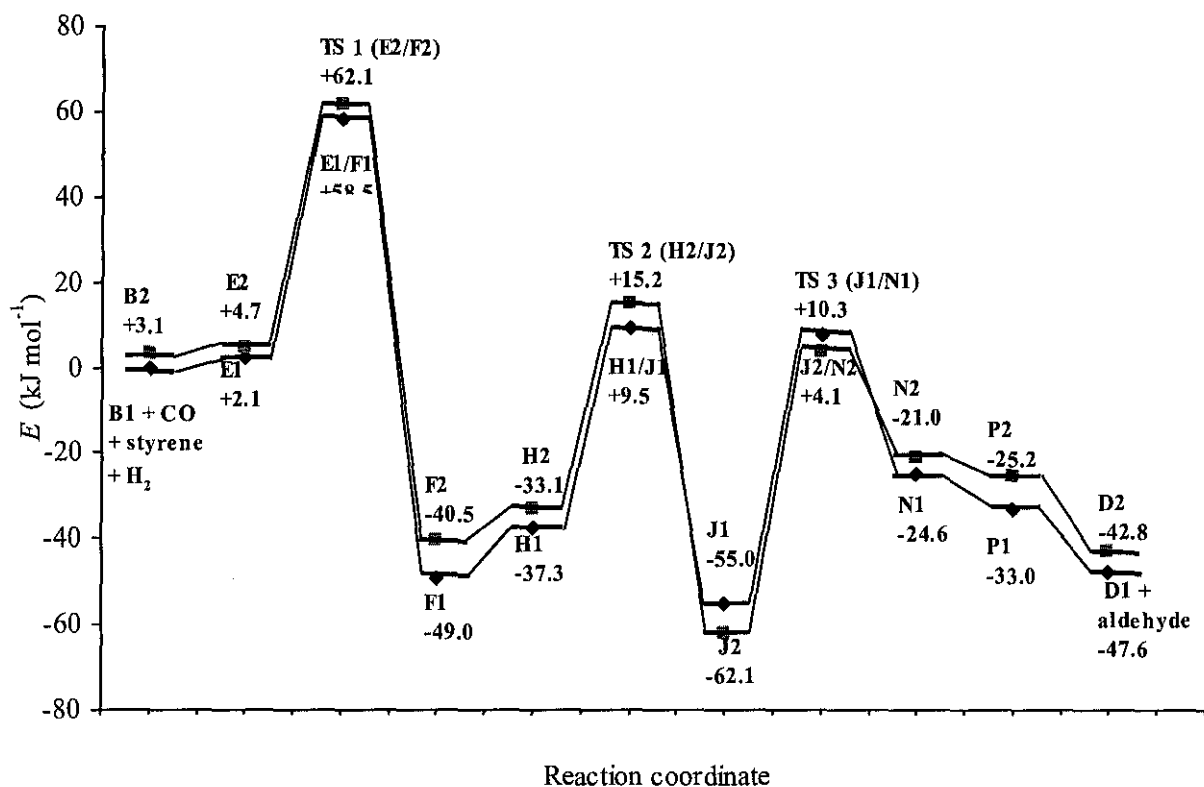


Figure 3.5c: The potential energy profile of styrene hydroformylation reaction

3.7.2. Development of the Mechanistic Rate Equation

Mechanistic rate equations for higher olefins were developed based on the reaction pathways depicted in Figure 3.1 using the conventional pre-equilibrium and quasi-steady state approximations. Three rate equations (M1, M2 and M3) have been developed corresponding to the three transition states identified by quantum chemical calculations. The following reaction steps are considered.





The Equations (3.9) to (3.16) and the simplifying assumptions were used to derive relationships between the rate of reaction and experimental parameters (i.e. concentrations of olefin, catalyst, dissolved CO, as well as H₂).

If the H₂ oxidative addition is rate-controlling, the rate of reaction is given by

$$\text{Rate} = k_7 [J][H_2] \quad (\text{where } k \text{ is the rate constant}) \quad (3.17)$$

Considering the conservation of the catalytic species, the overall balance at steady state is described by

$$[\text{catalyst}] = [B] + [C] + [D] + [F] + [G] + [J] + [M] \quad (3.18)$$

where [catalyst] is the concentration of catalyst loaded. The concentration of B, C, D, F, G and M are expressed in terms of J,

$$[B] = \frac{J}{K_1 K_2 K_4 K_6 [\text{alkene}]} \quad (3.19)$$

$$[C] = \frac{[J][CO]}{K_2 K_4 K_6 [\text{alkene}]} \quad (3.20)$$

$$[G] = \frac{K_5 [J]}{K_4 K_6} \quad (3.21)$$

$$[D] = \frac{[J]}{K_4 K_6 [\text{alkene}]} \quad (3.22)$$

$$[F] = \frac{[J]}{K_6[CO]} \quad (3.23)$$

$$[M] = K_8[J][CO] \quad (3.24)$$

and hence [catalyst],

$$[\text{catalyst}] = \frac{[J] \left(1 + K_1^*[CO] + K_2^*[CO]^2 + K_3^*[\text{alkene}] + K_4^*[CO][\text{alkene}] + K_5^*[CO][\text{alkene}] \right)}{K^*[CO][\text{alkene}]} \quad (3.25)$$

Equation (3.25) is rearranged to obtain the expression for [J] and in turn substituted in Equation (3.17) to give the rate model (M1) of the following form:

$$\text{Rate} = \frac{k[\text{catalyst}][CO][\text{alkene}][H_2]}{1 + K_1^*[CO] + K_2^*[CO]^2 + K_3^*[\text{alkene}] + K_4^*[CO][\text{alkene}] + K_5^*[CO]^2[\text{alkene}]} \quad (3.26)$$

where k is the reaction rate constant of the rate determining step and $K_1^* - K_5^*$ are constants derived from the equilibrium constants of the reactions 3.9-3.16. This model is similar to the empirical model proposed by Bhanage *et al.* (1997), van Rooy *et al.* (1995), Divekar *et al.* (1993) and Deshpande and Chaudhari (1988).

The second kinetic model (M2) was proposed considering the migration insertion of the alkene into R-H, as a rate limiting step (Eq. (3.12)). Therefore, the rate law is given by

$$\text{Rate} = k_4[D][\text{olefin}] \quad (3.27)$$

Following the derivation outlined previously, the corresponding rate equation is

$$\text{Rate} = \frac{k[\text{catalyst}][CO][\text{alkene}]}{1 + K_1^*[CO] + K_2^*[CO]^2 + K_3^*[\text{alkene}] + K_4^*[CO][\text{alkene}]} \quad (3.28)$$

Similarly, considering the formation of the acyl complex is rate-controlling (Eq. 3.14).

The rate law is given by

$$\text{Rate} = k_6 [\text{F}][\text{CO}] \quad (3.29)$$

and the final form of the rate equation is

$$\text{Rate} = \frac{k[\text{catalyst}][\text{CO}][\text{alkene}][\text{H}_2]}{1 + K_1^*[\text{CO}] + K_2^*[\text{CO}]^2 + K_3^*[\text{alkene}] + K_4^*[\text{CO}][\text{alkene}] + K_5^*[\text{H}_2]} \quad (3.30)$$

Models M1, M2 and M3 are called ‘generalized models’ corresponding to the three rate determining steps indicated by the quantum calculations and are independent of any particular olefin. The proposed rate equation (M1) is also consistent with the experimental observations, indicating a first-order dependence on $[\text{H}_2]$ and $[\text{catalyst}]$, first order in CO at low pressure and negative order at high pressures and fractional order in olefin concentration. The negative order with respect to CO concentration at high pressure may be explained by the accumulation of species **M**, which are outside of the cycle under these conditions and therefore should inhibit the rate of the reaction (Rosales et al., 2007a).

3.7.3 Determination of the Rate Parameters

Experimental hydroformylation rate data extracted from the published literature were used to evaluate the kinetic and equilibrium constants (k and K 's) of each of the three 1-alkenes. The data sources and the ranges of the process parameters (pressure, concentration, temperature) are listed in Table 3.4. The kinetic data used in the kinetic modeling is shown in Appendix D. The $\text{HRh}(\text{CO})(\text{PPh}_3)_3$ catalyst in an organic solvent was used for the alkene substrates except for 1-octene for which $\text{HRh}(\text{CO})[\text{P}(p\text{-CF}_3\text{C}_6\text{H}_4)_3]_3$ was used as catalyst in supercritical carbon dioxide ($sc\text{CO}_2$) solvent. Since no side reactions were reported by the researchers under the stated experimental conditions, the rate data represented the overall hydroformylation of an alkene to the corresponding aldehyde (Nair et al, (1999); Bhanage et al. (1997); Divekar et al. (1993)).

Table 3.4: Range of experimental conditions used for development of the mechanistic rate equation

Experimental conditions	Bhanage et al. (1997)	Divekar et al. (1993)	Palo and Erkey (1999)	Nair et al. (1999)
Substrate olefin	1-Dodecene (C ₁₂)	1-Decene (C ₁₀)	1-Octene (C ₈)	Styrene (C ₆)
Conc. of catalyst (mol/m ³)	1.0-8.0	0-1.0	0.63-2.54	0.131-1.01
Initial conc. of 1-alkene (kmol/m ³)	0.18-2.2	0-1.0	0-1.0	0.92-6.89
<i>P</i> _{H₂} (MPa)	0.68-1.7	0-1.38	5-13.8	1.03-4.12
<i>P</i> _{CO} (MPa)	0.17-2.04	0-8.11	5-13.8	0.3-4.12
<i>T</i> (°C)	50-70	50-70	50	60-80
Reaction volume (mL)	25	not available	not available	25
Solvent	toluene	benzene	scCO ₂	toluene

Non-linear least square regression based on the criterion of minimization of the mean residual sum of squares (MRSS) was performed to determine the kinetic parameters using the Solver in Microsoft Excel 2007.

$$\text{MRSS} = \frac{\sum_{i=1}^N (R_{\text{calc}} - R_{\text{expt}})^2}{N_{\text{expt}} - N_{\text{param}}} \quad (3.31)$$

where N_{expt} is the number of experimental data, N_{param} is number of model parameters, R_{calc} and R_{expt} represent calculated and experimental rates, respectively. Experimental rate data are available at different temperatures, partial pressures of CO and H₂ as well as concentrations of the olefin and of the catalyst (Table 3.4). The kinetic and equilibrium constant values can be estimated by optimizing the objective function given by the Equation (3.31) on a set of constant temperature rate data. Alternatively, a global error minimization can be done by considering all the available rate data at different temperatures and process conditions for a particular olefin. The second method is recognized as a robust technique that avoids the possible pitfalls of ending the optimization process at a local minimum. ‘Temperature centering’ is a tested strategy of estimating temperature-dependent parameters by global optimization over the entire temperature range (Pant and Kunzru, 1997; Wojciechowski and Rice, 2003; Patel and

Pant, 2007). In this technique the activation energy of the rate-controlling reaction step and the pre-exponential factor were obtained from the Arrhenius equation with ‘temperature centering’.

$$k_i = A_i \exp \left[\frac{-E_i}{R} \left(\frac{1}{T} - \frac{1}{T_m} \right) \right] \quad (3.32)$$

Here T_m is introduced for temperature centering. It is usually chosen at the middle of the temperature range (it is $T_m = 333$ K in this study). An ‘equilibrium constant’, K , was similarly determined as a function of temperature using the van’t Hoff equation also with temperature centering.

$$K_i^* = \exp \left[\frac{\Delta S_i}{R} - \frac{\Delta H_i}{R} \left(\frac{1}{T} - \frac{1}{T_m} \right) \right] \quad (3.33)$$

Suitable initial guess values are required for application of non-linear regression for parameter estimation using Equation (3.31) which, otherwise, may converge to local minima (Wojciechowski and Rice, 2003; Routray and Deo, 2005). In order to arrive at a suitable set initial guess values for global optimization over the entire experimental temperature range, isothermal rate data at individual temperatures were first fitted and the Arrhenius plots were done to make a judgment about the initial guess and the suitability of a model. The Arrhenius parameters from these plots were then used as the starting values for an “all up” fit of rate expression. A summary of the computational procedure is given in Figure 3.6.

The error estimate given by Equation (3.31) together with thermodynamic consistency of the calculated activation energy or negative kinetic parameter, if any, were used as the criteria of discrimination among the three macroscopic rate models (Patel and Pant, 2007; Hurtado et al., 2004; Pengpanich et al., 2002). Model M2 was rejected because of a high average standard error estimate ranging from 7% to 26% as shown in Appendix E. Model M3 displayed a non-linear Arrhenius plot besides a large error estimate (7% to 56%), therefore it was also rejected.

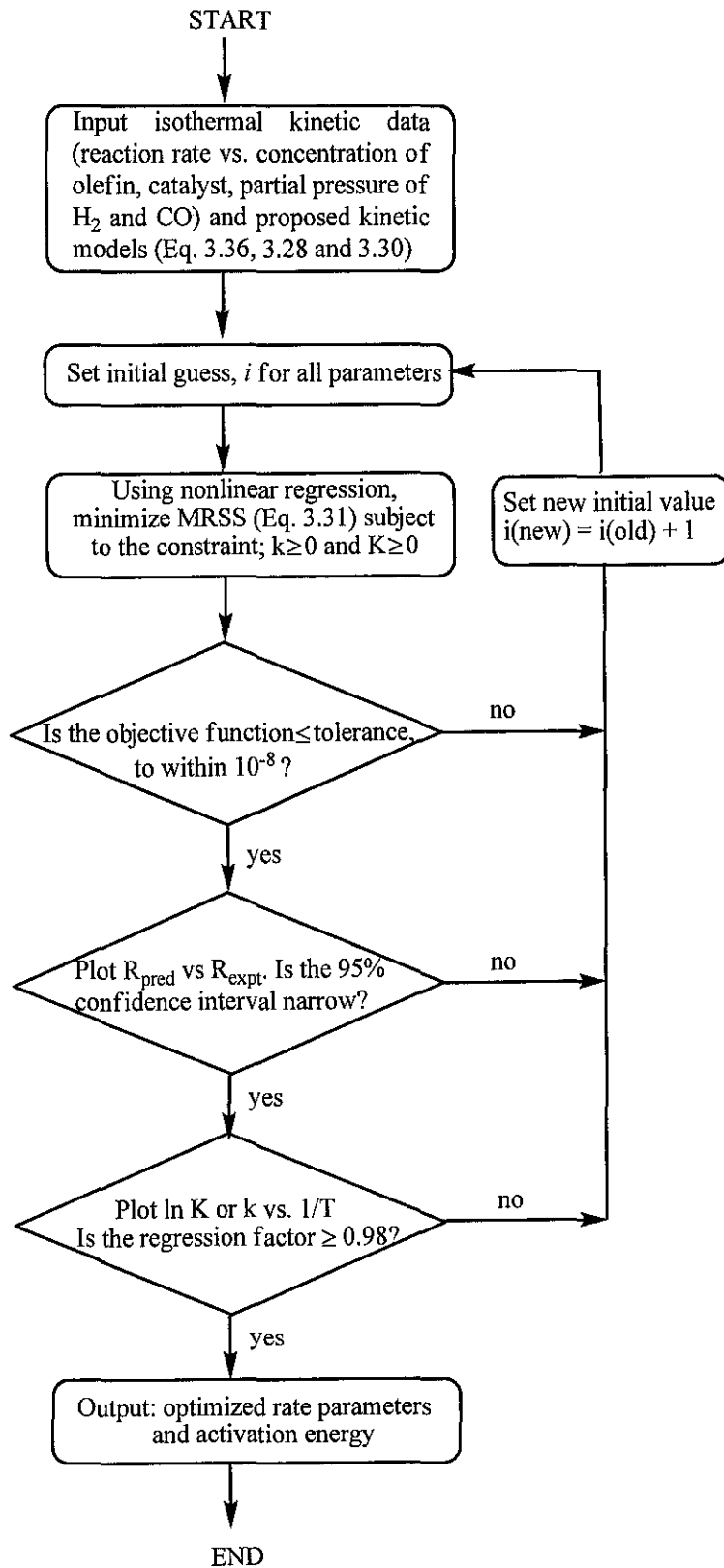


Figure 3.6: Flowchart illustrating the steps involved in kinetic modeling

Table 3.5: Estimated M1 kinetic model parameters with 95% confidence limits.

Substrate	T (K)	k	K_1^*	K_2^*	K_3^*	K_4^*	K_5^*	SEE	E_a (kJ·mol ⁻¹)
1-dodecene	323	3.1×10 ⁴ *3.4×10 ⁴	1.24×10 ³	2.5×10 ⁵	18.0	1.5×10 ⁴	9.0×10 ⁵	11.5	69.7
C ₁₂	333	6.0×10 ⁴ *5.8×10 ⁴	500	1.5×10 ⁵	5.0	1.1×10 ³	4.0×10 ⁵		*57.1 ^a
	343	10.0×10 ⁴ *9.9×10 ⁴	202	0.5×10 ⁵	2.2	9.4×10 ³	3.0×10 ⁵		
1-decene	323	3.9×10 ⁴ *1.1×10 ¹³	99.7	2.5×10 ⁵	19.9	63.4	1.05×10 ⁵	13.0	46.2
C ₁₀	333	6.5×10 ⁴ *1.4×10 ¹³	161	1.3×10 ⁵	24.5	80.0	1.10×10 ⁵		*49.2 ^b
	343	1.1×10 ⁵ *2.8×10 ¹³	447	8.0×10 ⁴	33.5	93.0	1.40×10 ⁵		
styrene	333	4.7×10 ⁴ *1.6	13.7	3.9×10 ⁴	5.2	3.0×10 ⁴	2.59×10 ⁵	2.0	63.0
C ₆	343	9.8×10 ⁴ *3.1	9.0	9.0×10 ²	11.4	3.5×10 ⁴	2.65×10 ⁵		*68.8 ^c
	353	21.3×10 ⁴ *6.6	5.0	3.0×10 ²	13.0	3.7×10 ⁴	2.95×10 ⁵		
1-octene	323	2.2×10 ⁵ *0.10	2.0×10 ³	3.0×10 ⁵	18.0	1.5×10 ⁴	8.0×10 ⁵	4.0	
C ₈									

(kmol, m³, s units)

*Activation energy and rate constant value reported in open literature:

^aBhanage et al. (1997)^bDivekar et al. (1993)^cNair et al.(1999)

The rate model M1 is able to describe the experimental data reasonably well over the whole range of pressure, olefin concentration and temperature. The estimated parameters as well as the activation energy and error estimates are presented in Table 3.5. These results suggest that a mechanism of reaction featuring oxidative addition of H₂ to acylrhodium intermediate species as rate determining is appropriate for describing the hydroformylation of all the substrates. Rates of hydroformylation of the olefins have been calculated for different concentrations and temperature using the generalized rate equation and estimated parameters. Comparisons of these calculated values with experimental data reported in the literature as well as the predictions of the reported empirical models shown in Figures 3.7, 3.8 and 3.9 appear to be satisfactory.

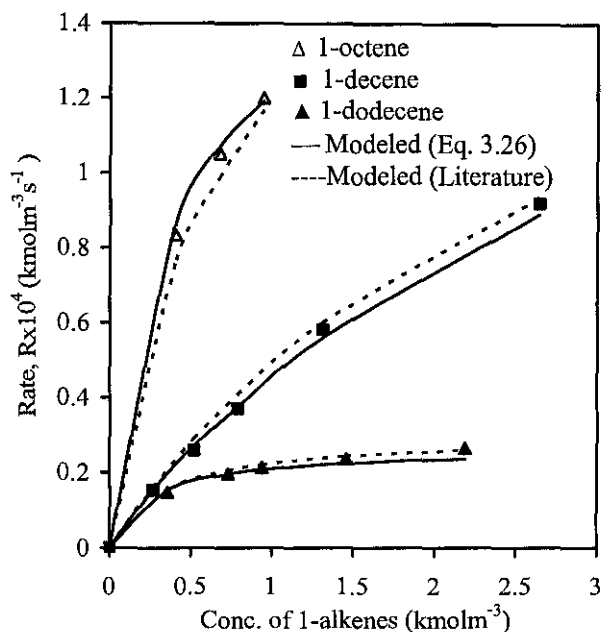


Figure 3.7: Experimental and predicted initial reaction rates vs. concentration of olefin, at temperature of 323 K. *References to experimental data: 1-octene, Palo and Erkey (1999); 1-decene, Divekar et al. (1993); 1-dodecene, Bhanage et al. (1997).

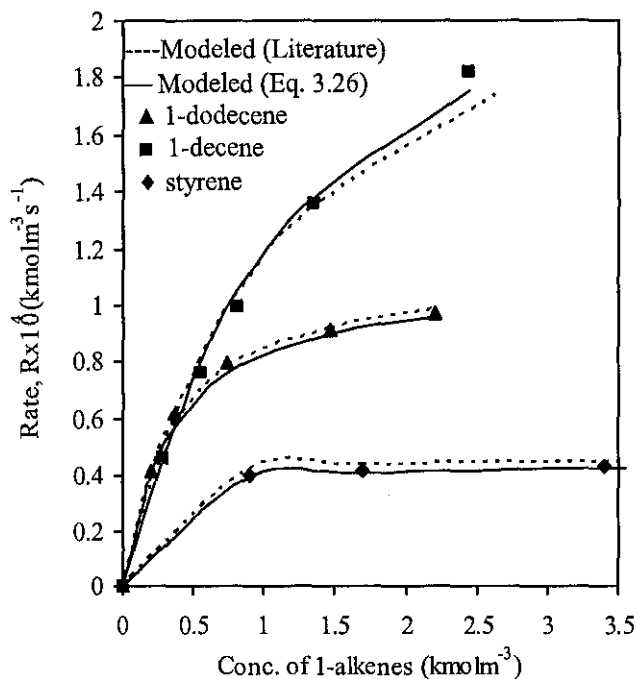


Figure 3.8: Experimental and predicted initial reaction rates vs. concentration of olefin, at temperature of 333 K. *References to experimental data: styrene, Nair et al.(1999); 1-decene, Divekar et al. (1993); 1-dodecene, Bhanage et al. (1997).

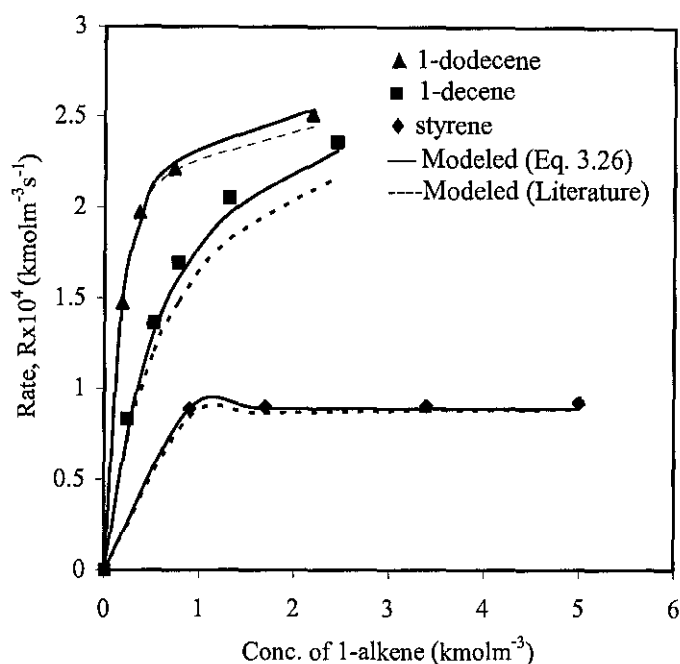


Figure 3.9: Experimental and predicted initial reaction rates vs. concentration of olefin, at temperature of 343 K. *References to experimental data: styrene, Nair et al. (1999); 1-decene, Divekar et al. (1993); 1-dodecene, Bhanage et al. (1997).

Since the concentration history of 1-dodecene during hydroformylation reaction is reported by Bhanage et al. (1997), we could check the capability of the generalized model M1 to predict the concentration transient. The derivation of the rate equation that links concentrations of reactants with time is presented in Appendix F. The results presented in Figure 3.10 for three different temperatures further establish the accuracy of the proposed model. As a final check, we plotted the calculated and experimental rate data of all the olefins at different process conditions in the form of a parity diagram shown in Figure 3.11. The average prediction error is 7.6% while the maximum error is 13.0%.

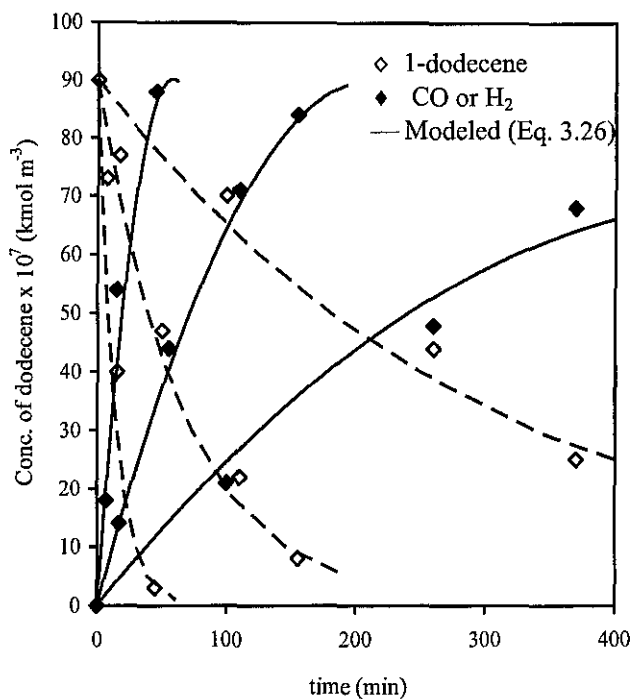


Figure 3.10: Experimental and predicted concentration of 1-dodecene and CO or H₂ as a function of contact time at temperature of 323, 333 and 343 K. References to experimental data: Bhanage et al.(1997).

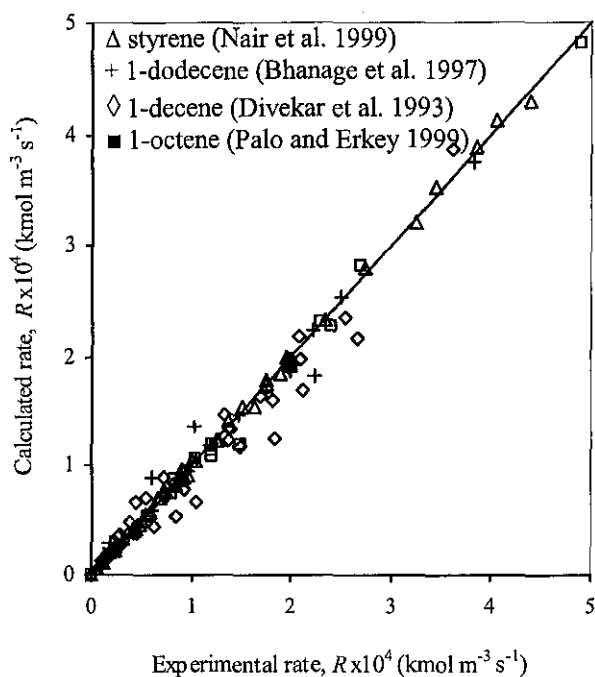


Figure 3.11: Parity plots of the model predictions of the rate of hydroformylation of styrene, 1-octene, 1-decene and 1-dodecene in homogeneous system.

The rate parameter values were determined at 95% confidence interval. Since the confidence interval is narrow, the sample mean may be considered to be reasonably accurate estimates of the population mean values. In addition, the values of rate parameters in the denominator of the kinetic rate expression versus temperature ($\ln K$ vs $1/T$) yielded good correlation (R^2) ranging from 0.97 to 0.99. The parameters K_i^* in the denominator of Equation (3.26) relate to the equilibrium constants of elementary steps in the reaction mechanism. The magnitudes of the parameters, that vary over a wide range, are representative of the importance of the different steps of the overall reaction. For instance, the large value of K_2^* implies that the rate of dissociation and association of ligand, step 2 and 4 are high. However, the value of K_1^* suggests that step 3 occurs at 3 orders of magnitude slower compared to step 4. On the other hand, difference of two orders of magnitude lower in the rate constant of the alkene insertion step (step 5 and 6) with respect to step 2 was also observed and reported in open literature (van Leeuwen et al., 2000). From the regressed value of K_4^* , the rate of the carbonyl insertion step (step 8) was found to be greater by one order of magnitude compared to the alkene insertion step.

The rate constant, k , is close to the value reported by Bhanage et al (1997). Furthermore, comparing the regressed values of the rate constant, k at 333 K, the values of k increase in the order of styrene (4.7×10^4), 1-dodecene (6.0×10^4) and 1-decene (6.5×10^4) which are also supported by our calculated activation energies for H_2 oxidative addition. On the other hand the rate constant of hydroformylation of 1-octene (2.2×10^5 at 323 K) in $scCO_2$ is found to be greatest due to the rate enhancing effect of CO_2 (Koeken et al., 2006).

A negative order with respect to P_{CO} has been observed experimentally, and therefore the concentration term of CO is expected to appear raised to a higher power in the denominator than in the numerator (Helfferich, 2001). The regressed values of K_1^* and K_2^* for all four substrates are relatively large and suggest that the effect of the P_{CO} inhibition on the rate of reaction is highly significant. The values of K_1^* and K_2^* are larger for 1-dodecene, than for 1-decene, which in turn is larger than styrene. As P_{CO} increases the denominator increases significantly compared to the numerator leading to a rapid decline

in the reaction rate. It is also to be noticed that at high concentration of alkene and low PPh_3 or CO concentrations leads to zero order in alkene, which has been observed experimentally for the high alkene/low PPh_3 case. According to Helfferich (2001), the rate equation giving an order between zero and plus one contains the respective concentration ($[\text{alkene}]$) as a factor in the numerator and in some but not all terms of the denominator, as it is seen in model M1, M2 and M3 [Eq.(3.23), (3.25) and (3.27)].

The values of the rate constant for 1-dodecene, was found to be 2.5 times higher, than that of styrene, which confirms the good intrinsic reactivity of 1-dodecene in spite of its large molecular size. van Rooy et al. (1995) also reported similar results whereby, the hydroformylation of styrene using $\text{Rh}(\text{CO})_2(\text{acac})$ as the catalyst precursor and tris(2-tert-butyl-4-methylphenyl) phosphite as the ligand ($T=40\text{-}100^\circ\text{C}$, $P_{\text{CO}}=2.5\text{-}44$ bar, $P_{\text{H}_2} = 2.5\text{-}50$ bar, toluene as a solvent), the rate is three times lower than that of 1-octene. For the hydroformylation of 1-dodecene, the activation energy of $57.7 \text{ kJ}\cdot\text{mol}^{-1}$ (ee species) was obtained for the rate determining step, which is close to that reported by Bhanage et al. (1997), $57.1 \text{ kJ}\cdot\text{mol}^{-1}$. The average deviation of predictions is 11.5 %. As for 1-decene, an activation energy of $52.9 \text{ kJ}\cdot\text{mol}^{-1}$ (ee species) was obtained, which is higher than that obtained from the empirical kinetic model ($49.2 \text{ kJ}\cdot\text{mol}^{-1}$) reported by Divekar et al (1993). The average deviation of prediction is 13.0 %. However the rate equation predicts the rate of hydroformylation of styrene in toluene and 1-octene in scCO_2 with high accuracy. An activation energy of $63.2 \text{ kJ}\cdot\text{mol}^{-1}$ (ee species) was obtained, which is lower than that obtained from the mechanistic model, ($68.8 \text{ kJ}\cdot\text{mol}^{-1}$) reported by Nair et al. (1999). The mechanistic equation reported by Nair et al. (1999) was derived from the catalytic cycle described by Evans et al. (1968) and the error between the predicted and experimental rate data was within ± 5 %. On the other hand, the predictions of the rate data by using model M1 were found to be within a maximum error of ± 2.4 %. The relatively small error compared to 1-dodecene and 1-decene is probably due to the presence of the aromatic ring and shorter alkyl chain of styrene. The compact molecular structure of styrene has reduced the occurrence of the isomerization reaction compared to the long carbon chain of 1-dodecene and 1-decene. As for the rate of hydroformylation of 1-octene in scCO_2 , the average deviation in the predicted and observed rates was found to be in the range of ± 4 %. This result also demonstrates that model M1 is able to predict

the rate of hydroformylation of higher alkenes in both organic solvent and $scCO_2$ although several major differences exist between the conventional organic solvent-based system and the $scCO_2$ system. According to Palo and Erkey (1999), the major differences are the higher concentration of H_2 and CO in the $scCO_2$ compared to those in organic solvent, higher total pressure of the $scCO_2$ system and significantly different fluid densities (ρ of $scCO_2 = 0.2-0.9 \text{ g}\cdot\text{cm}^{-3}$) from those of organic systems ($\rho \cong 0.7 \text{ g}\cdot\text{cm}^{-3}$).

Besides the rate-determining step of TS-3 which is corroborated by experimental rate data for all the four higher alkenes, further match between the quantum chemical calculation results and the experimental data is evident from the magnitudes of the activation energies. The calculated (range of 52.9-59.6, 57.7-62.3 and 63.2-66.2 $\text{kJ}\cdot\text{mol}^{-1}$) and experimental (49.2 ± 6 , 57.1 ± 8 and $68.8\pm 5 \text{ kJ}\cdot\text{mol}^{-1}$) relative energy of the third transition structure (TS 3) or the activation energy for the hydroformylation of 1-decene, 1-dodecene and styrene, respectively are in reasonable agreement (Nair et al., 1999; Bhanage et al, 1997; Divekar, et al., 1993). However, the *ab initio* computational approach overestimate the activation energy for the hydroformylation of 1-dodecene and 1-decene although the activation energy values are close to the actual values obtained experimentally. The activation barrier relative to $HRh(CO)(PPh_3)_3$ catalyst is larger for styrene, than for 1-dodecene, which in turn is larger than 1-decene. This suggests that the observed reactivity seems to be influenced by the increased steric hindrance of the alkyl group of the alkene substrate.

CHAPTER 4

MATERIAL AND METHOD

This chapter covers the details of the various experiments conducted as part of this work. The first section describes all the chemicals and gases used. Section 4.2 discusses the development of the TMS-system by performing the gas solubilities experiments. In Section 4.3 the reactor set-up and experimental procedure to study the effect of process parameters on the yield and selectivity of the linear aldehydes as well as the rate of reaction are described. The liquid-liquid equilibrium and solute distribution experiments are discussed in Section 4.4. Finally the analytical techniques are outlined in Section 4.5.

4.1. Materials

The following chemicals (supplier, purity) were used as received without further purification: propylene carbonate (Acros, 99.5%), dodecane (Acros, 98.0%), 1,4-dioxane (Fischer Scientific, 99.5%), 1-octene (Acros, 98.0%), 1-dodecene (Acros, 98.0%), nonanal (Acros, 98.5%), tridecanal (Acros, 98.0%) and triphenylphosphite (Acros, 99.0%). Gas chromatograph (GC) analysis did not detect any appreciable peaks of impurities. The catalyst, $\text{HRh}(\text{CO})(\text{PPh}_3)_3$ was purchased from ABCR, Germany, with purity of 98.0 %. Gas chromatographic analysis did not indicate any notable peaks of impurities. Hydrogen, carbon monoxide, nitrogen and syngas (1:1, 1:2, 1:3, 2:1, 3:1 CO/H_2) were supplied by Malaysian Oxygen (MOX), with purity of 99.99 %.

Densities of the solvents used in solubility study were measured with Mettler Toledo densimeter (model Densito 3OP) and are given in Table 4.1, along with the literature values (Lide, 2005). The densimeter measures the density of solvent by the oscillating body method. After loading in the cell, the liquid was allowed to equilibrate until a steady reading was obtained in about 1 minute to a resolution of 0.0001 g cm^{-3} . The densimeter was calibrated against distilled water.

Table 4.1: Physical properties of the pure components at $T=298.15$ K and $P=101.325$ kPa.

Compound	$\rho/(\text{g cm}^{-3})$	
	Expt.	Lide (2005)
Propylene carbonate	1.2000	1.200
Dodecane	0.7510	0.751
1,4-Dioxane	1.0311	1.034

4.2. Development of the TMS-System

Solubilities of H_2 and CO in pure solvent and solvent mixtures relevant to the hydroformylation process are studied in this work, particularly in the temperature-dependent multi-component solvent (TMS)-systems involving propylene carbonate, dodecane and 1,4-dioxane. These solvents are preferred because of high boiling point, thermal stability, and inert nature with respect to the homogeneous catalyst, olefin, hydrogen, carbon monoxide and the hydroformylation products (Tijani and Ali, 2006; Behr et al., 2005; Behr and Miao, 2004). However, neither experimental data nor any theoretical model on solubilities for CO and H_2 in the TMS-system are available in the literature. In the above context, the objectives of this work are to:

- i. experimentally determine solubilities of CO and H_2 in different types of solvent systems which include single phase propylene carbonate (PC), biphasic mixture of PC+ dodecane, and TMS-system of PC+dodecane+1,4-dioxane at temperature range of 298-343 K,
- ii. determine the Henry's law constant for solubility by data fitting, and
- iii. predict the gas solubilities by thermodynamic modeling using the regular solution theory (RST)-based model and the modified UNIFAC model and compare with the experimental data.

4.2.1. Composition of the TMS- Systems

The appropriate compositions of the TMS-system (PC+dodecane+1,4-dioxane) for the solubility study at different temperatures were determined by the cloud point method in an equilibrium glass cell. All mixtures were prepared by weighing with a Mettler balance

accurate to within $\pm 10^{-4}$ g. A mixture of PC and dodecane (1.0 g; 5:1, 3:1, 1:1, 1:3, 1:5 wt. ratio) was transferred into a 5 mL centrifuge tube and immersed in a silicone oil bath that was controlled within 1 K, under a stirring speed of 900 rpm. After having reached the desired temperature (298 K, 353 K and 373 K), a heterogeneous mixture of PC and dodecane was titrated with 1,4-dioxane until a homogeneous phase is formed. The transition from a heterogeneous mixture to a clear liquid phase was determined visually. The reliability of the method depends on the precision of the micro burette which had an accuracy of $\pm 0.005 \text{ cm}^3$, and is limited by the visual inspection of the transition across the apparatus. The accuracy of the visual inspection of the transition is achieved by waiting approximately 5 minutes at the transition point and observing the heterogeneity. All visual experiments were repeated at least three times in order to ensure reproducibility.

4.2.2. Determination of the Gas Solubility

The solubilities of pure H_2 and CO in PC, biphasic mixture of PC+dodecane and TMS-systems of PC+dodecene+1,4-dioxane were measured by the absorption method as a function of the gas pressure (1-15 bar) and temperature (298-343 K) in a 300 mL capacity high pressure gas solubility cell (SOLTEQ model BP 22). As shown in Figure 4.1, the equipment consists of a gas mixing vessel and an equilibrium cell, each immersed in a heating jacket. A PTFE coated magnetic stir-bar placed within the cell in conjunction with an external magnet is used to stir the liquid phase inside the cell. Other supporting components include the vacuum pump, thermostat heating bath, liquid feed pump, and instrumentations such as mass flow controllers, pressure and temperature indicators. High accuracy pressure sensors and platinum RTD sensors are used for high accuracy pressure and temperature measurements. Figure 4.2 shows the photograph of the high pressure solubility unit.

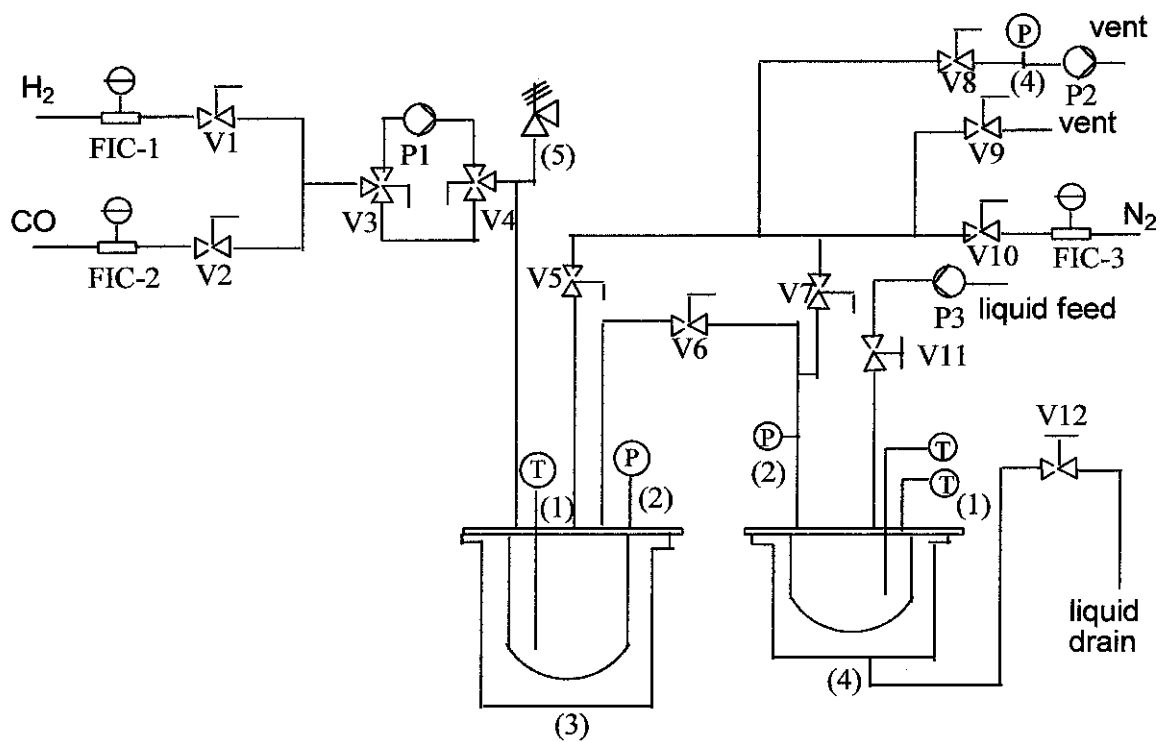


Figure 4.1: Schematic of the high pressure solubility cell unit: 1– thermocouple; 2– pressure transducer; 3– mixing vessel; 4– equilibrium cell; 5- pressure relief valve

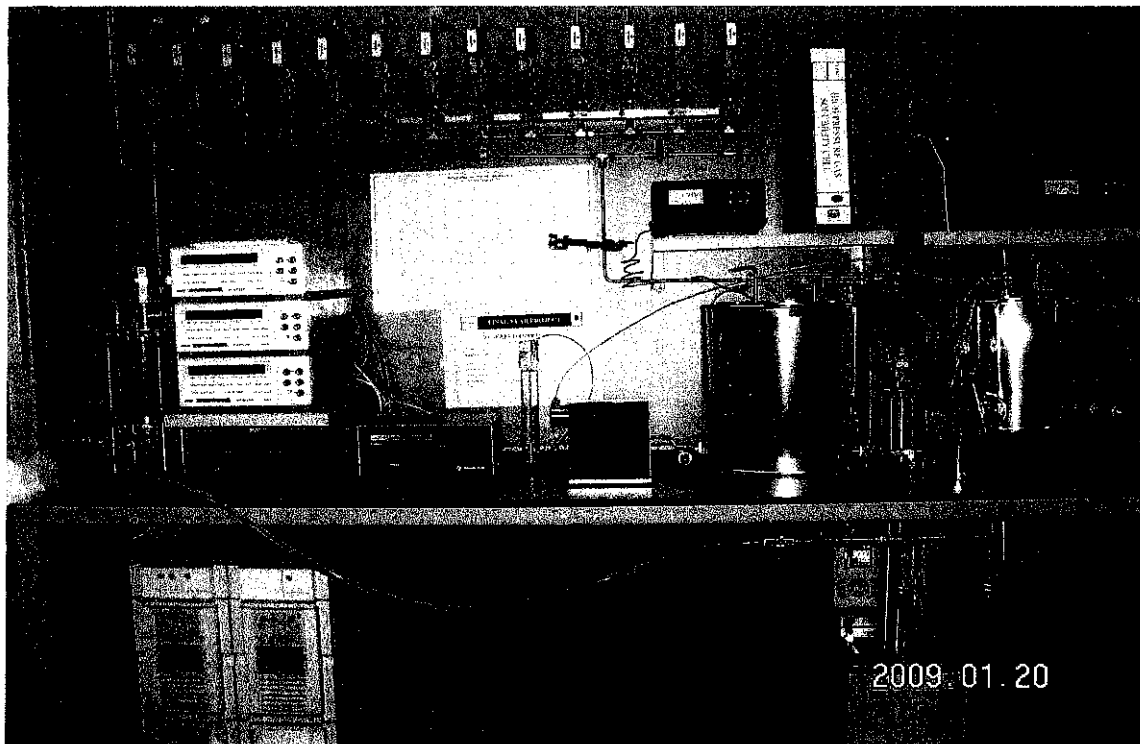


Figure 4.2: High pressure solubility cell unit

4.2.2.1. Pressure Test

After closing all valves, the gas solubility cell was tested for leakage by using SNOOP liquid leak detector (SNOOP, Swagelok). The unit was pressurized with N₂ by opening valves V5, V6 and V10 until the pressure reading reads 6.0 MPa. When visible bubbles were observed, the equipment was de-pressurised before the loose connection was tightened to stop the gas leakage. When the pressure stabilized within 15 minutes, the pressure release valve was set at 3.0 MPa.

4.2.2.2. Purging and Evacuation

The unit was purged with N₂ gas and fully evacuated before carrying out each solubility experiment. Purging was carried out before evacuation to avoid residue gas or liquid from passing through the vacuum pump during evacuation. Both the mixing vessel and the equilibrium cell were purged by allowing N₂ gas to flow through the unit for approximately 10 minutes by setting the flow rate at FIC-3 to 8 NL/min. Opening valves V5, V7 and V8, the mixing vessel and an equilibrium cell were then evacuated using a turbomolecular vacuum pump (Model DCU-200, Pfeiffer Vacuum). A pressure transducer (Model DPI 150, Druck) having a precision of $\pm 1 \times 10^{-4}$ bar was used to measure the pressure in the gas reservoir and in the equilibrium cell.

4.2.2.3. Solubility Experiment

After achieving the specified level of vacuum, which is approximately 1×10^{-3} mbar, the temperature of the heating bath was set at a desired value and the bath circulation was allowed to start. The temperature of the liquid in the mixing cell and equilibrium cell were controlled within ± 0.01 K and the temperature is measured by a digital thermometers (Model 7563, Yokogawa). Using the maximum flow rate, the gas was charged into the mixing vessel by opening the valves at the mass flow controller. Immediately the air drive supply was turned on to the gas booster P1. The gas booster is air driven, and therefore the air pressure was regulated to control the boosting speed. Once the pressure of the mixing vessel has reached the desired pressure, the air drive supply to the gas booster was turned off and valve V4 was switched towards the bypass line. After thermal equilibrium was attained, the pressurized gas in the mixing vessel was

charged into the equilibrium cell up to the desired pressure by slowly opening valve V6. When the pressure and temperature of the mixing vessel and equilibrium cell are equalized, the solvent (200 mL) was then quickly introduced into the cell using a liquid feed pump, P3. The contents were stirred at 1000 rpm for about 1 hr to equilibrate the liquid phase with the gas. A few preliminary experiments showed that this time was sufficient for equilibration. The total pressure change due to absorption was recorded on-line as a function of time till it attained a steady and constant value, indicating saturation of the liquid phase.

From the initial and final pressure readings, the solubility was calculated in mole fraction as:

$$x_2 = \frac{[P_i - (P_f - p^v)]V_g}{RTV_L\rho_L} \quad (4.1)$$

where x_g represents the mole fraction of the solute gas in the liquid phase, P_i and P_f are the initial and final pressure readings in the equilibrium cell; p^v is the vapour pressure of the solvent; V_g and V_L are the volumes of the gas and liquid phases, respectively; R is the gas constant; T is the absolute temperature; and ρ_L is the molar density of the liquid. The volume of the gas in the cell above the liquid is calculated by subtracting the measured volume of the liquid from the total volume of the cell. Within the temperature range of this study, propylene carbonate and dodecane have negligible vapour pressure. The vapour pressure of pure 1,4-dioxane was calculated with the Antoine equation:

$$\log (P/\text{kPa}) = A - B/(C + T/^\circ\text{C}) \quad (4.2)$$

where P is the vapor pressure (kPa), T , the temperature ($^\circ\text{C}$) and A , B and C are constants, which are 6.5564, 1554.679 and 240.337, respectively (Romero et al., 2005). In order to ensure the applicability of the ideal gas law in Equation 4.1, the H_2 and CO fugacity coefficients, were calculated using the Peng-Robinson equation of state (PR EoS)

$$\ln \phi_i^f = \frac{b_i}{b_m}(Z - 1) - \ln(Z - B) - \frac{A}{2B\sqrt{2}}$$

$$\times \left[\frac{2 \sum_j y_j \sqrt{a_i a_j} (1 - k_{ij})}{a_m} - \frac{b_i}{b_m} \right] \ln \frac{Z + (1 + \sqrt{2})B}{Z + (1 - \sqrt{2})B} \quad (4.3)$$

where Z is the compressibility factor and can be written as following:

$$Z^3 - (1 - B)Z^2 + (A - 3B^2 - 2B)Z - (AB - B^2 - B^3) = 0 \quad (4.4)$$

where Z is commonly defined as $Z = (PV/RT)$

To calculate fugacity coefficient, ϕ_i^f using Equation (4.3) or the compressibility factor, Z using Equation (4.4), pure component parameters a_i and b_i were found from Equations (4.5) to (4.9), using critical properties in Table 4.2 where M is the molecular weight (g mol^{-1}), T_c , the critical temperature, P_c , the critical pressure and ω , the acentric factor.

$$\alpha(T_r, \omega) = \left[1 + K_i \left(1 - \sqrt{T_{ri}} \right) \right]^2 \quad (4.5)$$

$$a_i(T) = a_i(T_c) \times \alpha(T_r, \omega) \quad (4.6)$$

where at critical point temperature

$$a_i(T_c) = 0.45724 \frac{R^2 T_{ci}^2}{P_{ci}} \quad (4.7)$$

$$b_i(T_c) = 0.0778 \frac{RT_{ci}}{P_{ci}} \quad (4.8)$$

and

$$K_i = 0.37464 + 1.54226\omega_i - 0.26992\omega_i^2 \quad (4.9)$$

Table 4.2: Critical properties and acentric factors used in the PR EoS

Component	M ($gmol^{-1}$)	T_C (K)	P_C (MPa)	ω	Ref.
H ₂	2.016	32.98	1.293	-0.217	Phiong and Lucien (2002)
CO	28.00	132.9	3.499	0.066	Chapoy (2004)

The value of the hydrogen and carbon monoxide fugacity coefficient, ϕ_i , calculated through the PR EoS is close to one (for example at 343.15 K and 1.5 MPa, $\phi_{H_2} = 0.998$ and $\phi_{CO} = 1.004$). Hence, according to Peng and Robinson (1976), the vapour phase can be considered as an ideal gas. Here it is also assumed that under the equilibrium conditions the amount of dissolved gas in the liquid has negligible contribution to the liquid volume.

4.3. Parametric Study of Reaction Variables and Kinetic Study

In the present work, the synthesis of *n*-nonanal and *n*-tridecanal, two commercially important linear aldehydes, by the hydroformylation reaction of 1-octene and 1-dodecene using a homogeneous catalyst consisting of HRh(PPh₃)₃(CO) and P(OPh)₃ in a TMS-system composed of propylene carbonate, dodecane and 1,4-dioxane was studied. The reaction scheme for hydroformylation of 1-octene is shown in Figure 4.3. In the above context, the specific objectives of this work are to:

- (i) experimentally determine the effects of reaction parameters of the hydroformylation of 1-octene with HRhCO(PPh₃)₃/P(OPh)₃ catalyst in TMS-system of PC/dodecane/1,4-dioxane over a temperature range of 353-383 K,
- (ii) study the kinetics of the hydroformylation of 1-octene and 1-dodecene with the above catalyst and reaction medium,
- (iii) develop empirical as well as mechanistic rate models of the reaction and evaluate the rate parameters by fitting experimental data, and
- (iv) assess the validity and quality of the developed mechanistic rate model by fitting experimental hydroformylation data.

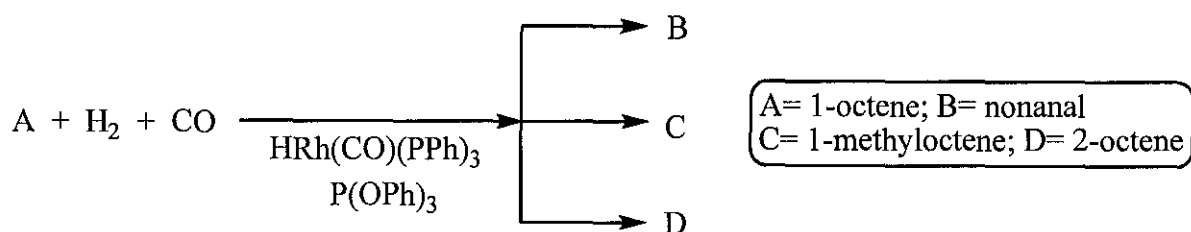


Figure 4.3: Reaction products of hydroformylation of 1-octene

The reaction proceeds via catalytic addition of H and formyl (CHO) groups across the double bond of olefin to give aldehydes. The main steps in the catalytic cycle follow the Heck and Breslow mechanism developed for the cobalt-catalyzed oxo reaction (van Leeuwen, 2004). The kinetics of the reaction has been investigated at three temperatures - 353, 363 and 373 K. The initial rates of hydroformylation were determined under the range of condition shown in Table 4.3. Since the reaction occurs in the liquid phase but two of the reactants are supplied as gas, mass transfer limitation may influence the rate of reaction. This was tested by conducting the reaction at different stirrer speeds under unchanged experimental conditions.

Table 4.3: Range of variables studied in the present work

	1-octene	1-dodecene
Conc. of catalyst (kmolm^{-3})	$8.66 \times 10^{-5} - 6.78 \times 10^{-4}$	$8.66 \times 10^{-5} - 3.46 \times 10^{-4}$
Conc. of 1-olefins (kmolm^{-3})	0.21-4.2	0.20-3.0
P_H (MPa)	0.3-1.5	0.3-1.5
P_{CO} (MPa)	0.3-1.5	0.1-1.5
T (K)	353-383	353-383
Reaction volume (mL)	240	220

Hydroformylation of 1-octene and 1-dodecene were carried out in a 1.8 L stirred high pressure reactor (model: Parr 4843). A schematic and photograph of the experimental set up are shown in Figure 4.4 and Figure 4.5, respectively. The design of the reactor has been taken into account the safety features and sampling considerations such as to avoid syngas leakage and protection against high pressure gas. The experimental work was

carried out at maximum pressure and temperature of 2.5 MPa and 383 K, respectively, therefore the equipment was designed to withstand the above conditions. The top of the reactor was connected tightly to a tree carrying needle valves to secure gas and liquid sampling, pressure release valve and pressure gauge by means of a union using Teflon tape around the threads. The reactor was equipped with an automatic temperature control system, which included an external electric heating jacket and an internal cooling loop. A pressure transducer-monitor system with high precision was also connected to the reactor for on-line measurement of reactor pressure in the course of semi-batch hydroformylation reaction.

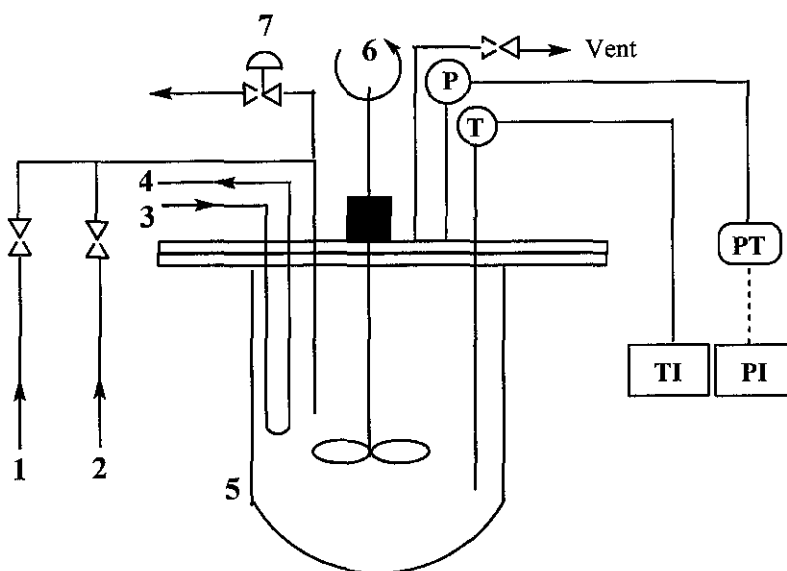


Figure 4.4: Schematic of the experimental setup: (1) nitrogen; (2) syngas (CO/H_2); (3) cooling water in; (4) cooling water out; (5) high pressure reactor; (6) stirrer; (7) sampling valve; (T) thermocouple; (P) pressure gauge; (PT) pressure transducer; (PI) pressure indicator; (TI) temperature indicator.



Figure 4.5: Parr high pressure reactor

4.3.1. Pressure Test

Since the gaseous reactant, carbon monoxide is a highly toxic gas with a threshold limit value (TLV) of 25 ppm, the pressure test was performed regularly to verify leak-tightness of piping and components of the reactor (Silk, 1975). After closing all valves, the reactor was tested for leakage by using a liquid leak detector (SNOOP, Swagelok). The reactor was pressurized with N_2 until the pressure reading reads 7.0 MPa. When visible bubbles were observed, the equipment was de-pressurised before the loose connection was tightened to stop the gas leakage. When the pressure stabilized within 15 minutes, the pressure release valve was set at 5.0 MPa. A portable CO gas detector was also placed adjacent to the reactor, for detecting CO leaks.

4.3.2. Reaction and Kinetic Measurement

The feed mixture with the catalyst (220 mL) was taken in the PTFE holding vessel within the preheated reactor. Before starting the run, the reactor was purged with nitrogen and syngas successively, and then adjusted to the desired temperature. It was then pressurized with a mixture of CO and H₂ to a desired total pressure gradually in avoiding the feed mixture from spilling out from the liner. The total pressure was monitored regularly and maintained constant during the whole run by using the pressure regulator. When over-pressure was observed, some gas was released by opening the venting valve. The stirrer was set at 450 rpm while the reaction continued. Liquid samples (each less than 1 mL) were withdrawn at regular time intervals to follow the progress of the reaction. The reaction was stopped quickly by cooling down the mixture to the room temperature. The gas was vented out and the biphasic mixture was left to separate overnight (24 hr) using a separatory funnel. The recovery of the catalyst and product was determined by collecting samples from the nonpolar and polar phases. The analysis of reactants and products was carried out by a gas chromatographic method. Each type of experiment was repeated three times to check for reproducibility. Measurements are, in general, reproducible within a maximum of 10 % but often within a few per cent.

4.3.3. Solubility Measurement

The solubilities of pure H₂ and CO in TMS-systems of PC/dodecene/1,4-dioxane with composition of 0.30/0.10/0.60 were measured by the absorption method at different pressures (0.1-2.5 MPa) and temperatures (353-373 K). Requisite volume of the solvent only was taken in the reactor which was then quickly pressurized. The contents were stirred at 450 rpm for about 1 hr to equilibrate the liquid phase with the gas. A few preliminary experiments showed that this time was sufficient for equilibration. The total pressure change due to absorption was recorded on-line as a function of time till it attained a steady and constant value, indicating saturation of the liquid phase. From the initial and final pressure readings, the solubility was calculated in kmolm⁻³ as:

$$C_L = \frac{[P_i - (P_f - p^v)]V_g}{RTV_L} \quad (4.10)$$

where C_L represents the concentration of the solute gas in the liquid phase, P_i and P_f are the initial and final pressure readings in the reactor; p^v is the vapour pressure of the solvent; V_g and V_L are the volumes of the gas and liquid phases, respectively. In order to ensure the applicability of the ideal gas law in Eq. (4.10), the H_2 and CO fugacity coefficients, were calculated using the Peng-Robinson equation of state as outlined in section 4.2.2.3. The reproducibility of the experimental measurement was checked by repeating a particular experiment 3 times. It was observed that the error in solubility values obtained was within 2-3 %.

4.4. Liquid-liquid Equilibria

Four different temperatures (298.15, 313.15, 333.15 and 353.15 K) at atmospheric pressure were selected to study the ternary equilibrium system of the TMS- system (PC+1,4-dioxane+dodecane) in order to obtain the binodal (solubility) curves and tie-lines. The binodal (solubility) curves were determined by the cloud point method which is outlined in Section 4.2.1. The major central part of the solubility curves was obtained by titrating heterogeneous mixtures of PC and dodecane (1.0 g) with 1,4-dioxane until the turbidity has disappeared. End-point determinations of the tie-lines of PC+dodecane+1,4-dioxane were based on the independent analysis of the conjugate phases that were regarded as being in equilibrium. For this purpose, 1.5 g mixtures of known masses of the component lying within the heterogeneous phase were introduced into a sealed glass tube and were stirred vigorously by a magnetic stirrer for at least 5 hr and then left for 5 hr to settle down into raffinate (polar phase) and extract (nonpolar) layers. After phase equilibrium has been reached, samples of two layers were withdrawn with a syringe and their compositions were analyzed gas chromatographically. The $HRh(CO)(PPh_3)_3$ catalyst concentration was analyzed by Atomic Absorption Spectrophotometer (AAS) with air-acetylene flame. All experiments were repeated at least two times as a check for accuracy.

4.4.1. Distribution Coefficient

The distribution coefficients for 1-octene, nonanal, triphenylphosphite and $\text{HRh}(\text{CO})(\text{PPh}_3)_3$ catalyst in the ternary systems were obtained at temperature of 298 K and 308 K. End-point determinations of the tie-lines of PC+dodecane+1,4-dioxane+1-octene, PC+dodecane+1,4-dioxane+nonanal, PC+dodecane+1,4-dioxane+1-octene+nonanal, PC+dodecane+1,4-dioxane+ $\text{HRh}(\text{CO})(\text{PPh}_3)_3$, PC+dodecane+1,4-dioxane+1-octene+nonanal+triphenylphosphite+ $\text{HRh}(\text{CO})(\text{PPh}_3)_3$ were determined by the same procedure as described for the TMS- system.

4.5. Analytical Techniques

4.5.1. Gas Chromatography

The reaction products were determined by Shimadzu GC 2010 using BPX5 capillary column and flame ionization detector. The length and inner diameter of the column and the film thickness was 30 m, 0.25 mm and 0.25 μm , respectively. The column used is a non polar column, so the polar compounds are eluted quicker than non polar compound. Since the analysis involved non-polar and polar compounds thus, the polarity of the solvents would affect the retention time. The non-polar components in a mixture are separated according to their boiling points with a substance of lower boiling point being detected first. Helium was used as a carrier gas. For the separation of the organic products a heating program was applied. The initial temperature of the column was adjusted to 323 K and kept constant for 2 min, then the column was heated with a rate of 293 K/min until 523 K and kept again constant at this temperature for 5 min. Products were identified by comparison of the retention times and spectral characteristics with authentic standard samples. Figures 4.4 and 4.5 show GC signal for hydroformylation of 1-octene and 1-dodecene, respectively.

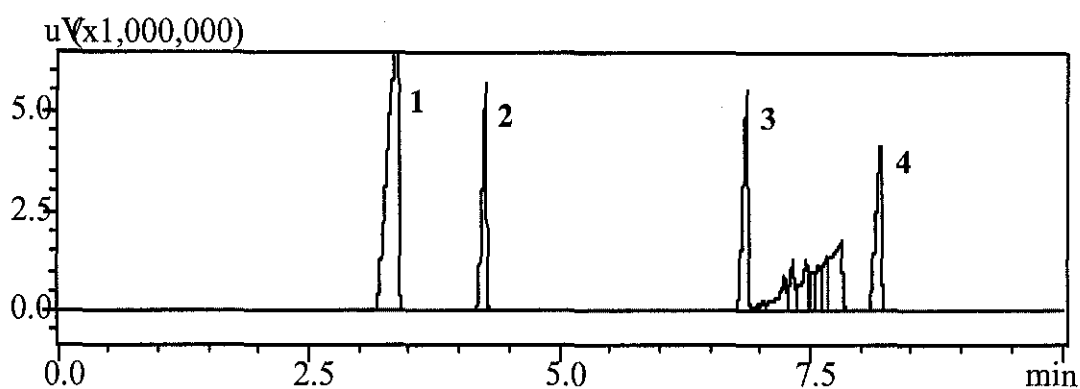


Figure 4.6: GC signal for hydroformylation of 1-octene (1: 1,4-dioxane, 2: 1-octene, 3: dodecane, 4: nonanal).

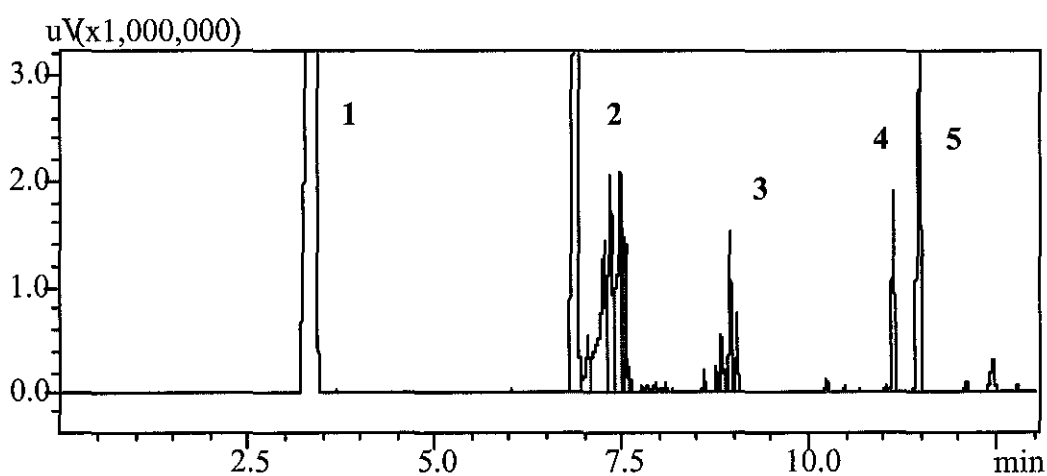


Figure 4.7: GC signal for hydroformylation of 1-dodecene (1: 1,4-dioxane, 2: dodecane, 3: 1-dodecene, 4: 2-methyldodecanal, 5: tridecanal)

4.5.2. Atomic Absorption Spectroscopy

Rhodium concentrations in both polar and non polar rich phases were determined after phase separation. Analysis was carried out by Hitachi Z5000. The measurement conditions were as follow: 343.5 nm wavelength, 0.2 nm gap, 0.4 air/acetylene ratio. The calibration curve of the Rh standard is presented in Appendix H.

CHAPTER 5

RESULTS AND DISCUSSION

This chapter presents the results and discussion of the experimental work conducted. The first section focuses on the solubility of gaseous reactants – CO and H₂ – in the individual components of the solvent as well as in their mixtures, and provides insight on how the different properties of the various gases and the solvent affect the solubility. Section 5.2 discusses the effect of reaction variables on the selectivity, conversion and yield of total aldehyde. Subsequently, section 5.3 presents the kinetics and modeling of the hydroformylation reaction of 1-octene and 1-dodecene using a homogeneous catalyst consisting of HRh(PPh₃)₃(CO) and P(OPh)₃ in a TMS- system composed of PC, dodecane and 1,4-dioxane. Finally, Section 5.4 provides the liquid-liquid equilibrium (LLE) behavior of the TMS system as well as the distribution of the reaction species in the non-polar and polar phases.

5.1. Development of the TMS- System

5.1.1. TMS-systems: PC+Dodecane+1,4-Dioxane

The phase diagram of this solvent system obtained by cloud titrations at 298, 353 and 373 K are shown in Figure 5.1. The isothermal 3-component phase diagram (PC+dodecane+1,4-dioxane) shows a closed loop at all studied temperature. The big miscibility gap of this solvent system facilitated a good operating range for the hydroformylation. The miscibility gap or heterogeneous sphere of the system seems to decrease with increasing temperature. The possible operating points are defined by the area between the two binodal curves at the temperatures of 298 K and 373 K. This point is located in the single-phase regime when the reaction temperature is above the phase separation temperature. Cooling down the reaction mixture to room temperature leads to the separation of the single phase into two phases. Therefore, the composition of the TMS-system selected for the solubility study was 1.31/1.29/7.40 weight ratio (point 1 in Figure 5.1). At this composition, the ternary mixture dissolved into a single phase at temperature range of 298-343 K with the highest amount of 1,4-dioxane.

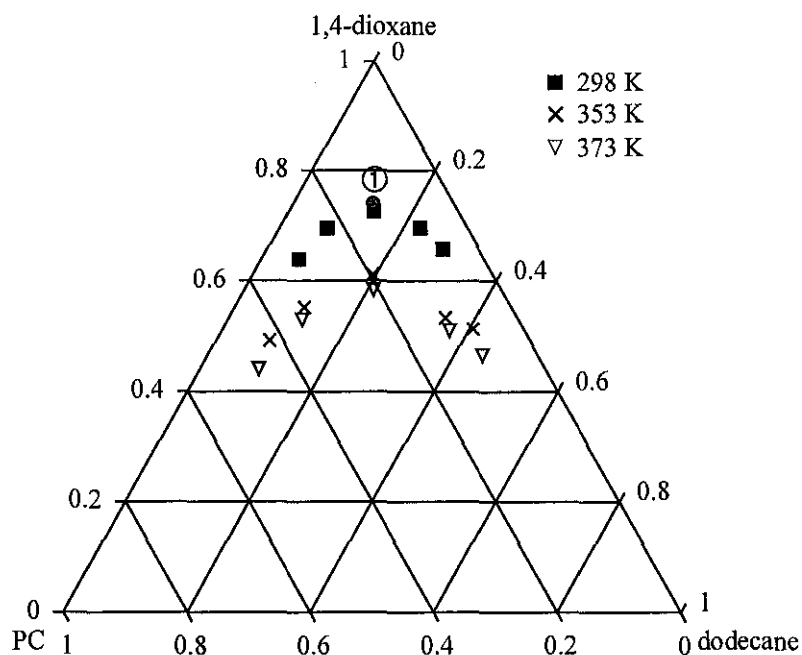


Figure 5.1: Phase diagram of the solvent system PC+dodecane+1,4-dioxane

5.1.2. Solubility Data

Figure 5.2 shows a plot of pressure vs. the mole fraction solubility of CO and H₂ in PC, biphasic PC+dodecane mixture and TMS-system of PC+dodecane+1,4-dioxane. Within the temperature and pressure ranges of this study, the equilibrium pressure was found to be almost linear in the liquid phase mole fraction for all the systems, conforming to Henry's law. Therefore the data are presented as equilibrium liquid phase mole fractions at 0.10325 MPa (1 atm) pressure of the gas. PC and TMS-systems have a considerably higher affinity for CO and H₂ compared to the biphasic solvent mixture. Figure 5.2 also shows that the TMS-system, particularly, 1,4-dioxane, has a higher affinity for carbon monoxide compared to hydrogen, whereas hydrogen is more soluble in PC. The biphasic mixture which contains higher amount of non-polar dodecane contributed to the lower solubility of CO and H₂ gas. Furthermore, the solubility of carbon monoxide in the three solvent systems does not vary significantly compared to hydrogen. Typical solubility data at 298 K for the three solvent systems are shown in Figure 5.2.

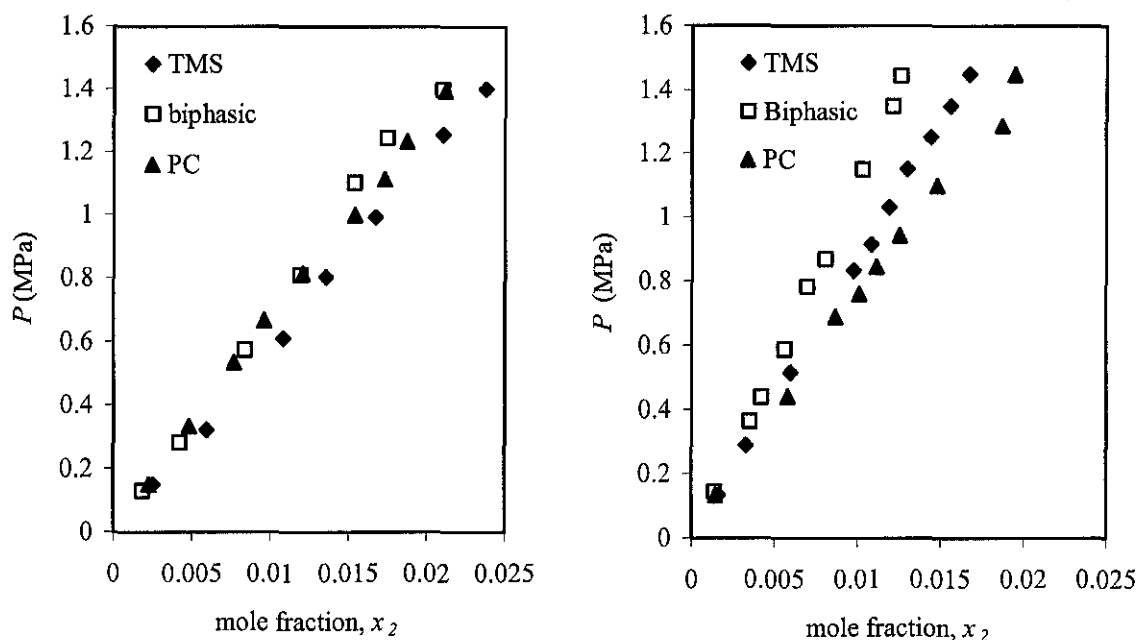


Figure 5.2: Experimental solubility of gases in PC, biphasic PC+dodecane mixture (1:1) and TMS-systems of PC+dodecane+1,4-dioxane (1.31:1.29:7.40) at 298 K. (A) CO; (B) H₂.

As it is seen in Figure 5.2 all liquids exhibit a relatively higher affinity for CO compared to H₂, which is an expected behavior since solubility increases with increasing molecular weight of the solute. The attractive forces between the gas and solvent molecules involved in this study are mainly of the London dispersion type, which increases with increasing size and mass of the gas molecules (Fogg and Gerrard, 1991). In Figure 5.3, the solubility of CO and H₂ in the solvent systems increases moderately with respect to temperature over the range of operating conditions, except for CO-propylene carbonate system. According to Le Chatelier's principle, an increase in the solubility with temperature indicates that the solution process is endothermic, and that the solubility is driven by the increase of disorder in the system. This phenomenon is common for gases having low solubilities (Prausnitz et al., 1999). Similar results have been reported for other oxygen containing solvents (Still et al., 2006; Deshpande et al., 1996; Fogg and Gerrard, 1991) and nonpolar solvents (Nair et al., 1999; Divekar et al., 1993; Miller et al., 1990).

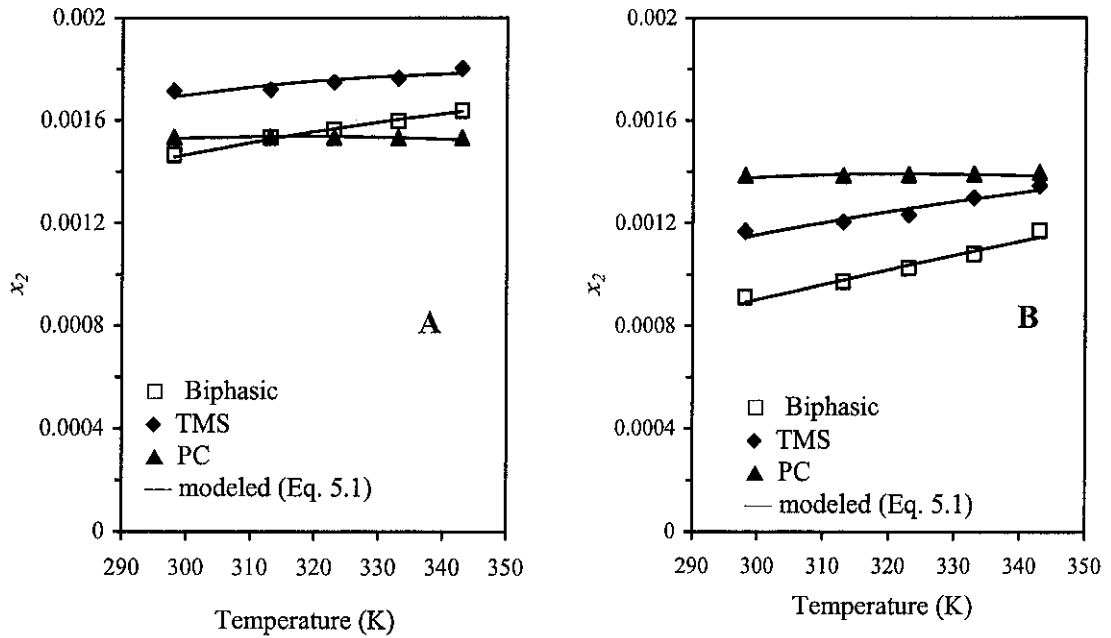


Figure 5.3: Experimental and predicted solubility of gases in PC, biphasic PC+dodecane mixture and TMS-systems of PC+dodecane+1,4-dioxane (1.31:1.29:7.40) at a partial pressure of 101.3 kPa. (A) CO; (B) H₂.

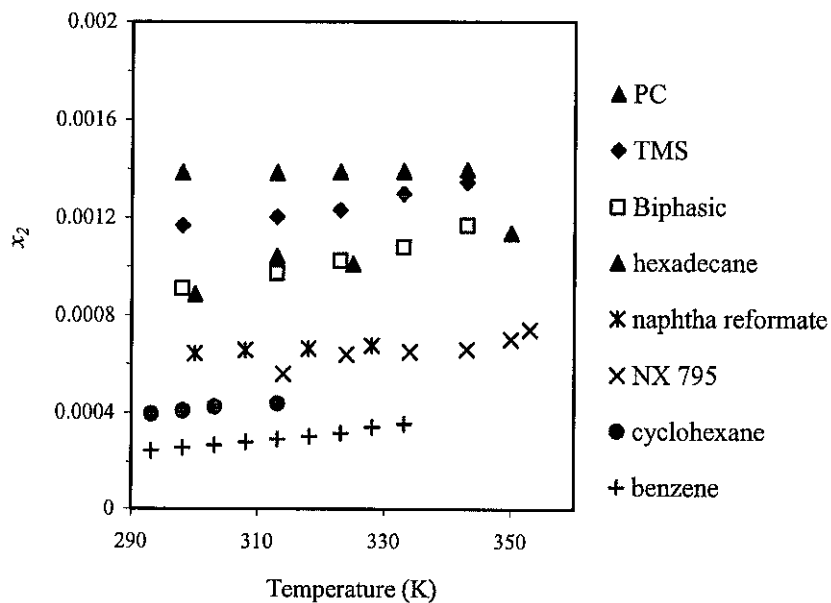


Figure 5.4: Experimental solubilities of H₂ at partial pressure of 101.3 kPa as a function of temperature. References to experimental data: NX 795, Still et al. (2006); naphtha, Fahim and Elkilani, (1991); *n*-hexadecane, Hu and Xu, (1985); cyclohexane, Hu and Xu, (1985); benzene, Hu and Xu, (1985).

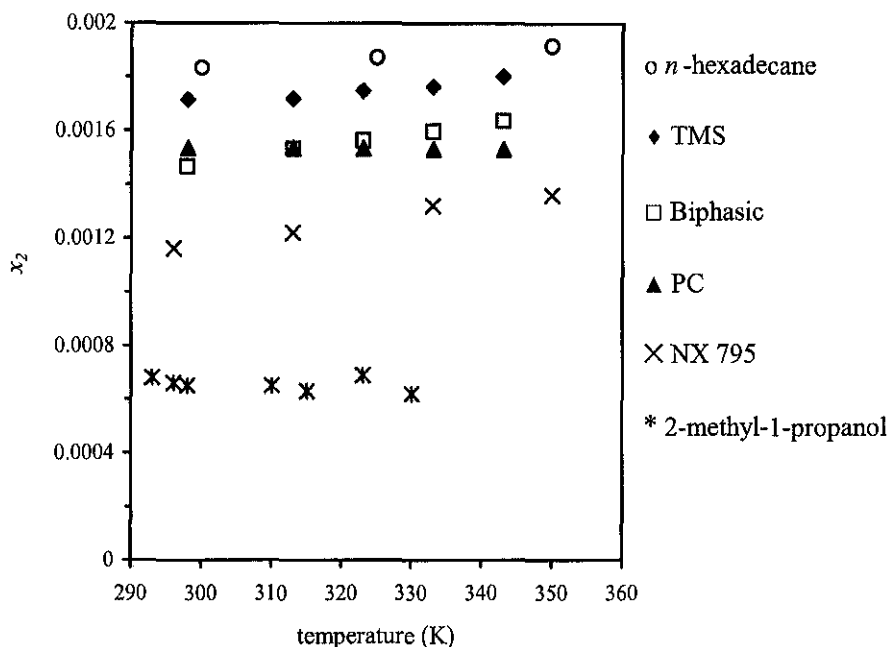


Figure 5.5: Experimental solubilities of CO at partial pressure of 101.3 kPa as a function of temperature. References to experimental data: NX 795, Still et al. (2006); *n*-hexadecane, Hu and Xu, (1985); 2-methyl-1-propanol, Sander et al., (1983).

Figures 5.4 and 5.5 compares the solubility of H₂ and CO from the current work with other organic solvents in open literature. The most notable attribute seen in these two figures is that CO is more soluble in non-polar solvent compared to H₂. Anthony (2004) reported that CO solubilities are not governed by its polarizability, even though CO has significant quadrupole moments. A reasonable explanation for this behaviour was not provided. On the other hand, the solubility of H₂ is greatest in PC. The large dipole moment of PC as well as specific interactions between H₂ and the carboxyl group are likely the governing forces leading to such high solubilities. The biphasic mixtures of PC+dodecane and *n*-hexadecane have basically the same solubility, although the biphasic mixture appears more soluble at higher temperature. The solubility of H₂ in TMS-systems of PC+dodecene+1,4-dioxane is higher compared to other non-polar solvents (naphtha, *n*-hexadecane, cyclohexane and benzene) and polar solvent of 2,2,4-trimethyl-1,3-pentanediolmono(2-methylpropanoate) (NX 795). This suggests that the interactions governing the higher solubility of H₂ in TMS-systems are influenced by the presence of

the ether group of 1,4-dioxane. Within the studied temperature range the solubility of H₂ increases with temperature in all cases. The maximum solubility (x_2) values for CO and H₂ in TMS-system are 0.0210 and 0.0172, respectively at temperature of 343 K. The TMS-system also shows high affinity for CO and H₂, which is comparable to the single phase propylene carbonate. The solubility data of the present work are compiled in Appendix G.

5.1.3. Empirical Modeling

The solubility data were fitted to the empirical equation (Fogg and Gerrard, 1991) at 1 atm pressure using the following equation,

$$\ln x_2 = A + \frac{B}{T} + C \ln T \quad (5.1)$$

where x_2 represents the mole fraction of the solute gas in the liquid phase, T is the absolute temperature and A , B and C are empirical constants. The accuracy of the empirical model is given by R^2 that quantifies the goodness of fit and was calculated as follows:

$$R^2 = 1.0 - \frac{\sum (y_{\text{expt}} - y_{\text{pred}})^2}{\sum (y_{\text{expt}} - \bar{y}_{\text{expt}})^2} \quad (5.2)$$

where y_{expt} is the experimental value, y_{pred} is the predicted value and \bar{y}_{expt} is the mean of the experimental values. Plots of experimental and predicted solubility versus temperature are shown in Figure 5.3. It is found that the logarithmic empirical model is able to describe the experimental data with good accuracy over the whole range of the operating pressure and temperature except for H₂-PC and CO-PC systems. Table 5.1 summarizes the values of the parameters A , B and C of Equation (5.1) and the parameter R^2 . Still et al. (2006) also reported a good fit of Equation (5.1) for their solubility data on H₂-CO-NX795 system. The values of the optimized parameters are consistent with that reported in the literature. (Still et al., 2006). The empirical model cannot be used to explain the behavior of a system. Nevertheless, such a model can be very useful to

predict the solubility within limited ranges of pressure and temperature. Thermodynamic models, on the other hand, are expectedly more robust and flexible than purely empirical models. Thermodynamic models also provide insights into the system being modeled.

Table 5.1: Parameters in Equation (5.1) for H₂ and CO solubilities at a partial pressure and temperature of 101.3 kPa and 298-343 K, respectively.

Gas-Liquid System	<i>A</i>	<i>B</i>	<i>C</i>	<i>R</i> ²
CO-PC	0.129	-300.0	-0.9833	0.802
CO-biphasic	10.000	-1000.0	-2.3128	0.992
CO-TMS systems	12.949	-1015.0	-2.7952	0.995
CO-NX 795	*17.413	*-1398.4	*-3.4190	*0.985
H ₂ -PC	17.486	-1200.0	-3.5218	0.750
H ₂ -biphasic	4.994	-1050.0	-1.4912	0.998
H ₂ -TMS systems	9.008	-1025.0	-2.1659	0.987
H ₂ -NX 795	*10.972	*-1466.0	*-2.3931	*0.955

*Values of the parameters *A*, *B*, *C* and *R*² reported by Still et al. (2006) for H₂-CO-NX 795 system

5.1.4. Thermodynamic modeling

The regular solution theory (RST)-based model and the modified *UNI*versal *F*unctional *A*ctivity Coefficient (UNIFAC) model are used to correlate and interpret the experimental solubility data. The regular solution model predicts activity coefficients from solubility parameters and the UNIFAC model uses the functional groups present on the molecules that make up the liquid mixture to calculate activity coefficients. By utilising interactions for each of the functional groups present on the molecules, as well as some binary interaction coefficients, the activity of each of the solutions can be calculated. The important advantage of RST is that its parameter is calculable without resorting to activity coefficient measurements. However, the parameters obtained may not be as accurate as those fitted to experimental data. On the other hand, the main advantages of the modified UNIFAC method are a better description of the real behavior in the dilute

region and that it can be applied more reliably for systems involving molecules of very different in size (Gmehling et al., 1993). A comparison is then made of the prediction accuracy of the models.

5.1.4.1. Prediction of H₂ and CO Solubility by the RST- based Model

A regular solution is a solution that diverges from the behavior of an ideal solution only moderately. In contrast to ideal solutions, regular solutions possess an enthalpy of mixing and the volumes are no longer strictly additive but must be calculated from the partial molar volumes that are a function of x . Two major assumptions were made in proposing the Regular Solution Theory (RST):

- i. The change in entropy and volume of mixing were considered to be negligible,
- ii. The molecular interaction was primarily due to London Dispersion Forces (LDF).

Solubility predictions of highly polar compounds based on solubility parameter difference were inconsistent due to the second assumption. The experimental solubility data for H₂ and CO in the three solvent systems were compared with the theoretical predictions using the equations suggested by Prausnitz and Shair (1961) and Yen and McKetta (1962). Since modeling according to the RST is essentially limited to dissolution of nonpolar gases in nonpolar, non-associating solvents, the modification to the RST by Yen and McKetta (Still et al., 2006) was applied in order to extend the RST to polar solvents, such as PC and 1,4-dioxane. The activity models are presented below in the way they were used for the solubility calculations:

RST:

$$\frac{1}{x_2} = \frac{f_2^L}{f_2^G} \exp \left(\frac{v_2 (\delta_1 + \delta_2)^2 \phi_1^2}{RT} \right) \quad (5.3)$$

RST with Yen and McKetta correction:

$$\frac{1}{x_2} = \frac{f_2^L}{f_2^G} \exp\left(\frac{v_2 (\delta_1 + \delta_2)^2 \phi_1^2}{RT} + \ln \frac{\phi_2}{x_2} + 1 - \frac{\phi_2}{x_2}\right) \quad (5.4)$$

In Equations (5.3) and (5.4), the subscripts 2 and 1 represent the gas and liquid (solvent), respectively; x_2 is the mole fraction of the dissolved solute in the solvent at atmospheric pressure (0.10325 MPa); f_2^G (MPa) and f_2^L (MPa) are the fugacities of pure gas and hypothetical liquid solute at atmospheric pressure, respectively; ϕ_1 and ϕ_2 are the volume fraction of solvent and gas, respectively; v_2 ($\text{m}^3 \cdot \text{mol}^{-1}$) is the molar volume of gas, and δ_1 and δ_2 are the solubility parameters ($\text{J} \cdot \text{m}^{-3}$)^{1/2} for the solvent and the solute gas, respectively, R is the gas constant and T is the absolute temperature. The regular solution theory also states that the solubility parameters and molar volume of solutes are independent of temperature. The δ -values were obtained from Katayama and Nitta (Purwanto et al., 1996). The quantity f_2^L was determined according to Prausnitz and Shair (1961).

The solubility parameter (δ_1) for PC, dodecane and 1,4-dioxane were calculated from the heat of vaporization as proposed by Hildebrand and Scott (1948)

$$\delta_1 = (\Delta H_v - RT / v_2)^{1/2} \quad (5.5)$$

where ΔH_v represents the heat of vaporization and v_2 the molar volume of the solvent. The heat of vaporization is generally reported at the normal boiling temperature (T_b). The correlation proposed by Reid and Prausnitz (1987) was used to calculate ΔH_v at the five chosen temperatures of study:

$$\Delta H_{v,T} = \Delta H_{v,T_b} \left(\frac{1 - T_r}{1 - (T_r)_{T_b}} \right)^{0.375} \quad T_r = T / T_c \quad \text{and} \quad (T_r)_{T_b} = T_b / T_c \quad (5.6)$$

where T_c is the critical temperature of the solvent. The solubilities of CO and H₂ in pure PC, dodecane and 1,4-dioxane were further used for calculating the solubilities of these

gases in a mixture of solvents by using the method proposed by Prausnitz and Shair (1961), and given by the following expression:

$$\frac{1}{x_2} = \frac{f_2^L}{f_2^G} \exp \left(\frac{v_2 (\delta_2 - \bar{\delta})^2}{RT} \right) \quad (5.7)$$

where $\bar{\delta}$ is the average solubility parameter defined as

$$\bar{\delta} = \sum_i \phi_i \delta_i \quad (5.8)$$

The liquid molar volumes, v_2 and solubility parameters δ used in the modeling are listed in Table 5.2.

Table 5.2: Parameters for modeling with RST model

Compound	v_2 (cm ³ mol ⁻¹)	δ (MPa ^{1/2})	T_c (K)	P_c (MPa)
	at 25 °C	at 25 °C		
Carbon monoxide	32.1 ^a	7.38 ^b	132.92 ^f	3.499 ^f
Hydrogen	37.3 ^a	7.84 ^b	33.18 ^f	1.300 ^f
Propylene carbonate	84.82 ^c	21.30 ^d	778.10 ^e	-
Dodecane	84.07 ^c	17.91 ^d	658.30 ^f	-
1,4-Dioxane	226.82 ^c	21.33 ^d	588.15 ^f	-

Not required in modeling; ^aPurwanto et al., (1996); ^bYen and McKetta (1962); ^cCalculated from molecular mass and density; ^dCalculated from Eq. (5.5); ^eKolář et al., (2005); ^fWashburn (2003)

5.1.4.2. Prediction of H₂ and CO Solubility by the Modified UNIFAC Group Contribution Model

The UNIFAC group-contribution model has been extensively used to predict activity coefficients for nonelectrolytic liquid mixtures. The method has become a reliable tool for the prediction of vapor-liquid equilibrium (VLE) as well as gas-liquid equilibrium (GLE) data (Gmehling et al., 1982; Hartounian and Allen, 1988; Fahim and Elkilani, 1991) for systems for which little or no experimental information is available. UNIFAC

assumes that a physical property of the fluid is the sum of the contributions made by the functional groups of the molecule. In the model, molecules are broken down into functional groups and the mixture is treated as a mixture of groups. The properties of each group are assumed to be independent of the rest of the molecule to which it is attached.

For a gas (component 2) dissolved in a solvent or solvent mixture (component 1) the gas phase fugacity becomes equal to the liquid phase fugacity at equilibrium.

$$f_2^G = f_2^L \quad (5.9)$$

The gas phase fugacity coefficients for H₂ and CO calculated using the Peng-Robinson equation of state (PR-EoS) and were found to be close to unity and the gas-phase was assumed ideal.

$$f_2^G = y_2 P \quad (5.10)$$

where P is the total pressure and y_2 is the mole fraction of gas in the gas phase. For non-volatile liquids such as dodecane and propylene carbonate, the mole fraction of the solute in the gas phase is unity. Liquid phase non-ideality can be taken into account through the activity coefficient. The fugacity of the solute in a solution can be written as

$$f_2^L = x_2 \gamma_2 f_2^0 \quad (5.11)$$

where x_2 and γ_2 are the mole fraction and activity coefficient of the gas in the solution, while f_2^0 represents the fugacity of a hypothetical pure liquid whenever the temperature is greater than the critical temperature of the gas. The quantity f_2^0 cannot be determined experimentally (Wilhelm, 1986). So the expression may be modified in terms of the Henry's law constant for the solute in a 'reference solvent' as follows (Sander et al., 1983):

$$f_2^0 = H_{2,r} / \gamma_{2,r}^\infty \quad (5.12)$$

where $\gamma_{2,r}^\infty$ is the infinite dilution activity coefficient of the gas in the reference solvent and $H_{2,r}$ is the Henry's law constant of the gas in the reference solvent. *n*-Propanol was selected as the reference solvent in this work. Equations (5.9) to (5.12) are used to obtain the mole fraction of the solute gas in the solution.

$$x_2 = \frac{y_2 P}{H_{2,r} \gamma_{2,r}^\infty} \quad (5.13)$$

The activity coefficients may be determined by the UNIFAC group contribution method. Since UNIFAC model deals with functional groups present in the components, the application of the model requires all the interaction parameters between the groups present in the liquid and gas phase as function of temperature. Two modifications of UNIFAC have been used in this work. The first modification expresses interaction parameters as a linear function of temperature given by Equation (5.14). A constant enthalpy of solution is assumed.

$$a_{nm} = A_{nm} + B_{nm}(T - 273.15) \quad (5.14)$$

The second modification, suggested by Kikic et al. (see Fahim and Elkilani, 1991), is concerned with the combinatorial activity coefficient according to the following expression

$$\ln \gamma_i^c = \frac{\ln \psi_i}{(x_i + 1 - \psi_i)/x_i} - 5q_i \frac{\ln \phi_i}{(\theta_i + 1 - \phi_i)/\theta_i} \quad (5.15)$$

where

$$\psi_i = \frac{x_i r_i^{2/3}}{\sum_j x_j r_j^{2/3}}; \quad \phi_i = \frac{x_i r_i}{\sum_j x_j r_j} \quad ; \quad \theta_i = \frac{x_i q_i}{\sum_j x_j q_j} \quad (5.16)$$

The van der Waals relative volume and surface of the components (*r* and *q*), needed for UNIFAC calculations, are listed in Table 5.3.

Table 5.3: UNIFAC parameters r and q of the components

Compound	r	q	References
Carbon monoxide	2.094	2.120	Li et al., 1997
Hydrogen	0.832	1.141	Li et al., 1997
Propylene carbonate	3.282	2.736	Ali et al., 2003
Dodecane	17.092	14.192	Sander et al., 1983
1,4-Dioxane	3.185	2.640	Bandrés et al., 2007

However, the UNIFAC parameters for the interaction between H₂, CO and the functional groups present in the solvents (PC and 1,4-dioxane) as a function of temperature are not available in the literature. Therefore, it has been necessary to estimate these parameters before the suitability of the model can be tested. These parameters for the systems studied have been estimated by using one-half of the experimental solubility data set. In fact, the alternate data points of gas solubility (x_2 against pressure) were used for UNIFAC parameter estimation and the rest were used to test the applicability of the model. The Henry's law constant for hydrogen and carbon monoxide in the reference solvent (n -propanol), $H_{2,r}$, were calculated (Sander et al., 1983) and subsequently the ratio $(\gamma_i/\gamma_{i,r}^\infty)_{\text{exp}}$ was calculated from Equation (5.13). The following objective function was used to minimize the errors in the estimation of UNIFAC interaction parameters between the gas (2) and the functional group

$$\Phi_{\min} = \sum_n [\ln(\gamma_i/\gamma_{i,r}^\infty)_{\text{exp}} - \ln(\gamma_i/\gamma_{i,r}^\infty)_{\text{calc}}]^2 \quad (5.17)$$

where Φ_{\min} is the objective function to be minimized, n is the number of data points and γ_i is the activity coefficient of the solute gas calculated by using modified UNIFAC. By using the new predicted interaction parameters presented in Table 5.4, the gas solubility in liquid and liquid mixtures can be calculated from Equation (5.13). The quality of the UNIFAC correlation, obtained as a result of the parameter regression, was also compared with the remaining data set.

Table 5.4: Modified UNIFAC group interaction parameters for Equation (5.14).

a_{nm}	A_{nm}	B_{nm}
$a_{CO,PC}$	-339.4	-1.24
$a_{PC,CO}$	858.6	1.86
$a_{CO,dioxane}$	-363.1	1.45
$a_{dioxane,CO}$	490.6	6.37
$a_{H_2,PC}$	-440.1	0.57
a_{PC,H_2}	1201.9	-3.96
$a_{H_2,dioxane}$	-1747.5	6.00
$a_{dioxane,H_2}$	300.0	-3.47

5.1.3.3. Results of the Thermodynamic Modeling

The experimental and predicted solubilities based on the RST and UNIFAC model are plotted and compared in Figures 5.6-5.8. As Figures 5.6, 5.7 and 5.8 displayed convincingly, the UNIFAC activity coefficient model leads to the best description of the experimental results. The mean relative deviation between experimental and predicted mole fraction solubilities is not more than 7.8 %. The RST and UNIFAC predictions for H_2 in all three solvent systems were satisfactory with an average error 8.2 % and 5.8 %, respectively. UNIFAC also gave a fairly good prediction of the solubilities of CO in the three systems studied with an average deviations of 7.2 %. However, the RST based predictions for CO in pure PC and binary mixture PC/dodecane were found to agree within ± 6.7 %, except for the tertiary TMS (PC+dodecane+1,4-dioxane) system which predicted with a maximum error of 14.8 %. This suggests that the regular-solution assumption, whereby the change in entropy and volume of mixing were considered to be negligible cannot be applied to the tertiary multi-component TMS system due to the large differences in size or molar volume between components. Still et al. (2005) and Cuevas et al. (1995) incorporated the Flory-Huggins entropy of mixing into the RST model and good agreement is observed with experimental data. In addition the RST based model did not give as good description compared to UNIFAC model, which is most likely due to the polarity of CO and the polarity of PC and 1,4-dioxane.

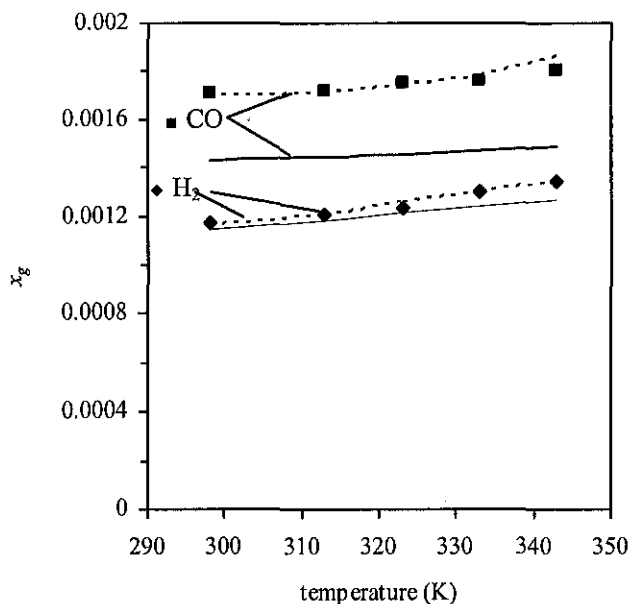


Figure 5.6: Solubility of CO and H₂ in TMS-systems PC+dodecane+1,4-dioxane at a partial pressure of 101.3 kPa. Experimental (■ ◆), modeled with regular solution theory (RST) with Yen and McKetta extension for polar solvent (—), and UNIFAC model (---).

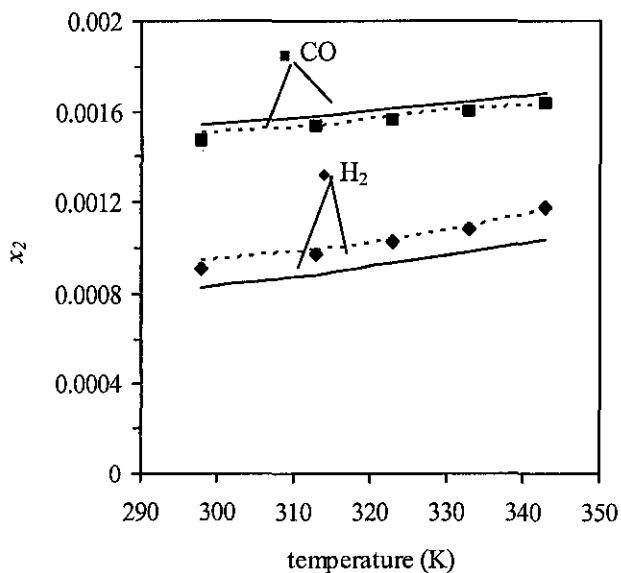


Figure 5.7: Solubility of CO and H₂ in biphasic PC+dodecane mixture at partial pressure of 101.3 kPa. Experimental (■ ◆), modeled with regular solution theory (RST) with Yen and McKetta extension for polar solvent (—), and UNIFAC model (---).

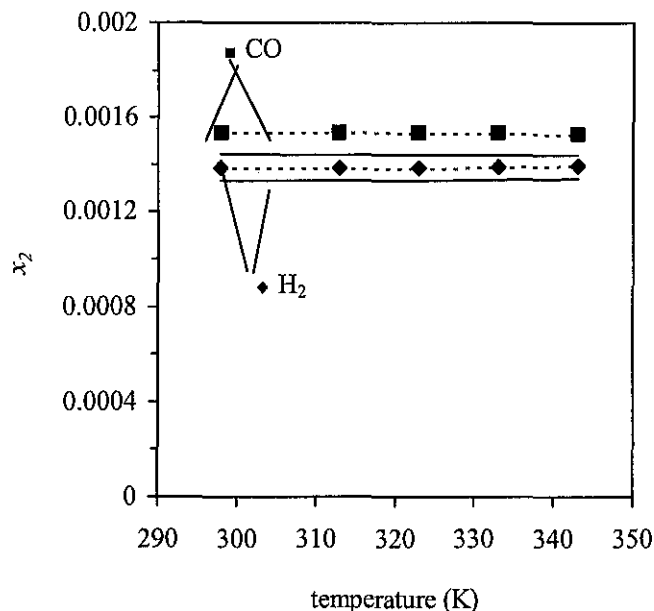


Figure 5.8: Solubility of CO and H₂ in propylene carbonate at partial pressure of 101.3 kPa. Experimental (■, ◆), modeled with regular solution theory (RST) with Yen and McKetta extension for polar solvent (—), and UNIFAC model (---).

Figure 5.9 shows the comparison of experimental and predicted values of solubility of H₂ and CO in the studied solvent systems. The theoretical predictions of solubility by using modified UNIFAC were found to be within a maximum error of $\pm 8.5\%$, whereas RST with the extension of Yen and McKetta (1962) predicts within $\pm 11.0\%$ error. Modeling also showed that the RST based model can be used for prediction of CO and H₂ gas solubilities in the studied solvent systems except for CO-TMS system. On the other hand, the UNIFAC model is able to describe the experimental data with a better accuracy over the whole range of the operating pressure and temperature.

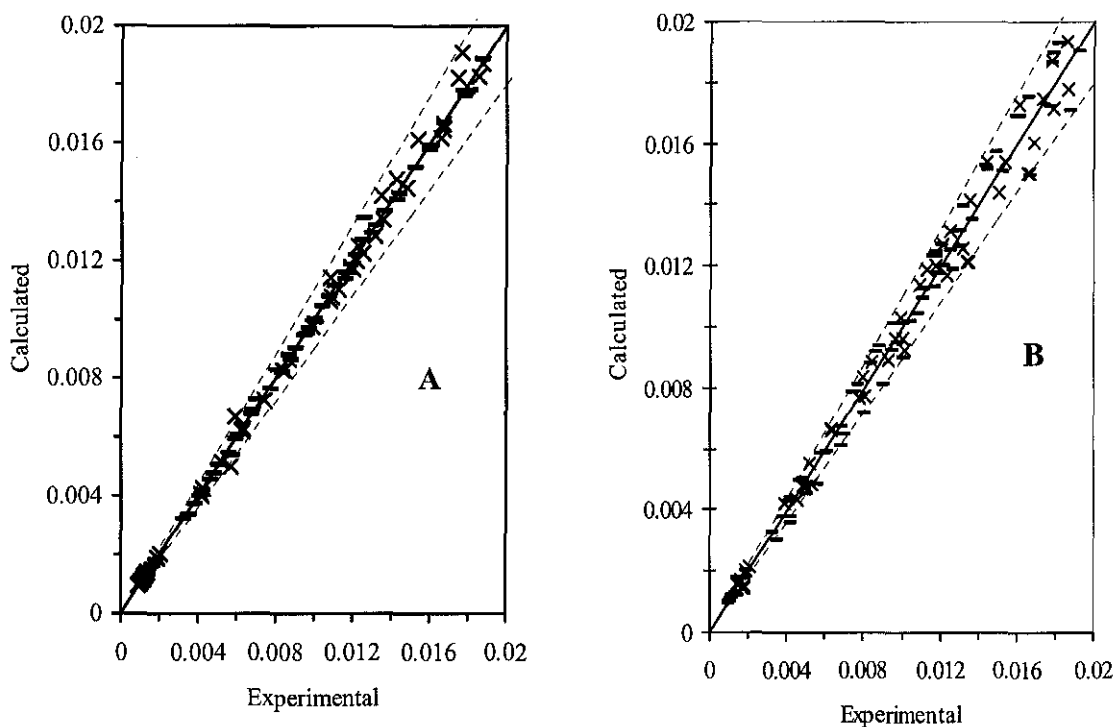


Figure 5.9: Parity plots of the model predictions of the solubility of CO and H₂ in PC, biphasic PC+dodecane mixture and TMS-systems PC+dodecane+1,4-dioxane at temperature range of 298-343 K. (A) UNIFAC model; (B) RST based model.

5.2. Parametric Study of Reaction Variables

5.2.1. Selection of Solvent Composition

Figure 5.10 shows the phase diagram with the corresponding working points obtained by cloud-point titration. The hydroformylation of 1-octene has been carried out in PC/dodecane/1,4-dioxane with varying compositions, A, B, C and D listed in Table 5.10. At a reaction temperature of 90°C and syngas pressure of 1.5 MPa and 0.17 mM catalyst concentrations, the conversion of 1-octene and the yield of total aldehyde were 53 % and 47 %, respectively. With a reaction-time of 2 h and a selectivity of approximately 90 %, this catalytic system can be considered as highly reactive and selective.

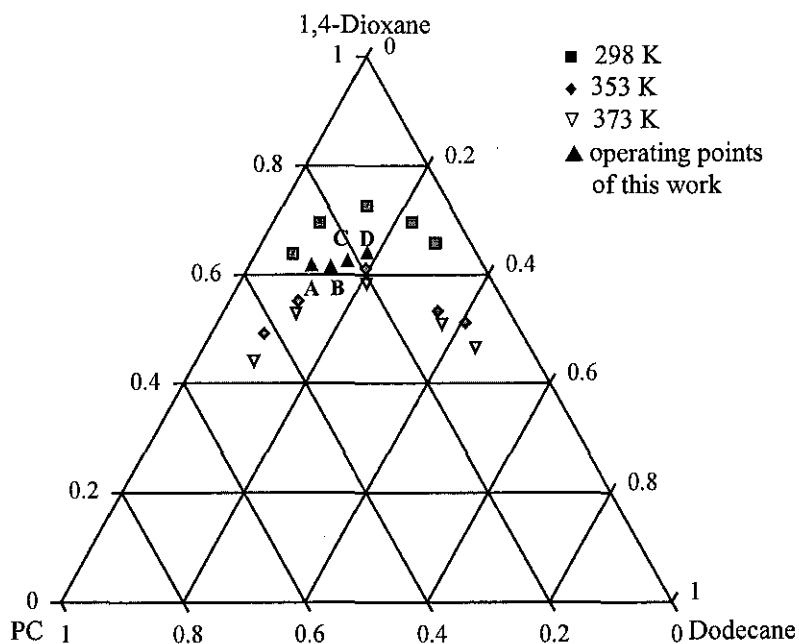


Figure 5.10: Phase diagram of the solvent system PC/dodecane/1,4 dioxane

The total turnover number was 600 while the turnover frequency was 400 h^{-1} . The turnover number (TON) is the number of moles of product obtained by the number of moles of Rh catalyst used:

$$\text{TON} = \frac{\text{moles of aldehyde product}}{\text{moles of catalyst}} \quad (5.18)$$

The TON is a measure of the efficiency of a catalyst. Particularly in using expensive catalysts, the TON should be as high as possible to reduce the final production cost. On the other hand, the turnover frequency (TOF), is for describing the activity of the catalyst and is defined as:

$$\text{TOF} = \frac{n_s}{n_{\text{cat}} \cdot t} \quad (5.19)$$

where n_s is the moles of converted starting material, t is the time for conversion and n_{cat} is moles of catalyst. The TOF allows an evaluation of the performance between different catalytic systems.

Upon reaction completion, the solution is phase separated by cooling to form the polar rich phase, PC and non-polar rich phase, dodecane. Gas chromatographic analysis of the two liquid phases obtained at the end of the reaction showed that the product preferentially remained in the nonpolar phase. The percentage yield of nonanal distributed into the non polar phase was found to be in the range of 67 to 85 %. Table 5.5 shows that the n -selectivity increases at a higher PC concentration in the TMS-system. Similar results on the effect of PC concentration were reported by Behr et al. (2005) for the hydroformylation of trans-1-octene using Rh(acac)(CO)₂/BIPHEPHOS catalyst. From the calculated turnover frequency (TOF), the TOF was well above 300 h⁻¹, showing high catalytic activity although significantly less concentration of catalyst was used compared to the amount of catalyst loading in industrial hydroformylation processes. The TOF obtained are comparable with the biphasic system for hydroformylation of 1-dodecene (Zhang et al., 2002). The solvent composition according to the operation point A (PC/dodecane/1,4-dioxane: 0.30/0.10/0.60) given in Table 5.5, was selected as a practical one for further study.

Table 5.5: Effect of the composition of TMS-systems.

Serial	PC/dodecane/1,4-dioxane [wt %]	Yield of total aldehyde [%]	<i>n/iso</i>	TON	TOF, h ⁻¹	Rh loss, %
A	30.0/10.0/60.0	47.5	10.5:1	600.5	404.0	2.8
B	25.5/13.5/61.0	47.0	9.7:1	574.9	383.3	3.0
C	21.8/15.8/62.4	47.9	9.5:1	463.2	308.8	6.3
D	17.8/18.2/64.0	50.6	8.5:1	618.3	412.2	10.4

Reaction conditions: $P = 1.5$ MPa, $y_{H_2}/y_{CO} = 1/1$, $HRh(CO)(PPh_3)_3 = 1.7 \times 10^{-4}$ kmol·m⁻³, 1-octene = 1.9 kmol·m⁻³, $P(OPh)_3/HRh(CO)(PPh_3)_3 = 12$, temperature = 363 K, reaction-time = 2 h.

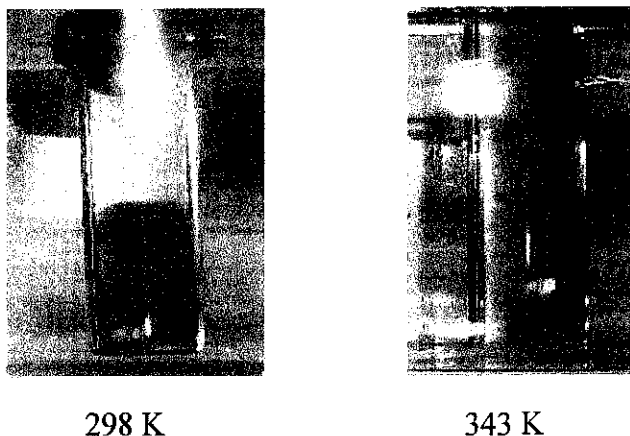


Figure 5.11: An organic solvent mixture composed of PC/dodecane/1,4-dioxane (30.0/10.0/60.0) formed the biphasic system at 298 K (a lower PC layer was colored due to the presence of the catalyst).

As shown in Figure 5.11, the catalyst remained in the propylene carbonate phase giving it a light yellow colour. However, the catalyst loss into the product or nonpolar phase was found to be within 2.8 to 10.4 % and it could be correlated to the polarity and the solubility of the solvent mediator in the product phase. 1,4-Dioxane proved to be a better solvent mediator with low catalyst loss of 3 % only compared to *p*-xylene which caused a higher rhodium leaching of about 47 % (Behr et al, 2005b).

5.2.2. Effect of Reaction Parameters

5.2.2.1. Effect of Catalyst Concentration

Industrial hydroformylation processes carried out in a single phase solvent using rhodium catalyst generally require high catalyst loadings, up to 1 mM $\text{HRh}(\text{CO})(\text{PPh}_3)_3$. In this study, a significantly less amount of catalyst was found to give satisfactory conversion and selectivity. In Figure 5.12, at catalyst concentration of 0.68 mM, the conversion of 1-octene increased with time until it reached a plateau at 98 % conversion and reaction time of 2.0 h, indicating the end point of the reaction. The initial rate and conversion increased with the concentration of the $\text{HRhCO}(\text{PPh}_3)_3$ catalyst. After 2.0 h, conversion of 1-octene to C_9 -aldehyde increased from 50.0 to 95.3 % for a change of catalyst concentration from 0.0866 to 0.68 mM. The yield of total aldehyde in nonpolar phase, dodecane increased

steadily from 0.0866 mM concentration of catalyst until it reached equilibrium at 0.68 mM of catalyst concentration. The catalyst also increases the rate at which equilibrium is achieved. The rate of reaction decreases as the percent completion increases until the point where the system reaches dynamic equilibrium. The high rates of total reaction and yields of aldehydes may be due to the addition of excess $P(O\text{Ph})_3$ ligand. According to Beller et al., (1995), by using phosphite-modified catalyst, even less reactive olefins such as 1-octene, 2,3- and 2,5-dihydrofuran, 1-butene and 2-butene are hydroformylated at much higher rates compared to those achieved with phosphine-modified catalysts. Similar observation was reported before in the case of hydroformylation of 1-octene at 10 bar and 353 K, where the addition of excess ligand ($P\text{Ph}_3:\text{Rh} = 5:1$ molar ratio) systematically led to high rates of hydroformylation and selectivity with reduced rates of isomerization and hydrogenation of the olefin (Huang et al., 2004).

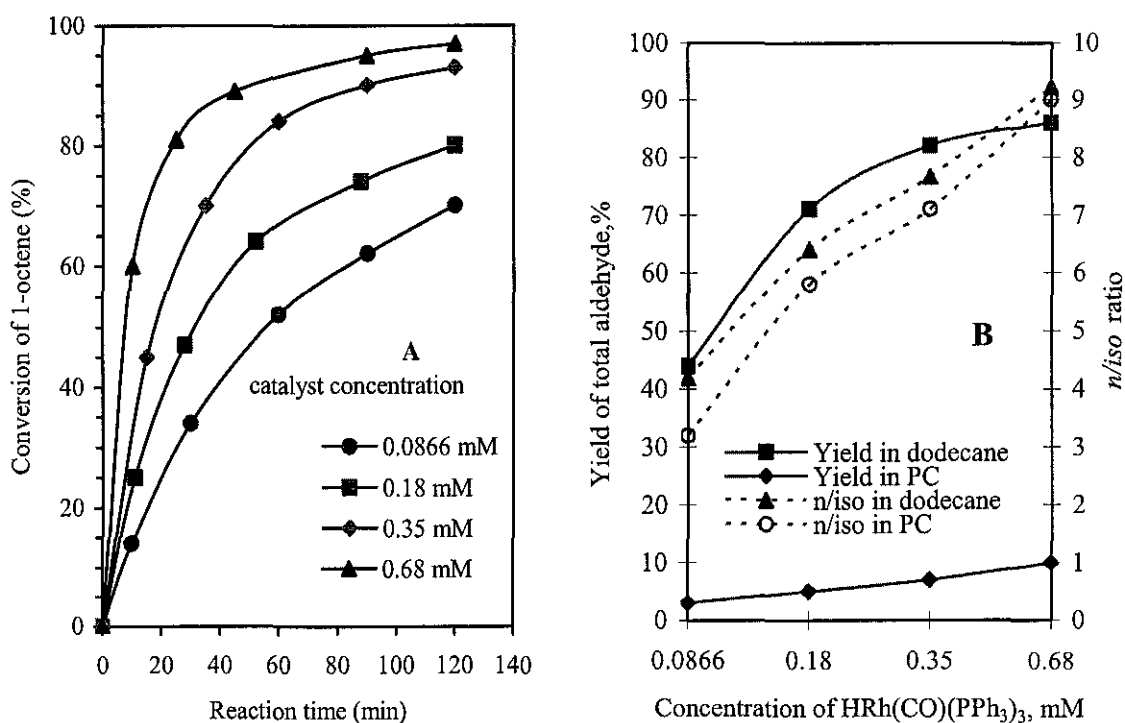


Figure 5.12: **A:** Time evolution of the yield of total aldehyde at different concentration of $\text{HRh}(\text{CO})(\text{PPh}_3)_3$ catalyst; **B:** Effect of $\text{HRh}(\text{CO})(\text{PPh}_3)_3$ concentration on the yield of total aldehyde and selectivity. Reaction conditions: $P = 1.5$ MPa, $y_{\text{H}_2}/y_{\text{CO}} = 1/1$, $T = 363$ K, $1\text{-octene} = 1.9 \text{ kmol}\cdot\text{m}^{-3}$, $P(\text{OPh})_3/\text{HRh}(\text{CO})(\text{PPh}_3)_3 = 12$, $\text{PC}/\text{dodecane}/1,4\text{-dioxane} = 0.30/0.10/0.60$.

Similarly, the regioselectivity for linear aldehyde increased with the increase of catalyst loading. The *n*-product was favoured under all conditions studied even though the regioselectivity to *n*-nonanal decreased with time. This could be attributed to the ratio of phosphite ligand (**L**) to rhodium metal affecting the coordination equilibrium of catalytic active species. According to the catalytic cycle of hydroformylation, with the increase of the ratio of phosphite ligand to rhodium metal, the rhodium metal complex converted from $\text{HM}(\text{CO})_2\text{L}$ to $\text{HM}(\text{CO})\text{L}_2$ and then to $\text{HM}(\text{CO})\text{L}_3$, among which $\text{HM}(\text{CO})\text{L}_2$ was the main active species most favorable for the coordination and dissociation of reactants, exhibiting higher catalytic activity and selectivity. With 0.68 mM $\text{HRh}(\text{CO})(\text{PPh}_3)_3$, the conversion of 1-octene and the yield of total aldehyde were 97% and 95 %, respectively. The *n/iso* aldehyde ratio was 8.4 and formation of only 1.6 % of the 2-octene and 0.5 % of 1-octane were observed after 2.0 h as shown in Figure 5.13 and 5.14. A comparison of conversion and selectivity of hydroformylation reported in the literature for a few systems with that achieved in the present work is presented in Appendix H. The percentage yield of aldehyde distributed into the nonpolar phase was found to be in the range of 89.5 to 93.3 %.

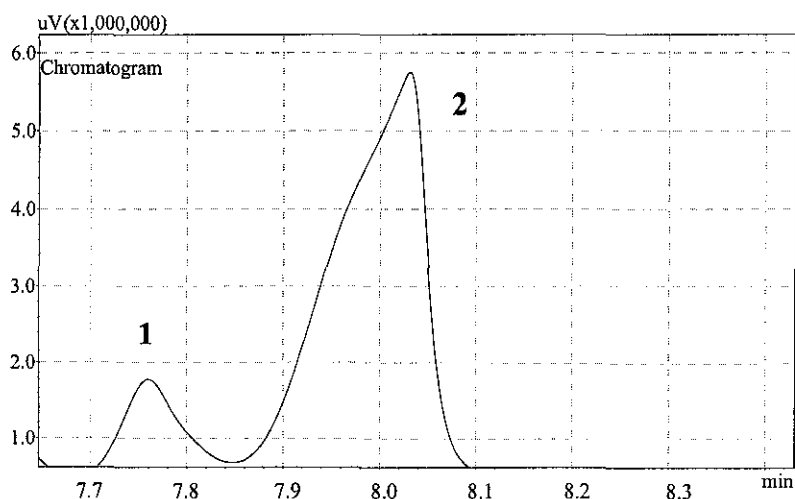


Figure 5.13: Expanded GC signal for the formation for C_9 -aldehyde isomers (1: 2-methyloctanal, 2: nonanal)

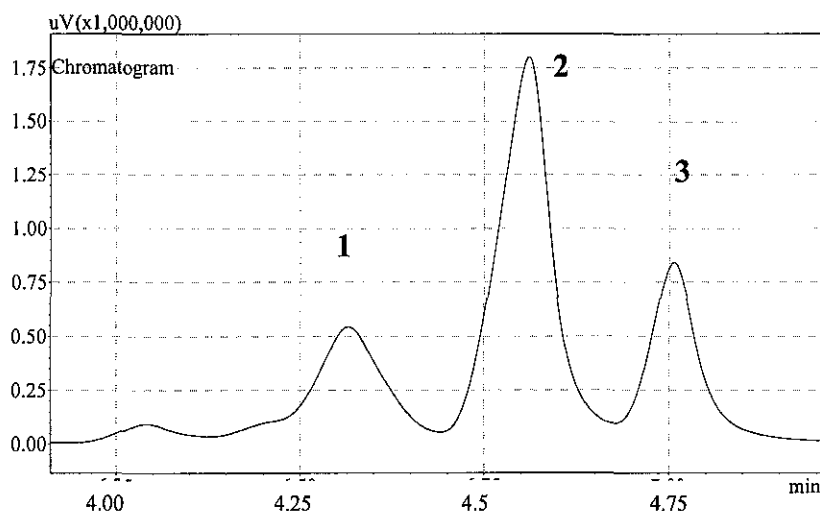


Figure 5.14: Expanded GC signal for the octene isomers and octane (1: 1-octene, 2: 2-octene, 3: octane)

5.2.2.2. Effect of Temperature

The reaction temperature significantly influences the conversion as well as the distribution of products due to enhanced isomerization of the double bonds and the dissociation of ligand from the catalytic complexes at higher temperature (van Leeuwen, 2004). From the collision theory, an increase in temperature is accompanied by an increase in the reaction rate. Temperature is a measure of the kinetic energy of a system, so higher temperature implies higher average kinetic energy of molecules and more collisions per unit time. A general rule of thumb for most (not all) chemical reactions is that the rate at which the reaction proceeds will approximately double for each 10 K increase in temperature. Once the temperature reaches a certain point, the chemical species may be altered (e.g., decomposition of ligands and denaturing of proteins) and the rate of the chemical reaction will be reduced.

As it is seen in Figure 5.15, an increase in temperature from 353 to 373 K, increases the initial rate of the reaction. This suggests that an increase of temperature from 353 to 373 K accelerated the formation of catalytic active species and enhanced the reaction activity. At a higher temperature of 383 K, the initial rate dropped thereafter which might be caused by the partial ligand degradation, leading to a decrease of conversion of 1-octene and selectivity for aldehyde. Although the rate of reaction increases with temperature up

to 373 K, the percentage yield of aldehyde dropped significantly from 90 % to 72 % with respect to an increase of temperature from 363 K to 373 K. In addition at the higher temperature (373 K) an orange colour develops in the reaction mixture due to the decomposition of the triphenylphosphite ligand which simultaneously affects the activity and stability of catalyst (van Leeuwen and Claver, 2000). After 2.0 h, the total yield of aldehyde was as high as 95 % and the ratio of *n/iso* aldehydes was 8.4. Thus, a higher temperature increases the rate of the hydroformylation but decreases the *n/iso* ratio. The isomerization of 1-octene into other internal octenes are favorable at higher temperature and subsequently the concentrations of the branched octenes are enhanced, and hence lower *n/iso* ratio. The optimal temperature of 363 K was observed, offering the highest initial rate and reasonably high selectivity (*n/iso* = 8.8-9) for aldehyde. The percentage yield of aldehyde distributed into the nonpolar phase was found to be in the range of 84.2 to 84.9 %.

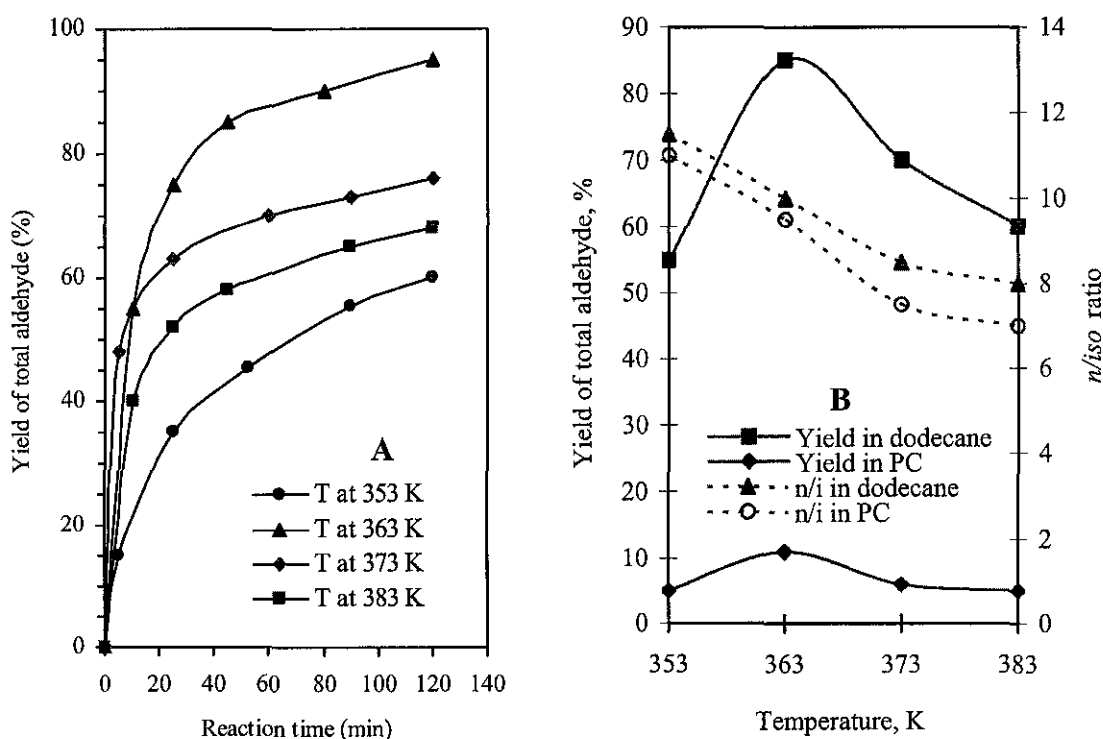


Figure 5.15: **A:** Time evolution of the yield of total aldehyde at different reaction temperatures; **B:** Effect of temperature. Reaction conditions: $P = 1.5$ MPa, $y_{H_2}/y_{CO} = 1/1$, $HRh(CO)(PPh_3)_3 = 6.8 \times 10^{-4}$ kmol·m⁻³, 1-octene = 1.9 kmol·m⁻³, $P(OPh)_3/HRh(CO)(PPh_3)_3 = 12$, PC/dodecane/1,4-dioxane=0.30/0.10/0.60.

5.2.2.3. Effect of the Total Pressure of Syngas

The effect of total pressure ($y_{H_2}/y_{CO} = 1/1$) on the conversion of 1-octene, total yield of aldehyde and the selectivity are presented in Figure 5.16. An increase in the total pressure increased the rate and conversion of 1-octene but the total yield of aldehydes were in the range of 88-90 % and did not vary significantly. However, with the increase of the total pressure, a decrease in selectivity of the linear aldehyde was observed. The n/iso ratio decreased from 7.7 at total pressure of 1.5 MPa to 3.8 at 2.5 MPa. Typical experimental results on conversion and selectivity are given in Table 5.6.

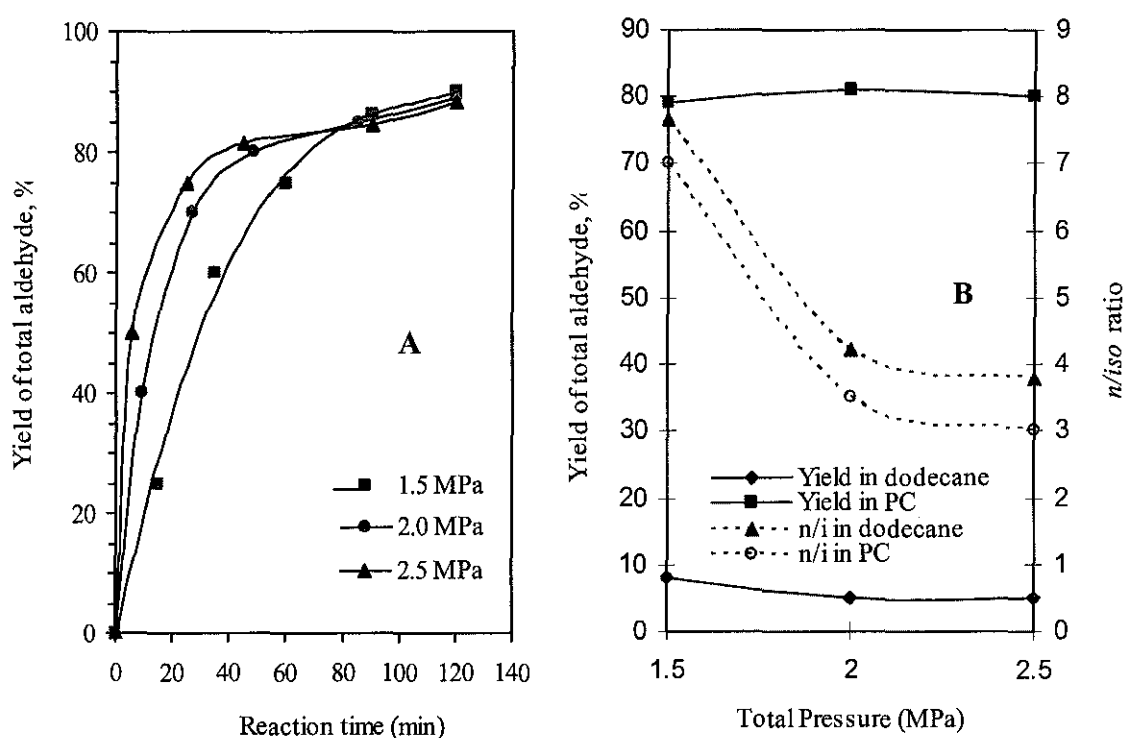


Figure 5.16: A: Yield of total aldehyde as a function of reaction time at different total syngas pressure; B: Effect of total pressure. Reaction conditions: $y_{H_2}/y_{CO} = 1/1$, $HRh(CO)(PPh_3)_3 = 6.8 \times 10^{-4} \text{ kmol} \cdot \text{m}^{-3}$, $1\text{-octene} = 1.9 \text{ kmol} \cdot \text{m}^{-3}$, $P(OPh)_3/HRh(CO)(PPh_3)_3 = 12$, $PC/dodecane/1,4\text{-dioxane} = 0.30/0.10/0.60$, temperature = 363 K.

The catalyst was found to be more stable at higher concentrations of dissolved CO and H_2 (gas pressure = 2.0-2.5 MPa), and the initial light colour of the reaction mixture sustained. Deshpande et al. (1992) reported that a higher partial pressure of CO could prevent the formation of inhibiting species that led to catalyst deactivation. Wilkinson

also reported the formation of orange dirhodium species, $\text{Rh}_2(\text{CO})_5\text{L}_3$ at a low partial pressure of H_2 and high Rh catalyst concentration (van Leeuwen and Claver, 2000). Since the formation of dirhodium species is a reversible process, at a high partial pressure of H_2 , the active rhodium hydrides ($\text{HRh}(\text{CO})_2\text{L}_2$) are regenerated and might be another cause for the positive rate response to increase in the total pressure of the syngas. The increase of total pressure led to an increase of catalytic activity. However, side-hydrogenation and isomerization of 1-octene also increased at a pressure above 1.5 MPa, which made the selectivity for nonanal drop correspondingly.

Table 5.6: Typical results on conversion of 1-octene, selectivity and yields.

Temperature K	[catalyst] mol/m^3	[1-octene] kmol/m^3	P atm	Conversion of 1-octene %	Yield of aldehyde %	n/i
353	0.68	1.90	15.0	95.3	60.0	10.5
363	0.68	1.90	15.0	97.2	95.0	8.4
373	0.68	1.90	15.0	98.6	83.0	7.5
383	0.68	1.90	15.0	99.1	68.0	7.0
363	0.086	1.90	15.0	50.0	48.2	3.0
363	0.18	1.90	15.0	53.0	47.0	5.0
363	0.35	1.90	15.0	93.0	89.7	7.7
363	0.35	1.90	20.0	95.3	89.0	5.5
363	0.35	1.90	25.0	98.8	88.2	3.8

Reaction conditions: $\text{H}_2/\text{CO} = 1$, reaction time = 2 h, catalyst: $\text{P}(\text{OPh})_3 = 5:1$ molar ratio

5.2.2.4. Effect of CO/H_2 Ratio

The effect of composition of syngas on the conversion of 1-octene, total yield of aldehyde and the selectivity are presented in Figure 5.17. A decrease in the partial pressure of CO increased the rate and selectivity of the linear aldehyde but a decrease in the total yield of aldehydes was observed. A sudden increase of the total yield of aldehydes was observed when equimolar ratio of CO/H_2 was used. The negative-order dependence with CO in a certain range of partial pressures appears to be a common feature in hydroformylation reaction, using $\text{HRh}(\text{CO})(\text{PPh}_3)$ as a catalyst. As proposed by Evans et al. (1968) the inhibition in the hydroformylation rates at higher CO pressures is mainly due to the formation of $(\text{RCO})\text{Rh}(\text{CO})_2(\text{PPh}_3)_2$ and/or $(\text{RCO})\text{Rh}(\text{CO})_3(\text{PPh}_3)$ species which are unreactive toward hydrogen. These species are likely to be formed by

equilibrium reactions, thus reducing the effective concentration of the active catalytic species. The equilibrium leading to the formation of unreactive species will be more pronounced at higher pressures of CO causing a sharp decrease in the total yield of aldehydes and rate of reaction as observed in this work. At lower partial pressures of CO, the formation of these species is expected to be negligible, and therefore a positive-order dependence of the rate on P_{CO} is observed. We also observed an increase in the rate of reaction with partial pressure of H_2 . Regeneration of rhodium hydrides from dormant rhodium species formed by impurities is another cause for the positive rate response to raising the H_2 pressure.

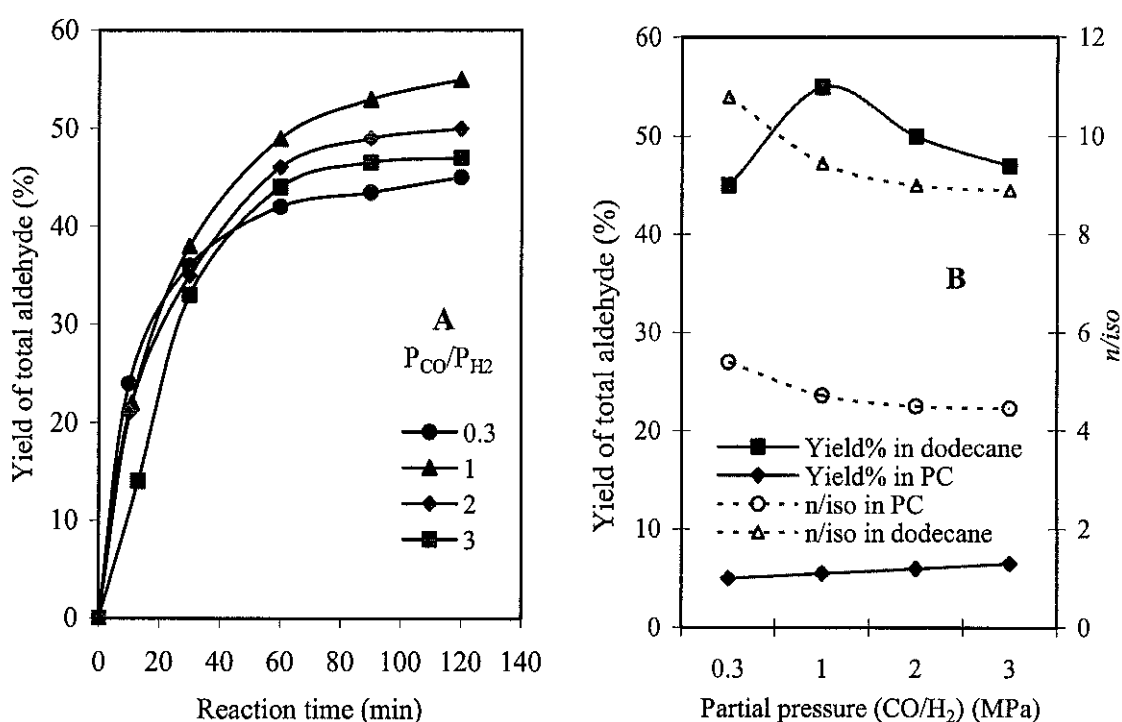


Figure 5.17: A: Yield of total aldehyde as a function of reaction time at different CO/ H_2 pressure ratio; B: Effect of CO/ H_2 ratio. Reaction conditions: $p = 1.5$ MPa, $HRh(CO)(PPh_3)_3 = 2.1 \times 10^{-4}$ kmol·m $^{-3}$, 1-octene = 1.9 kmol·m $^{-3}$, $P(OPh)_3/HRh(CO)(PPh_3)_3 = 12$, PC/deodecane/1,4-dioxane=0.30/0.10/0.6017, temperature = 363 K.

5.2.2.5. Effect of Ligand to Catalyst [$P(OPh)_3/HRh(CO)(PPh_3)_3$] Ratio

On the basis of the above catalytic results in 1-octene hydroformylation, an excess of $P(OPh)_3$ was added to $HRh(CO)(PPh_3)_3$, and the effects of $P(OPh)_3$ at 15 bar ($H_2/CO = 1$) and 363 K was investigated. It is clearly seen from Figure 5.18 that addition

of excess P(OPh)_3 systematically leads to great increases in the rates of hydroformylation and in the ratio of *n/iso* aldehydes when the molar ratio of P(OPh)_3 :Rh is in the range of 10-12 and eventually dropped thereafter. The need for excess ligand (L) arises from the facile Rh-L dissociation equilibrium shown in Figure 5.19 (van Leeuwen and Claver, 2000). As the concentration of P(OPh)_3 increases, the formation of inactive catalyst HRhL_3 lowers the total yield. In addition, at high P(OPh)_3 concentrations, where the catalyst resting state is $(\text{P(OPh)}_3)_3\text{Rh(CO)H}$, phosphite dissociation must occur to form the coordinatively unsaturated intermediates. This dissociation is suppressed by increased P(OPh)_3 concentration, which serves to reduce the concentration of active Rh species in the catalytic cycle.

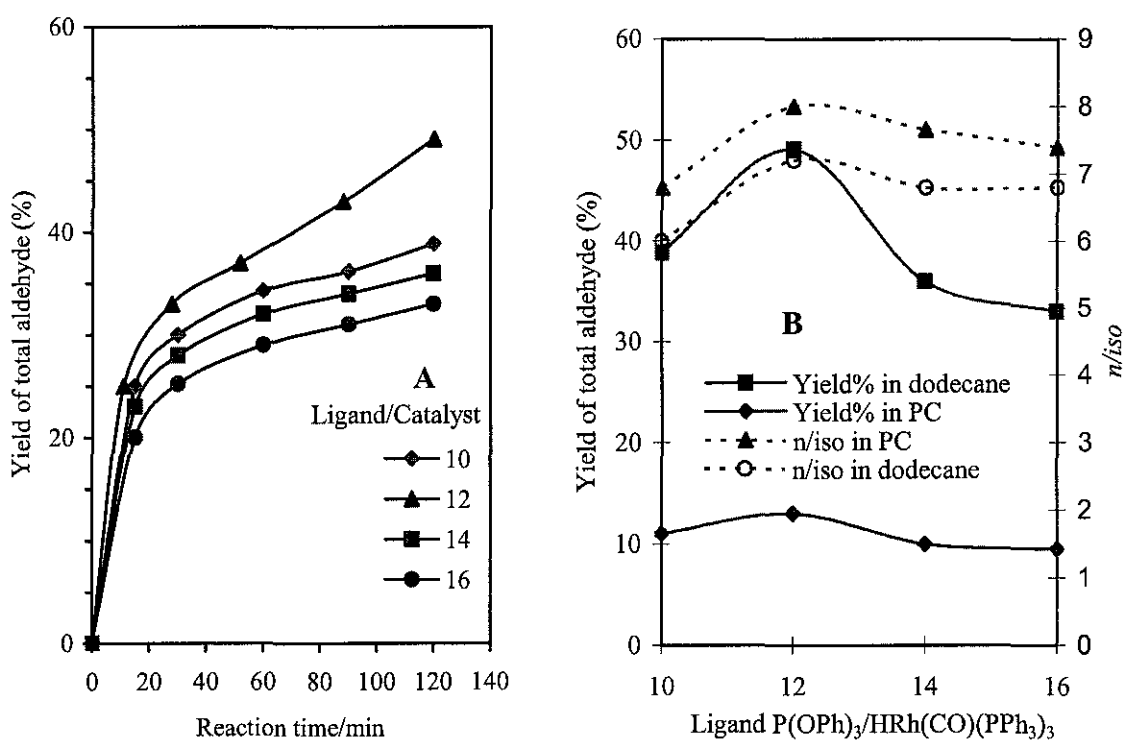


Figure 5.18: A: Yields of total aldehyde as a function of reaction time at different ratio of ligand to catalyst concentration. B: Effect of $\text{P(OPh)}_3/\text{HRh(CO)(PPh}_3)_3$ ratio. Reaction conditions: $p = 1.5 \text{ MPa}$, $\text{HRh(CO)(PPh}_3)_3 = 2.1 \times 10^{-4} \text{ kmol} \cdot \text{m}^{-3}$, $1\text{-octene} = 1.9 \text{ kmol} \cdot \text{m}^{-3}$, $\text{P(OPh)}_3/\text{HRh(CO)(PPh}_3)_3 = 12$, $\text{PC/deodecane/1,4-dioxane} = 0.30/0.10/0.60$, temperature = 363 K.

With $\text{HRh(CO)(PPh}_3)_3$ concentration of $2.1 \times 10^{-4} \text{ kmol} \cdot \text{m}^{-3}$ and $\text{P(OPh)}_3/\text{Rh} = 12$, the yield of total aldehyde went up to 48.0 %, the *n/iso* aldehyde ratio reached 8.0 after 2 h. The observations in catalytic behaviour of a phosphite-containing rhodium complex can

be interpreted in terms of electronic and steric factors of donor ligands. $\text{HRh}(\text{CO})(\text{P}(\text{OPh})_3)$ contains the strong electronegativity of the oxygen. Electron-withdrawing ligands lead to a decrease of the back-donation to CO ligands via the rhodium by π -back donation. Consequently, the Rh–CO bond is weaker in $\text{HRh}(\text{CO})(\text{P}(\text{OPh})_3)_2$ than in $\text{HRh}(\text{CO})(\text{PPh}_3)_2$ so that the former can be catalytically more active than the latter for hydroformylation. This will affect the formation of species **J** (in Figure 5.29), such that the rate of formation, or the equilibrium concentration increases.

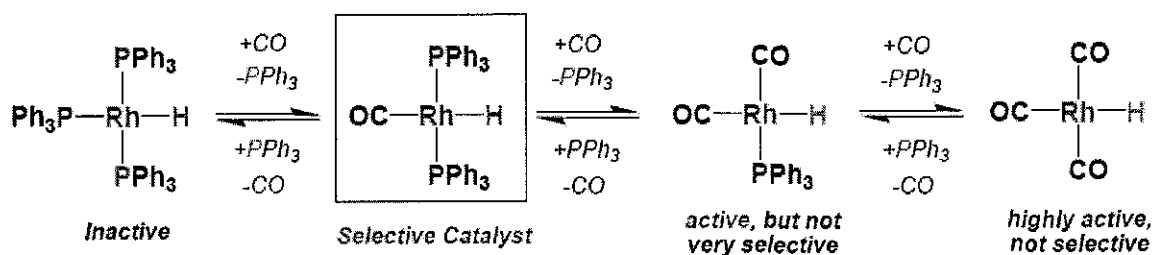


Figure 5.19: $\text{HRh}(\text{CO})(\text{PPh}_3)_3$ dissociation equilibrium

Alkene complexation, giving complexes **E**, may also be accelerated or become more favored thermodynamically. Migratory insertions are not particularly sensitive to electronic properties of the ligand, but it is important to note that oxidative addition will slow down when electron-withdrawing ligands are used (Broussard et al., 1993). $\text{HRh}(\text{CO})(\text{P}(\text{OPh})_3)_2$ presents a greater steric hindrance than PPh_3 for the coordination of 1-octene to the rhodium center and thus can lead to lower rates of the 1-octene reactions. The greater steric hindrance relatively favours anti-Markownikov addition (van Leeuwen and Claver, 2000), which can produce more nonanal than 2-methyloctanal and 2-octene. The addition of excess PPh_3 makes a significant impact on the enhancement of catalytic activity and selectivity of rhodium complexes for 1-octene hydroformylation (Deshpande et al., 1993). Consistent with the results reported with other rhodium complex systems for 1-octene hydroformylation, our catalyst systems in the presence of excess $\text{P}(\text{OPh})_3$ ($\text{P}(\text{OPh})_3:\text{Rh} = 12:1$ molar ratio) show a marked increase in the *n/iso* aldehyde ratio and great decreases in the activities for the formation of 2-octene and *n*-octane. The increase

in the *n/iso* aldehyde ratio and the suppression of the side reactions of 1-octene are mainly due to strong steric effect of P(OPh)₃. However, the increase in the activity for the formation of aldehydes by addition of excess PPh₃ or P(OPh)₃ remains unclear.

5.2.2.6. Effect of 1-Octene Concentration

As shown in Figure 5.20, a higher concentration of 1-octene increases the rate of the hydroformylation but the *n/iso* ratio in the product or non-polar phase was in the range 6.0-6.5 and did not vary significantly. An increase in the 1-octene concentration resulted in a higher reaction rate and conversion of 1-octene, while the linear aldehyde selectivity remains unaffected. The increase in olefin concentration will predictably cause an increase of the addition of olefin to the active catalyst species **B** in Figure 5.29, to form the alkyl complex and hence will cause enhancement in the rates of reaction as observed.

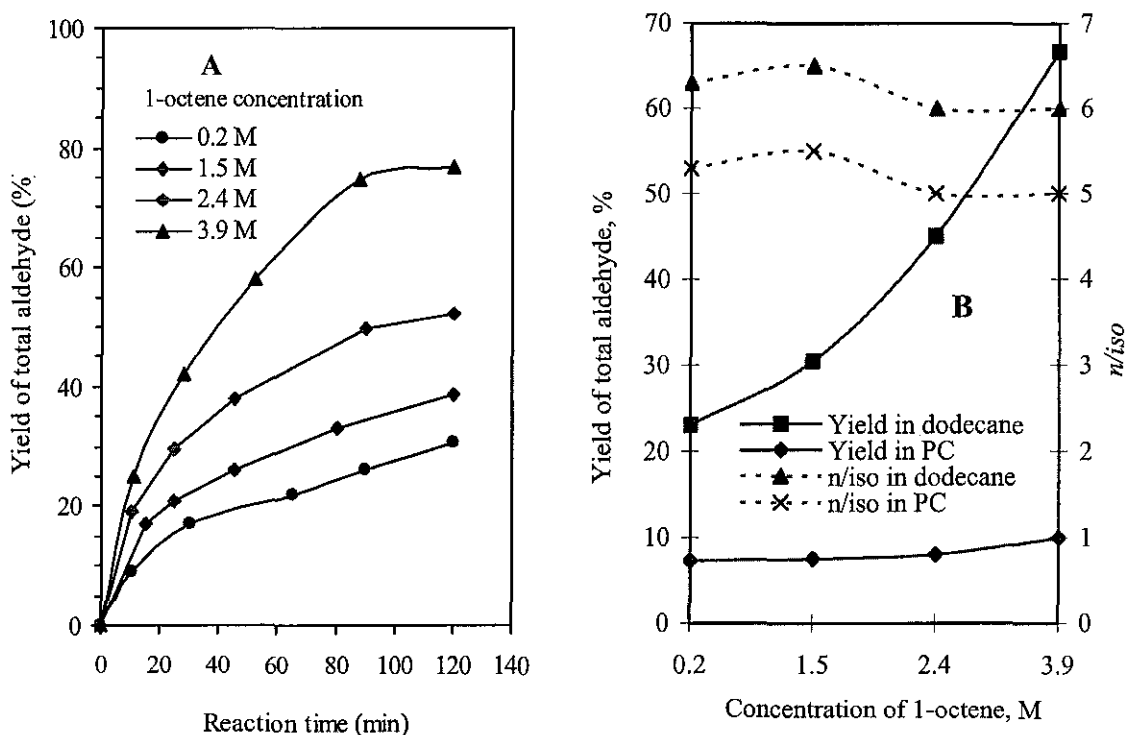


Figure 5.20: A: Yield of total aldehyde as a function of reaction time at different 1-octene concentrations; B: Effect of 1-octene concentration. Reaction conditions: $p = 1.5$ MPa, $y_{H_2}/y_{CO} = 1/1$, $HRh(CO)(PPh_3)_3 = 1.73 \times 10^{-4} \text{ kmol} \cdot \text{m}^{-3}$, $P(OPh)_3/HRh(CO)(PPh_3)_3 = 12$, $PC/dodecane/1,4\text{-dioxane} = 0.30/0.10/0.60$, temperature = 363 K.

5.3. Kinetic Study

5.3.1. Solubility of CO and H₂ in TMS-system

For the kinetic study, a knowledge of the solubility of gaseous reactants in the reaction medium is essential. Therefore, the solubilities of H₂ and CO in TMS-system of PC/dodecane/1,4-dioxane (0.30/0.10/0.60) were determined using the high pressure reactor over the temperature and pressure range of 353-373 K and 0.1-2.5 MPa, respectively. The solubility of H₂ and CO in the TMS system is linearly dependent on the pressure in the pressure range of 0.1 to 2.5 MPa as illustrated in Figure 5.21.

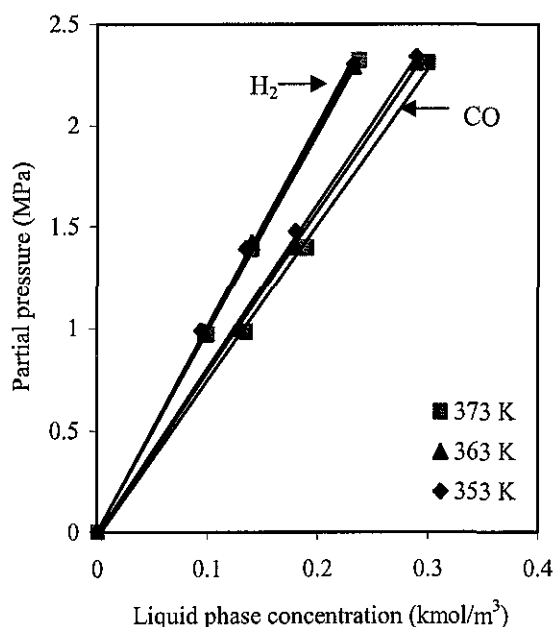


Figure 5.21: Effect of partial pressure of H₂ and CO on solubility

Table 5.7: Solubility of H₂ and CO in TMS-system of PC/dodecane/1,4-dioxane (0.30/0.10/0.60).

Temperature (K)	Henry's law constant (m ³ ·MPa·kmol ⁻¹)	
	H ₂	CO
353	10.13	8.05
363	9.98	7.88
373	9.79	7.56

The plots are linear with a high correlation coefficient (>0.995). Henry's law constants for solubilities of CO and H₂ in TMS system of PC/dodecane/1,4-dioxane with composition of 0.30/0.10/0.60 are presented in Table 5.7. These values were used in the calculation of the concentrations of dissolved CO and H₂ in the reaction medium. However, the temperature of 353 to 373 K has no significant effect on the solubility of both H₂ and CO in TMS-system.

5.3.2. Kinetics

The initial rates of hydroformylation were determined under the range of condition shown in Table 4.3. Since the reaction occurs in the liquid phase but two of the reactants are supplied as gas, mass transfer limitation may influence the rate of reaction. The common technique to apply in order to avoid external mass transfer limitations is by conducting the reaction at increasing agitation speeds under unchanged experimental conditions. Once this variable does not affect the reaction rate, it can be concluded that external mass transfer effect is negligible and the reaction rate is in the chemical or slow kinetic regime. As shown in Figure 5.22, increase of the agitation speed above 430 rpm had no effect on the rate of reaction and existence of the kinetic regime was confirmed.

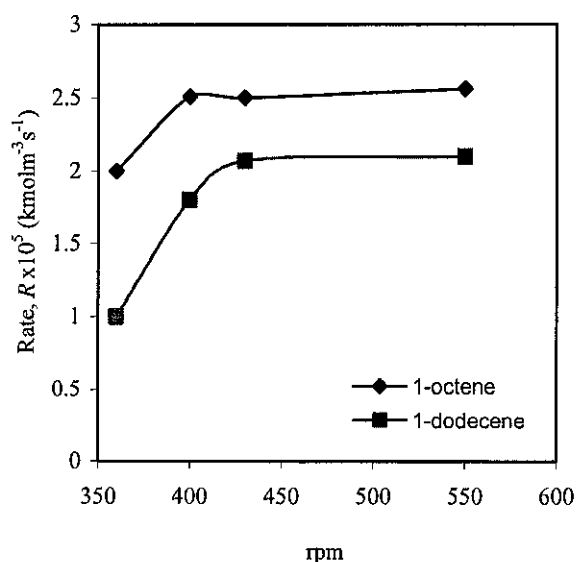


Figure 5.22: Effect of agitation speed on the rate of reaction in hydroformylation of 1-octene and 1-dodecene. Reaction conditions: $p = 1.5$ MPa, $y_{H_2}/y_{CO} = 1/1$, $HRh(CO)(PPh_3)_3 = 1.73 \times 10^{-4}$ kmol·m⁻³, 1-olefins = 1.9 kmol·m⁻³, $P(OPh)_3/HRh(CO)(PPh_3)_3 = 12$, PC/deodecane/1,4-dioxane=0.30/0.10/0.60, temperature = 363 K.

5.3.2.1. Effect of Catalyst Concentration

Initial reaction rate as a function of catalyst concentration for the TMS system is plotted in Figure 5.23. The plots are linear with a high correlation coefficient (0.990). Therefore, the reaction rate shows a first order rate dependence on the concentration of catalyst over the concentration range studied. The studies conducted by Brown and Wilkinson (1970) and Chaudhari and co-workers (Deshpande et al., 1988,1992; Bhanage et al., 1997; Divekar et al., 1993; Nair et al., 1999) using $\text{HRh}(\text{CO})(\text{PPh}_3)_3$ catalyst showed first-order rate dependence on catalyst concentration in benzene, toluene, or ethanol for several different unsaturated substrates. However, when vinyl acetate or 1-hexene was the substrate, Chaudhari noted a critical catalyst concentration (C^*) of $0.2\text{-}0.4 \times 10^{-3} \text{ kmol m}^{-3}$, below which no reaction was observed. Beyond C^* , the dependence on catalyst concentration was first order (Deshpande et al., 1988, 1989). The inactivity at low catalyst concentrations was attributed to a high substrate/catalyst ratio, leading to catalytically inactive dimer formation. This dimer formation probably involves the species F and G of Figure 5.30 (Palo and Erkey, 1999). The data lie on a curve that passes through the origin, indicating that there is no critical catalyst concentration in the TMS system using $\text{HRh}(\text{CO})(\text{PPh}_3)_3/\text{P}(\text{OPh}_3)_3$ as catalyst when 1-octene is the substrate.

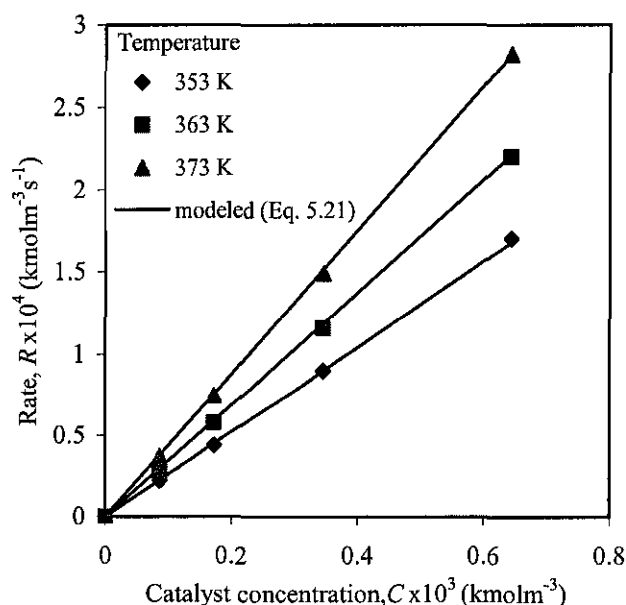


Figure 5.23: Effect of catalyst concentration on the rate of reaction. Reaction conditions: $P = 1.5 \text{ MPa}$, $y_{\text{H}_2}/y_{\text{CO}} = 1/1$, $1\text{-octene} = 1.9 \text{ kmol}\cdot\text{m}^{-3}$, $\text{P}(\text{OPh})_3/\text{HRh}(\text{CO})(\text{PPh}_3)_3 = 12$, $\text{PC}/\text{dodecane}/1,4\text{-dioxane}=0.30/0.10/0.60$.

5.3.2.2. Effect of 1-Octene Concentration

Initial reaction rate as a function of 1-octene concentration for the TMS system is plotted in Figure 5.24.

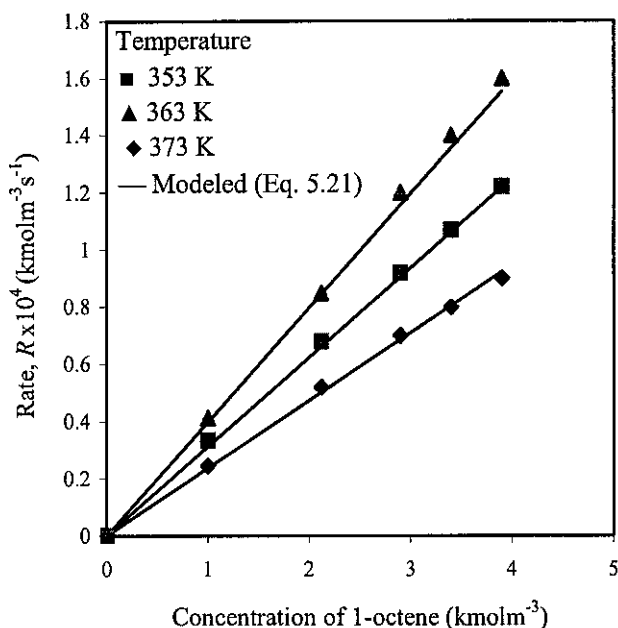


Figure 5.24: Effect of 1-octene concentration on the rate of reaction. Reaction conditions: $P = 1.5$ MPa, $y_{H_2}/y_{CO} = 1/1$, $HRh(CO)(PPh_3)_3 = 1.73 \times 10^{-3}$ kmol·m⁻³, $P(OPh)_3/HRh(CO)(PPh_3)_3 = 12$, $PC/dodecane/1,4\text{-dioxane} = 0.30/0.10/0.60$.

The reaction rate shows a first order rate dependence on the concentration of catalyst over the concentration range studied. Substrate inhibition was absent over the range of substrate and catalyst concentrations selected, where the substrate/catalyst ratio varied from 580 to 2300. This may be due to several factors - solvent effects, the phosphite ligands, and the increased H₂ and CO concentrations relative to conventional systems (Shaharun et al., 2008). The parametric effect on the reaction kinetics was found to be similar to that observed for a homogeneous hydroformylation system under industrial operating conditions (van Leeuwen and Claver, 2000). The studies conducted by Brown and Wilkinson (1970) and Chaudhari and co-workers (Deshpande et al., 1988,1992; Bhanage et al., 1997; Divekar et al., 1993; Nair et al., 1999) using HRh(CO)(PPh₃)₃ catalyst showed first-order rate dependence on catalyst concentration in benzene, toluene, or ethanol for several different unsaturated substrates. However, when vinyl acetate or 1-hexene was the substrate, Chaudhari noted a critical catalyst concentration (C^*) of 0.2-

$0.4 \times 10^{-3} \text{ kmol m}^{-3}$, below which no reaction was observed. Beyond C^* , the dependence on catalyst concentration was first order (Deshpande et al., 1988, 1989). The inactivity at low catalyst concentrations was attributed to a high substrate/catalyst ratio, leading to catalytically inactive dimer formation. This dimer formation probably involves the species F and G of Figure 5.30 (Palo and Erkey, 1999). The data lie on a curve that passes through the origin, indicating that there is no critical catalyst concentration in the TMS system using $\text{HRh}(\text{CO})(\text{PPh}_3)_3/\text{P}(\text{OPh}_3)_3$ as catalyst when 1-octene is the substrate.

5.3.2.3. Effect of Hydrogen Partial Pressure

Initial reaction rate as a function of partial pressure of hydrogen for the TMS system is plotted in Figure 5.25.

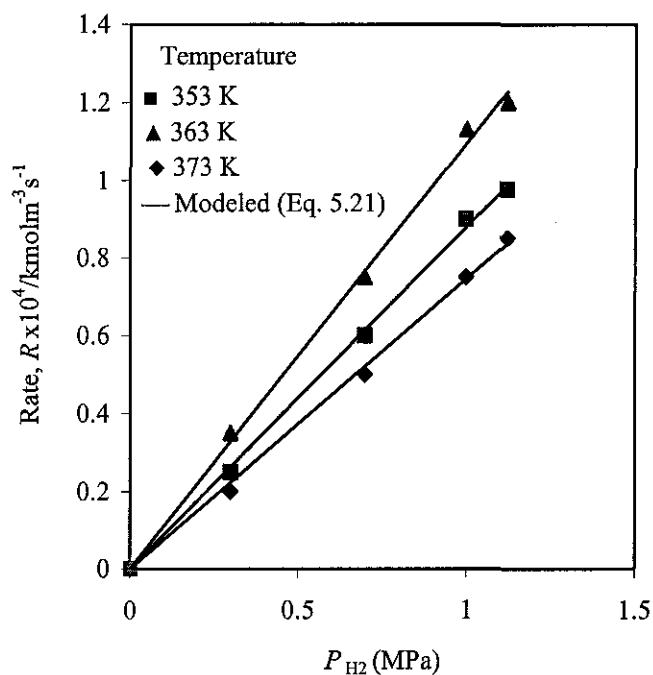


Figure 5.25: Effect of partial pressure of H_2 on the rate of reaction. Reaction conditions: $P_{\text{CO}} = 10 \text{ atm}$, 1-octene = $1.9 \text{ kmol} \cdot \text{m}^{-3}$, $\text{HRh}(\text{CO})(\text{PPh}_3)_3 = 1.73 \times 10^{-4} \text{ kmol} \cdot \text{m}^{-3}$, $\text{P}(\text{OPh}_3)_3/\text{HRh}(\text{CO})(\text{PPh}_3)_3 = 12$, $\text{PC}/\text{dodecane}/1,4\text{-dioxane} = 0.30/0.10/0.60$.

The plots are also linear with a high correlation coefficient (0.995). Therefore, the reaction rate shows a first order rate dependence, which is commonly observed in conventional solvent system. It is important to note that, a first order rate dependence was observed, although the solubility of H_2 is higher in the TMS system compared to the

conventional non polar solvent system. Such first-order dependency is commonly interpreted to mean that the oxidative addition of H_2 (step 11 in Figure 5.30) is the rate determining step (Nair et al., 1999; Deshpande et al 1998; Bhanage et al., 1997). This result illustrates the usefulness of the TMS-system not only as an alternative solvent, but also as a mechanistic tool for investigating kinetic behavior over a much wider range of conditions than normally employed.

5.3.2.4. Effect of Carbon Monoxide Partial Pressure

Initial reaction rate as a function of partial pressure of carbon monoxide for the TMS system is plotted in Figure 5.26.

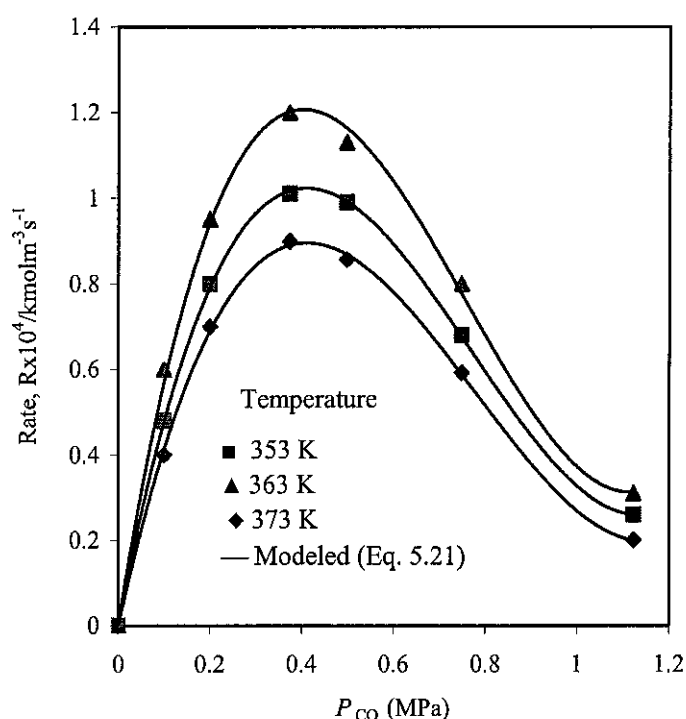


Figure 5.26: Effect of partial pressure of CO on the rate of reaction. Reaction conditions: $P_{H_2} = 10$ atm, 1-octene = $1.9 \text{ kmol}\cdot\text{m}^{-3}$, $\text{HRh}(\text{CO})(\text{PPh}_3)_3 = 1.73 \times 10^{-4} \text{ kmol}\cdot\text{m}^{-3}$, $\text{P}(\text{OPh})_3/\text{HRh}(\text{CO})(\text{PPh}_3)_3 = 12$, PC/dodecane/1,4-dioxane=0.30/0.10/0.60.

The rate was found to be inversely dependent on the CO partial pressure in the range of 4.0 to 11.5 atm. Increasing P_{CO} had no positive effect on the reaction rate at all, which is explained by the high initial concentration of CO in the reactor. The conventional system exhibits positive dependence on $[\text{CO}]$ only at very low concentrations $[(0-17) \times 10^{-3}]$

kmol·m⁻³] and shows drastic rate inhibition at higher concentrations, due to the formation of inactive species **M** as illustrated Figure 5.30. These species are coordinatively saturated, so oxidative addition of H₂ cannot take place, preventing aldehyde formation. Since the TMS system is performed at [CO] values of at least 0.046 kmol·m⁻³, the purely negative rate dependence on [CO] is expected. Generally, the parametric effects were found to be similar to that of kinetics in homogeneous system under the industrial operating conditions. According to van Leeuwen (2004), under the “standard” catalytic conditions (1.0-3.0 MPa, temperature 343-393 K, [Rh] = ≈10⁻³ kmol·m⁻³, [alkene] = 0.1-2 kmol·m⁻³, [L] depending on complex stability) the rhodium phosphite catalyzed reaction is first order in the concentration of alkene, first order in the rhodium concentration, first order in hydrogen, and the reaction shows a negative order in ligand concentration (phosphine or CO, or both).

5.3.3. Kinetic Modeling

5.3.3.1. Empirical Model

A comparison of the experimental rates of reaction and those predicted by the developed kinetic model of M1, M2 and M3 showed high average standard error estimate ranging from 15% to 45% besides having negative kinetic parameters. This result suggests that a different mechanism is operating when excess ligands are presence in the reaction system. Hence a new empirical and mechanistic model were developed for the hydroformylation of 1-octene and 1-dodecene in the TMS system of PC/dodecane/1,4-dioxane using HRhCO(PPh₃)₃/P(OPh)₃ catalyst for the ranges of process conditions listed in Table 4.2. Figure 5.27 is a typical profile obtained at 363 K and initial concentrations of 1.9 kmol·m⁻³ 1-octene and 0.17 mol·m⁻³ HRh(CO)(PPh₃)₃. Similar profiles were obtained for 353 and 373 K. In each case, the reaction was allowed to proceed until the nonanal concentration was asymptotic to its equilibrium value.

The concentration–time profiles of nonanal and 2-methyloctanal were curve fitted by a cubic polynomial of the form

$$[C_{ald}] = \alpha + \beta t + \gamma t^2 \quad (5.20)$$

where $[C_{ald}]$ is the concentration of aldehyde ($\text{kmol}\cdot\text{m}^{-3}$) and t is the time (s), to determine the reaction rate of the formation of nonanal and 2-methyloctanal at the initial time. Values of the constants α , β , and γ which were found are given in Table 5.8. The polynomials were subsequently differentiated to give reaction rates (in $\text{kmol}\cdot\text{m}^{-3}\cdot\text{s}^{-1}$) as a function of time to produce initial reaction rates for fitting against those predicted by a suitable model.

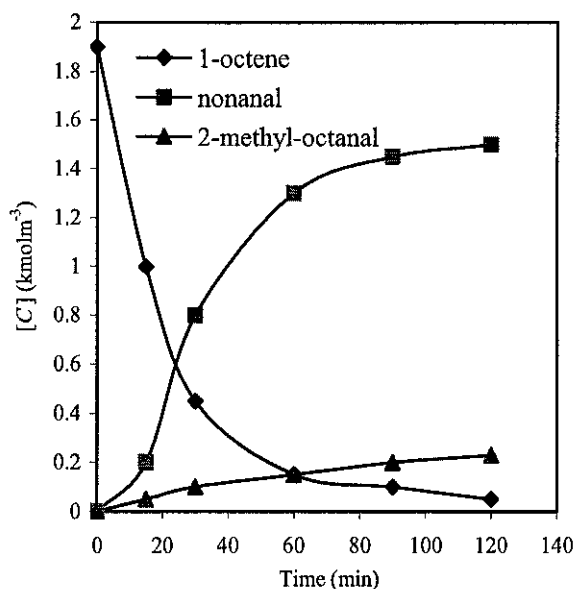


Figure 5.27: Typical plot of concentrations of 1-octene, nonanal and 2-methyloctanal versus reaction time.

Table 5.8: Constants in polynomial fitting nonanal concentration vs. time*

T (K)	$\alpha \times 10^2$ ($\text{kmol}\cdot\text{m}^{-3}$)	$\beta \times 10^5$ ($\text{kmol}\cdot\text{m}^{-3}\cdot\text{s}^{-1}$)	$\gamma \times 10^9$ ($\text{kmol}\cdot\text{m}^{-3}\cdot\text{s}^{-2}$)	R^2
353	1.02	2.73	-2.57	0.985
363	1.33	4.48	-4.34	0.987
373	1.63	5.07	-4.64	0.980

*Reaction conditions: $P = 1.5$ MPa, $y_{H_2}/y_{CO} = 1/1$, 1-octene = $1.9 \text{ kmol}\cdot\text{m}^{-3}$, $\text{HRh}(\text{CO})(\text{PPh}_3)_3 = 1.73 \times 10^{-3} \text{ kmol}\cdot\text{m}^{-3}$, $\text{P}(\text{OPh})_3/\text{HRh}(\text{CO})(\text{PPh}_3)_3 = 12$, $\text{PC}/\text{dodecane}/1,4\text{-dioxane} = 0.30/0.10/0.60$.

In order to validate the model, the rate versus concentration data was then used to determine the parameters by fitting with the experimental rate. The non-linear least square regression based on the criterion of minimization of the statistical parameter mean residual sum of squares (Φ) was performed to determine the selectivity and kinetic parameters. Activation energy was obtained by means of Arrhenius equation with 'temperature centering' as outlined in Section 3.7.3. In the present study $T_m = 363$ K was used for temperature centering and parameter estimation. The following models were found to best fit the data at all the temperatures studied.

$$\text{Rate} = \frac{k[\text{octene}][\text{catalyst}]P_{\text{CO}}P_{\text{H}_2}}{(1 + K_{\text{CO}}P_{\text{CO}})^m} \quad (5.21)$$

$$\text{Selectivity} = 0.75[\text{octene}]^{-0.15}[\text{catalyst}]^{0.26}P_{\text{CO}}^{-1.2}P_{\text{H}_2}^{-0.77}T^{-1.3}(L/R)^{0.25} \quad (5.22)$$

where [octene] is the concentration of 1-octene; [catalyst] is the concentration of HRh(CO)(P(OPh)₃)₃ in the reaction mixture; P_{CO} is the partial pressure of CO; P_{H_2} is the partial pressure of H₂; T is the absolute temperature and L/R is the ratio of P(OPh)₃/HRh(CO)(PPh₃)₃. Table 5.9 summarizes the values of the optimized parameters and the average standard error of estimation (SEE) and Φ values of the non-linear regression analysis for the empirical rate model (Equation (5.21)) at 353, 363 and 373 K.

Table 5.9: Estimated kinetic model parameters with 95% confidence limit

T (K)	k $\text{m}^3 \text{ kmol}^{-1} \text{ MPa}^{-2} \text{ s}^{-1}$	K_{CO} (MPa^{-1})	m	Φ_{min} ($\times 10^{-11}$)	SEE (%)
353	5.5	0.52	1.72	1.54	5.97
363	11.1	1.18	1.60	5.00	6.35
373	19.7	2.24	1.36	3.79	4.26

The rate constant, k increased with increasing temperature from 353 to 373 K. Generally, the rate constant doubled with every ten degree increase in temperature. However, the optimized values of the rate parameter, K_{CO} , suggests that the effect of inhibition of CO on the rate of reaction increases with a change of temperature from 353 to 373 K. The optimized values of the rate parameter m (1.36 to 1.72) also suggests that the inhibition of CO in the TMS-system is comparatively lower compared to those in conventional organic solvent based system, biphasic system and $scCO_2$ which is probably due to the lower solubility of CO in the TMS- system (Palo and Erkey, 1999; Deshpande et al., 1996; Divekar et al., 1993; Deshpande and Chaudhari, 1988).

The selectivity model (Equation (5.22)) describes the dependence of selectivity (n/iso) on the concentration of 1-octene and catalyst, partial pressure of H_2 and CO and also the ratio of ligand to catalyst. The regressed values of the parameter for P_{H_2} is -0.77 which means that the formation of branched aldehyde is more favoured at increasing H_2 pressure. Similar findings were reported by van Rooy et al. (1995) for the hydroformylation of styrene using $Rh(CO)_2(acac)$ as the catalyst precursor and tris(2-tert-butyl-4-methylphenyl)phosphite as the ligand ($T = 353$ K, $[Rh(CO)(acac)] = 0.25$ mol·m⁻³, $P/Rh = 20$, $[styrene] = 0.89$ kmol·m⁻³ in 20 mL of toluene). The regressed values of the parameter for P_{CO} suggests that increases in P_{CO} have a detrimental effect on the $n:iso$ ratio. Mechanistically, increases in $[CO]$ enhance the formation of the active species F over against the active species G (Figure 5.30). Since the CO ligand is much less sterically demanding than the phosphine, selectivity decreases as the $[G]/[F]$ ratio increases. $[1-Octene]_0$ does not significantly affect the final $n:iso$ ratio. However, it was observed that selectivity decreased slightly over the course of the reaction for each experiment in this study. Similar results were observed for the hydroformylation of 1-octene in $scCO_2$ solvent system (Palo and Erkey, 1999). However, in an aqueous biphasic solvent system, high selectivity was achieved with increase in olefin concentration (Yang et al., 2002), whereby the reported parameter was 0.156. Catalyst concentration also had a direct effect on the $n:iso$ ratio of the aldehyde products. Such selectivity dependence on catalyst concentration is typical of rhodium/phosphine systems and is related to the degree of phosphine dissociation from B in solution. The selectivity dependence on the ratio of ligand to catalyst concentration follows the same trend. The isomerization step is

slightly suppressed towards high ligand/metal ratios in homogeneous and microemulsion systems (Unveren, 2004). Under such conditions the metal center presents a more sterically hindered environment to the alkene and the formation of linear alkyl and acyl species are favored. As only the branched alkyl rhodium species will form internal alkenes, the amount of the internal alkenes diminish. With the ligand/metal ratio of 20, the internal octenes that are formed via isomerization are not hydroformylated as the 1-octene conversion begins to decrease. As in the hydroformylation of other substrates such as styrene and cyclohexene in conventional solvent system, an increase in temperature leads to a considerable decrease of selectivity toward the linear aldehyde (van Leeuwen and Claver, 2000).

A comparison of the experimental rates of reaction and selectivity and those predicted by the model are presented in Figures 5.28 and 5.29, respectively, for all the temperatures, which show a good agreement.

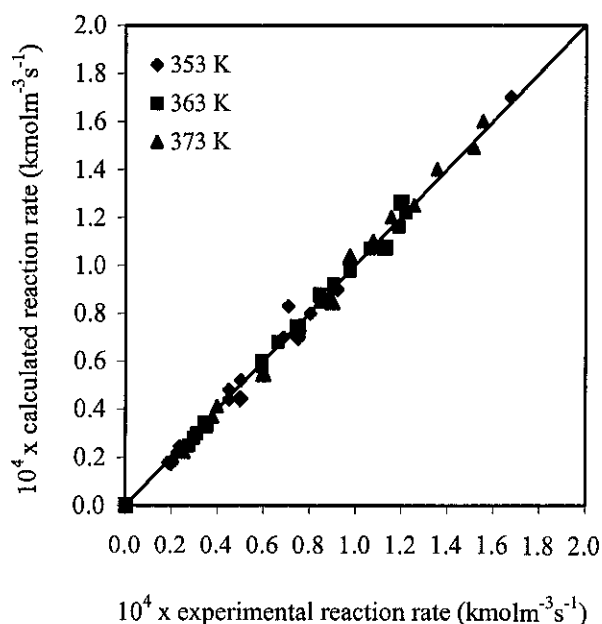


Figure 5.28: Parity plot of the experimental and calculated reaction rates using Eq.(5.21).

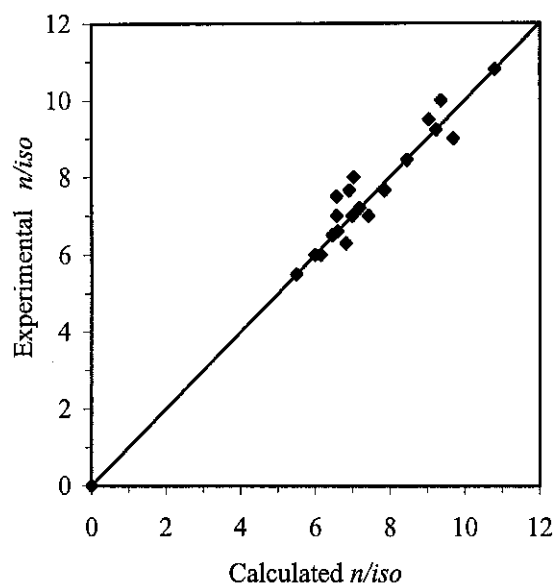


Figure 5.29: Parity plot of the experimental and calculated selectivity (n/iso) using Equation (5.22).

The prediction of the selectivity by using Equation (5.22) was found to be within $\pm 3.2\%$ error, whereas the rate equation predicts within $\pm 5.5\%$ error. The activation energy was found to be $69.8 \text{ kJ}\cdot\text{mol}^{-1}$, which lies in the range of activation energy values ($66\text{-}75 \text{ kJ}\cdot\text{mol}^{-1}$) reported by other workers for the hydroformylation of 1-octene with different Rh-complexes by homogeneous, biphasic and supported aqueous phase catalysis, SAPC (Jáuregui-Haza et al., 2001; Deshpande et al., 1996; Hermann et al., 1992; Arhancet et al., 1991).

5.3.3.2. Mechanistic model

In this work, a model based on key mechanisms is also proposed. The main objective is to establish a molecular mechanism for the hydroformylation of 1-olefin in the presence of excess $\text{P}(\text{OPh})_3$ ligand. Experimental results have shown that the hydroformylation reaction is sensitive to experimental conditions. Therefore, the plausible reaction pathway described in Figure 5.30, for the hydroformylation reaction in the presence of excess ligand and Rh-catalyst is different than the one proposed in Chapter 3.

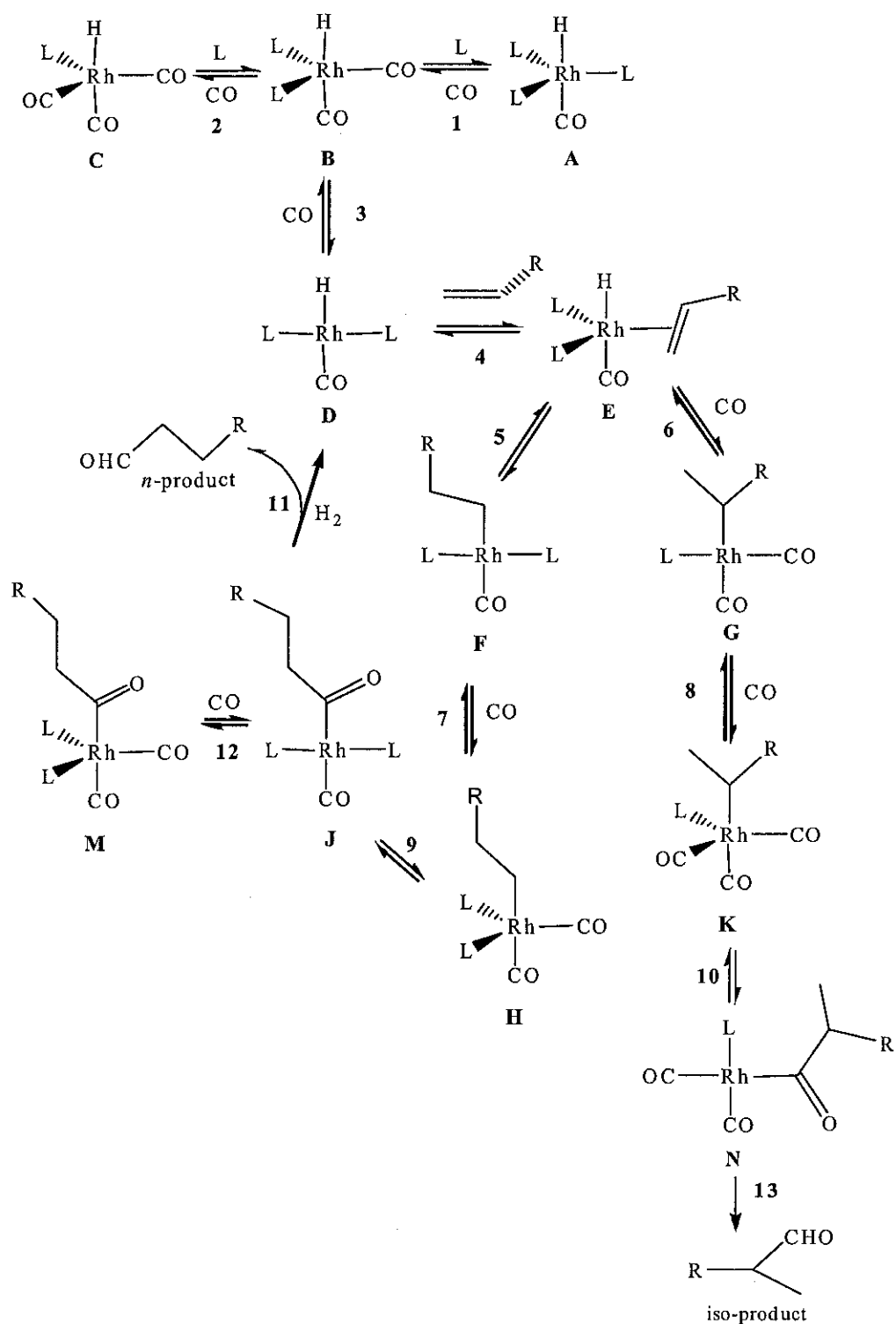


Figure 5.30: Plausible steps for rhodium catalyzed hydroformylation in the presence of excess concentration of $P(OPh)_3$ ligand (L = ligand).

Qualitative reasoning and some available experimental observations as outlined in Section 3.5, form the basis of the scheme (van Leeuwen, 2004; van der Veen et al., 2000; Musaev et al, 1995; Jongsma et al., 1991; Brown and Kent, 1987). In the presence of excess ligand, the dissociation of phosphite ligand to form monophosphite catalyst is less feasible. According to van Leeuwen and Claver (2000), at moderate $P(OPh)_3$ concentrations, the resting state of the catalyst is **B**, which undergoes $P(OPh)_3$ dissociation to form selectively 4-coordinate intermediate **D**. Since the reaction was carried out using excess $P(OPh)_3$ ligand, the complexes shown in Figure 5.30 contain at least two coordinated $P(OPh)_3$ ligands. The reaction pathways depicted in Figure 5.30 was used to develop mechanistic rate equations using the conventional quasi-steady state formalism.

Assumptions used in Chapter 3 to develop the mechanistic model for the hydroformylation of higher olefins in homogeneous system were also applied. Three rate equations (Model A1, A2 and A3) have been developed corresponding to the three transition states identified by the quantum chemical calculations. The following reaction steps (Figure 5.30) are considered.



Equations (5.23) to (5.28) and the simplifying assumptions were used to derive relationships between the rate of reaction and experimental parameters (i.e. concentrations of olefin, catalyst, dissolved CO, as well as H_2). Kinetic model (A1) has been developed using the oxidative addition of hydrogen as a rate determining step (RDS) (Equation (5.28)). Taking into account that the overall hydroformylation rate is given by the rate of this step, the rate equation is expressed as

$$\text{Rate} = k_6 [\text{J}] [\text{H}_2] \quad (5.29)$$

The following expressions for the concentrations of the different intermediates can be written in terms of the equilibrium constants of the reactions and intermediate J.

$$[\text{B}] = \frac{[\text{J}]}{K_2 K_3 K_5 [\text{alkene}]} \quad (5.30)$$

$$[\text{D}] = \frac{[\text{J}]}{K_3 K_5 [\text{CO}] [\text{alkene}]} \quad (5.31)$$

$$[\text{C}] = \frac{K_1 [\text{J}] [\text{CO}]}{K_2 K_3 K_5 [\text{alkene}]} \quad (5.32)$$

$$[\text{F}] = \frac{[\text{J}]}{K_5 [\text{CO}]} \quad (5.33)$$

$$[\text{G}] = \frac{K_4 [\text{J}]}{K_3 K_5} \quad (5.34)$$

An expression for the concentration of the species [J] can be obtained from a total catalyst balance at steady state.

$$[\text{Catalyst}] = [\text{B}] + [\text{C}] + [\text{D}] + [\text{F}] + [\text{J}] \quad (5.35)$$

where [Catalyst] is the concentration of catalyst loaded and hence,

$$[\text{catalyst}] = \frac{[\text{J}] \left(1 + K_1^* [\text{CO}] + K_2^* [\text{CO}]^2 + K_3^* [\text{alkene}] + K_4^* [\text{alkene}] [\text{CO}] \right)}{K^* [\text{CO}] [\text{alkene}]} \quad (5.36)$$

Equation (5.36) was rearranged to obtain the expression for [J] and in turn substituted in Equation (5.29) to give the rate Model A1 of the following form:

$$\text{Rate} = \frac{k[\text{catalyst}][\text{alkene}][\text{CO}][\text{H}_2]}{1 + K_1^*[\text{CO}] + K_2^*[\text{CO}]^2 + K_3^*[\text{alkene}] + K_4^*[\text{CO}][\text{alkene}]} \quad (5.37)$$

where K^* , $K_1^* - K_4^*$ are constant derived from the equilibrium constants of elementary steps in the reaction mechanism in Figure 5.30.

The second kinetic model (A2) was proposed considering the migration insertion of the alkene into R-H, is assumed as a rate limiting step (Equation (5.25)). The rate of the reaction is given by

$$\text{Rate} = k_3[\text{D}][\text{alkene}] \quad (5.38)$$

The corresponding rate equation can be derived in the form (Model A2)

$$\text{Rate} = \frac{k[\text{catalyst}][\text{alkene}][\text{CO}][\text{H}_2]}{\left(1 + K_1^*[\text{CO}]^2 + K_2^*[\text{alkene}] + K_3^*[\text{CO}][\text{alkene}]\right)[\text{H}_2] + K_4^*[\text{CO}][\text{alkene}]} \quad (5.39)$$

Similarly, considering the formation of the acyl complex is rate-controlling (Equation 5.27), the rate equation is expressed as

$$\text{Rate} = k_5[\text{F}][\text{CO}] \quad (5.40)$$

and the following rate equation (Model A3) was obtained

$$\text{Rate} = \frac{k[\text{catalyst}][\text{alkene}][\text{CO}][\text{H}_2]}{\left(1 + K_1^*[\text{CO}] + K_2^*[\text{CO}]^2 + K_3^*[\text{alkene}] + K_4^*[\text{CO}][\text{alkene}]\right)[\text{H}_2] + K_5^*[\text{CO}][\text{alkene}]} \quad (5.41)$$

The ‘equilibrium constant’, K , was similarly determined as a function of temperature using the van’t Hoff equation also with temperature centering. The error estimate (SEE) given by Equation (3.6) together with thermodynamic consistency of the calculated activation energy or negative kinetic parameter, if any, were used as the criteria of discrimination among the three rate models (Patel and Pant, 2007; Hurtado et al., 2004; Pengpanich et al., 2002).

As shown in Table E-2, Appendix E, Model A3 showed high average standard error estimate ranging from 7% to 15% besides having negative kinetic parameters. In addition the obtained activation energies are lower than the range of activation energy values (57-75 kJmol^{-1}) reported by other workers for the hydroformylation of 1-octene and 1-dodecene with different Rh-complexes by homogeneous, biphasic and supported aqueous phase catalysis, SAPC (Jáuregui-Haza et al., 2003; Bhanage et al., 1998; Deshpande et al., 1996; Hermann et al., 1992; Arhancet et al., 1991). On the other hand, Model A2 was rejected because it displayed a non-linear Arrhenius plot. As it is seen in Figure 5.31-5.34, the rate model A1 is able to describe the experimental data reasonably well over the whole range of pressure, concentrations of the olefins (1-octene and 1-dodecene) and temperature.

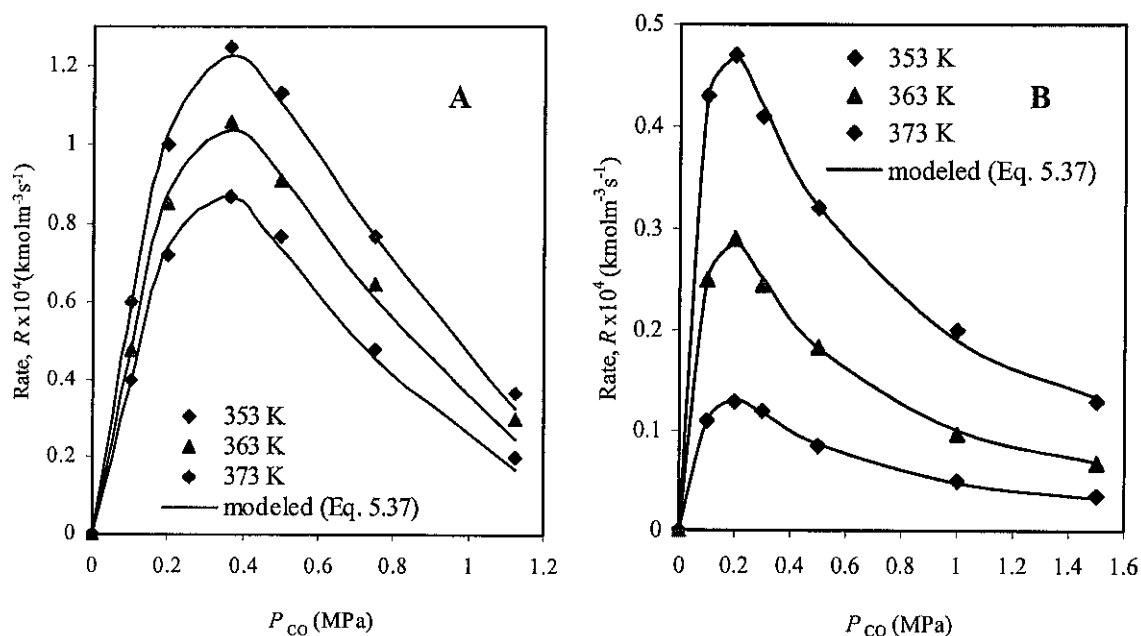


Figure 5.31: Effect of partial pressure of CO on the rate of hydroformylation of 1-octene (A) and 1-dodecene (B). Reaction conditions: $P_{H_2} = 1.5$ MPa, 1-olefins = $1.9 \text{ kmol}\cdot\text{m}^{-3}$, $\text{HRh}(\text{CO})(\text{PPh}_3)_3 = 1.73 \times 10^{-4} \text{ kmol}\cdot\text{m}^{-3}$, $\text{P}(\text{OPh})_3/\text{HRh}(\text{CO})(\text{PPh}_3)_3 = 12$, $\text{PC}/\text{dodecene}/1,4\text{-dioxane} = 0.30/0.10/0.60$.

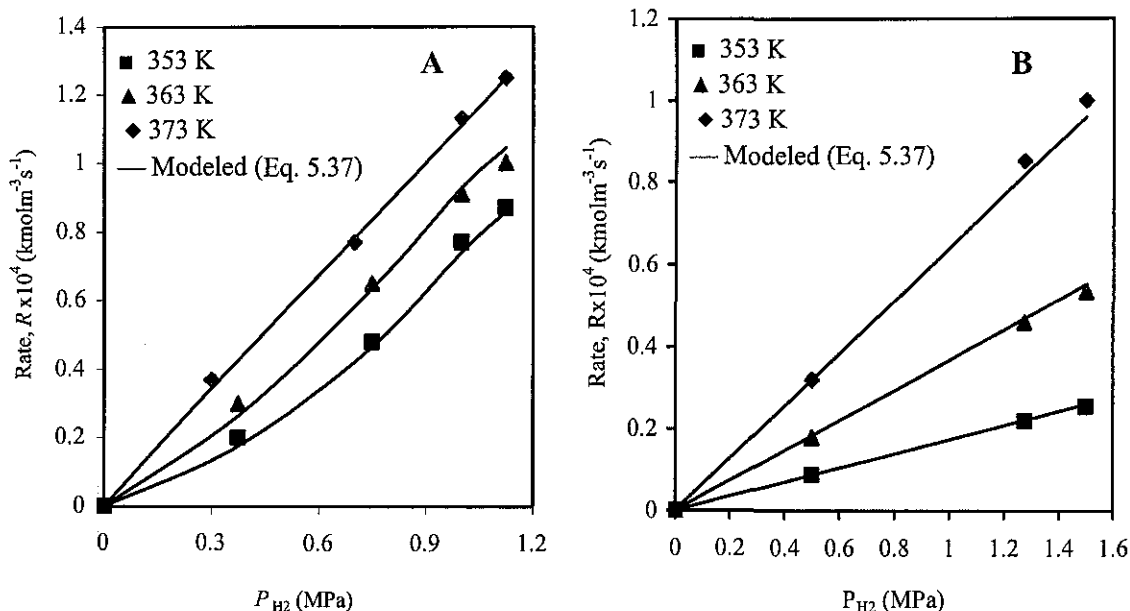


Figure 5.32: Effect of partial pressure of H₂ on the rate of hydroformylation of 1-octene (A) and 1-dodecene (B). Reaction conditions: $P_{CO} = 1.0$ MPa, $y_{H_2}/y_{CO} = 1/1$, 1-olefins = 1.9 kmol·m⁻³, HRh(CO)(PPh₃)₃ = 1.73×10^{-4} kmol·m⁻³, P(OPh)₃/HRh(CO)(PPh₃)₃ = 12, PC/dodecane/1,4-dioxane=0.30/0.10/0.60.

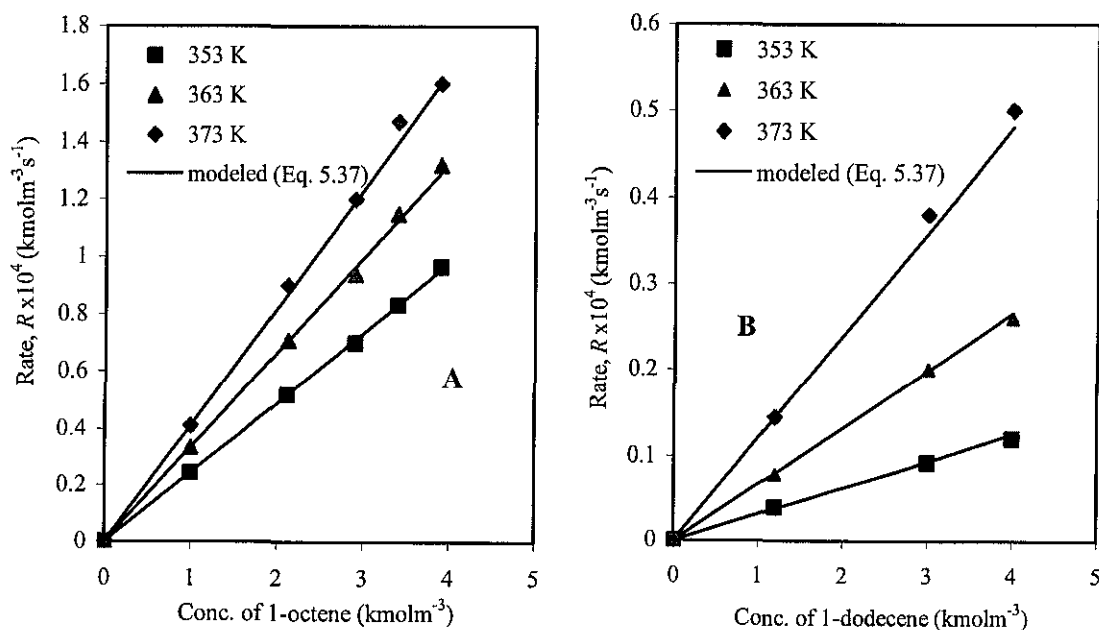


Figure 5.33: Effect of concentration of 1-olefin on the rate of hydroformylation of 1-octene (A) and 1-dodecene (B). Reaction conditions: $P = 1.5$ MPa, $y_{H_2}/y_{CO} = 1/1$, HRh(CO)(PPh₃)₃ = 1.73×10^{-4} kmol·m⁻³, P(OPh)₃/HRh(CO)(PPh₃)₃ = 12, PC/dodecane/1,4-dioxane=0.30/0.10/0.60.

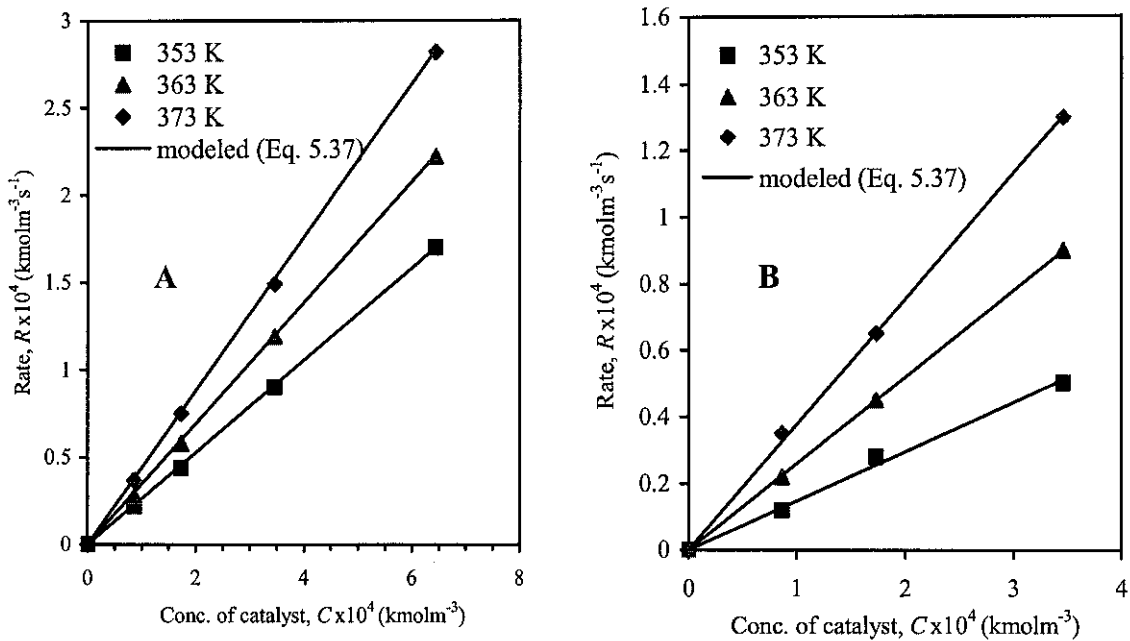


Figure 5.34: Effect of concentration of catalyst on the rate of reaction: 1-octene (A) and 1-dodecene (B). Reaction conditions: $P = 1.5$ MPa, $y_{H_2}/y_{CO} = 1/1$, 1-octene = 1.9 kmol·m⁻³, $P(OPh)_3/HRh(CO)(PPh_3)_3 = 12$, PC/dodecene/1,4-dioxane=0.30/0.10/0.60.

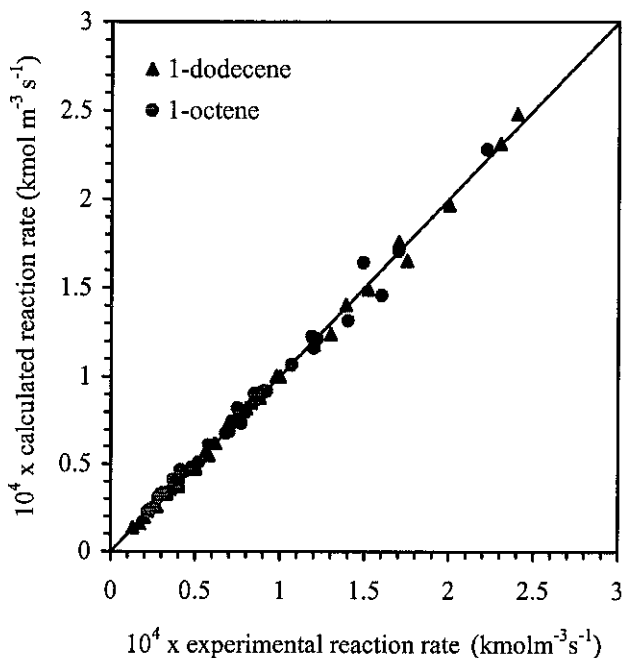


Figure 5.35: Parity plot of the model predictions of the rate of hydroformylation of 1-octene and 1-dodecene in TMS-systems of PC/dodecene/1,4-dioxane (0.30/0.10/0.60).

As Figure 5.35 displayed convincingly, the rate model A1 describes the experimental data of both substrates satisfactorily. The estimated parameters as well as the activation energy and error estimates are presented in Table 5.10.

Table 5.10: Estimated A1 kinetic model parameters with 95% confidence limits

Substrate	T (K)	k	K_1^*	K_2^*	K_3^*	K_4^*	SEE (%)	E_a (kJ mol ⁻¹)
1-octene	353	5.1×10^3	1.2×10^2	1.5×10^3	0.88	0	4.5	66.3
C ₈	363	8.0×10^3	2.0×10^2	1.3×10^3	6.8×10^{-3}	0		
	373	1.0×10^4	2.3×10^2	9.7×10^2	9.7×10^{-6}	0		
1-dodecene	353	7.1×10^2	0.99	2.4×10^3	0.63	9.0×10^{-2}	3.6	76.1
C ₁₂	363	1.3×10^3	5.28	2.2×10^3	0.17	4.8×10^{-2}		
	373	2.8×10^3	34.8	2.0×10^3	2.0×10^{-2}	0.10		

Since a negative order with respect to P_{CO} is observed experimentally, the concentration term of CO is raised to a higher power in the denominator than in the numerator (Helfferich, 2001). The regressed values of K_1^* and K_2^* for both substrates are relatively large and suggest that the effect of the P_{CO} inhibition on the rate of reaction is highly significant. As P_{CO} increases the denominator increases significantly compared to the numerator leading to a rapid decline in the reaction rate. On the other hand, high concentration of alkene in the presence of excess $P(OPh_3)_3$ ligand leads to a first order kinetic, and, in turn, the alkene-containing terms in the denominator is expected to have insignificant effect on the rate of reaction.

Equation (5.37) explains the inverse order dependence of the reaction rate on dissolved carbon monoxide concentration at high CO pressure. The rate parameters in the denominator are derived from the equilibrium constants of elementary steps in the reaction mechanism. Therefore, the regressed rate parameters can be used to estimate the rate of the elementary steps. For instance, the large value of K_2^* implies that the rate of dissociation and association of ligand, step 2 in Figure 5.30 is high. However, the value of K_1^* suggests that step 3 occurs at 3 orders of magnitude slower compared to step 2. On the other hand, difference of two orders of magnitude lower in the rate constant of the

alkene insertion step (step 5 and 6) with respect to step 3 was also observed and consistent with the experimental value reported in open literature (van Leeuwen, 2000). From the regressed value of K_4^* , the rate of the carbonyl insertion step (step 8) was found to be greater by three orders of magnitude compared to the alkene insertion step.

Comparing the regressed values of the rate constant, k at 353, 363 and 373 K, the values of k are higher for 1-octene than 1-dodecene. Activation energy of 66.3 and 76.1 kJ·mol⁻¹ were determined for the hydroformylation of 1-octene and 1-dodecene, respectively. Generally, the results suggest that the activation energy of the hydroformylation of higher olefins in the TMS-system is higher compared to the conventional organic solvent based system (46.2 to 69.7 kJ·mol⁻¹). The average deviation between experimental and calculated rate of reaction was found to be in the range of ± 4.0 %. Model A1 seems to give a slightly better description compared to the empirical model (±5.5 %) but this could be mainly attributed to the great flexibility arising from their structure having five (model A1) instead of three (empirical model, Equation (5.22)) rate parameters. The results also support previous findings in demonstrating that under the experimental conditions listed in Table 4.3, the acylrhodium complex is the resting state and oxidative addition of H₂ is rate determining (van Leeuwen and Claver, 2000).

5.4. Liquid-liquid Equilibrium Study

This work presented the liquid-liquid ternary equilibrium data of a TMS-system consisting of PC, dodecane and 1,4-dioxane, at atmospheric pressure and four different temperatures (298.15, 313.15, 333.15 and 353.15 K). The distributions of 1-octene, nonanal, triphenylphosphite ligand and HRh(CO)(PPh₃)₃ catalyst were measured at atmospheric pressure and two different temperatures (298.15 and 308.15 K) to model the extraction efficiency for a typical reaction, the hydroformylation of 1-octene. The liquid-liquid equilibria and solute distributions were also predicted using the UNIFAC and UNIQUAC models.

5.4.1. Liquid-liquid Equilibrium Data

The experimental binodal curves of the TMS-system obtained by cloud titrations at 298, 313, 333 and 353 K are shown in Figures 5.36, 5.37, 5.38 and 5.39, respectively. The isothermal 3-component phase diagram (PC+dodecane+1,4-dioxane) shows a closed loop at all the experimental temperatures.

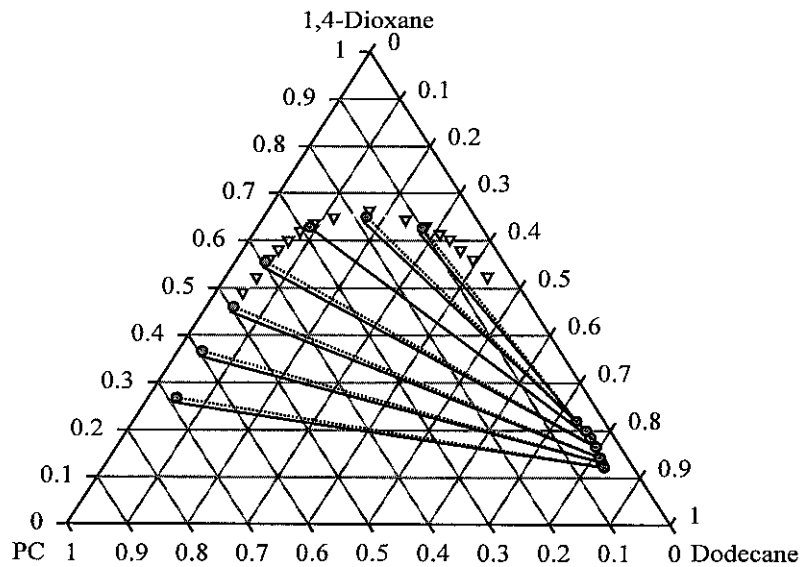


Figure 5.36: LLE ternary diagram for PC+dodecane+1,4-dioxane at 298.15 K; (▽) experimental binodal curve; (●) experimental tie lines data; (---) calculated (UNIQUAC) tie lines and (—) calculated (UNIFAC) tie lines.

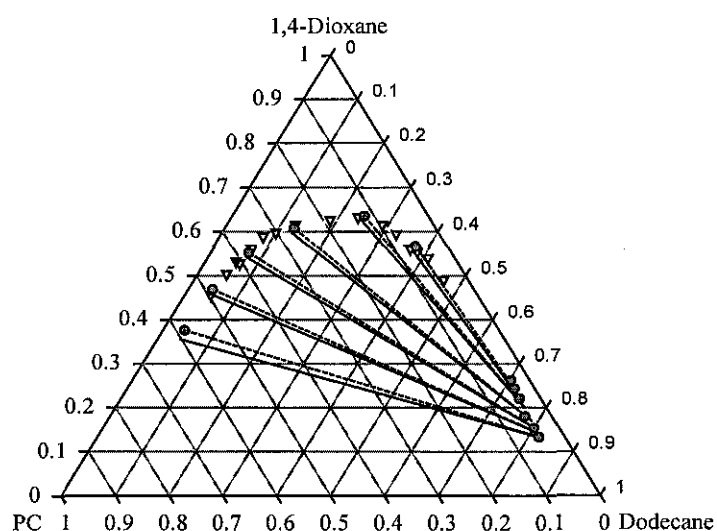


Figure 5.37: LLE ternary diagram for PC+dodecane+1,4-dioxane at 313.15 K; (∇) experimental binodal curve; (●) experimental tie lines data; (---) calculated (UNIQUAC) tie lines and (—) calculated (UNIFAC) tie lines.

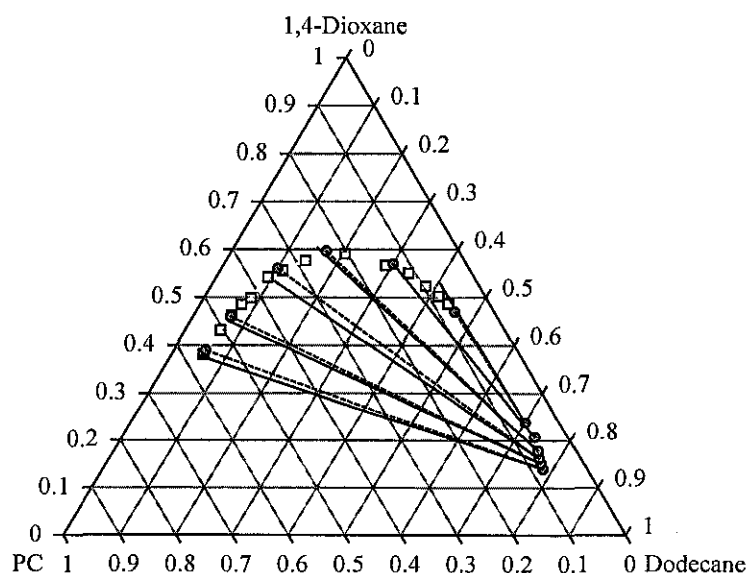


Figure 5.38: LLE ternary diagram for PC+dodecane+1,4-dioxane at 333.15 K; (∇) experimental binodal curve; (●) experimental tie lines data; (---) calculated (UNIQUAC) tie lines and (—) calculated (UNIFAC) tie lines.

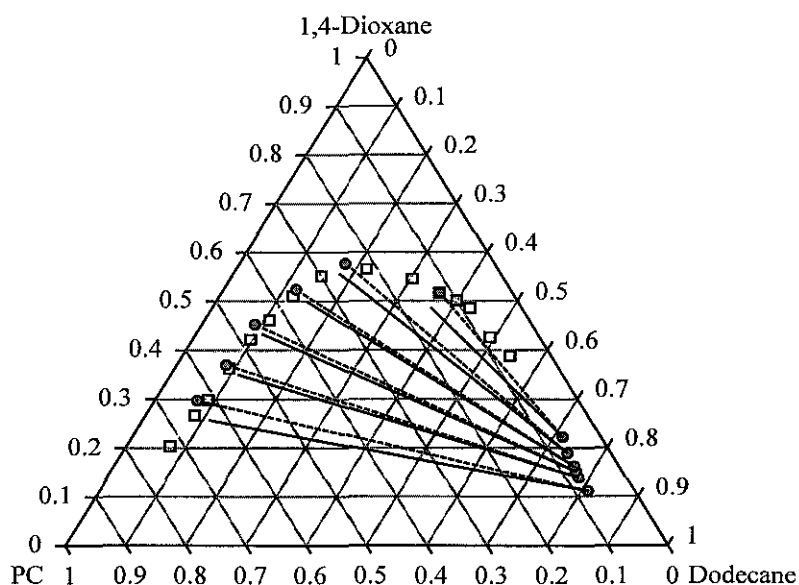


Figure 5.39: LLE ternary diagram for PC+dodecane+1,4-dioxane at 353.15 K; (V) experimental binodal curve; (●) experimental tie lines data; (---) calculated (UNIQUAC) tie lines and (—) calculated (UNIFAC) tie lines.

The miscibility gap or heterogeneous sphere of the system decreased with increasing temperature. The experimental tie-line compositions of the equilibrium phases at 298 and 308 K for the (TMS-system+1-octene), (TMS-system + nonanal), (TMS-system+1-octene+nonanal), and (TMS-system+1-octene+nonanal+ triphenylphosphite+catalyst) systems were summarized in Appendix J. To show the selectivity of the TMS-system in extracting the reactant (1-octene), product (nonanal), ligand (triphenylphosphite) and catalyst (HRh(CO)(PPh₃)₃), distribution coefficients (D_i) for these compounds (1-octene, nonanal, triphenylphosphite, HRh(CO)(PPh₃)₃) are defined as follows:

$$D_i = \frac{\text{Weight fraction in nonpolar phase}}{\text{Weight fraction in polar phase}} \quad (5.42)$$

The distribution coefficients for each equilibrium system and temperature are given in significantly decreases the distribution coefficient of 1-octene and nonanal. According to Behr et al. (2005), the addition of *trans*-4-octene into the ternary system of

PC+dodecane+*p*-xylene does not affect the position of the binodal curve. On the other hand, the addition of nonanal has a significant effect on the phase behavior of the solvent system. The binodal curves at 298 K and 353 K move closer to each other. However, the distributions of catalyst remain unchanged with or without the presence of 1-octene, nonanal and triphenylphosphite. The minimum distribution coefficient for 1-octene and nonanal are 1.33 and 1.75, respectively and on the other hand the maximum distribution coefficient for HRh(CO)(PPh₃)₃ and P(OPh)₃ are 0.034 and 0.23, respectively. These results suggest that the extraction of 1-octene, nonanal, HRh(CO)(PPh₃)₃ and P(OPh)₃ by the TMS-system from a 1-octene+nonanal+HRh(CO)(PPh₃)₃+P(OPh)₃ mixture is possible. The extraction capacity of the TMS- system at each temperature, plots D vs, x , for 1-octene, nonanal and HRh(CO)(PPh₃)₃ are given in Figures 5.40-5.42, respectively.

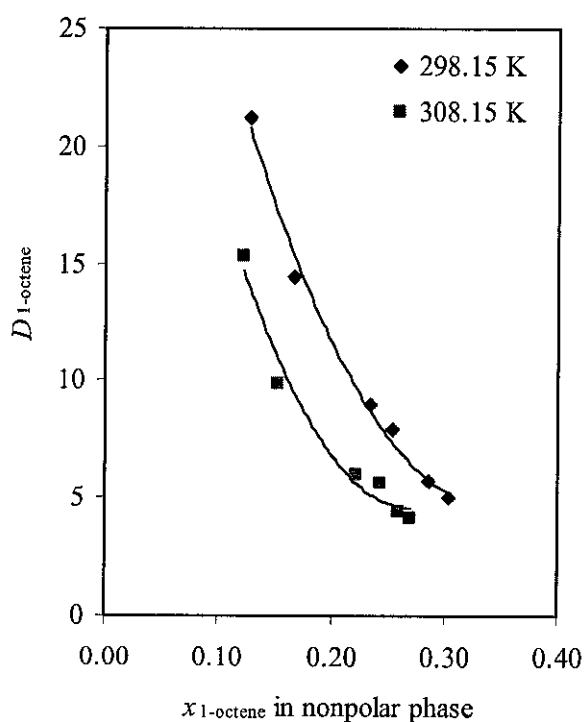


Figure 5.40: Distribution coefficient D of 1-octene as a function of the mass fraction x of 1-octene in the non polar phase.

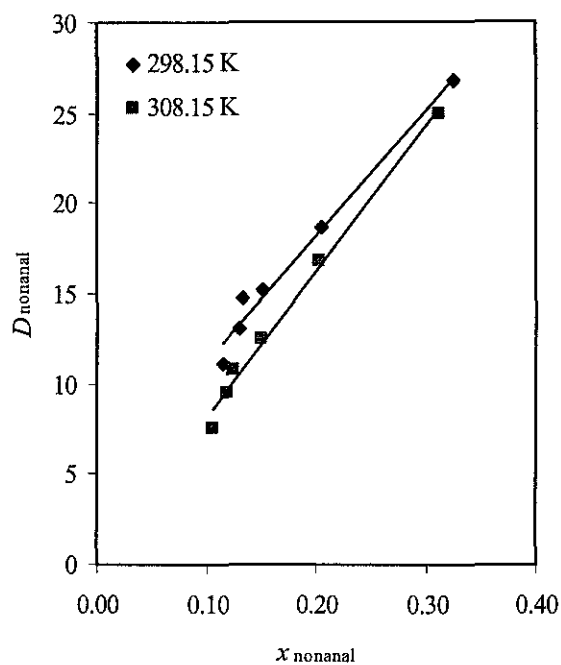


Figure 5.41: Distribution coefficient D of nonanal as a function of the mass fraction x of nonanal in the non polar phase.

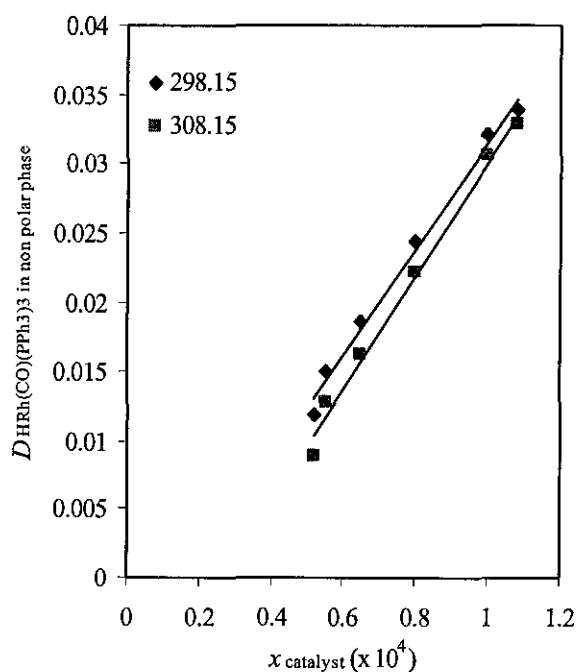


Figure 5.42: Distribution coefficient D of $\text{HRh(CO)(PPh}_3)_3$ catalyst as a function of the mass fraction x of $\text{HRh(CO)(PPh}_3)_3$ in the non polar phase.

The capacity of the extraction of the TMS system towards 1-octene decreases with the concentration of 1-octene in non polar phase at both 298 and 308 K. However, the data in Table 5.11 shows that capacity of extraction of the TMS system towards nonanal and $\text{HRh}(\text{CO})(\text{PPh}_3)_3$ increases with the concentration of nonanal and $\text{HRh}(\text{CO})(\text{PPh}_3)_3$ in the nonpolar phase. The effect of temperature change on the distribution is expected because the phase behavior of the TMS system is temperature dependent.

Table 5.11: Distribution coefficients of species in TMS- system

TMS+octene	298.15	13.05	
		7.78	
		4.12	
	308.15	8.33	
		7.04	
		3.70	
TMS+nonanal	298.15		22.96
			13.71
			18.40
	308.15		20.80
			12.02
			16.81
TMS+ $\text{HRh}(\text{CO})(\text{PPh}_3)_3$	298.15		0.0188
			0.0156
			0.0301
	308.15		0.0000
			0.0167
			0.0132
TMS+1-octene+nonanal	298.15	12.69	21.25
		7.57	12.64
		4.04	17.59
		2.32	33.97
		2.92	2.63
	308.15	8.17	17.48
		6.85	11.39
		3.64	15.53
		2.01	26.66
		1.52	1.75

According to Sorensen and Artl (Cháfer et al., 2008), PC+dodecane+1,4-dioxane ternary system is a type-1 system with only one liquid pair having very low miscibility (PC+dodecane) and two liquid pairs being miscible (PC+1,4-dioxane and 1,4-dioxane+dodecane). In this system, the non polar phase is on an average 78 wt % dodecane while the polar phase contains up to 75 wt % 1,4-dioxane. From these results, a highly effective extraction of the polar catalyst is expected, with nonpolar products easily extracted using dodecane. The differences in organic partitioning arise mainly from differences in polarity of the semi-polar solvent used in each system. 1,4-Dioxane has a non polar backbone, which causes it to be soluble in nonpolar dodecane, but because 1,4-dioxane has a compact chemical structure and polar ether bonds, it is partially soluble in the C₁₂ nonpolar phase. The amphiphilic character of this molecule causes it to distribute favourably in the polar phase. Although this property may not allow for effective product extraction (Robbins et al., 2007), it may be good for catalyst extraction.

5.4.2 Thermodynamic modeling

Liquid-liquid equilibrium (LLE) calculations were carried out by solving the thermodynamic criteria and mass balance equation

$$(\gamma_i x_i)^I = (\gamma_i x_i)^{II} \quad (5.43)$$

$$\sum_i x_i^I = \sum_i x_i^{II} = 1 \quad (5.44)$$

where I and II represent equilibrium phases and x is liquid phase mole fraction and γ the activity coefficient. Several models are available for the calculation of activity coefficients. In the present work UNIQUAC and UNIFAC models were used to correlate and interpret the experimental LLE data. The UNIQUAC and UNIFAC equations have found wide application for the description of liquid phase excess properties, owing to its sound theoretical background (Fredenslund, 1989; Robbins et al., 2007; Fahim and Merchant, 1998). However, LLE data are often fitted by UNIQUAC, because it provides a satisfactory description for many typical mixtures and because it is relatively simple

with its only two adjustable parameters. Its wide range of applicability is also one of the advantages. A comparison is then made of the prediction accuracy of the models.

5.4.2.1. UNIQUAC (UNIversal QUAsi-Chemical) model

Abrams and Prausnitz (1975) extended the quasi-chemical theory of liquid mixtures to solutions containing molecules of different sizes. This extension is called the UNIQUAC theory. The UNIQUAC model consists of two parts, the combinatorial part, which describes the prominent entropic contribution and residual part, which is due to the intermolecular forces that are responsible for the enthalpy of mixing. The combinatorial part involves the sizes and shape of the molecules and requires only pure component data. The residual part depends on the intermolecular forces and involves two adjustable binary parameters. The UNIQUAC equation expresses the molar excess Gibbs energy as a sum of a combinatorial part and residual part.

$$g^E = g^E(\text{combinatorial}) + g^E(\text{residual}) \quad (5.45)$$

The combinatorial part accounts for differences in the size and shape of the molecules, whereas the residual contribution accounts for energetic interactions.

The UNIQUAC activity coefficient for multicomponent systems is given by

$$\begin{aligned} \ln \gamma_i = & \ln \left(\frac{\phi}{x_i} \right) + \left(\frac{z}{2} \right) q_i \ln \left(\frac{\theta}{\phi} \right) + l_i \\ & - \left(\frac{\phi}{x_i} \right) \sum_{j=1}^m x_j l_j + q_i \left\{ 1 - \ln \left(\sum_{j=1}^m \theta_j \tau_{ji} \right) - \sum_{j=1}^m \left[\frac{\theta_j \tau_{ji}}{\sum_{i=1}^m \theta_i \tau_{ij}} \right] \right\} \end{aligned} \quad (5.46)$$

where

$$l_i = \left(\frac{1}{2} \right) z (r_i - q_i) - (r_i - 1) \quad (5.47)$$

z is a co-ordination number (= 10 usually), θ_i and ϕ_i are the volume fraction and the surface area fraction of the component i , respectively and given by:

$$\phi_i = \frac{x_i r_i}{\sum_{j=1}^3 x_j r_j}; \quad (5.48)$$

$$\theta_i = \frac{x_i q_i}{\sum_{j=1}^3 x_j q_j} \quad (5.49)$$

where r_i is the molecular-geometric volume parameter of pure component, and q_i is the molecular-geometric surface parameter of pure component that can be estimated by the Bondii's method.

The interaction parameter is given by

$$\tau_{ij} = \exp\left(\frac{-a_{ij}}{T}\right) \quad (5.50)$$

where the interaction parameter a_{ij} is a temperature dependent function which is assumed as

$$a_{ij} = A_{ij}^0 + \frac{A_{ij}^1}{T} \quad (5.51)$$

Thus, there are two binary parameters a_{ij} and a_{ji} in the UNIQUAC model and these are found by fitting LLE data.

5.4.2.2. The UNIFAC (UNIQUAC Functional Group Activity Coefficients) model

The group contribution method is more effective in predicting the activity coefficient of the components compared to other methods. The effectiveness of this method depends on the division of solution into number of interacting groups. As the mutual behavior of interacting groups cannot be determined experimentally, only certain thermodynamic model can be used, where the interaction parameters are determined from the behavior of

a real system. The group contribution method, namely UNIFAC has found wide application in practice.

The UNIFAC model is also based on the assumption that the contribution to the activity coefficient of component i can be separated into two parts, namely, combinatorial part (molecular size contribution) and residual part (intermolecular forces):

$$\ln \gamma_i = \ln \gamma_i^C + \ln \gamma_i^R \quad (5.52)$$

The size of a molecule is accounted in the combinatorial part and the actual interaction between the groups is accounted in the residual part. The other assumption is that, the contribution from interaction between molecular groups can be expressed as the sum of the individual contributions of each solute group in the solution minus the sum of the individual contributions of the pure molecular species:

$$\ln \gamma_i^R = \sum_{m=1}^g \nu_{mi} \left(\ln \Gamma_m - \ln \Gamma_m^{(i)} \right) \quad (5.53)$$

where Γ_m is the activity coefficient of group m in the mixture and $\Gamma_m^{(i)}$ is the activity coefficient of group m in pure compound i . Γ_m are functions of group fraction. The group fraction is defined as

$$X_k = \frac{\sum_{i=1}^N x_i \nu_{ki}}{\sum_{i=1}^N x_i \sum_{m=1}^g \nu_{mi}} \quad (5.54)$$

where ν_{ki} is the content of the group k in molecules of component i , N the number of components and g is the number of various groups in the mixture.

The combinatorial part of the UNIFAC equation can be expressed as follows:

$$\ln \gamma_i^C = \left(\frac{\ln \phi_i}{x_i} + 1 - \frac{\phi_i}{x_i} \right) - \frac{1}{2} z q_i \left(\frac{\ln \phi_i}{\theta_i} + 1 - \frac{\phi_i}{\theta_i} \right) \quad (5.55)$$

where

$$\phi_i = \frac{x_i r_i}{\sum_{j=1}^N x_j r_j} \quad (5.56)$$

$$\theta_i = \frac{x_i q_i}{\sum_{j=1}^N x_j q_j} \quad (5.57)$$

q_i and r_i are proportional to the surface area and volume of molecule i , which were estimated on the basis of R_k and Q_k values of the corresponding individual groups in the i th molecule, using the following relationship:

$$r_i = \sum_{k=1}^g \nu_{ki} R_k \quad (5.58)$$

$$q_i = \sum_{k=1}^g \nu_{ki} Q_k \quad (5.59)$$

where ν_{ki} is the number of k groups in the molecule of component i .

The residual part of the group activity coefficient was found using

$$\ln \Gamma_m = Q_m \left\{ 1 - \ln \left(\sum_{k=1}^g \Theta_k^g \Psi_{mk} \right) - \sum_{k=1}^g \left(\frac{\Theta_k^g \Psi_{mk}}{\sum_{j=1}^g \Theta_k^g \Psi_{jk}} \right) \right\} \quad (5.60)$$

where

$$\Theta_k^g = \frac{X_k Q_k}{\sum_{j=1}^g Q_j X_j} \quad (5.61)$$

Interaction parameter Ψ_{jk} is considered to be dependent on temperature as given below

$$\Psi_{jk} = \exp \left(\frac{-a_{jk}}{T} \right) \quad (5.62)$$

where parameters a_{jk} were estimated on the basis of experimental data (Magnussen et al., 1981). The van der Waals relative volume and surface of the components (r and q), needed for UNIQUAC and UNIFAC calculations, were estimated using group

contribution method and the required data were collected from Magnussen et al. (1981) and Bondi (1964). Since the study of LLE systems contain a maximum of 7 components, the calculations of the residual component of the UNIQUAC and UNIFAC models will be too complex. Therefore, PC, dodecane and 1,4-dioxane molecules are considered to be one 'test' molecule which is called TMS. This has been assumed for simplicity. The estimated components surface area (r) and volume (q) are given in Table 5.12.

Table 5.12: UNIFAC parameters r and q of the components

Compound	r	q
TMS (PC+dodecane+1,4-dioxane)	13.5629	12.790
HRh(CO)(PPh ₃) ₃	12.210	10.778
P(OPh) ₃	3.290	2.900
1-Octene	4.715	3.875
Nonanal	6.620	5.576
Propylene carbonate	3.584	3.178
Dodecane	17.092	14.192
1,4-Dioxane	3.185	2.640

However, the UNIFAC and UNIQUAC parameters for the interaction between TMS (PC+dodecane+1,4-dioxane), HRhCO(PPh₃)₃, P(OPh)₃ and other functional groups studied are not available in the literature. Therefore, it has been necessary to estimate these parameters before the suitability of the model can be tested. These parameters for the systems studied have been estimated by using one-half of the experimental LLE data set. In fact, the alternate data points were used for parameter estimation and the rest were used to test the applicability of the model. The following objective function was used to minimize the errors in the estimation of the interaction parameters where n denotes tie-lines $k = 1$ to n , phases $j=1$ and 2 , components $i=1,2$ and 3 , x^{exp} and x^{cal} are the experimental and calculated liquid phase mole fraction, respectively.

$$F = 100 \left\{ \frac{\sum_k^n \sum_i^3 \sum_j^2 (x_{ijk}^{\text{exp}} - x_{ijk}^{\text{cal}})^2}{6n} \right\}^{0.5} \quad (5.63)$$

The interaction parameters of the UNIQUAC and UNIFAC model were estimated using different initial guess values. Different sets of the interaction parameters were obtained based on the different initial guess values with minimum error difference or for same error in the calculated values. These results indicate the importance of the initial guess, and the possibility of the multiple parameters sets resulting from the minimization procedure of the UNIQUAC model. This may be due to the inter-correlation of the interaction parameters. The estimated interaction parameters of UNIQUAC and UNIFAC equations are given in Table 5.13 and 5.14, respectively.

Table 5.13: Binary interaction parameters of UNIQUAC equation

Temperature (K)	<i>i-j</i>	UNIQUAC interaction parameters (K)	
		a_{ij}	a_{ji}
298.15 K	TMS-catalyst	-6934.9	468.9
	TMS-1-octene	6131.3	-467.2
	TMS-nonanal	310.9	-61.8
	TMS-triphenylphosphite	-6013.1	-203.7
	HRh(CO)(PPh ₃) ₃ -1-octene	-100.7	-1019.8
	HRh(CO)(PPh ₃) ₃ -nonanal	-79.6	79.5
	HRh(CO)(PPh ₃) ₃ -triphenylphosphite	10.0	-486.4
	1-octene-nonanal	-232.7	-126.0
	1-octene-triphenylphosphite	276.8	757.9
	Nonanal-triphenylphosphite	12.0	2760.8
308.15 K	TMS-catalyst	-6934.9	400.3
	TMS-1-octene	6131.3	-460.6
	TMS-nonanal	335.6	-48.0
	TMS-triphenylphosphite	-6013.1	-175.8
	HRh(CO)(PPh ₃) ₃ -1-octene	-311.7	-1019.8
	HRh(CO)(PPh ₃) ₃ -nonanal	-411.8	79.5
	HRh(CO)(PPh ₃) ₃ -triphenylphosphite	10.0	-486.4
	1-octene-nonanal	-142.2	-125.5
	1-octene-triphenylphosphite	276.8	808.4
	Nonanal-triphenylphosphite	12.0	2760.7

Table 5.14: Interaction parameter a_{jk} of the UNIFAC equation

m/n	CH ₃	C=C	CHO	TMS	P(OPh) ₃	HRh(CO)(PPh ₃) ₃
CH ₃	0	76.54	158.1	4671.05	1001.03	-2909.55
C=C	292.3	0	-214.7	-293.92	-1141.79	1937.54
CHO	146.1	517	0	5782.18	1333.07	1575.04
TMS	-9159.88	730.33	154.72	0	-2952.94	774.23
P(OPh) ₃	845.93	6988.01	2149.36	-36.81	0	-3191.55
HRh(CO)(PPh ₃) ₃	-10.74	5207.96	1668.82	-566.36	-294.60	0

Table 5.15: The average deviation (%) of the experimental data from the calculated weight fractions using UNIQUAC and UNIFAC model

LLE system	Temperature	
	298.15 K	308.15 K
UNIQUAC model		
TMS-1-octene	0.33	0.66
TMS-nonanal	0.26	0.55
TMS- HRh(CO)(PPh ₃) ₃	0.10	0.16
TMS+1-octene+nonanal	0.42	0.86
TMS+1-octene+nonanal+ triphenylphosphite+ HRh(CO)(PPh ₃) ₃	1.13	1.49
UNIFAC model		
TMS-1-octene	0.30	1.38
TMS-nonanal	0.81	1.95
TMS- HRh(CO)(PPh ₃) ₃	3.31	3.30
TMS+1-octene+nonanal	1.25	1.35
TMS+1-octene+nonanal+ triphenylphosphite+ HRh(CO)(PPh ₃) ₃	3.05	3.09

Using the estimated interaction parameters of the models, the tie line data at different temperatures were predicted. The distribution coefficient of 1-octene, nonanal, triphenylphosphite and catalyst was also measured. The average deviation of the predicted results by UNIQUAC and UNIFAC methods were reported. The deviation is defined by the following equation:

$$\text{dev} = \frac{1}{N} \sum_{i=1}^N |x_i^{\text{ca}} - x_i^{\text{exp}}| \times 100 \quad (5.64)$$

where N is the number of experimental points and the superscripts 'exp' and 'cal' denote the experimental and calculated values, respectively. The average deviation of the calculated mole fractions from the experimental values for the UNIQUAC and UNIFAC method is shown in Table 5.15. The comparison of experimental tie line data of the ternary PC+1,4-dioxane+dodecane and TMS+1-octene+nonanal system with those calculated from the UNIQUAC and UNIFAC model is shown in Figure 5.36 to 5.39 and Figure 5.43 to 5.44, respectively. Both models fit the data well in the both ternary system at the given temperature. On the basis of the obtained deviations we conclude that both UNIQUAC and UNIFAC methods can be satisfactorily used to predict all the LLE system. However, UNIQUAC activity coefficient model leads to the best description of the experimental results for all LLE system. The limitation of the UNIQUAC model is the inability to explain the physical significance of the interaction parameters and their values. On the other hand, multiple set of interaction parameters is able to predict the LLE data equally good, hence the uniqueness of the interaction parameters was not there.

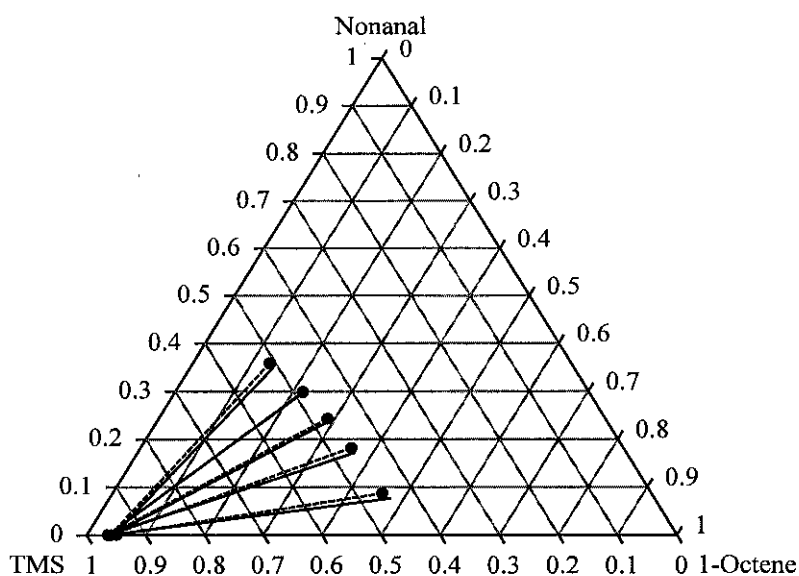


Figure 5.43: LLE ternary diagram for ternary (TMS+nonanal+1-octene) systems at 298.15 K; (●) experimental tie lines data; (---) calculated (UNIQUAC) tie lines and (—) calculated (UNIFAC) tie lines.

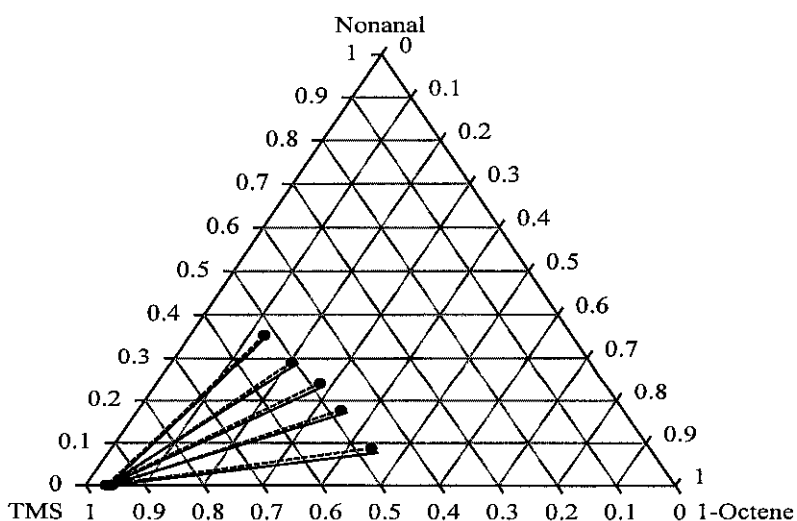


Figure 5.44: LLE ternary diagram for ternary (TMS+nonanal+1-octene) systems at 308.15 K; (●) experimental tie lines data; (---) calculated (UNIQUAC) tie lines and (—) calculated (UNIFAC) tie lines.

While the predictions of the ternary behavior were similar for both UNIFAC and UNIQUAC, there was a significant difference in predicting the distribution coefficients as shown in Table 5.16. UNIQUAC predicted well the distribution coefficients in all LLE system. For the UNIFAC model, the prediction of the distribution of the $\text{HRh}(\text{CO})(\text{PPh}_3)_3$ catalyst deviated from the measured values by several orders of magnitude and consistently over predicted the concentration of 1-octene, nonanal and $\text{HRh}(\text{CO})(\text{PPh}_3)_3$ catalyst in the polar phase. The deviations may be due to the limitations of the UNIFAC model. One deficiency is the limited availability of information on functional groups. In addition UNIFAC method only accounts for first-order structural differences and therefore, cannot distinguish between isomers or account for group-proximity effects within molecules. Therefore, further studies are required to better quantify the interactions between functionalities, as well as the role of molecular structure in multifunctional compounds.

Table 5.16: Experimental and predicted distribution of 1-octene, nonanal and $\text{HRh}(\text{CO})(\text{PPh}_3)_3$ in $\text{TMS}+1\text{-octene}+\text{nonanal}+\text{P}(\text{OPh}_3)_3+\text{HRh}(\text{CO})(\text{PPh}_3)_3$ system

$D_{1\text{-octene}}$			D_{nonanal}			$D_{\text{HRh}(\text{CO})(\text{PPh}_3)_3}$		
Expt	UNIQUAC	UNIFAC	Expt	UNIQUAC	UNIFAC	Expt	UNIQUAC	UNIFAC
298 K								
14.4	15.8	11.4	26.78	25.8	5.6	0.019	0.045	0.0036
7.9	9.6	5.6	13.08	18.7	3.5	0.015	0.016	0.0075
5.7	6.3	2.8	15.26	21.4	1.9	0.034	0.012	0.0014
2.6	3.7	2.1	18.67	28.7	1.3	0.024	0.010	0.0034
5.0	6.8	4.7	14.80	14.7	2.0	0.012	0.0097	0.0022
308 K								
8.2	9.9	6.1	24.93	29.3	5.2	0.016	0.025	0.0013
6.9	7.9	5.8	10.71	17.8	3.2	0.013	0.038	0.0008
3.6	4.3	2.7	12.49	16.2	1.7	0.033	0.052	0.0022
2.0	3.8	1.7	16.80	21.9	1.2	0.022	0.012	0.0019
1.5	2.7	0.6	9.50	13.5	1.9	0.009	0.0038	0.0021

5.5. Additional Validation of UNIQUAC and UNIFAC Model

Additional validation of the UNIQUAC and UNIFAC model was also performed to judge the overall model performance and provides one indication of expected model accuracy. The UNIFAC and UNIQUAC model were validated by comparing model predictions to existing LLE data obtained from the semi-batch hydroformylation reactor. It should be noted that the sample data used for model parameterization do not include reactor data. Therefore the validation represents a “fair test” of the model’s predictive abilities given the constraints of the data set. The experimental LLE data at temperature of 298 K were compared with those predicted using the UNIQUAC and UNIFAC model. As it is seen in Figure 5.45, the theoretical predictions of LLE data using UNIQUAC model were found to be within a maximum error of $\pm 6.5\%$, whereas UNIFAC predicts within $\pm 8.2\%$ error. Modeling showed that the UNIFAC model can be used for prediction of solute distribution in the studied solvent systems. However, UNIQUAC model is able to describe the experimental data with a better accuracy over the whole range of the operating conditions. The predicted LLE data using UNIQUAC model was close to that obtained from reaction runs. The results also indicate that the UNIQUAC and UNIFAC model can be extended to predict the distribution data of real catalytic systems.

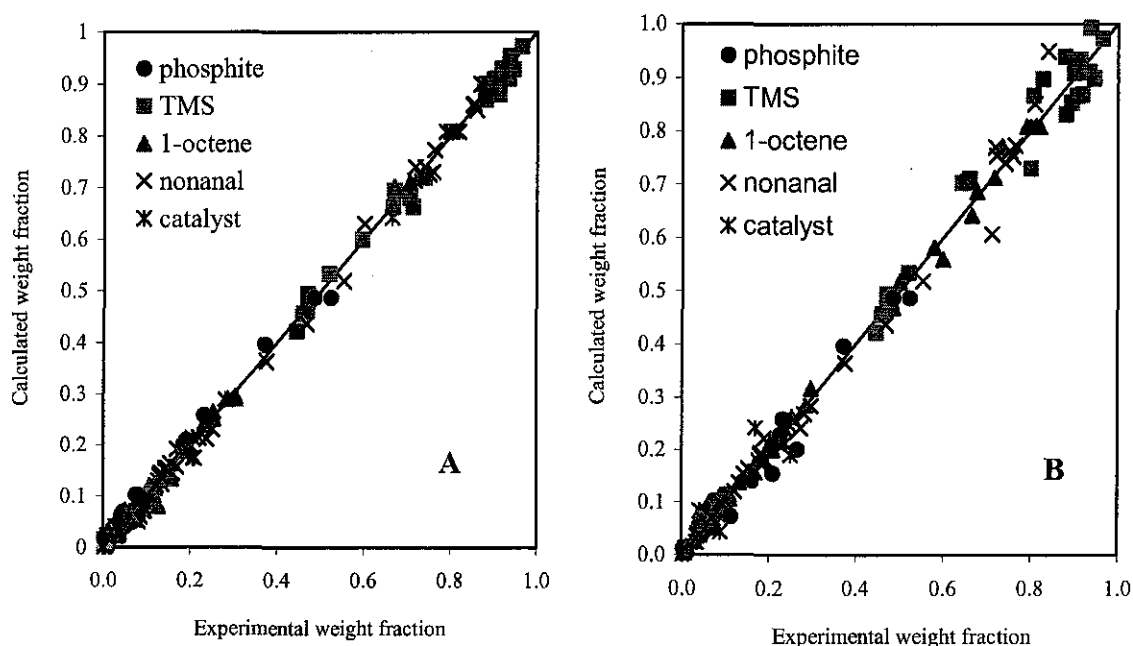


Figure 5.45: Parity plots of the model predictions of the LLE data of TMS+1-octene+nonanal+triphenylphosphite+HRh(CO)(PPh₃)₃ system at temperature of 298 K. (A) UNIQUAC model; (B) UNIFAC model

CHAPTER 6

CONCLUSION AND RECOMMENDATIONS

6.1 Conclusion

In this work, a thermomorphic solvent (TMS) system composed of propylene carbonate (PC), dodecane and 1,4-dioxane were developed for investigating hydroformylation of two higher olefins – 1-octene and 1-dodecene, using a homogeneous catalyst consisting of $\text{HRh}(\text{PPh}_3)_3(\text{CO})$ and $\text{P}(\text{OPh})_3$. The study began with the determination of the solubilities of H_2 and CO in pure solvent and solvent mixtures relevant to the hydroformylation process, particularly in the TMS-systems involving PC, dodecane and 1,4-dioxane. Findings indicated that PC and TMS-systems have a considerably higher affinity for CO and H_2 compared to the biphasic solvent mixture. The measured solubilities were tested against empirical model and activity coefficient models based on the regular solution theory (RST) with Yen and McKetta extension for polar solvents and the UNIFAC group contribution method. The logarithmic empirical model provided good fit to the experimental data except for H_2 -PC and CO -PC systems. The theoretical predictions of solubility by using modified UNIFAC were found to be within a maximum error of $\pm 8.5\%$, whereas RST based model predicts within 11.0 % error.

The effects of reaction condition including solvent composition, partial pressures of the gaseous reactants – CO and H_2 , reaction temperature and catalyst loading on the yield and selectivity of the linear aldehydes were investigated. Experimental results show that the shift of equilibria between various active species with varied reaction conditions seems to be a determining factor in the hydroformylation reactions. Low ligand/metal ratios and high syngas pressure lead to the formation of unmodified rhodium carbon species with the characteristic of high reaction rates and low selectivities. Isomerization and hydroformylation were in competition in the reaction of 1-octene. Hydroformylation of isomerization products (2-octene, 3-octene) disturbs the initial linear aldehyde selectivity. This disturbance should be taken into consideration for process improvement. Moreover, the initial aldehyde selectivity seems to be affected by reaction conditions such as temperature, total pressure of syngas, partial pressure of CO and ligand to catalyst

ratio. No significant change was observed in the selectivity by varying the concentration of the substrate, olefin. In addition, it is observed that the TMS- system leads to an enhancement in the catalytic activity, which is also comparable with the one under homogeneous conditions. In the hydroformylation of 1-octene using TMS-system of PC/dodecane/1,4-dioxane, highest selectivity for *n*-nonanal with average activity is observed at temperature of 363 K, equimolar of CO/H₂, total syngas pressure of 1.5 MPa, ligand/catalyst ratio of 12 and TMS composition of 0.1/0.3/0.6. Although most of the rhodium in the TMS- system can be separated by simple phase separation, the determined rhodium loss (in the range of 0.6-6 ppm) is still not economically acceptable. Further separation process is required accompanied by the phase separation for the complete catalyst recovery. However, the thermomorphic solvent system proved to have potential as a reaction medium in practical applications of the higher olefins hydroformylation.

Kinetic results obtained for the hydroformylation of 1-octene and 1-dodecene, are in good accordance with each other. The hydroformylation activity using 1-octene seems to be higher than 1-dodecene. The effects of concentration of the olefins, catalyst loading, partial pressure of CO and H₂ and temperature on the rate of reaction have been studied at 353, 363 and 373 K. The rate was found to be first order with respect to catalyst, 1-octene and partial pressure of H₂. The rate vs. P_{CO} shows a typical case of substrate inhibited kinetics. The rate model with H₂-addition as the controlling step was found to represent the rate data. The rate model predicted the conversion of the two alkenes satisfactorily with an average absolute error of ± 4.0 % only.

Experimental liquid-liquid equilibrium (LLE) data for the ternary system PC+dodecane+1,4-dioxane at varying temperature and the distribution of 1-octene, nonanal, and HRh(CO)(PPh₃)₃ catalyst in this system indicate that the TMS- system may serve as a feasible reaction medium and could be useful in extracting products from systems containing recyclable amphiphilic ligands and organometallic catalysts. The experimental tie lines were compared to the values predicted by the UNIQUAC and UNIFAC models. UNIQUAC predicted well the distribution coefficients in all LLE systems. For the UNIFAC model, the predictions of distribution coefficient consistently over predicted the concentration of 1-octene, nonanal and HRh(CO)(PPh₃)₃ in the polar phase. The UNIFAC and UNIQUAC model were further validated by comparing model

predictions to existing LLE data obtained from the semi-batch hydroformylation reactor. The theoretical predictions of LLE data using UNIQUAC model were found to be within a maximum error of $\pm 6.5\%$, whereas UNIFAC predicts within $\pm 8.2\%$ error indicating that both models can be extended to predict the distribution data of real catalytic systems.

Mechanistic studies of the hydroformylation of higher olefins using Rh-phosphine catalyst were investigated using theoretical approaches. The *ab initio* computational methodology is found to be a reliable tool for arriving at the reaction energetics and pathways in the hydroformylation of higher olefins. These information together with experimental data proves to be effective in developing macroscopic practically useful rate models. Mechanism of reaction featuring oxidative addition of H_2 to acylrhodium intermediate species as rate determining is found to describe the hydroformylation of all the four substrates – namely, 1-dodecene, 1-decene, 1-octene and styrene without the addition of free phosphine ligand. The rate model predicted the conversion of all the four olefins quite satisfactorily with an average deviation of 7.6% and maximum deviation of 13% . As for the potential energy surface fitting, the current approach is still limited to small molecules. In this study, although the PPh_3 was used in experiments, we had to use PH_3 due to the computational limitations. This limitation comes from the lack of efficient representation of molecules, the complexity in computing the primary and secondary invariants, and the cost in obtaining the high quality *ab initio* energies. Considering the fast development of the computer techniques, it is still very promising to construct highly accurate potential energy surfaces for large molecule systems.

6.2 Recommendations for Future Work

The capabilities of computational chemistry have expanded rapidly over the last 3 – 4 decades, as hardware has become orders of magnitude more powerful and software has become more efficient and sophisticated. In this study, the kinetic and equilibrium parameters of the kinetic models were estimated by nonlinear least square regression of experimental data. In future work it will be interesting to determine the kinetic and equilibrium parameters in the mechanistic model as well as the activation energy from the first-principles calculations, in combination with statistical mechanics, although some additional assumptions may be required to derive the pre-exponential factors. In order to

evaluate the accuracy of this approach, the predictions of the first-principles based kinetic model should be validated by comparison with experimental data for the hydroformylation of higher olefins. Similarly, the approach should also apply to the hydroformylation of higher olefins using Rh/P(OPh)₃ catalyst in TMS- system. According to Matsubara et al., (1997), the coordinatively unsaturated intermediates in the catalytic cycle are strongly coordinated and stabilized by a solvent olefin molecule, while the transition states are not solvated. However, we believe that higher olefin coordination to coordinatively unsaturated intermediates is less favourable kinetically because of the size of the carbon chain which would sterically inhibit an olefin from solvating the intermediate. Therefore, the role of solvation in hydroformylation of higher olefins should be assessed and compared with lower olefins.

Developing a TMS-system with an efficient catalyst recycling capacity for hydroformylation of higher olefins should be a realistic possibility. The simple and efficient catalyst recycling concept gives the TMS-system the unique feature to perform hydroformylation reaction at a lower operating cost. An important aspect for industrial application is the complete recovery of the catalyst. Rhodium loss by organic phase after phase separation is in a range of 0.6-6 ppm in the nonpolar phase, therefore additional separation step is necessary for the total recovery of the expensive catalyst. Since basic task of separating catalyst from product has already be achieved by the phase separation additional membrane processes can enhance further work-up of the homogeneous catalyst. The Rh-phosphite catalyst can be separated using a solvent resistant nanofiltration (SRNF) membrane or a rugged inorganic membrane. For example, use of asymmetric polyamide membranes have been investigated in the nanofiltration of phase transfer catalysts and Wilkinson catalyst (chlorotris(triphenylphosphine)-rhodium(I), from reaction mixtures (Luthra et al., 2002; Scarpello et al., 2002)

REFERENCES

- Abrams, D.S., Prausnitz, J.M. (1975). Statistical thermodynamics of liquid mixtures: A new expression for the excess Gibbs energy of partly or completely miscible systems. *AIChE J.*, 14, 135-144.
- Annesini, M.C., Gironi, F., Marreill, L., Kikic, I. (1985). Liquid-Liquid Equilibria for Ternary Systems Containing Hydrocarbons and Propylene Carbonate *J. Chem. Eng. Data*, 30, 195-196.
- Anthony, J.L. (2004). Gas solubilities in ionic liquids: experimental measurements and applications. PhD thesis, Univ. of Notre Dame, p. 93.
- Antunes, C., Tassios, D. (1983). Modified UNIFAC model for the prediction of Henry's constants. *Ind. Eng. Chem. Process Des. Dev.* 22,457-462.
- Arhancet, J.P., Davis M.E., Merola, J.S., Hanson, B.E. (1990). Supported aqueous-phase catalysts. *J. Catal.* 121, 327-339.
- Bahrmann, H., Bogdanovic, S., Leeuwen, P.W.N.M.V. (2004). *Aqueous-Phase Organometallic Catalysis*, second ed. Wiley-VCH, 391-395.
- Bandrés, I., Giner, I., Pera, G., Giner, B., Lafuente, C. (2007). Vapour-liquid equilibrium of cyclic ethers with 1-chlorohexane: Experimental results and UNIFAC predictions. *Fluid Phase Equilib.*, 257, 70-77.
- Becke, A.D. (1993). Density-functional thermochemistry. III. The role of exact exchange. *J. Chem. Phys.* 98, 5648.
- Behr, A., Fangewisch, C. (2003). Rhodium-catalysed synthesis of branched fatty compounds in temperature-dependent solvent systems. *J. Mol. Catal. A: Chem.*, 197: 115-126
- Behr, A., Henze, G., Obst, D., Turkowski, B. (2005a). Selection process of new solvents in temperature-dependent multi-component solvent systems and its application in isomerising hydroformylation. *Green Chem.*, 7, 645-649.
- Behr, A., Obst, D., Turkowski, B. (2005b). Isomerizing hydroformylation of trans-4-octene to n-nonanal in multiphase systems: acceleration effect of propylene carbonate. *J. Mol. Catal. A: Chem.*, 226:215-219.

- Behr, A., Miao, Q. (2004). A new temperature-dependent solvent system based on polyethylene glycol 1000 and its use in rhodium catalyzed co-oligomerization. *J. Mol. Catal. A: Chem.*, 222:127-132.
- Behr, A., Roll, R. (2005). Hydroaminomethylation in thermomorphic solvent systems. *J. Mol. Catal A: Chem.*, 239:180-184.
- Bell, S., Dines, T.J., Chowdhry, B.Z., Withnall, R. (2007). Computational chemistry using modern electronic structure methods. *J. Chem. Edu.* 84, 1364-1370.
- Beller, M., Cornils, B., Frohning, C.D., Kohlpaintner, C.W. (1995). Progress in hydroformylation and carbonylation. *J. Mol. Catal. A*, 104, 17-85.
- Bergbreiter, D.E., Liu, Y.S., Osburn, P.L. (1998). Thermomorphic Rhodium(I) and Palladium (0) Catalysts. *J. Am. Chem. Soc.*, 120, 4250-4251.
- Bhaduri, S., Mukesh, D. (2000). Homogeneous Catalysis: Mechanisms and Industrial Applications. John Wiley and Sons, ISBN 0471372218, 9780471372219.
- Bhanage, B.M., Divekar, S.S., Deshpande, R.M., Chaudari R.V. (1997). Kinetics of hydroformylation of 1-dodecene using homogeneous HRh(CO)(PPh₃)₃ catalyst. *J. Mol. Catal. A Chem.* 115, 247-257.
- Bianchi, M., Piacenti, F., Frediani, P., Matteoli, U. (1977). Hydroformylation of deuterated olefins in the presence of cobalt catalysts : II. Experiments at low pressure of carbon monoxide. *J. Organomet. Chem.*, 137:361, 1977.
- Bianchini, C.P., Sernau, V. (1995). Zwitterionic Metal Complexes of the New Triphosphine NaO₃S(C₆H₄)CH₂C(CH₂PPh₂)₃ in Liquid Biphasic Catalysis: An Alternative to Teflon "Ponytails" for Facile Catalyst Separation without Water *Organometallics*, 14: 5458-5459.
- Bohnen, H., Cornils, B. (2003). Hydroformylation of Alkenes: An Industrial View of the Status and Importance. *ChemInform*, 34, 17.
- Bondi, A. (1964) van der Waals volumes and radii. *The Journal of Physical Chemistry*, 68, 441-451.
- Brady, C.J., Cunningham, J.R., Wilson, G.M. (1982). Water-hydrocarbon liquid-liquid-vapour equilibrium measurements to 530°F, Research report RR-62, Gas Processors' Association, Provo, UT.

- Breman, B.B., Beenackers, A.A. (1996). Thermodynamic models to predict gas-liquid solubilities in the methanol synthesis, the methanol-higher alcohol synthesis, and the Fischer-Tropsch synthesis via gas-slurry processes. *Ind. Eng. Chem. Res.* 35, 3763-3775.
- Broussard, M.E., Juma, B., Train, S.G., Peng, W.J., Laneman, S.A., Stanley, G.G. (1993). *Science*, 260, 1784.
- Brown, C.K., Wilkinson, G. (1970). Homogeneous hydroformylation of alkenes with hydridocarbonyltris-(triphenylphosphine)rhodium(I) as catalyst. *J. Chem Soc. (A)*, 2753-2764.
- Brown, J.M., Kent, A.G. (1987). Structural characterisation in solution of intermediates in rhodium-catalysed hydroformylation and their interconversion pathways. *J. Chem. Soc., Perkin Trans. 2*, 1597-1607.
- Cavallotti, C., Rota, R., Faravelli, T., Ranzi, E. (2007). *Ab initio* evaluation of primary cyclo-hexane oxidation reaction rates. *Proceedings of Combustion Inst.* 31, 201-209.
- Cháfer, A., de la Torre, J., Monton, J.B., Lladosa, E. (2008). Liquid-liquid equilibria of the systems isobutyl acetate+isobutyl alcohol+water and isobutyl acetate+isobutylalcohol+glycerol at different temperatures. *Fluid Phase Equilibria*, 265, 122-128.
- Chapoy, A. 2004. Phase behaviour in water/hydrocarbon mixtures involved in gas production systems. Ph.D. Thesis, Ecole Des Mines De Paris, p. 241.
- Chen, H., Li, Y.Z., Chen, J.R., Cheng, P.M., He, Y.E., Li, X.J., (1999). Micellar effect in high olefin hydroformylation catalyzed by water-soluble rhodium complex. *J. Mol. Catal. A*, 149, 1-6.
- Chen, J., Alper, H. (1997). A Novel Water-Soluble Rhodium-Poly(enolate-co-vinyl alcohol-co-vinyl acetate) Catalyst for the Hydroformylation of Olefins. *J. Am. Chem. Soc.*, 119 (5): 893-895.
- Chernyak, Y. (2008). Phase Equilibria in Binary Mixtures of Water with Cyclic Alkylene Carbonates. *J. Chem. Eng. Data*, 53, 603–606.
- Chiba, K., Kono, Y., Kim, S., Nishimoto, K., Kitano, Y., Tada, M. (2002). A liquid-phase peptide synthesis in cyclohexane-based biphasic thermomorphic systems. *Chem. Commun.*, 1766-1767.

- Cornils, B., Herrmann, W.A. (2004). *Aqueous-phase Organometallic Catalysis*; 2nd ed. Wiley-VCH.
- Cornils, B., Herrmann, W.A. (2002). *Applied Homogeneous Catalysis with Organometallic Compounds*, second ed. Wiley-VCH, pp. 31-103.
- Costa, R., Kristbergsson, K. (2009). *Predictive Modeling and Risk Assessment*; Springer, ISBN: 978-0-387-33512-4.
- Cotton, F. A., Wilkinson, G. (1988). *Advanced Inorganic Chemistry*; 5th ed. Wiley Interscience: USA.
- Coutinho, K.J., Dickson, R.S., Fallon, G.D. Jackson, W.R., De Simone, T., Skelton, B.W., White, A.H. (1997). Isolation and characterization of hydroformylation 'intermediates' from stoichiometric reactions between phosphinoalkenes and some heterobinuclear complexes. *J. Chem. Soc., Dalton Trans.*, 3193–3199.
- Cuevas, R.M., Eustaquio-Rincón, R., Romero-Martínez, A., Trejo, A. (1995). Experimental liquid-liquid miscibility curves for binary systems: ethanenitrile and butanenitrile with n-alkanes. *Fluid Phase Equilibria*, 107, 201-212.
- De Paz, J.L., Ciller, J. (1993). On the use of AM1 and PM3 methods on energetic compounds. *Propellants, Explosives, Pyrotechnics*, 18, 33-40.
- Deshpande, R.M., Chaudhari, R.V. (1988). Kinetics of 1-hexene using homogeneous HRh(CO)(PPh₃)₃ complex catalyst. *Ind. Eng. Chem. Res.* 27, 1996-2002.
- Deshpande, R. M., Chaudhari, R. V. (1989). Hydroformylation of Vinyl Acetate Using Homogeneous HRh(CO)(PPh₃)₃ Catalyst: A Kinetic Study. *J. Mol. Catal.*, 57, 177.
- Deshpande, R.M., Divekar, S.S., Bhanage, B.M., Chaudhari, R.V. (1992). Effect of solvent on the kinetics of hydroformylation of 1-hexene using HRh(CO)(PPh₃)₃ catalyst. *J. Mol. Catal.* 77, L13-L17.
- Deshpande, R.M., Bhanage, B.M., Divekar, S.S., Chaudhari, R.V. (1993). Solvent effects in hydroformylation of 1-octene using HRh(CO)(PPh₃)₃: Effect of PPh₃ addition on the rate of reaction. *J. Mol. Catal.* 78, L37-L40.
- Deshpande, R.M., Purwanto, R.P., Delmas, H., Chaudhari, R.V. (1996). Kinetics of Hydroformylation of 1-Octene using [Rh(COD)Cl]₂-TPPTS complex catalyst in a two-phase system in the presence of a cosolvent. *Ind. Eng. Chem. Res.* 35, 3927.

- Divekar, S.S., Deshpande, R.M., Chaudhari, R.V. (1993). Kinetics of hydroformylation of 1-decene using homogeneous $\text{HRh}(\text{CO})(\text{PPh}_3)_3$ catalyst: a molecular approach. *Catal. Lett.*, 21, 191-200.
- Diwakar, M.M., Deshpande, R.M., Chaudhari, R.V. (2005). Hydroformylation of 1-hexene using Rh/TPPTS complex exchanged on anion exchange resin: kinetic studies. *J. Mol. Catal. A: Chem.*, 232:179-186.
- Dorset, D.L. (1990). Binary phase behavior of perfluoroalkanes. *Macromolecules*, 23: 894-901.
- Drent, E and Jager, W.W. (1995). Shell Int. Res., GB 2.282.137.
- Evans, D., Osborn, J., Wilkinson, G. (1968). Hydroformylation of alkenes by use of rhodium complex catalysts. *J. Chem. Soc. A.* 3133-3142.
- Fahim, M.A., Elkilani, A.S. (1991). Prediction of the solubility of hydrogen in naphtha reformat using the modified UNIFAC Group Contribution Method. *Ind. Eng. Chem. Res.* 30, 255-259.
- Fahim, M.A., Merchant, S.Q. (1998). Liquid-liquid equilibria of systems containing propylene carbonate and some hydrocarbons. *J. Chem. Eng. Data*, 43, 884-888.
- Fogg, P.G.T., Gerrard, W., (1991). Solubility of Gases in Liquids: A Critical Evaluation of Gas/Liquid Systems in Theory and Practice. Wiley, Chichester.
- Foster, D. F., Gudmunsen, D., Adams, D. J., Stuart, A. M., Hope, E. G., Cole-Hamilton, D. J.; Schwarz, G. P.; Pogorzelec, P. (2002). Hydroformylation in perfluorinated solvents; improved selectivity, catalyst retention and product separation. *Tetrahedron*, 58, 3901-3910.
- Fredenslund, A. (1989). UNIFAC and related group-contribution models for phase equilibria. *Fluid Phase Equilibria*, 52, 135-150.
- Fredenslund, A., Gmehling, J., Rasmussen, P. (1977). Vapor-liquid equilibria using UNIFAC. Elsevier, Amsterdam.
- Garton, R.D., Ritchie, J.T., Caers, R.E. (2003). Hydroformylation process improvement in catalyst recovery. PCT International Applications, WO 2003/082789 A2: 20.
- Gholap, R.V., Kunt, O.M., Bourne, J.R., (1992). Hydroformylation of propylene using unmodified cobalt carbonyl catalyst: Selectivity Studies. *Ind. Eng. Chem Res.*, 31, 2446-2450.

- Gmehling, J., Li, J., Schiller, M. (1993). A Modified UNIFAC Model. 2. Present Parameter Matrix and Results for Different Thermodynamic Properties. *Ind. Eng. Chem. Res.*, 32, 178-193.
- Gmehling, J., Rasmussen, P., Fredenslund, A. (1982). Vapour-liquid equilibria by UNIFAC group contribution: revision and extension 2. *Ind. Eng. Chem., Proc. Des. Dev.*, 21, 118-127.
- Hartounian, H. and Allen, D.T. (1988). Group Contribution Methods for Coal-Derived Liquids. *Fuel*, 67, 1609-1614.
- Haumann, M., Koch, H., Hugo, P., Schomacker, R. (2002). Hydroformylation of 1-dodecene using Rh-TPPTS in a microemulsion. *Applied Catal. A: General* 225: 239-249.
- Heck, R.F. and Breslow, D.S. (1961). The reaction of cobalt hydrotetracarbonyl with olefins. *J. Am. Chem. Soc.*, 83, 4023-4027.
- Hehre, W.J., Radom, L., Schleyer, P.V., Pople, A.J. (1986). *Ab initio Molecular Orbital Theory* New York: John Wiley and Sons, ISBN: 9780471812418.
- Helfferich FG. Kinetics of homogeneous multistep reactions. (2001). Elsevier Science, Amsterdam, Netherlands. 38, pp.167-168.
- Herrmann, W.A., Kohlpaintner, C.W., Bahrmann, H., Konkol, W. (1992). Water-soluble metal complexes and catalysts Part 6. A new, efficient water-soluble catalyst for two-phase hydroformylation of olefins. *J. Mol. Catal.*, 73, 191-201.
- Hildebrand, J.H., Cochran, D.R.F. (1949). Liquid-Liquid Solubility of Perfluoromethylcyclohexane with Benzene, Carbon Tetrachloride, Chlorobenzene, Chloroform and Toluene. *J. Am. Chem. Soc.*, 71: 22-25.
- Hildebrand, J.H., Scott, R.L. (1948). Solubility of electrolytes and non-electrolytes. *J. Am. Chem. Soc.* 424, 9.
- Hohenberg, P., Kohn, W. (1964). Inhomogeneous Electron Gas. *Phys. Rev.* 136, B864.
- Horváth, I.T., Rábai, J. (1994). Facile Catalyst Separation Without Water: Fluorous Biphasic Hydroformylation of Olefins. *Science*, 266, 72-75.
- Horváth, I.T. (1990). Hydroformylation of Olefins with the Water Soluble $\text{HRh(CO)[P(m-C}_6\text{H}_4\text{SO}_3\text{Na)}_3\text{]}_3$ in Supported Aqueous-Phase. Is it Really Aqueous? *Catal. Lett.*, 6, 43-48.

- Hu, Y. and Xu, Y. (1985). Molecular thermodynamics of gas solubility. *Fluid Phase Equilib.*, 23: 15-40.
- Huang, L., He, Y., Kawi, S. (2004). Catalytic studies of aminated MCM-41-tethered rhodium complexes for hydroformylation of 1-octene and styrene. *J. Mol. Catal. A*, 213, 241-249.
- Hurtado, P., Ordonez, S., Sastre, H., Diez, F.V. (2004). Development of a kinetic model for the oxidation of methane over Pd/Al₂O₃ at dry and wet conditions. *Applied Catal. B: Environmental*. 51, 229-238.
- Jáuregui-Haza, U.J., Dessoudeix, M., Ph. Kalck, Wilhelm, A.M., Delmas, H. (2001). Multifactorial analysis in the study of hydroformylation of oct-1-ene using supported aqueous phase catalysis. *Catal. Today*, 66, 297-302.
- Jáuregui-Haza, U.J., Pardillo-Fontdevila, E., Wilhelm, A.M., Delmas, H., (2004). Solubility of hydrogen and carbon monoxide in water and some organic solvents. *Latin American Applied Research* 34, 71-74.
- Jin, Z.L., Zheng, X., Fell, B. (1997). Thermoregulated phase transfer ligands and catalysis. I. Synthesis of novel polyether-substituted triphenylphosphines and application of their rhodium complexes in two-phase hydroformylation. *J. Mol. Catal. A: Chem.*, 116: 55-58.
- Johnson, T.H. (1985). US Patent, 4.584.411.
- Jongsma, T., Challa, G., van Leeuwen, P.W.N.M. (1991). A mechanistic study of rhodium tri(*o*-*t*-butylphenyl)phosphite complexes as hydroformylation catalysts. *Organometal. Chem.* 421, 121.
- Karakhanov, E.A., Yu. S. Kardasheva, A. L. Maksimov, V. V. Predeina, E. A. Runova and A. M. Utukin (1996). Macrocomplexes on the basis of functionalized polyethylene glycols and copolymers of ethylene oxide and propylene oxide: synthesis and catalysis. *J. Mol. Catal. A: Chem.*, 107, 235-240.
- Katayama, H. (1999). Liquid-liquid equilibria of two ternary systems: methanol-cyclohexane including 1,3-dioxolane or 1,4-dioxane in the range of 277.79–308.64 K. *Fluid Phase Equilibria* 164, 83–95.

- Kiss, G., Mozeleski, E.J., Nadler, K.C. Van Driessche, E., DeRoover, C. (1999). Hydroformylation of ethene with triphenylphosphine modified rhodium catalyst: kinetic and mechanistic studies. *J. Mol. Catal. A: Chem.* 138, 155-176.
- Kojima, K and Tochigi, K. (1979). Prediction of vapor-liquid equilibria by the ASOG method. Elsevier, Kodansha, Tokyo.
- Kolar, P., Nakata, H., Shen, J.-W., Tsuboi, A., Suzuki, H., Ue, M. (2005). Prediction of gas solubility in battery formulations. *Fluid Phase Equilib.*, 228-229, 59-66.
- Köllhofer, A., Plenio, H. (2003). Homogeneous Catalysts Supported on Soluble Polymers: Biphasic Sonogashira Coupling of Aryl Halides and Acetylenes Using MeOPEG-Bound Phosphine-Palladium Catalysts for Efficient Catalyst Recycling. *Chemistry- A European Journal*, 9, 1416-1422.
- Le Bris, C., Defranceschi, M. (2000). Mathematical Models and Methods for ab initio Quantum Chemistry, Lecture Notes in Chemistry, vol. 74, Springer, Berlin.
- Lee, C., Yang, W., Parr, R.G. (1988). Development of the Colle-Salvetti correlation-energy formula into a functional of the electron density. *Phys. Rev. B*, 37, 785.
- Lee, K.Y. and Peters, C.A. (2004). UNIFAC Modeling of Cosolvent Phase Partitioning in Nonaqueous Phase Liquid-Water Systems. *Envir. Engrg.*, 130, 478-483.
- Li, J., Vanderbeken, I., Ye, S., Carrier, H., Xans, P. (1997). Prediction of the solubility of gas-liquid equilibria for gas-water and light hydrocarbon –water systems at high temperatures and pressures with a group contribution equation of state. *Fluid Phase Equilib.*, 131, 107-118.
- Lide, D.R. (2005). CRC Handbook of Chemistry and Physics, Internet Version. CRC Press, available from: <http://www.hbcpnetbase.com>
- Liu, C., Jiang, J., Wang, Y., Cheng, F., Jin, Z. (2003). Thermoregulated phase transfer ligands and catalysis XVIII: synthesis of N,N-dipolyoxyethylene-substituted-2-(diphenylphosphino)phenylamine (PEO-DPPPA) and the catalytic activity of its rhodium complex in the aqueous-organic biphasic hydroformylation of 1-decene. *J. Mol. Catal. A: Chem.*, 198, 23-27.
- Liu, X., Li, H., Wang, Y., Jin, Z.J. (2002). Polyether phosphite for hydroformylation of higher olefins in non-aqueous system and catalyst recovery. *J. Organomet. Chem.*, 654: 83-92.

- Luo, X., Tang, D., Li, M. (2005). Quantum investigation on the mechanism of isomerization of 1-butylene catalyzed by Rh-complex. *J. Mol. Struct.: THEOCHEM.* 731, 139-147.
- Luthra, S.S., Yang, X., Freitas dos Santos, L.M., White, L.S., Livingston, A.G. (2002). Homogeneous phase transfer catalyst recovery and re-use using solvent resistant membranes. *J. Membrane Science* 201, 65–75.
- Magnussen, T., Rasmussen, P., Fredenslund, A. (1981). UNIFAC parameter table for prediction of liquid-liquid equilibria. *Ind. Eng. Chem. Process Des. Dev.* 20, 331-339.
- Master, C. Homogeneous Transition Metal Catalysis, Chapman Hall, New York, 1977.
- Matsubara, T., Koga, N., Ding, Y., Musaev, D.G. Morokuma, K. (1997). Ab Initio MO Study of the Full Cycle of Olefin Hydroformylation Catalyzed by a Rhodium Complex, $\text{RhH}(\text{CO})_2(\text{PH}_3)_2$. *Organometallics* 16, 1065-1078.
- Merrick, J.P., Moran, D., Radom, L. (2007). Evaluation of harmonic frequency scale factors. *J. Phys. Chem. A*, 111, 11683-11700.
- Miller, S.A., Ekstrom, A., Foster N.R. (1990). Solubility and mass transfer coefficients for hydrogen and carbon monoxide in *n*-octacosane. *J. Chem. Eng. Data* 35, 125-127.
- Mohsen-Nia, M., Nekoei, E., Mohammad Doulabi, F.S. (2007). Ternary (liquid + liquid) equilibria for mixtures of (methanol + aniline + *n*-octane or *n*-dodecane) at $T = 298.15 \text{ K}$. *J. Chem. Thermodynamics* 40, 330-333.
- Monteil, F., Queau, R., Kalck, P. (1994). Behaviour of water-soluble dinuclear rhodium complexes in the hydroformylation reaction of oct-1-ene. *J. Organomet. Chem.* 480, 177-184.
- Musaev, D.G., Matsubara, T., Mebel, A.M., Koga, N., Morokuma, K. (1995). Ab initio molecular orbital studies of elementary reactions and homogeneous catalytic cycles with organometallic compounds. *Pure & Appl. Chem.* 67, 257-263.
- Nair, V.S., Mathew, S.P., Chaudhari, R.V. (1999). Kinetics of hydroformylation of styrene using homogeneous rhodium complex. *J. Mol. Catal. A: Chem.* 143, 99-110.
- Natta, G., Ercoli, R., Castello, S., Barbieri, F.H., (1954). The influence of hydrogen and carbon monoxide partial pressures on the rate of the hydroformylation reaction, *J. Am. Chem. Soc.*, 76, 4049.
- Novak, J.P., Mautous, J., Fick, J. (1987). Liquid-liquid equilibria. Elsevier.

- Ollis, D.F., Turchi, C., (1990). Heterogeneous Photocatalysis for Water-Purification – Contaminant Mineralization Kinetics and Elementary Reactor Analysis. *Environmental Progress*. 4, 229-234.
- Onada, T. (1993). Staying ahead in hydroformylation technology. *Chemtech*, 23, 34-37.
- Osborn, J.A., Wilkinson, G., Young, J.F. (1965). Mild hydroformylation of olefins using rhodium catalysts. *Chem. Commun. (London)*, 2, 17.
- Othmer, D.F., Tobias, P.E. (1942). Liquid-Liquid Extraction Data -Toluene and Acetaldehyde Systems. *Ind. Eng. Chem.* 34, 690-692.
- Palo, D.R., Erkey, C. (1999). Kinetics of the homogeneous catalytic hydroformylation of 1-octene in supercritical carbon dioxide with $\text{HRh}(\text{CO})[\text{P}(\text{p-CF}_3\text{C}_6\text{H}_4)_3]_3$. *Ind. Eng. Chem. Res.* 38, 3786-3792.
- Pant, K.K., Kunzru, D. (1997). Catalytic pyrolysis of n-heptane: Kinetic and modeling. *Ind. Eng. Chem. Res.* 36, 2059-2065.
- Patel, S., Pant, K.K. (2007). Experimental study and mechanistic kinetic modeling for selective production of hydrogen via catalytic steam reforming of methanol. *Chem. Eng. Sc.* 62, 5425-5435.
- Peng, D.Y., Robinson, D.B. (1976). A new two parameters Equation of State. *Ind. Eng. Chem. Fundam.* 15, 59-64.
- Pengpanich, S., Meeyoo, V., Rirksomboon, T., Bunyakiat, K. (2002). Catalytic oxidation of methane over $\text{CeO}_2\text{-ZrO}_2$ mixed oxide solid solution catalysts prepared via urea hydrolysis. *Appl Catal. A: Gen.* 234, 221-233.
- Phiong, H.S. and Lucien, F.P. (2002). Solubility of Hydrogen in α -Methylstyrene and Cumene at Elevated Pressure *J. Chem. Eng. Data*, 47, 474-477.
- Piacenti, F., Bianchi, M., Benedetti, E., Frediani, P. (1970). Hydroformylation of propene in the presence of $\text{Co}_2(\text{CO})_6[\text{P}(\text{C}_4\text{H}_9)]$. *J. Organomet. Chem.*, 23:257-264.
- Pople, J.A., Schlegel, H.B., Krishnan, R., DeFrees, D.J., Binkley, J.S., Frisch, M.J., Whiteside, R.A., Hout, R.F., Hehre, W.J. (1981). Molecular-orbital studies of vibrational frequencies. *Int. J. Quantum Chem. Quantum Chem. Symp.* 15, 269-278.
- Praunitz, J.M., Lichtenthaler, R.N., de Azevedo, E.G. (1999). Molecular Thermodynamics of Fluid-Phase Equilibria. 3rd ed., Upper Saddle River, NJ: Prentice Hall.

- Prausnitz, J.M., Shair, F.H., (1961). A thermodynamic correlation of gas solubilities. *AIChE J.* 7, 682-687.
- Purwanto, P., Delmas, H. (1995). Gas-liquid-liquid reaction engineering: hydroformylation of 1-octene using a water soluble rhodium complex catalyst. *Catal. Today*, 24, 135-140.
- Purwanto, P., Deshpande, R.M., Chaudhari, R.V., Delmas, H. (1996). Solubility of hydrogen, carbon monoxide, and 1-octene in various solvents and solvent mixture. *J. Chem Eng Data* 41, 1414-1417.
- Radhakrishnan, K., Ramachandran, P.A., Brahme, P.H., Chaudhari, R.V., (1983). Solubility of hydrogen in methanol, nitrobenzene and their mixtures: experimental data and correlation. *J. Chem. Eng. Data* 28, 1-4.
- Reid, R.C., Prausnitz, J.M., (1987). The properties of gases and liquids. Mc-Graw-Hill, 4th Edition, 335.
- Renon, H., Prausnitz, J.M. (1968). Local compositions in thermodynamic excess functions for liquid mixtures. *AIChE J.* 14, 135-144
- Riisager, A., Eriksen, K.M., Hjortkjaer, J., Fehrmann, R. (2003). Propene hydroformylation by supported aqueous-phase Rh-NORBOS catalysts. *J. Mol. Catal. A: Chem.* 193, 259-272.
- Roat-Malone, R.M. (2002). Bioinorganic chemistry: a short course. John Wiley and Sons. ISBN 047115976X, 9780471159766
- Robbins, G.P., Hallet, J.P., Bush, D., Eckert, C.A. (2007). Liquid-liquid equilibria and partitioning in organic-aqueous systems. *Fluid Phase Equilibria*, 253, 48-53
- Rocha, W.R. (2004). Hydrogen activation and aldehyde elimination promoted by homogeneous Pt-Sn catalyst: a theoretical study. *J. Mol. Struct.: THEOCHEM.* 677, 133-143.
- Rocha, W.R., Milagro, H.M.S., De Almeida, W.B. (2001). On the isomerization of β -pinene: a theoretical study. *J. Mol. Struct.: THEOCHEM* 544, 213-220.
- Romero, C., Villares, A., Haro, M., Giner, B., Lafuente, C. (2005). Experimental and predicted vapor-liquid equilibrium of 1,4-dioxane with cycloalkanes and benzene. *Fluid Phase Equilib.*, 238:1-6.

- Rosales, M., Gonz'alez, A., Guerrero, Y., Pacheco, I., S'anchez-Delgado, R.A. (2007a). Kinetics and mechanisms of homogeneous catalytic reactions Part 6. Hydroformylation of 1-hexene by use of Rh(acac)(CO)₂/dppe [dppe = 1,2-bis(diphenylphosphino)ethane] as the precatalyst. *J. Mol. Catal. A: Chem.* 270, 241–249
- Rosales, M., Duran, J.A., Gonzalez, A., Pacheco, I., Sanchez-Delgado, R.A. (2007b). Kinetics and mechanisms of homogeneous catalytic reactions. Part 7. Hydroformylation of 1-hexene catalyzed by cationic complexes of rhodium and iridium containing PPh₃. *J. Mol. Catal. A: Chem.*, 270, 250-256.
- Routray, K., Deo, G. (2005). Kinetic parameter estimation for a multi-response non-linear reaction model, *AIChE Journal*. 51,1733.
- Saeyns, M., Reyniers, M., Marin, G.B., Neurock, M. (2002). Density functional theory of benzene adsorption on Pt(111). *J. Phys. Chem. B*, 106, 7489-7498.
- Saeyns, M., Reyniers, M., Thybaut, J.W., Neurock, M., Marin, G.B. (2005). First-principles based kinetic model for the hydrogenation of toluene. *J. Catal.*, 236, 129-138.
- Sander, B., Jørgensen, S.S., Rasmussen, P., (1983). Gas solubility calculations, I. UNIFAC. *Fluid Phase Equilib.*, 11:105-126.
- Scarpello, J.T., Nair, D., Freitas dos Santos, L.M., White, L.S., Livingston, A.G. (2002). The separation of homogeneous organometallic catalysts using solvent resistant nanofiltration. *J. Membrane Science*, 203, 71–85.
- Schlegel, H.B. (1994). Some thoughts on reaction-path following. *J. Chem. Soc. Faraday Trans.*, 90, 1569-1574.
- Schlegel, H.B., Yarkony, D.R. (1994). *Modern Electronic Structure Theory*, World Scientific Publication, Singapore, 459-500.
- Scott, R.L. (1948). The Solubility of Fluorocarbons. *J. Am. Chem. Soc.*, 70: 4090-4093.
- Shaik, S.S., Hiberty, P.C. (2007). *A Chemist's guide to valence bond theory*. John Wiley & Sons. ISBN: 978-0-470-03735-5, pp. 254-256.
- Shriver, D.F., Atkins, P.W., Langford, C.H. (1998). *Inorganic Chemistry*, 2nd ed., Oxford University Press: Oxford.

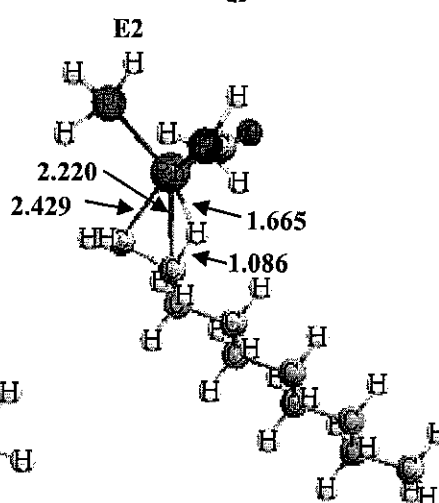
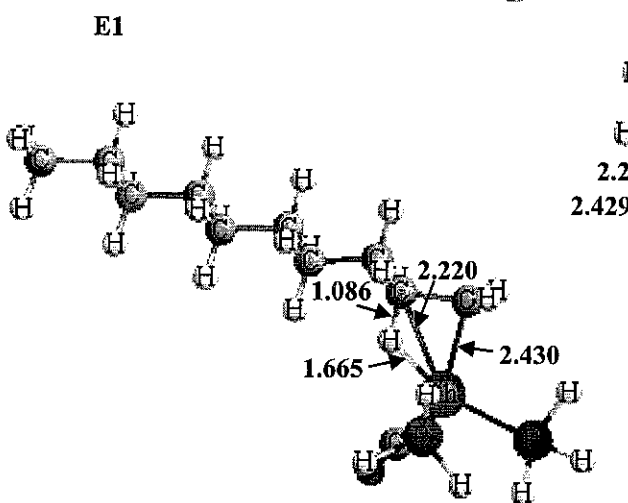
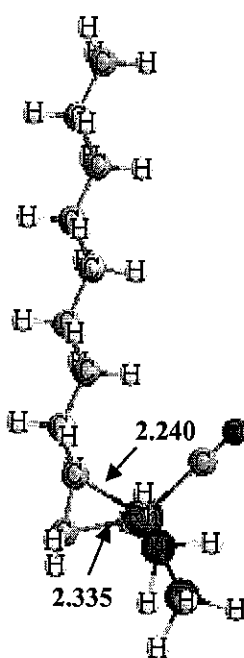
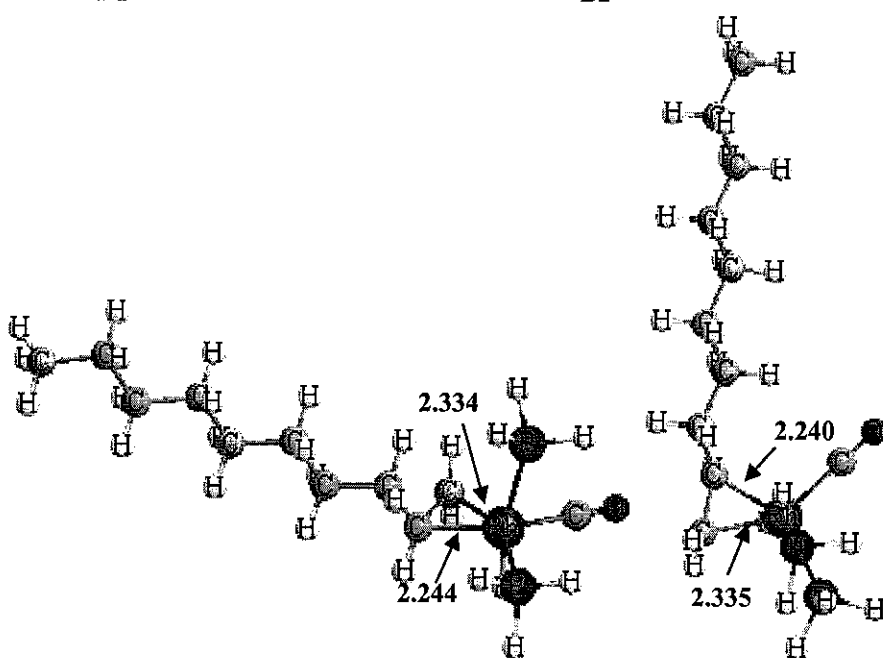
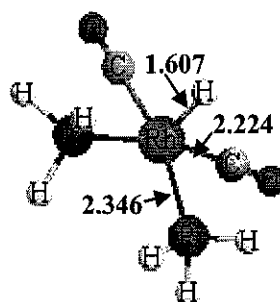
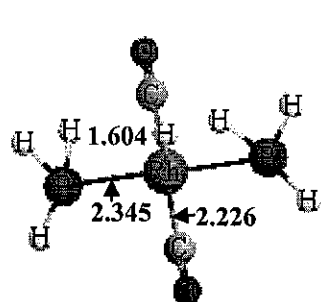
- Silk, S.J. (1975). The threshold limit value for carbon monoxide. *Ann. occup. Hyg.*, 18, 29-35.
- Sobieszuk, P., Cygański, P., Pohorecki, R. (2008). Volumetric liquid mass transfer coefficient in a gas-liquid microreactor. *Chemical and Process Engineering*. 29, 651-661.
- Still, C., Salmi, T., Mäki-Arvela, P., Eränen, K., Murzin, D.Y., Lehtonen, J. (2006). Solubility of gases in a hydroformylation solvent. *Chemical Eng. Science* 61, 3698-3704.
- Streitwieser, A. (1961). *Molecular Orbital Theory for Organic Chemists*. John Wiley & Sons; 1st Ed.
- Tang, D., Qin, S., Su, Z., Hu, C. (2007). Comprehensive theoretical study on the mechanism of regioselective hydroformylation of phosphinibutene catalyzed by a heterobinuclear rhodium(I)-chromium complex. *Organometallics*, 26, 33-47.
- Terreros, P., Pastor, E., Fierro, J. L. G. (1989). Heptene hydroformylation on phosphinated polystyrene-anchored rhodium complexes. *J. Mol. Catal.*, 53, 359-369.
- Tijani, J., Ali B.E. (2006). Selective thermomorphic biphasic hydroformylation of higher olefins catalyzed by HRhCO(PPh₃)₃/P(OPh)₃. *Applied Catal. A: General* 303, 158-165.
- Unveren, H.H.Y. (2004). Hydroformylation of long chain olefins in microemulsion. MSc thesis, der Technische Universität Berlin.
- van der Veen, L.A., Keeven, P.H., Schoemaker, G.C., Reek, J.N.H., Kramer, P.C.J., van Leeuwen, P.W.N.M., Lutz, M., Spek, A.L. (2000). Origin of the Bite Angle Effect on Rhodium Diphosphine Catalyzed Hydroformylation. *Organometallics* 19, 872.
- van Leeuwen, P.W.N.M. (2004). *Homogeneous catalysis, understanding the art*. Kluwer Academic Publishers, Dordrecht (The Netherlands): Springer-Verlag.
- van Leeuwen, P.W.N.M., Claver, C. (2000). *Rhodium Catalyzed Hydroformylation*. Kluwer Academic Publishers, Dordrecht (The Netherlands): Springer-Verlag. <http://www.knovel.com/knovel2/Toc.jsp?>
- van Leeuwen, P.W.N.M., Roobeek, C.F. (1983). Hydroformylation of less reactive olefins with modified rhodium catalysts. *J. Organomet. Chem.*, 258, 343-350.

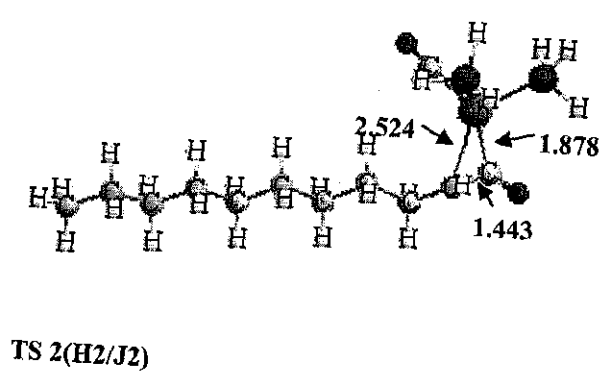
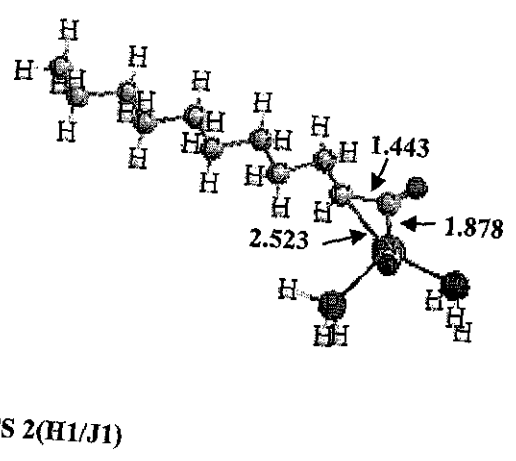
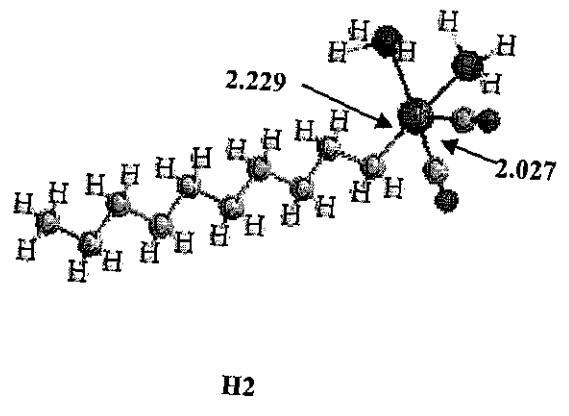
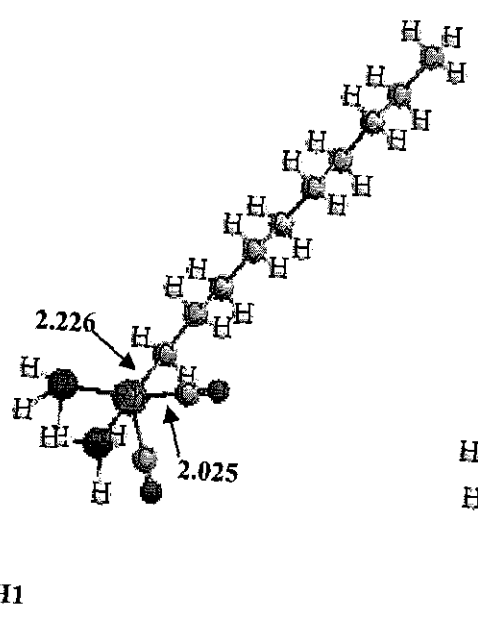
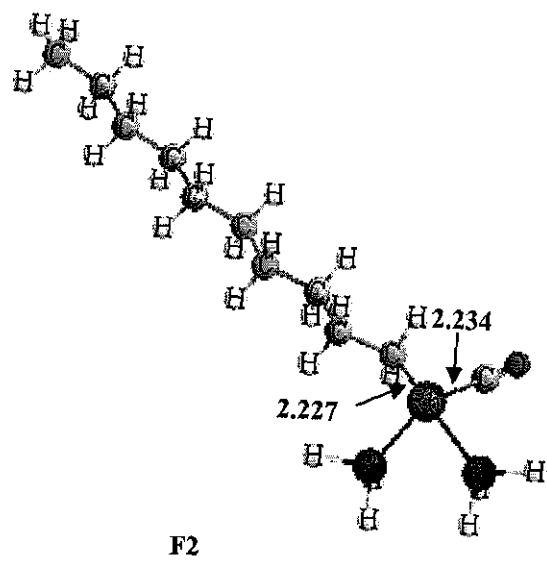
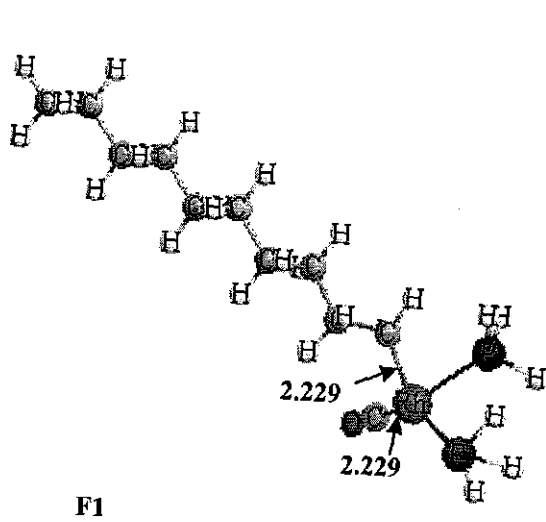
- van Leeuwen, P.W.N.M., Jongsma, T., Challa, G. (1991). A mechanistic study of rhodium tri(o-t-butylphenyl)phosphite complexes as hydroformylation catalysts. *J. Organomet. Chem.*, 421,121.
- van Rooy, A., de Bruijn, J.N.H., Roobeek, K.F., Kamer, P.C.J., van Leeuwen, P.W.N.M. (1996). Rhodium-catalysed hydroformylation of branched 1-alkenes; bulky phosphite vs. triphenylphosphine as modifying ligand. *J. Organometallic Chem.*, 507, 69-73.
- van Rooy, A., Orij, E.N., Kamer, P.C.J., van Leeuwen, P.W.N.M. (1995). Hydroformylation with a rhodium/bulky phosphite modified catalyst. Catalyst comparison for oct-1-ene, cyclohexene and styrene. *Organometallics*, 14, 34-43.
- van der Veen, L.A., Keeven, P.H., Schoemaker, G.C., Reek, J.N.H., Kramer, P.C.J., van Leeuwen, P.W.N.M., Lutz, M., Spek, A.L., (2000) Origin of the Bite Angle Effect on Rhodium Diphosphine Catalyzed Hydroformylation. *Organometallics*, 19, 872.
- Washburn, E.W. (2003). International Critical Tables of Numerical Data, Physics, Chemistry and Technology. Knovel: Physical constants and thermodynamics of phase transition. pp. 5094, 5320, 10961.
- Weissermel, K., Arpe, H. (1997). Industrial Organic Chemistry. John Wiley & Sons; 3rd Ed. ISBN 3-527-28838-4
- Wilhelm, E. (1986). Dilute solutions of gases in liquids. *Fluid Phase Equilib.*, 27, 233-261.
- Wilson, G.M. (1964). Vapor-Liquid Equilibrium. XI. A New Expression for the Excess Free Energy of Mixing. *J. Am. Chem. Soc.*; 86, 127-130.
- Wojciechowski, B.W., Rice, N.M. (2003). Experimental methods in kinetic studies. Elsevier Science B.V., Amsterdam.
- Yang, C., Bi, X., Mao, Z. (2002a). Effect of reaction engineering factors on biphasic hydroformylation of 1-dodecene catalyzed by water-soluble rhodium complex. *J. Mol. Catal. A*, 187, 35-46.
- Yang, C., Mao, Z., Wang, Y., Chen., J. (2002b). Kinetics of hydroformylation of propylene using $\text{RhCl}(\text{CO})(\text{TPPTS})_2/\text{TPPTS}$ complex catalyst in aqueous system. *Catal. Today*, 74, 111-119.
- Yen, C.L., McKetta, J.J., (1962). A thermodynamic correlation of nonpolar gas solubilities in polar, non-associated liquids. *AIChE J.* 8, 501-507.

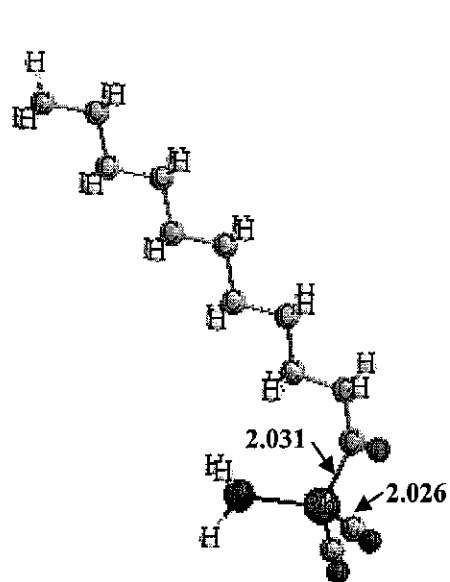
- Zaretskii, M.I., Rusak, V.V. and Chartov, E.M. (2008). Using Propylene Carbonate in Extraction and Absorption: A Review. *Coke and Chemistry*, 51, 101–104.
- Zhang, H., Ramachandran, B., Senekowitsch, J., Wyatt, R.E. (1999). Determination of spectroscopic constants and anharmonic force-fields for HOCl and DOCl using scaled external correlation. *J. Mol. Struct.: THEOCHEM* 487, 75-85.
- Zhang, Y.Q., Mao, Z., Chen, J. (2002). Macro-kinetics of biphasic hydroformylation of 1-dodecene catalyzed by water soluble rhodium complex. *Catal. Today*, 74, 23-35.
- Zheng, X.L., Jiang, J.Y., Liu, X.Z., Jin, Z.L. (1998). Thermoregulated phase transfer ligands and catalysis. III. Aqueous/organic two phase hydroformylation of higher olefins by thermoregulated phase-transfer catalysis. *Catal. Today* 44, 175-182.
- Zhu, H., Ding, Y., Yin, H., Yan, L., Xiong, J., Lu, Y., Luo, H., Lin, L. (2003). Supported rhodium and supported aqueous-phase catalyst, and supported rhodium catalyst modified with water-soluble TPPTS ligands. *Applied Catal. A: General* 245, 111-117.

Appendix A

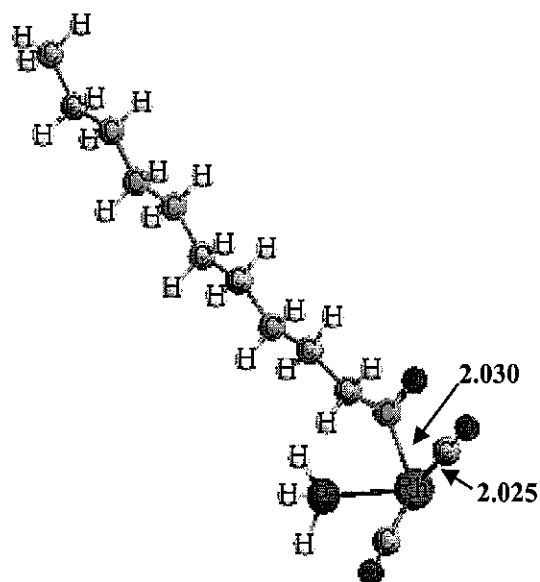
Key Structures Involved in the Catalytic Cycle of Hydroformylation of 1-Decene and Selected Parameters



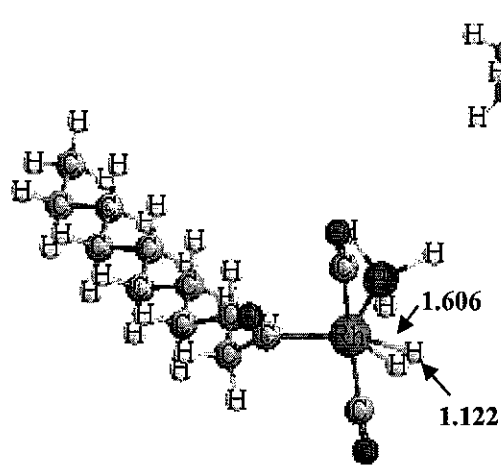




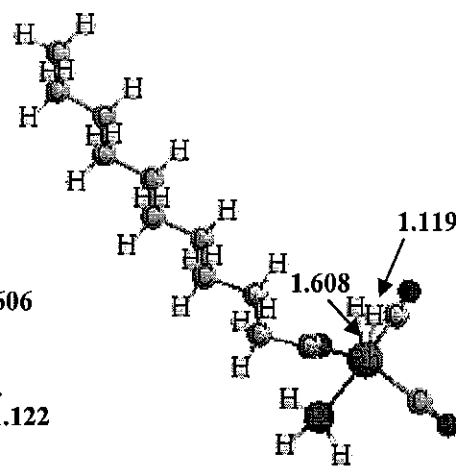
J1



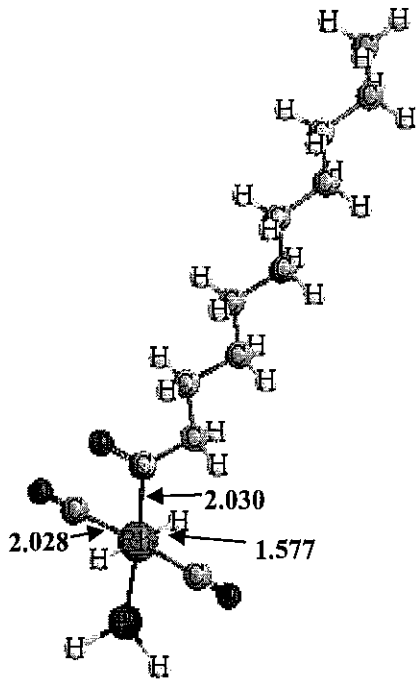
J2



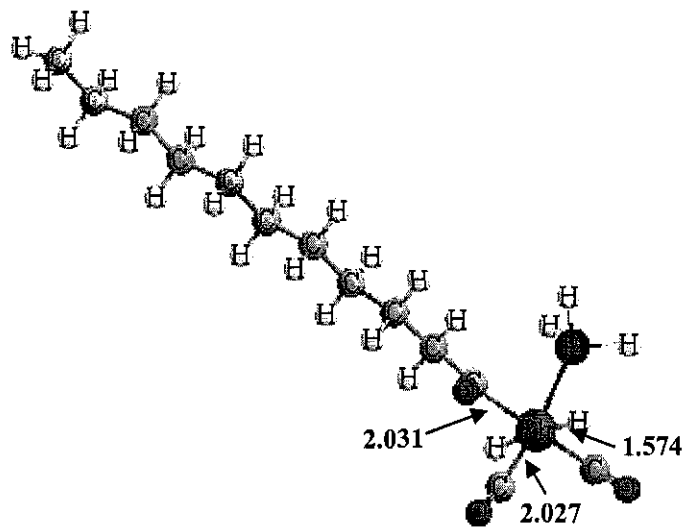
TS 3(J1/N1)



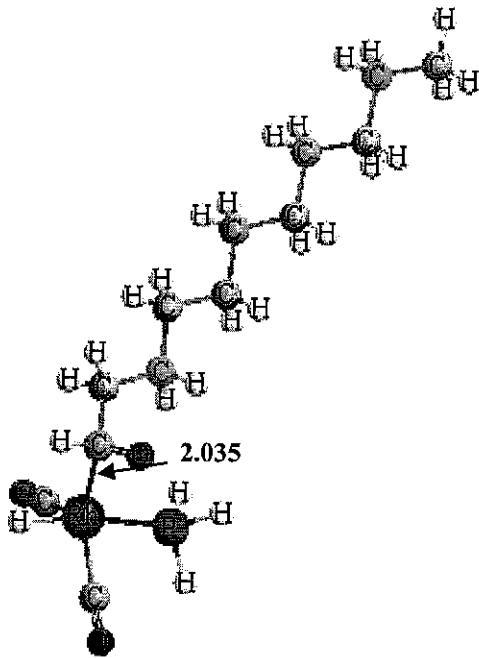
TS 3(J2/N2)



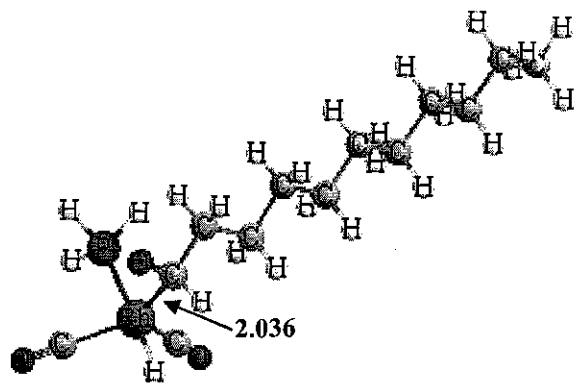
N1



N2



P1

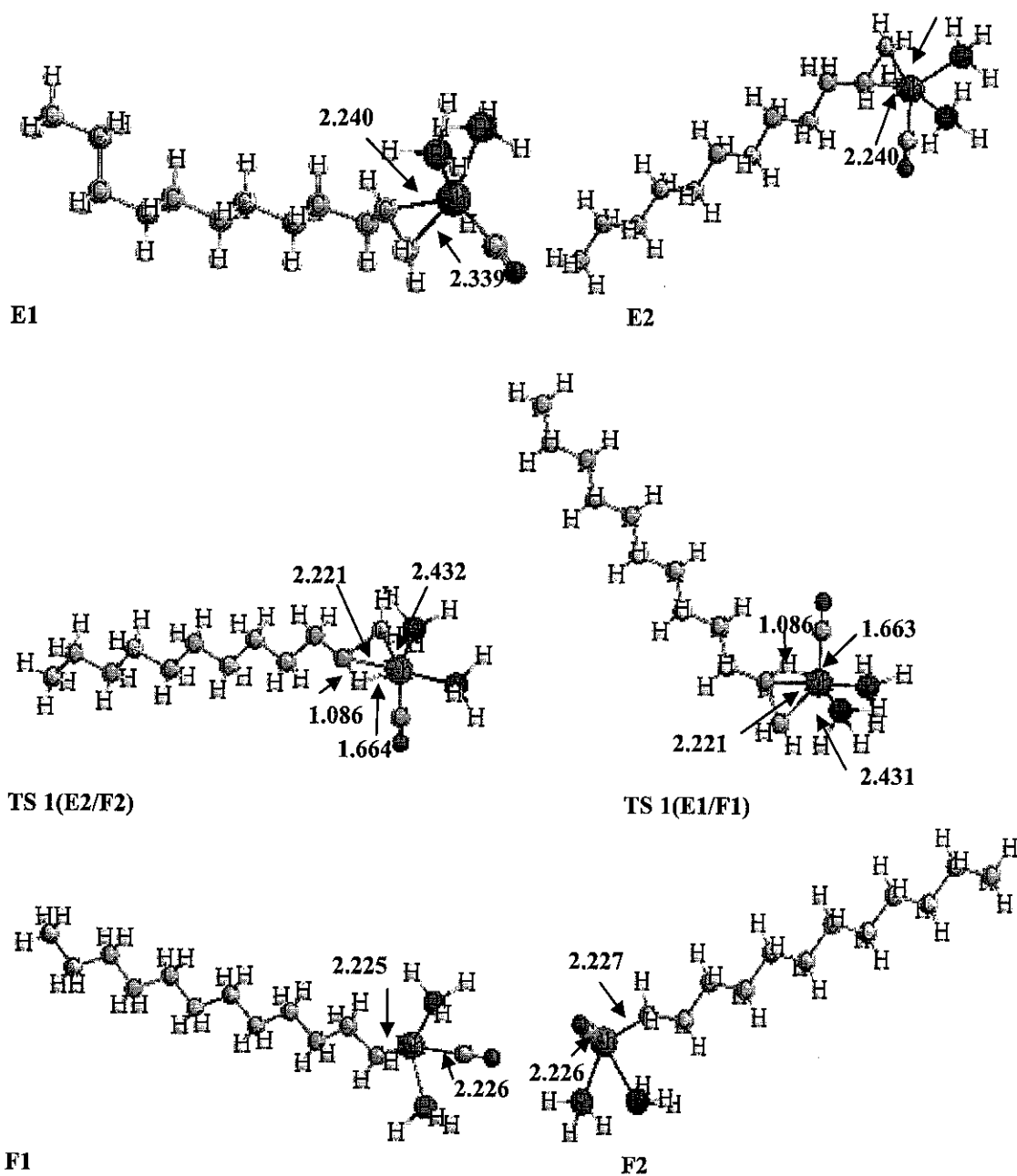


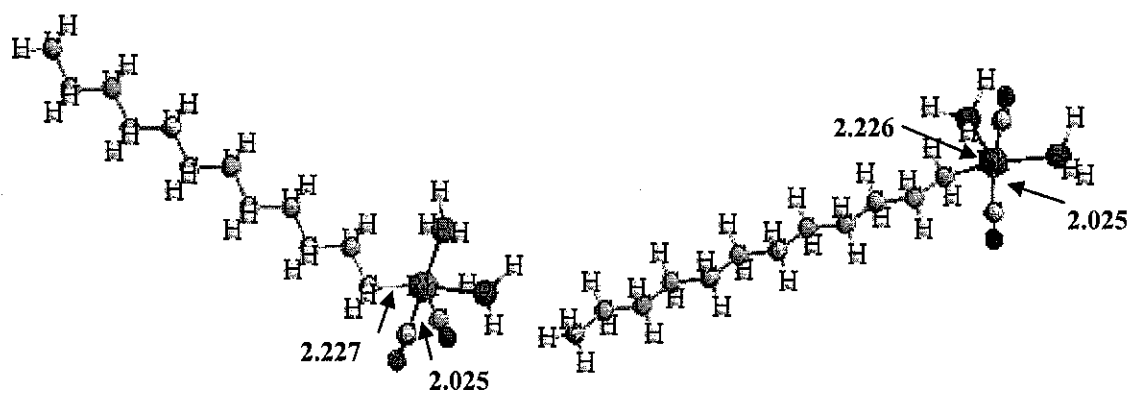
P2

(bond lengths are in angstrom)

Appendix B

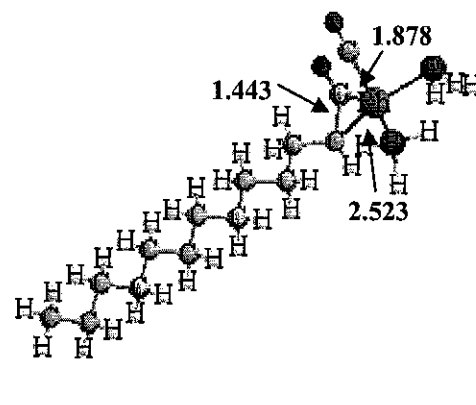
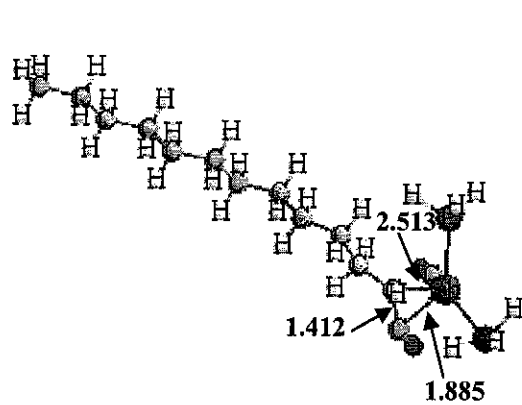
Key Structures Involved in the Catalytic Cycle of Hydroformylation of 1-Dodecene and Selected Parameters





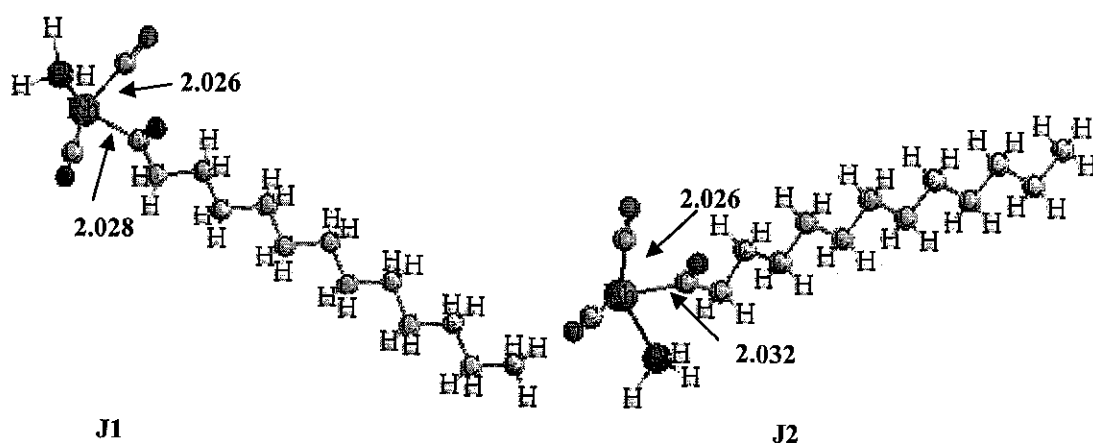
H1

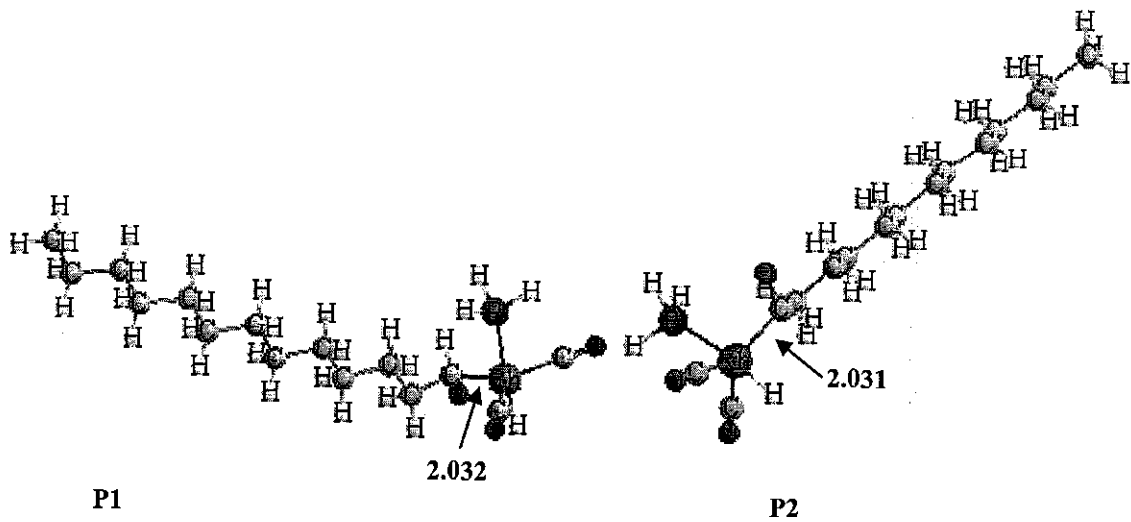
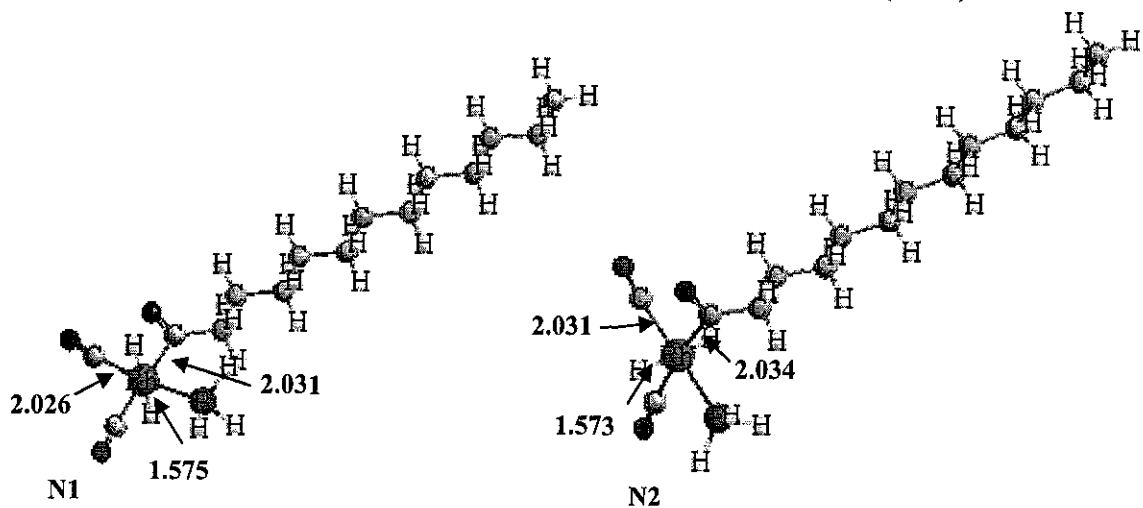
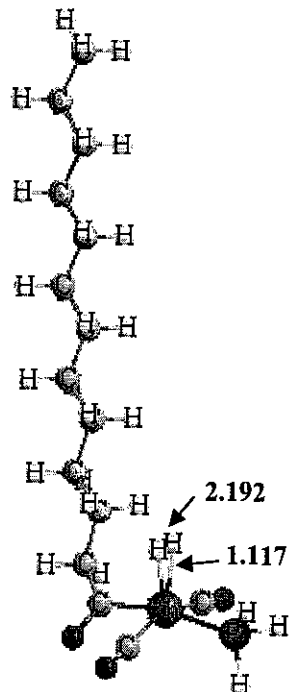
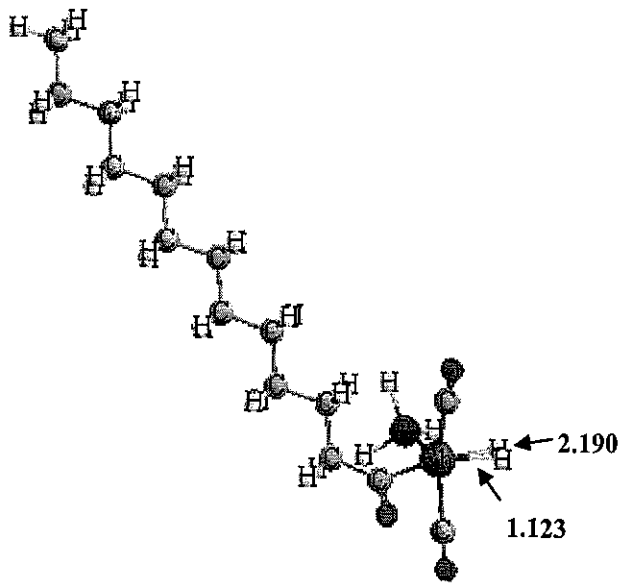
H2



TS 2(H1/J1)

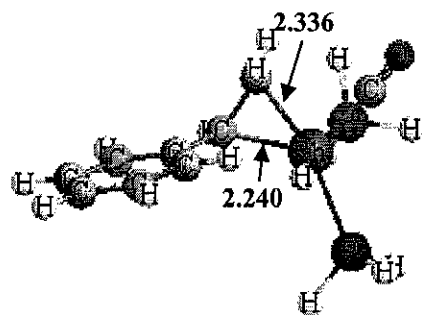
TS 2(H2/J2)



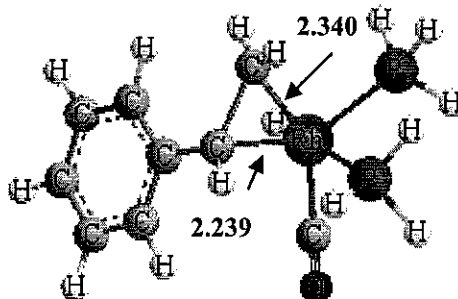


Appendix C

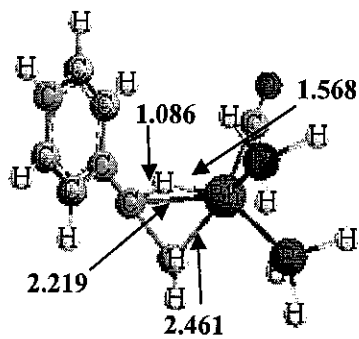
Key Structures Involved in the Catalytic Cycle of Hydroformylation of Styrene and Selected Parameters



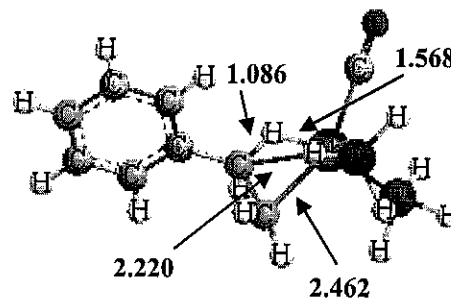
E1



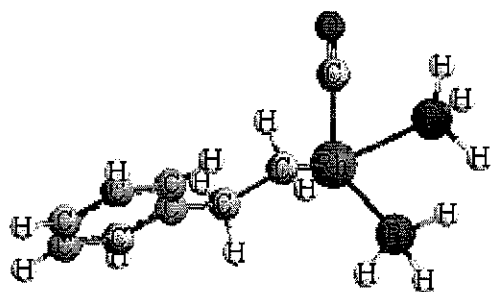
E2



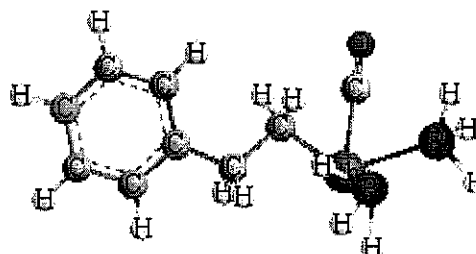
TS (E2/F2)



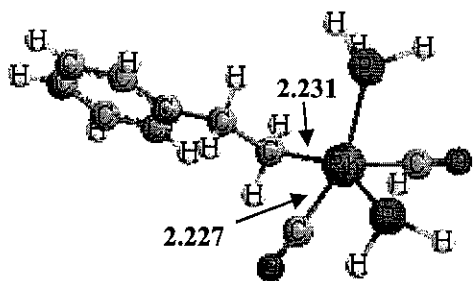
TS (E1/F1)



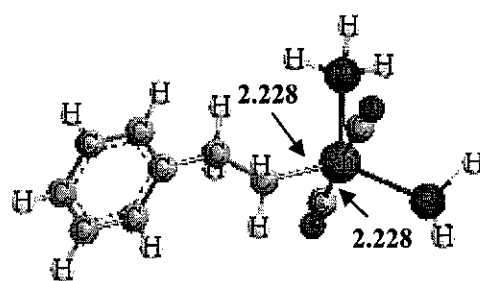
F1



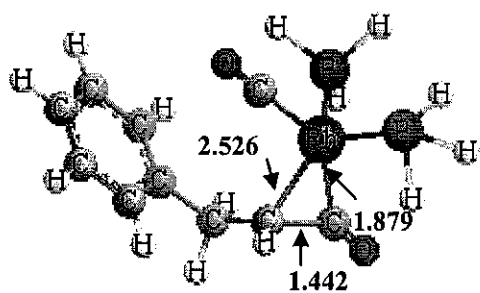
F2



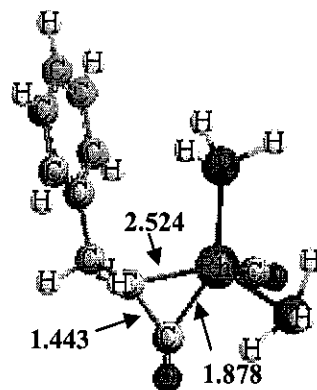
H1



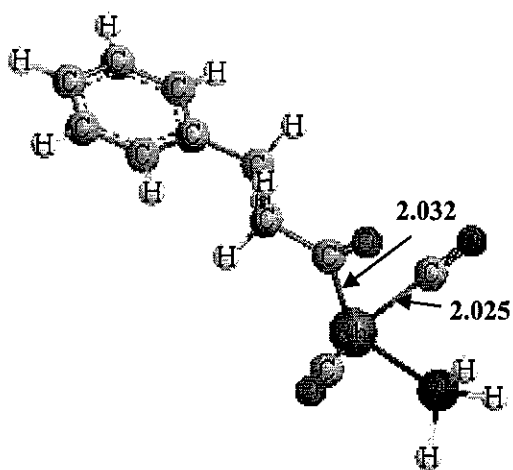
H2



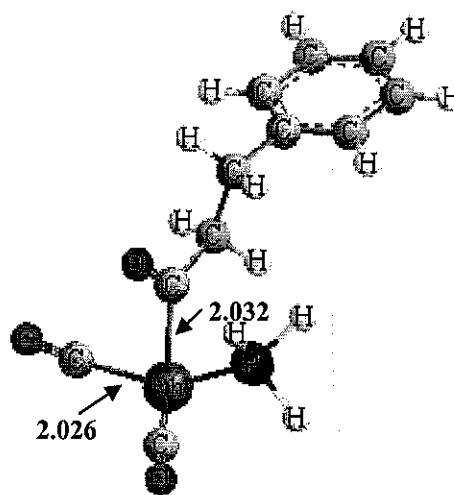
TS 1 (H1/J1)



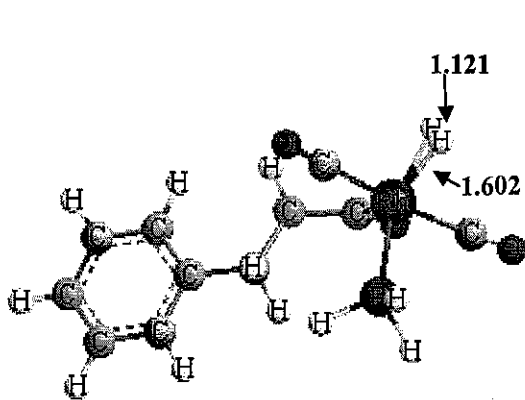
TS 1 (H2/J2)



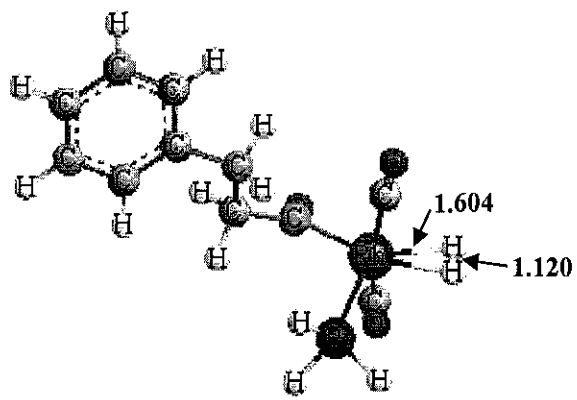
J1



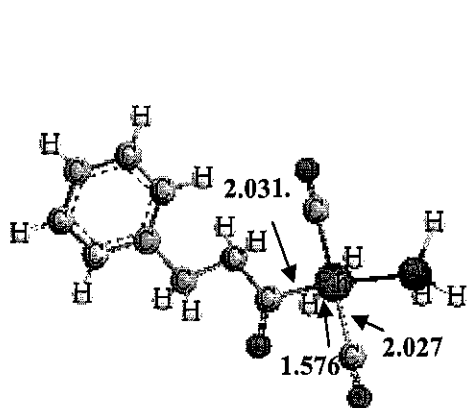
J2



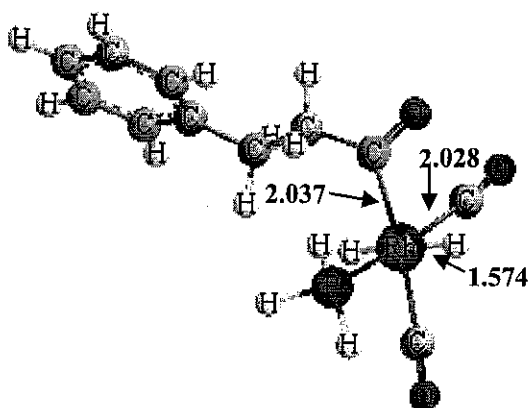
TS 2 (J1/N1)



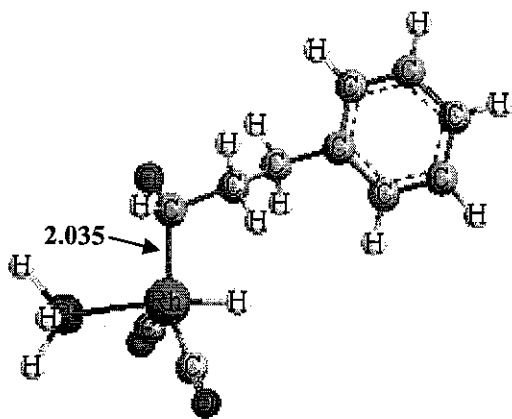
TS 2 (J2/N2)



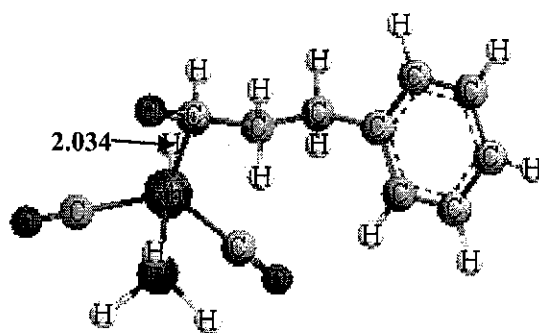
N1



N2



P1



P2

(bond lengths are in angstrom)

Appendix D

Kinetic Data for Hydroformylation of Higher Alkenes in Homogeneous System

Table D-1: Kinetic data for hydroformylation of 1-dodecene at temperature of 323 K (Bhanage *et al.*, 1997).

Exp. Rate ($\text{kmolm}^{-3}\text{s}^{-1}$)	H ₂ (kmolm^{-3})	CO (kmolm^{-3})	1-dodecene (kmolm^{-3})	catalyst (kmolm^{-3})
0	0.00000	0.2248	0.36	0.0020
7.50E-06	0.02145	0.2248	0.36	0.0020
1.50E-05	0.04538	0.2248	0.36	0.0020
1.80E-05	0.05611	0.2248	0.36	0.0020
0	0.08977	0.0000	0.36	0.0020
2.20E-04	0.08977	0.0066	0.36	0.0020
1.60E-04	0.08977	0.0083	0.36	0.0020
9.40E-05	0.08977	0.0140	0.36	0.0020
6.00E-05	0.08977	0.0273	0.36	0.0020
1.00E-05	0.08977	0.1116	0.36	0.0020
5.00E-06	0.08977	0.1405	0.36	0.0020
0	0.08977	0.2248	0	0.0020
1.50E-05	0.08977	0.2248	0.37	0.0020
1.80E-05	0.08977	0.2248	0.75	0.0020
2.00E-05	0.08977	0.2248	0.95	0.0020
2.30E-05	0.08977	0.2248	1.45	0.0020
2.50E-05	0.08977	0.2248	2.18	0.0020
0	0.08977	0.2248	0.36	0.0000
1.00E-05	0.08977	0.2248	0.36	0.0010
1.80E-05	0.08977	0.2248	0.36	0.0020
3.00E-05	0.08977	0.2248	0.36	0.0040
6.00E-05	0.08977	0.2248	0.36	0.0080

Table D-2: Kinetic data for hydroformylation of 1-dodecene at temperature of 333 K (Bhanage *et al.*, 1997).

K_H	29.3	11.9		
Exp. Rate ($\text{kmolm}^{-3}\text{s}^{-1}$)	H_2 (kmolm^{-3})	CO (kmolm^{-3})	1-dodecene (kmolm^{-3})	catalyst (kmolm^{-3})
0	0.00000	0.2286	0.3600	0.0020
3.00E-05	0.02304	0.2286	0.3600	0.0020
6.30E-05	0.04693	0.2286	0.3600	0.0020
7.30E-05	0.05802	0.2286	0.3600	0.0020
0.00E+00	0.09283	0.0000	0.3600	0.0020
7.50E-04	0.09283	0.0059	0.3600	0.0020
6.00E-04	0.09283	0.0084	0.3600	0.0020
4.00E-04	0.09283	0.0143	0.3600	0.0020
2.00E-04	0.09283	0.0277	0.3600	0.0020
1.00E-04	0.09283	0.0588	0.3600	0.0020
6.00E-05	0.09283	0.1134	0.3600	0.0020
3.50E-05	0.09283	0.1697	0.3600	0.0020
0.00E+00	0.09283	0.2286	0.0000	0.0020
4.40E-05	0.09283	0.2286	0.1800	0.0020
6.30E-05	0.09283	0.2286	0.3800	0.0020
8.10E-05	0.09283	0.2286	0.7000	0.0020
9.20E-05	0.09283	0.2286	1.4500	0.0020
9.80E-05	0.09283	0.2286	2.1800	0.0020
0.00E+00	0.09283	0.2286	0.3600	0.0000
3.50E-05	0.09283	0.2286	0.3600	0.0010
6.00E-05	0.09283	0.2286	0.3600	0.0020
1.20E-04	0.09283	0.2286	0.3600	0.0040
2.30E-04	0.09283	0.2286	0.3600	0.0080

Table D-3: Kinetic data for hydroformylation of 1-dodecene at temperature of 343 K (Bhanage *et al.*, 1997).

K_H	28.1	11.7		
Exp. Rate ($\text{kmolm}^{-3}\text{s}^{-1}$)	H_2 (kmolm^{-3})	CO (kmolm^{-3})	1-dodecene (kmolm^{-3})	catalyst (kmolm^{-3})
0	0.00000	0.2325	0.3600	0.0020
1.03E-04	0.02402	0.2325	0.3600	0.0020
1.99E-04	0.04893	0.2325	0.3600	0.0020
2.30E-04	0.06050	0.2325	0.3600	0.0020
0.00E+00	0.09680	0.0000	0.3600	0.0020
1.60E-03	0.09680	0.0085	0.3600	0.0020
1.13E-03	0.09680	0.0145	0.3600	0.0020
6.25E-04	0.09680	0.0282	0.3600	0.0020
1.88E-04	0.09680	0.1154	0.3600	0.0020
1.25E-04	0.09680	0.1726	0.3600	0.0020
0.00E+00	0.09680	0.2325	0.0000	0.0020
1.48E-04	0.09680	0.2325	0.1800	0.0020
1.90E-04	0.09680	0.2325	0.3800	0.0020
2.20E-04	0.09680	0.2325	0.7000	0.0020
2.50E-04	0.09680	0.2325	2.1500	0.0020
0.00E+00	0.09680	0.2325	0.3600	0.0000
1.00E-04	0.09680	0.2325	0.3600	0.0010
2.00E-04	0.09680	0.2325	0.3600	0.0020
3.80E-04	0.09680	0.2325	0.3600	0.0040
7.30E-04	0.09680	0.2325	0.3600	0.0080

Table D-4: Kinetic data for hydroformylation of styrene at temperature of 333 K (Nair *et al.*, 1999).

Exp. Rate ($\text{kmolm}^{-3}\text{s}^{-1}$)	K_H		styrene (kmolm^{-3})	catalyst (kmolm^{-3})
	29.3 H ₂ (kmolm^{-3})	11.9 CO (kmolm^{-3})		
0	0.00000	0.1714	3.4500	0.0010
1.90E-05	0.03413	0.1714	3.4500	0.0010
4.20E-05	0.06826	0.1714	3.4500	0.0010
8.40E-05	0.13652	0.1714	3.4500	0.0010
0	0.06962	0.0000	3.4500	0.0010
9.73E-05	0.06962	0.0045	3.4500	0.0010
8.94E-05	0.06962	0.0165	3.4500	0.0010
7.50E-05	0.06962	0.0420	3.4500	0.0010
6.84E-05	0.06962	0.0588	3.4500	0.0010
5.92E-05	0.06962	0.0924	3.4500	0.0010
5.00E-05	0.06962	0.1261	3.4500	0.0010
4.21E-05	0.06962	0.1739	3.4500	0.0010
3.16E-05	0.06962	0.2521	3.4500	0.0010
2.50E-05	0.06962	0.3504	3.4500	0.0010
0.00E+00	0.06962	0.1714	0.0000	0.0010
4.05E-05	0.06962	0.1714	0.9000	0.0010
4.17E-05	0.06962	0.1714	1.7000	0.0010
4.28E-05	0.06962	0.1714	3.4000	0.0010
4.40E-05	0.06962	0.1714	6.8700	0.0010
0.00E+00	0.06962	0.1714	3.4500	0.0000
5.25E-06	0.06962	0.1714	3.4500	0.0001
1.10E-05	0.06962	0.1714	3.4500	0.0003
2.31E-05	0.06962	0.1714	3.4500	0.0005
4.41E-05	0.06962	0.1714	3.4500	0.0010

Table D-5: Kinetic data for hydroformylation of styrene at temperature of 343 K (Nair *et al.*, 1999).

Exp. Rate ($\text{kmolm}^{-3}\text{s}^{-1}$)	H_2 (kmolm^{-3})	CO (kmolm^{-3})	styrene (kmolm^{-3})	catalyst (kmolm^{-3})
0	0.00000	0.1744	3.4500	0.0010
4.20E-05	0.03559	0.1744	3.4500	0.0010
9.03E-05	0.07117	0.1744	3.4500	0.0010
1.75E-04	0.14235	0.1744	3.4500	0.0010
0.00E+00	0.07260	0.0000	3.4500	0.0010
1.89E-04	0.07260	0.0046	3.4500	0.0010
1.76E-04	0.07260	0.0168	3.4500	0.0010
1.51E-04	0.07260	0.0427	3.4500	0.0010
1.37E-04	0.07260	0.0598	3.4500	0.0010
1.26E-04	0.07260	0.0872	3.4500	0.0010
1.01E-04	0.07260	0.1282	3.4500	0.0010
8.94E-05	0.07260	0.1769	3.4500	0.0010
6.71E-05	0.07260	0.2521	3.4500	0.0010
5.52E-05	0.07260	0.3504	3.4500	0.0010
0.00E+00	0.07260	0.1744	0.0000	0.0010
8.89E-05	0.07260	0.1744	0.9000	0.0010
9.00E-05	0.07260	0.1744	1.7000	0.0010
9.05E-05	0.07260	0.1744	3.4000	0.0010
9.22E-05	0.07260	0.1744	6.8700	0.0010
0	0.07260	0.1744	3.4500	0.0000
1.16E-05	0.07260	0.1744	3.4500	0.0001
2.47E-05	0.07260	0.1744	3.4500	0.0003
4.78E-05	0.07260	0.1744	3.4500	0.0005
9.08E-05	0.07260	0.1744	3.4500	0.0010

Table D-6: Kinetic data for hydroformylation of styrene at temperature of 353 K (Nair *et al.*, 1999).

Exp. Rate ($\text{kmolm}^{-3}\text{s}^{-1}$)	K_H 26.8 H ₂ (kmolm^{-3})	11.53 CO (kmolm^{-3})	styrene (kmolm^{-3})	catalyst (kmolm^{-3})
0	0.00000	0.1769	3.4500	0.0010
9.14E-05	0.03731	0.1769	3.4500	0.0010
2.00E-04	0.07463	0.1769	3.4500	0.0010
3.84E-04	0.14925	0.1769	3.4500	0.0010
0.00E+00	0.07612	0.0000	3.4500	0.0010
4.39E-04	0.07612	0.0047	3.4500	0.0010
4.05E-04	0.07612	0.0170	3.4500	0.0010
3.45E-04	0.07612	0.0434	3.4500	0.0010
3.25E-04	0.07612	0.0607	3.4500	0.0010
2.75E-04	0.07612	0.0885	3.4500	0.0010
2.34E-04	0.07612	0.1301	3.4500	0.0010
1.97E-04	0.07612	0.1795	3.4500	0.0010
1.63E-04	0.07612	0.2602	3.4500	0.0010
1.25E-04	0.07612	0.3617	3.4500	0.0010
0.00E+00	0.07612	0.1769	0.0000	0.0010
1.97E-04	0.07612	0.1769	0.9000	0.0010
2.00E-04	0.07612	0.1769	1.7000	0.0010
1.97E-04	0.07612	0.1769	3.4000	0.0010
2.01E-04	0.07612	0.1769	6.8700	0.0010
0	0.07612	0.1769	3.4500	0.0000
2.52E-05	0.07612	0.1769	3.4500	0.0001
5.04E-05	0.07612	0.1769	3.4500	0.0003
1.04E-04	0.07612	0.1769	3.4500	0.0005
1.96E-04	0.07612	0.1769	3.4500	0.0010

Table D-7: Kinetic data for hydroformylation of 1-decene at temperature of 323 K
(Divekar *et al.*, 1993).

Exp. Rate ($\text{kmolm}^{-3}\text{s}^{-1}$)	H_2 (kmolm^{-3})	CO (kmolm^{-3})	1-decene (kmolm^{-3})	catalyst (kmolm^{-3})
0	0.00000	0.1000	0.5280	0.0010
9.57E-06	0.02010	0.1000	0.5280	0.0010
2.97E-05	0.04053	0.1000	0.5280	0.0010
8.42E-05	0.08106	0.1000	0.5280	0.0010
0	0.04080	0.0000	0.5280	0.0010
2.08E-04	0.04080	0.0087	0.5280	0.0010
1.84E-04	0.04080	0.0202	0.5280	0.0010
1.06E-04	0.04080	0.0404	0.5280	0.0010
6.27E-05	0.04080	0.0606	0.5280	0.0010
2.74E-05	0.04080	0.1029	0.5280	0.0010
1.57E-05	0.04080	0.1538	0.5280	0.0010
1.18E-05	0.04080	0.2038	0.5280	0.0010
0.00E+00	0.04080	0.1000	0.0000	0.0010
1.53E-05	0.04080	0.1000	0.2683	0.0010
2.58E-05	0.04080	0.1000	0.5244	0.0010
3.71E-05	0.04080	0.1000	0.7927	0.0010
5.81E-05	0.04080	0.1000	1.3170	0.0010
9.19E-05	0.04080	0.1000	2.6460	0.0010

Table D-8: Kinetic data for hydroformylation of 1-decene at temperature of 333 K
(Divekar *et al.*, 1993).

Exp. Rate ($\text{kmolm}^{-3}\text{s}^{-1}$)	H_2 (kmolm^{-3})	CO (kmolm^{-3})	1-decene (kmolm^{-3})	catalyst (kmolm^{-3})
0	0.00000	0.1076	0.5280	0.0010
2.58E-05	0.02200	0.1076	0.5280	0.0010
7.27E-05	0.04407	0.1076	0.5280	0.0010
2.28E-04	0.08890	0.1076	0.5280	0.0010
0.00E+00	0.04470	0.0000	0.5280	0.0010
3.61E-04	0.04470	0.0106	0.5280	0.0010
3.72E-04	0.04470	0.0231	0.5280	0.0010
2.12E-04	0.04470	0.0442	0.5280	0.0010
1.49E-04	0.04470	0.0663	0.5280	0.0010
7.45E-05	0.04470	0.1096	0.5280	0.0010
3.92E-05	0.04470	0.1634	0.5280	0.0010
2.74E-05	0.04470	0.2192	0.5280	0.0010
0.00E+00	0.04470	0.1076	0.0000	0.0010
4.60E-05	0.04470	0.1076	0.2805	0.0010
7.34E-05	0.04470	0.1076	0.5366	0.0010
9.52E-05	0.04470	0.1076	0.7927	0.0010
1.36E-04	0.04470	0.1076	1.3170	0.0010
1.81E-04	0.04470	0.1076	2.6340	0.0010

Table D-9: Kinetic data for hydroformylation of decene at temperature of 343 K
(Divekar *et al.*, 1993).

Exp. Rate ($\text{kmolm}^{-3}\text{s}^{-1}$)	H ₂ (kmolm^{-3})	CO (kmolm^{-3})	1-decene (kmolm^{-3})	catalyst (kmolm^{-3})
0	0.00000	0.1148	0.5280	0.0010
5.36E-05	0.02322	0.1148	0.5280	0.0010
1.34E-04	0.04840	0.1148	0.5280	0.0010
3.79E-04	0.09719	0.1148	0.5280	0.0010
0.00E+00	0.04470	0.0000	0.5280	0.0010
6.98E-04	0.04470	0.0125	0.5280	0.0010
6.74E-04	0.04470	0.0240	0.5280	0.0010
4.04E-04	0.04470	0.0471	0.5280	0.0010
2.67E-04	0.04470	0.0702	0.5280	0.0010
1.39E-04	0.04470	0.1163	0.5280	0.0010
7.25E-05	0.04470	0.1760	0.5280	0.0010
4.51E-05	0.04470	0.2346	0.5280	0.0010
0.00E+00	0.04470	0.1148	0.0000	0.0010
8.31E-05	0.04470	0.1148	0.2439	0.0010
1.36E-04	0.04470	0.1148	0.5244	0.0010
1.69E-04	0.04470	0.1148	0.7805	0.0010
2.11E-04	0.04470	0.1148	1.3170	0.0010
2.53E-04	0.04470	0.1148	2.6460	0.0010

Table D-10: Kinetic data for hydroformylation of 1-octene at temperature of 323 K
(Palo and Erkey, 1999).

Exp. Rate ($\text{kmolm}^{-3}\text{s}^{-1}$)	H ₂ (kmolm^{-3})	CO (kmolm^{-3})	1-octene (kmolm^{-3})	catalyst (kmolm^{-3})
0.00E+00	0.000	1.100	0.960	0.001
1.50E-04	1.100	1.100	0.960	0.001
2.40E-04	2.100	1.100	0.960	0.001
2.70E-04	2.600	1.100	0.960	0.001
0	1.000	0.000	0.960	0.001
1.20E-04	1.000	1.100	0.960	0.001
8.00E-05	1.000	1.600	0.960	0.001
5.70E-05	1.000	2.200	0.960	0.001
0.00E+00	1.100	1.100	0.000	0.001
8.33E-05	1.100	1.100	0.410	0.001
1.05E-04	1.100	1.100	0.680	0.001
1.20E-04	1.100	1.100	0.950	0.001
0.00E+00	1.100	1.100	0.960	0.000
1.2E-04	1.100	1.100	0.960	0.001
2.30E-04	1.100	1.100	0.960	0.001
4.90E-04	1.100	1.100	0.960	0.003

Appendix E

Estimated Rate Parameters

Table E-1: Estimated rate parameters of Model M2 with 95% confidence limits.

Substrate	T (K)	k	K_1^*	K_2^*	K_3^*	K_4^*	K_5^*	SEE	E_a (kJ mol ⁻¹)
Model M2									
1-dodecene	323	2.6×10 ⁴ *3.4×10 ⁴	1.4×10 ⁴	2.5×10 ⁵	5.9×10 ⁵	1.9×10 ⁴	9.0×10 ⁵	25.8	88.3
C ₁₂	333	5.9×10 ⁴ *5.8×10 ⁴	1.0×10 ⁴	1.0×10 ⁵	3.7×10 ⁵	1.5×10 ⁴	5.0×10 ⁵		*57.1 ^a
	343	11.0×10 ⁴ *9.9×10 ⁴	0.77×10 ⁴	0.52×10 ⁵	2.3×10 ⁵	1.2×10 ⁴	3.0×10 ⁵		
1-decene	323	1.0×10 ⁴ *1.1×10 ¹³	7.0×10 ³	2.0×10 ⁵	4.0×10 ⁴	60.0	9.0×10 ⁴	24.3	49.4
C ₁₀	333	3.0×10 ⁴ *1.4×10 ¹³	8.0×10 ³	1.3×10 ⁵	5.7×10 ⁴	900	1.2×10 ⁵		*49.0 ^b
	343	5.0×10 ⁴ *2.8×10 ¹³	2.5×10 ³	8.0×10 ⁴	6.9×10 ⁴	1.2×10 ³	1.4×10 ⁵		
styrene	333	1.1×10 ⁴ *1.6	11.0	3.7×10 ¹	4.6	1.1×10 ⁵	8.4×10 ⁵	9.7	74.5
C ₆	343	1.8×10 ⁴ *3.1	9.0	9.4×10 ¹	0.50	8.8×10 ⁴	6.0×10 ⁵		*68.8 ^c
	353	2.9×10 ⁴ *6.6	5.0	1.4×10 ²	0.050	6.0×10 ⁴	4.8×10 ⁵		
1-octene C ₈	323	3.2×10 ⁵ *0.10	1.4×10 ⁴	2.5×10 ⁵	5.9×10 ⁵	1.9×10 ⁴	9.0×10 ⁵	7.0	
Model M3		Non-linear Arrhenius constant and relatively high Φ_{min}							

(kmol, m³, s units)

*Activation energy and rate constant value reported in open literature:

^aBhanage et al. (1997)

^bDivekar et al. (1993)

^cNair et al.(1999)

Table E-2: Estimated rate parameters of Model A2 with 95% confidence limits.

Substrate	T (K)	k	K_1^*	K_2^*	K_3^*	K_4^*	K_5^*	SEE	E_a (kJ mol ⁻¹)
Model A3									
1-octene C ₁₀	353	1.1×10^3	5.3×10^1	2.4×10^1	2.4×10^1	-4.3×10^2	7.0×10^2	15.3	36.8
	363	2.0×10^3	3.8×10^2			-1.6×10^2	1.1×10^3		
	373	3.1×10^3	2.5×10^1	3.4×10^1	3.4×10^1	-8.5×10^1	6.8×10^1		
1-dodecene C ₁₂	353	1.1×10^3	5.7×10^2	-1.1×10^2	-1.4×10^2	-4.1×10^3	3.0×10^2	7.4	51.0
	363	1.8×10^3	1.0×10^3	-1.2×10^2	-1.4×10^2	-4.1×10^3	1.9×10^2		
	373	2.9×10^3	4.9×10^2	-5.3×10^2	-1.5×10^2	-4.3×10^3	6.6×10^2		
Model A2 Non-linear Arrhenius constant and relatively high Φ_{min}									

(kmol, m³, s units)

Appendix F

Derivation of the Rate Equation

Rate equation is a differential equation, and it can be integrated in order to obtain an integrated rate equation that links concentrations of reactant with time. In a semi-batch reactor, the concentration of 1-dodecene varies as a function of time and hence, it was necessary to check the validity of the rate equation over the entire range of conditions involved in a batch reactor operated at higher conversions. The data was developed to observe the variation in the concentrations of 1-dodecene as a function of time, at constant P_{CO} and P_{H_2} . Using model M1 (equation 3.14), the variation of the concentration of 1-dodecene can be expressed by the following mass balance equations for the kinetic regime:

$$\frac{-d[\text{dodecene}]}{dt} = \frac{k[H_2][CO][\text{catalyst}][\text{dodecene}]}{(1 + K_{co}[CO]^2)(1 + K_{\text{dodecene}}[\text{dodecene}])} \quad \text{F-1}$$

with initial conditions, $t = 0$ and $[\text{dodecene}] = [\text{dodecene}]_0$

For constant H_2 and CO pressure conditions, the following equation for the variation of 1-dodecene concentration with time can be derived,

$$\ln \frac{[\text{dodecene}]_0}{[\text{dodecene}]_t} + K_{\text{dodecene}}([\text{dodecene}]_0 - [\text{dodecene}]_t) = \frac{k[H_2][CO][\text{catalyst}]}{1 + K_{co}[CO]^2} \quad \text{F-2}$$

In deriving the equation, it was assumed that the change in reactant and products concentration do not affect the solubility of H_2 and CO significantly. Using Equation (B-2), the concentration of 1-dodecene, as a function of time was predicted for different temperatures and compared with literature data (Bhanage et al., 1997).

Appendix G

Table G-1: Solubility of CO at different pressure and temperature (x_2), calculated solubility (x_{calc}) and standard error of estimation (SEE) from the RST-based model.

$T = 298.15 \text{ K}$				$T = 313.15 \text{ K}$				$T = 323.15 \text{ K}$			
$P(\text{kPa})$	x_2	x_{calc}	$SEE (\%)$	$P(\text{kPa})$	x_2	x_{calc}	$SEE (\%)$	$P(\text{kPa})$	x_2	x_{calc}	$SEE (\%)$
Propylene carbonate											
131	0.00155	0.00150	3.22	122	0.00156	0.00152	2.56	128	0.00157	0.00155	1.27
333	0.0048	0.0043	10.42	370	0.0049	0.0045	8.16	332	0.0049	0.0048	2.04
535	0.0077	0.0079	2.62	613	0.0078	0.0082	5.13	523	0.0078	0.0084	7.69
767	0.0106	0.0101	4.76	865	0.0107	0.0110	2.80	755	0.0109	0.0111	1.83
995	0.0134	0.0129	3.73	1082	0.0136	0.0132	2.94	997	0.0138	0.0135	2.17
1115	0.0160	0.0165	3.12	1315	0.0162	0.0164	1.23	1361	0.0163	0.0167	2.45
1496	0.0183	0.0179	2.19	1489	0.0184	0.0187	1.63	1533	0.0184	0.0189	2.72
Biphasic PC+dodecane											
136	0.00145	0.00152	4.83	117	0.00150	0.00155	3.33	156	0.00155	0.00157	1.29
282	0.0042	0.0042	0.00	399	0.0043	0.0044	2.33	399	0.0045	0.0047	4.44
574	0.0074	0.0077	4.05	576	0.0075	0.0080	6.67	576	0.0077	0.0082	6.49
809	0.0110	0.0092	16.36	821	0.0112	0.0094	16.07	821	0.0113	0.0096	15.04
1004	0.0135	0.0133	1.48	1005	0.0136	0.0136	0.00	1015	0.0138	0.0138	0.00
1245	0.0163	0.0165	1.23	1355	0.0165	0.0168	1.82	1350	0.0165	0.0170	3.03
1515	0.0180	0.0176	2.22	1523	0.0182	0.0178	2.20	1535	0.0183	0.0181	1.09
TMS-systems PC+dodecane+1,4-dioxane											
125	0.00169	0.00165	2.37	120	0.00172	0.00167	2.91	138	0.00175	0.00171	2.29
321	0.0050	0.0052	4.00	368	0.0053	0.0054	1.89	388	0.0056	0.0056	0.00
610	0.0093	0.0089	4.30	595	0.0100	0.0092	8.00	625	0.0107	0.0095	11.21
803	0.0125	0.0127	1.60	885	0.0130	0.0129	0.77	890	0.0135	0.0132	2.22
1005	0.0147	0.0139	5.44	995	0.0149	0.0142	4.70	987	0.0150	0.0145	3.33
1355	0.0173	0.0174	0.58	1116	0.0174	0.0176	1.15	1126	0.0178	0.0179	0.56
1523	0.0198	0.0205	3.54	1515	0.0200	0.0207	3.50	1510	0.0205	0.0209	1.95

Table G1 (continue)

<i>T</i> = 333.15 K				<i>T</i> = 343.15 K			
<i>P</i> (kPa)	<i>x</i> ₂	<i>x</i> _{calc}	<i>SEE</i> (%)	<i>P</i> (kPa)	<i>x</i> ₂	<i>x</i> _{calc}	<i>SEE</i> (%)
Propylene carbonate							
131	0.00157	0.00157	0.00	145	0.00158	0.00159	0.63
399	0.0052	0.0050	3.85	328	0.0050	0.0052	4.00
622	0.0079	0.0085	7.59	576	0.0080	0.0087	8.75
875	0.0109	0.0112	2.75	850	0.0111	0.0113	1.80
1056	0.0139	0.0137	1.44	999	0.0140	0.0139	0.71
1216	0.0165	0.0169	2.42	1189	0.0165	0.0171	3.64
1495	0.0186	0.0190	2.15	1545	0.0187	0.0192	2.67
Biphasic PC+dodecane							
146	0.00158	0.00159	0.63	126	0.00160	0.00161	0.63
362	0.0050	0.0049	2.00	378	0.0051	0.0051	0.00
665	0.0078	0.0084	7.69	643	0.0081	0.0086	6.17
788	0.0113	0.0098	13.27	885	0.0116	0.0100	13.79
1006	0.0138	0.0140	1.45	1182	0.0144	0.0142	1.39
1301	0.0165	0.0171	3.64	1315	0.0166	0.0173	4.22
1503	0.0185	0.0183	1.08	1495	0.0187	0.0185	1.07
TMS-systems PC+dodecane+1,4-dioxane							
122	0.00178	0.00174	2.25	135	0.00182	0.00176	3.30
376	0.0055	0.0058	5.45	339	0.0056	0.0060	7.14
576	0.0109	0.0098	10.09	592	0.0113	0.0100	11.50
799	0.0133	0.0134	0.75	811	0.0140	0.0137	2.14
995	0.0153	0.0147	3.92	1015	0.0155	0.0150	3.23
1255	0.0181	0.0181	0.00	1242	0.0183	0.0183	0.00
1496	0.0207	0.0211	1.93	1519	0.0210	0.0213	1.43

Table G-2: Solubility of H₂ at different pressure and temperature (x_2), calculated solubility (x_{calc}) and standard error of estimation (SEE) from the RST-based model.

$T = 298.15$ K				$T = 313.15$ K				$T = 323.15$ K			
P (kPa)	x_2	x_{calc}	SEE (%)	P (kPa)	x_2	x_{calc}	SEE (%)	P (kPa)	x_2	x_{calc}	SEE (%)
Propylene carbonate											
131	0.00135	0.00132	2.22	122	0.00138	0.00135	2.17	128	0.00139	0.00137	1.44
333	0.0048	0.0047	2.08	370	0.0049	0.0050	2.04	332	0.0051	0.0053	3.92
535	0.0075	0.0080	6.67	613	0.0076	0.0082	7.89	523	0.0077	0.0084	9.09
767	0.0101	0.0105	3.96	865	0.0102	0.0107	4.90	755	0.0102	0.0109	6.86
995	0.0124	0.0128	3.23	1082	0.0126	0.0129	2.38	997	0.0127	0.0130	2.36
1215	0.0145	0.0149	2.76	1315	0.0147	0.0150	2.04	1361	0.0148	0.0153	3.38
1496	0.0178	0.0175	1.69	1489	0.0179	0.0178	0.56	1533	0.0180	0.0181	0.56
Biphasic PC+dodecane											
136	0.00092	0.00096	4.35	117	0.00098	0.00097	1.02	156	0.00104	0.00099	4.81
282	0.0022	0.0026	9.09	399	0.0024	0.0027	12.50	399	0.0027	0.0029	7.41
574	0.0044	0.0046	4.55	576	0.0046	0.0049	6.52	576	0.0047	0.0051	8.51
809	0.0072	0.0070	2.78	821	0.0073	0.0074	1.37	821	0.0075	0.0077	2.67
1004	0.0093	0.0089	4.30	1005	0.0095	0.0094	1.05	1015	0.0098	0.0097	1.02
1245	0.0103	0.0106	2.91	1355	0.0104	0.0107	2.88	1350	0.0106	0.0109	2.83
1515	0.0126	0.0129	2.38	1523	0.0128	0.0130	1.56	1535	0.0129	0.0132	2.33
TMS-systems PC+dodecane+1,4-dioxane											
125	0.00115	0.00118	2.61	120	0.00122	0.00120	1.64	138	0.00126	0.00124	1.59
321	0.0032	0.0029	9.38	368	0.0033	0.0033	0.00	388	0.0036	0.0035	2.78
610	0.0059	0.0055	6.78	595	0.0060	0.0057	5.00	625	0.0062	0.0059	4.84
803	0.0097	0.0095	2.06	885	0.0099	0.0097	2.02	890	0.0105	0.0101	3.81
1005	0.0119	0.0122	2.52	995	0.0121	0.0123	1.65	987	0.0122	0.0126	3.28
1355	0.0154	0.0158	2.60	1116	0.0155	0.0159	2.58	1126	0.0157	0.0161	2.55
1523	0.0166	0.0167	0.60	1515	0.0168	0.0169	0.60	1510	0.0169	0.0173	2.37

Table G-2 (Continue)

<i>T</i> = 333.15 K				<i>T</i> = 343.15 K			
<i>P</i> (kPa)	<i>x</i> ₂	<i>x</i> _{calc}	<i>SEE</i> (%)	<i>P</i> (kPa)	<i>x</i> ₂	<i>x</i> _{calc}	<i>SEE</i> (%)
Propylene carbonate							
131	0.00140	0.00145	3.57	145	0.00140	0.00148	-5.71
399	0.0051	0.0055	7.84	328	0.0051	0.0057	-11.76
622	0.0077	0.0086	11.69	576	0.0082	0.0089	-8.54
875	0.0103	0.0110	6.80	850	0.0103	0.0112	-8.74
1056	0.0127	0.0133	4.72	999	0.0127	0.0135	-6.30
1216	0.0148	0.0156	5.41	1189	0.0148	0.0158	-6.76
1495	0.0181	0.0185	2.21	1545	0.0181	0.0188	-3.87
Biphasic PC+dodecane							
146	0.00109	0.00103	5.50	126	0.00115	0.00108	6.09
362	0.0028	0.0032	14.29	378	0.0031	0.0035	12.90
665	0.0049	0.0053	8.16	643	0.0052	0.0056	7.69
788	0.0078	0.0079	1.28	885	0.0080	0.0083	3.75
1006	0.0099	0.0102	3.03	1182	0.0102	0.0106	3.92
1301	0.0106	0.0115	8.49	1315	0.0109	0.0117	7.34
1503	0.0129	0.0136	5.43	1495	0.0131	0.0139	6.11
TMS-systems PC+dodecane+1,4-dioxane							
122	0.00129	0.00127	1.55	135	0.00133	0.00136	2.26
376	0.0037	0.0038	2.70	339	0.0039	0.0043	10.26
576	0.0062	0.0064	3.23	592	0.0065	0.0067	3.08
799	0.0104	0.0108	3.85	811	0.0105	0.0112	6.67
995	0.0124	0.0130	4.84	1015	0.0125	0.0133	6.40
1255	0.0158	0.0165	4.43	1242	0.0160	0.0166	3.75
1496	0.0169	0.0178	5.33	1519	0.0172	0.0182	5.81

Table G-3: Solubility of CO at different pressure and temperature (x_2), calculated solubility (x_{calc}) and standard error of estimation (SEE) from the modified UNIFAC model.

$T = 298.15 \text{ K}$				$T = 313.15 \text{ K}$				$T = 323.15 \text{ K}$			
$P(\text{kPa})$	x_2	x_{calc}	$SEE (\%)$	$P(\text{kPa})$	x_2	x_{calc}	$SEE (\%)$	$P(\text{kPa})$	x_2	x_{calc}	$SEE (\%)$
Propylene carbonate											
131	0.00155	0.00145	6.45	122	0.00156	0.00158	1.28	128	0.00157	0.00160	1.91
333	0.0048	0.0050	4.17	370	0.0049	0.0052	6.12	332	0.0049	0.0054	10.20
535	0.0077	0.0080	3.90	613	0.0078	0.0083	6.41	523	0.0078	0.0085	8.97
767	0.0106	0.0109	2.83	865	0.0107	0.0112	4.67	755	0.0109	0.0114	4.59
995	0.0134	0.0130	2.99	1082	0.0136	0.0135	0.74	997	0.0138	0.0137	0.72
1115	0.0160	0.0155	3.13	1315	0.0162	0.0158	2.47	1361	0.0163	0.0160	1.84
1496	0.0183	0.0188	2.73	1489	0.0184	0.0190	3.26	1533	0.0184	0.0192	4.35
Biphasic PC+dodecane											
136	0.00145	0.00149	2.76	117	0.00150	0.00153	2.00	156	0.00155	0.00156	0.65
282	0.00423	0.0045	6.38	399	0.0043	0.0048	11.63	399	0.0045	0.0052	15.56
574	0.0074	0.0078	5.41	576	0.0075	0.0081	8.00	576	0.0077	0.0084	9.09
809	0.0110	0.0115	4.55	821	0.0112	0.0118	5.36	821	0.0113	0.0121	7.08
1004	0.0135	0.0140	3.70	1005	0.0136	0.0145	6.62	1015	0.0138	0.0147	6.52
1245	0.0163	0.0168	3.07	1355	0.0165	0.0172	4.24	1350	0.0165	0.0175	6.06
1515	0.0180	0.0175	2.78	1523	0.0182	0.0185	1.65	1535	0.0183	0.0187	2.19
TMS-systems PC+dodecane+1,4-dioxane											
125	0.00169	0.00165	2.37	120	0.00172	0.00169	1.74	138	0.00175	0.00173	1.14
321	0.0050	0.0045	10.00	368	0.0053	0.0049	7.55	388	0.0056	0.0053	5.36
610	0.0093	0.0099	6.45	595	0.0100	0.0105	5.00	625	0.0107	0.0109	1.87
803	0.0125	0.0129	3.20	885	0.0130	0.0135	3.85	890	0.0135	0.0139	2.96
1005	0.0147	0.0151	2.72	995	0.0149	0.0155	4.03	987	0.0150	0.0159	6.00
1355	0.0173	0.0178	2.89	1116	0.0174	0.0182	4.60	1126	0.0178	0.0186	4.49
1523	0.0188	0.0195	3.72	1515	0.0190	0.0199	4.74	1510	0.0191	0.0204	6.81

Table G-3 (Continue)

<i>T</i> = 333.15 K				<i>T</i> = 343.15 K			
<i>P</i> (kPa)	<i>x</i> ₂	<i>x</i> _{calc}	<i>SEE</i> (%)	<i>P</i> (kPa)	<i>x</i> ₂	<i>x</i> _{calc}	<i>SEE</i> (%)
Propylene carbonate							
131	0.00157	0.00157	0.00	145	0.00157	0.00159	1.27
399	0.0052	0.0050	3.85	328	0.0050	0.0052	4.00
622	0.0079	0.0085	7.59	576	0.0080	0.0087	8.75
875	0.0109	0.0112	2.75	850	0.0111	0.0113	1.80
1056	0.0139	0.0137	1.44	999	0.0140	0.0139	0.71
1216	0.0165	0.0169	2.42	1189	0.0165	0.0171	3.64
1495	0.0186	0.0190	2.15	1545	0.0187	0.0192	2.67
Biphasic PC+dodecane							
146	0.00158	0.00159	0.63	126	0.00160	0.00161	0.63
362	0.0050	0.0049	2.00	378	0.0051	0.0051	0.00
665	0.0078	0.0084	7.69	643	0.0081	0.0086	6.17
788	0.0113	0.0098	13.27	885	0.0116	0.0100	13.79
1006	0.0138	0.0140	1.45	1182	0.0144	0.0142	1.39
1301	0.0165	0.0171	3.64	1315	0.0166	0.0173	4.22
1503	0.0185	0.0183	1.08	1495	0.0187	0.0185	1.07
TMS-systems PC+dodecane+1,4-dioxane							
122	0.00178	0.00174	2.25	135	0.00182	0.00176	3.30
376	0.0055	0.0058	5.45	339	0.0056	0.0060	7.14
576	0.0109	0.0098	10.09	592	0.0113	0.0100	11.50
799	0.0133	0.0134	0.75	811	0.0140	0.0137	2.14
995	0.0153	0.0147	3.92	1015	0.0155	0.0150	3.23
1255	0.0181	0.0181	0.00	1242	0.0183	0.0183	0.00
1496	0.0207	0.0211	1.93	1519	0.0210	0.0213	1.43

Table G-4: Solubility of H₂ at different pressure and temperature (x_2), calculated solubility (x_{calc}) and standard error of estimation (SEE) from the modified UNIFAC model.

$T = 298.15$ K				$T = 313.15$ K				$T = 323.15$ K			
P (kPa)	x_2	x_{calc}	SEE (%)	P (kPa)	x_2	x_{calc}	SEE (%)	P (kPa)	x_2	x_{calc}	SEE (%)
Propylene carbonate											
131	0.00135	0.00137	1.48	122	0.00138	0.00138	0.00	128	0.00139	0.00140	0.72
333	0.0048	0.0050	4.17	370	0.0049	0.0051	4.08	332	0.0051	0.0052	1.96
535	0.0075	0.0074	1.33	613	0.0076	0.0075	1.32	523	0.0077	0.0076	1.30
767	0.0101	0.0100	0.99	865	0.0102	0.0101	0.98	755	0.0102	0.0103	0.98
995	0.0124	0.0123	0.81	1082	0.0126	0.0125	0.79	997	0.0127	0.0127	0.00
1215	0.0145	0.0143	1.38	1315	0.0147	0.0145	1.36	1361	0.0148	0.0147	0.68
1496	0.0178	0.0179	0.56	1489	0.0179	0.0180	0.56	1533	0.0180	0.0182	1.11
Biphasic PC+dodecane											
136	0.00092	0.00095	3.26	117	0.00098	0.00097	1.02	156	0.00104	0.00099	4.81
282	0.0022	0.0024	9.09	399	0.0024	0.0025	4.17	399	0.0027	0.0028	3.70
574	0.0044	0.0045	2.27	576	0.0046	0.0047	2.17	576	0.0047	0.0049	4.26
809	0.0072	0.0073	1.39	821	0.0073	0.0075	2.74	821	0.0075	0.0077	2.67
1004	0.0093	0.0091	2.15	1005	0.0095	0.0094	1.05	1015	0.0098	0.0097	1.02
1245	0.0103	0.0102	0.97	1355	0.0104	0.0105	0.96	1350	0.0106	0.0106	0.00
1515	0.0126	0.0128	1.59	1523	0.0128	0.0130	1.56	1535	0.0129	0.0132	2.33
TMS-systems PC+dodecane+1,4-dioxane											
125	0.00115	0.00118	2.61	120	0.00122	0.00121	0.82	138	0.00126	0.00124	1.59
321	0.0032	0.0035	9.38	368	0.0035	0.0036	2.86	388	0.0037	0.0038	2.70
610	0.0059	0.0062	5.08	595	0.0060	0.0064	6.67	625	0.0062	0.0066	6.45
803	0.0097	0.0096	1.03	885	0.0099	0.0098	1.01	890	0.0105	0.0102	2.86
1005	0.0119	0.0121	1.68	995	0.0121	0.0124	2.48	987	0.0124	0.0126	1.61
1355	0.0154	0.0152	1.30	1116	0.0155	0.0155	0.00	1126	0.0157	0.0157	0.00
1523	0.0166	0.0165	0.60	1515	0.0168	0.0167	0.60	1510	0.0169	0.0170	0.59

Table G-4: (Continue)

<i>T</i> = 333.15 K				<i>T</i> = 343.15 K			
<i>P</i> (kPa)	<i>x</i> ₂	<i>x</i> _{calc}	<i>SEE</i> (%)	<i>P</i> (kPa)	<i>x</i> ₂	<i>x</i> _{calc}	<i>SEE</i> (%)
Propylene carbonate							
131	0.00140	0.00142	1.43	145	0.00142	0.00143	0.70
399	0.0051	0.0053	3.92	328	0.0053	0.0054	1.89
622	0.0077	0.0078	1.30	576	0.0079	0.0079	0.00
875	0.0103	0.0104	0.97	850	0.0105	0.0104	0.95
1056	0.0127	0.0128	0.79	999	0.0129	0.0128	0.78
1216	0.0148	0.0149	0.68	1189	0.0150	0.0149	0.67
1495	0.0181	0.0183	1.10	1545	0.0185	0.0183	1.08
Biphasic PC+dodecane							
146	0.00109	0.00105	3.67	126	0.00115	0.00110	4.35
362	0.0028	0.0030	7.14	378	0.0031	0.0034	9.68
665	0.0049	0.0051	4.08	643	0.0052	0.0055	5.77
788	0.0078	0.0080	2.56	885	0.0080	0.0083	3.75
1006	0.0099	0.0102	3.03	1182	0.0102	0.0105	3.05
1301	0.0106	0.0109	2.83	1315	0.0109	0.0110	0.92
1503	0.0129	0.0134	3.88	1495	0.0131	0.0136	3.82
TMS-systems PC+dodecane+1,4-dioxane							
122	0.00129	0.00127	1.55	135	0.00133	0.00130	2.26
376	0.0037	0.0039	5.41	339	0.0039	0.0042	7.69
576	0.0062	0.0068	9.68	592	0.0065	0.0070	7.69
799	0.0104	0.0105	0.96	811	0.0105	0.0108	2.86
995	0.0124	0.0128	3.23	1015	0.0125	0.0131	4.80
1255	0.0158	0.0159	0.63	1242	0.0160	0.0161	0.62
1496	0.0169	0.0172	1.78	1519	0.0172	0.0175	1.74

Appendix H

Table H-1: A summary of the effect of reaction conditions on the conversion and selectivity involving Rh-catalyzed hydroformylation reaction

Reference	Catalyst Precursor	Substrate	[Catalyst] mol/m ³	P bar	T K	t h	Solvent	Olefin Conversion (%)	Yield of Aldehyde (%)	<i>n/iso</i>
Klein et al. (2001)	Rh(acac)(CO) ₂ NAPHOS; NAPHOS:Rh=5,	1-pentene	0.080	10	393	16	anisole	-	76.0	99.0
Huang et al. (2004)	Rh ₄ (CO) ₁₂	1-octene	11.6	10	353	1.5	THF	96.7	6.5	1.4
	Rh ₄ (CO) ₁₂ + PPh ₃ ; P:Rh=5							97.7	93.1	2.4
	Rh ₄ (CO) ₁₂ /MCM-41(NH ₂)							25.2	5.9	1.7
	Rh ₄ (CO) ₁₂ /MCM-41(NH ₂) + PPh ₃ ; P:Rh=5							98.9	95.9	2.7
	RhCl(PPh ₃) ₃							20.1	21.4	3.0
	RhCl(PPh ₃)/ MCM-41(NH ₂)							73.6	61.0	2.9
van Rooy et al., (1995)	RhCl(PPh ₃)/ MCM-41(NH ₂) + PPh ₃ ; P:Rh=5							92.9	94.5	2.7
	Rh(CO) ₂ (acac)tris(2-tertbutyl-4-methylphenyl) phosphate; P:Rh=50	1-octene	0.1	10	353	-	toluene	-	44.0	1.9
Behr et al. (2005)	Rh(acac)(CO) ₂ Biphephos; Biphephos:Rh = 5	4-octene	3.33	10	398	4	PC/dodecane/ <i>p</i> -xylene	99.0		9.0
Tijani and Ali (2006)	HRh(CO)(PPh ₃) ₃ P(OPh) ₃ ; P:Rh = 12	1-octene	0.83	14	363	1.5	PC/heptane	-	84.0	8.1

Table H-1: (Continue)

Reference	Catalyst Precursor	Substrate	[Catalyst] mol/m ³	P bar	T K	t h	Solvent	Olefin Conversion (%)	Yield of Aldehyde (%)	<i>n</i> / <i>i</i>
Suárez et al. (2006)	RhCl(CO)(TPPMS) ₂ [TPPMS=P(C ₆ H ₅) ₂ (C ₆ H ₄ SO ₃)]	1-hexene	0.19	68	373	1.5	biphasic toluene/H ₂ O	95.0	73.2	1.1
	RhCl(CO)(TPPDS) ₂ [TPPDS=P(C ₆ H ₅)(C ₆ H ₄ SO ₃) ₂]							96.0	73.9	1.3
	RhCl(CO)(TPPTS) ₂ [TPPTS=P(C ₆ H ₄ SO ₃) ₃]							94.0	74.3	1.1
Present work	HRh(CO)(PPh ₃) ₃ P(OPh) ₃ ; P:Rh = 12	1-octene	0.17	15	363	1.5	PC/dodecane/ 1,4-dioxane	53.0	47.0	9.0

Appendix J

Kinetic Data

Table J-1: Kinetic data, estimated rate parameters, mean residual sum of squares (MRSS) and standard error of estimation (SEE) from the empirical rate model.

Hydroformylation of 1-octene with $\text{HRh}(\text{CO})(\text{PPh}_3)_3/\text{P}(\text{OPh})_3$ catalyst in TMS-system at temperature of 353 K.

k 0.55
 K_{CO} 0.52
 m 1.72

[1-octene]	[catalyst]	P_{H_2}	P_{CO}	R_{expt}	R_{calc}	MRSS	SEE	%SEE
0.19	8.66E-05	7.485	7.485	2.00E-05	2.13E-05	1.57273E-12	6.27E-02	6.27E+00
0.19	0.000173	7.485	7.485	4.00E-05	4.25E-05	6.04712E-12	6.15E-02	6.15E+00
0.19	0.000346	7.485	7.485	8.00E-05	8.49E-05	2.41885E-11	6.15E-02	6.15E+00
0.19	0.000644	7.485	7.485	1.55E-04	1.58E-04	9.33789E-12	1.97E-02	1.97E+00
0.1	1.73E-04	7.485	7.485	2.45E-05	2.23E-05	4.80974E-12	8.94E-02	8.94E+00
0.212	1.73E-04	7.485	7.485	5.20E-05	4.74E-05	2.13869E-11	8.89E-02	8.89E+00
0.29	1.73E-04	7.485	7.485	7.00E-05	6.48E-05	2.69779E-11	7.42E-02	7.42E+00
0.34	1.73E-04	7.485	7.485	8.33E-05	7.60E-05	5.35909E-11	8.79E-02	8.79E+00
0.39	1.73E-04	7.485	7.485	8.67E-05	8.72E-05	2.05087E-13	5.22E-03	5.22E-01
0.19	1.73E-04	11.23	3.74	8.99E-05	8.79E-05	3.99698E-12	2.22E-02	2.22E+00
0.19	1.73E-04	10	4.98	7.06E-05	7.01E-05	2.25464E-13	6.73E-03	6.73E-01
0.19	1.73E-04	7.485	7.48506	4.62E-05	4.25E-05	1.39959E-11	8.10E-02	8.10E+00
0.19	1.73E-04	3.74	11.23	1.80E-05	1.63E-05	2.95579E-12	9.55E-02	9.55E+00
						1.05807E-11	7.56E-01	5.82E+00

Table J-2: Kinetic data, estimated rate parameters, mean residual sum of squares (MRSS) and standard error of estimation (SEE) from the empirical rate model.

Hydroformylation of 1-octene with $\text{HRh}(\text{CO})(\text{PPh}_3)_3/\text{P}(\text{OPh})_3$ catalyst in TMS-system at temperature of 363 K.

k 1.11
 K_{CO} 1.18
 m 1.60

[1-octene]	[catalyst]	P_{H_2}	P_{CO}	R_{expt}	R_{calc}	MRSS	SEE	%SEE
0.19	8.66E-05	7.485	7.485	2.50E-05	2.64E-05	1.9815E-12	5.63E-02	5.63E+00
0.19	0.000173	7.485	7.485	5.20E-05	5.28E-05	5.69011E-13	1.45E-02	1.45E+00
0.19	0.000346	7.485	7.485	1.00E-04	1.06E-04	3.03453E-11	5.51E-02	5.51E+00
0.19	0.000644	7.485	7.485	1.85E-04	1.96E-04	1.29511E-10	6.15E-02	6.15E+00
0.1	1.73E-04	7.485	7.485	3.05E-05	2.78E-05	7.42325E-12	8.94E-02	8.94E+00
0.212	1.73E-04	7.485	7.485	6.50E-05	5.89E-05	3.76662E-11	9.44E-02	9.44E+00
0.29	1.73E-04	7.485	7.485	8.40E-05	8.05E-05	1.2112E-11	4.14E-02	4.14E+00
0.34	1.73E-04	7.485	7.485	1.00E-04	9.44E-05	3.13322E-11	5.60E-02	5.60E+00
0.39	1.73E-04	7.485	7.485	1.12E-04	1.08E-04	1.37997E-11	3.32E-02	3.32E+00
0.19	1.73E-04	11.23	3.74	9.77E-05	1.03E-04	2.56597E-11	5.18E-02	5.18E+00
0.19	1.73E-04	10	4.98	8.50E-05	8.31E-05	3.62952E-12	2.24E-02	2.24E+00
0.19	1.73E-04	7.485	7.48506	5.80E-05	5.28E-05	2.7519E-11	9.04E-02	9.04E+00
0.19	1.73E-04	3.74	11.23	2.45E-05	2.18E-05	7.08915E-12	1.09E-01	1.09E+01
						2.00968E-11	6.66E-01	5.96E+00

Table J-3: Kinetic data, estimated rate parameters, mean residual sum of squares (MRSS) and standard error of estimation (SEE) from the empirical rate model.

Hydroformylation of 1-octene with $\text{HRh}(\text{CO})(\text{PPh}_3)_3/\text{P}(\text{OPh})_3$ catalyst in TMS-system at temperature of 373 K.

k 1.97
 K_{CO} 2.24
 m 1.36

[1-octene]	[catalyst]	P_{H_2}	P_{CO}	R_{expt}	R_{calc}	MRSS	SEE	%SEE
0.19	8.66E-05	7.485	7.485	3.50E-05	3.63E-05	1.63815E-12	3.66E-02	3.66E+00
0.19	0.000173	7.485	7.485	7.00E-05	7.25E-05	6.13065E-12	3.54E-02	3.54E+00
0.19	0.000346	7.485	7.485	1.35E-04	1.45E-04	9.90429E-11	7.37E-02	7.37E+00
0.19	0.000644	7.485	7.485	2.60E-04	2.70E-04	9.59441E-11	3.77E-02	3.77E+00
0.1	1.73E-04	7.485	7.485	4.12E-05	3.81E-05	9.45396E-12	7.46E-02	7.46E+00
0.212	1.73E-04	7.485	7.485	8.50E-05	8.09E-05	1.70736E-11	4.86E-02	4.86E+00
0.29	1.73E-04	7.485	7.485	1.20E-04	1.11E-04	8.79603E-11	7.82E-02	7.82E+00
0.34	1.73E-04	7.485	7.485	1.37E-04	1.30E-04	5.33788E-11	5.33E-02	5.33E+00
0.39	1.73E-04	7.485	7.485	1.60E-04	1.49E-04	1.2619E-10	7.02E-02	7.02E+00
0.19	1.73E-04	11.23	3.74	1.20E-04	1.30E-04	9.14029E-11	7.97E-02	7.97E+00
0.19	1.73E-04	10	4.98	1.13E-04	1.08E-04	2.55121E-11	4.47E-02	4.47E+00
0.19	1.73E-04	7.485	7.48506	8.00E-05	7.25E-05	5.66128E-11	9.41E-02	9.41E+00
0.19	1.73E-04	3.74	11.23	3.50E-05	3.21E-05	8.35294E-12	8.26E-02	8.26E+00
						4.18963E-11	7.27E-01	6.06E+00
								5.97E+00

Table J-4: Estimated rate parameters, mean residual sum of squares (MRSS) and standard error of estimation (SEE) from the mechanistic rate model.

Hydroformylation of 1-octene with $\text{HRh}(\text{CO})(\text{PPh}_3)_3/\text{P}(\text{OPh})_3$ catalyst in TMS-system at temperature of 353 K

k 5.11E+03
 K1* 1.22E+02
 K2* 1.50E+03
 K3* 8.80E-01
 K4* 8.12E-13

[H ₂]	[CO]	[1-octene]	[catalyst]	R _{expt}	R _{expt} X 10 ⁴	R _{calc}	R _{calc} X 10 ⁴	MRSS	SEE	%SEE
0.0747	0.0930	0.19	8.66E-05	2.200E-05	2.200E-01	2.293E-05	2.293E-01	8.712E-13	4.243E-02	4.243E+00
0.0747	0.0930	0.19	1.73E-04	4.400E-05	4.400E-01	4.581E-05	4.581E-01	3.290E-12	4.122E-02	4.122E+00
0.0747	0.0930	0.19	3.46E-04	9.000E-05	9.000E-01	9.163E-05	9.163E-01	2.649E-12	1.808E-02	1.808E+00
0.0747	0.0930	0.19	6.44E-04	1.700E-04	1.700E+00	1.705E-04	1.705E+00	2.956E-13	3.198E-03	3.198E+00
0.0747	0.0930	0.1	1.73E-04	2.454E-05	2.454E-01	2.419E-05	2.419E-01	1.241E-13	1.435E-02	1.435E+00
0.0747	0.0930	0.212	1.73E-04	5.200E-05	5.200E-01	5.108E-05	5.108E-01	8.471E-13	1.770E-02	1.770E+00
0.0747	0.0930	0.29	1.73E-04	7.000E-05	7.000E-01	6.969E-05	6.969E-01	9.905E-14	4.496E-03	4.496E+00
0.0747	0.0930	0.34	1.73E-04	8.000E-05	8.000E-01	8.156E-05	8.156E-01	2.432E-12	1.949E-02	1.949E+00
0.0747	0.0930	0.39	1.73E-04	9.000E-05	9.000E-01	9.339E-05	9.339E-01	1.151E-11	3.770E-02	3.770E+00
0.1397	0.0124	0.19	1.73E-04	1.000E-04	1.000E+00	1.100E-04	1.100E+00	8.493E-37	9.216E-15	9.216E+00
0.1120	0.0373	0.19	1.73E-04	8.200E-05	8.200E-01	8.998E-05	8.998E-01	6.372E-11	9.734E-02	9.734E+00
0.0998	0.0618	0.19	1.73E-04	7.200E-05	7.200E-01	7.176E-05	7.176E-01	5.545E-14	3.271E-03	3.271E-01
0.0747	0.0930	0.19	1.73E-04	4.800E-05	4.800E-01	4.581E-05	4.581E-01	4.780E-12	4.555E-02	4.555E+00
0.0373	0.1395	0.19	1.73E-04	2.000E-05	2.000E-01	1.847E-05	1.847E-01	2.328E-12	7.629E-02	7.629E+00
Average:								8.454E-12	4.211E-01	4.161E+00

Table J-5: Estimated rate parameters, mean residual sum of squares (MRSS) and standard error of estimation (SEE) from the mechanistic rate model.

Hydroformylation of 1-octene with $\text{HRh}(\text{CO})(\text{PPh}_3)_3 / \text{P}(\text{OPh})_3$ catalyst in TMS-system at temperature of 363 K.

k	8.01E+03
K1*	2.02E+02
K2*	1.30E+03
K3*	6.80E-03
K4*	4.33E-14

[H ₂]	[CO]	[1-octene]	[catalyst]	R _{expt}	R _{expt} X 10 ⁴	R _{calc}	R _{calc} X 10 ⁴	MRSS	SEE	%SEE
0.0754	0.0949	0.19	8.66E-05	2.800E-05	2.800E-01	2.962E-05	2.962E-01	2.618E-12	5.779E-02	5.779E+00
0.0754	0.0949	0.19	1.73E-04	5.800E-05	5.800E-01	5.917E-05	5.917E-01	1.364E-12	2.014E-02	2.014E+00
0.0754	0.0949	0.19	3.46E-04	1.190E-04	1.190E+00	1.183E-04	1.183E+00	4.411E-13	5.581E-03	5.581E+00
0.0754	0.0949	0.19	6.44E-04	2.220E-04	2.220E+00	2.203E-04	2.203E+00	3.045E-12	7.860E-03	0.000E+00
0.0754	0.0949	0.1	1.73E-04	3.000E-05	3.000E-01	3.114E-05	3.114E-01	1.303E-12	3.805E-02	3.805E+00
0.0754	0.0949	0.212	1.73E-04	6.800E-05	6.800E-01	6.602E-05	6.602E-01	3.926E-12	2.914E-02	2.914E+00
0.0754	0.0949	0.29	1.73E-04	9.200E-05	9.200E-01	9.031E-05	9.031E-01	2.866E-12	1.840E-02	1.840E+00
0.0754	0.0949	0.34	1.73E-04	1.070E-04	1.070E+00	1.059E-04	1.059E+00	1.263E-12	1.050E-02	1.050E+00
0.0754	0.0949	0.39	1.73E-04	1.220E-04	1.220E+00	1.214E-04	1.214E+00	3.083E-13	4.551E-03	4.551E+00
0.1411	0.0127	0.19	1.73E-04	1.250E-04	1.250E+00	1.250E-04	1.250E+00	7.347E-40	2.168E-16	2.168E+00
0.1132	0.0381	0.19	1.73E-04	9.770E-05	9.770E-01	1.074E-04	1.074E+00	9.372E-11	9.909E-02	9.909E+00
0.1008	0.0632	0.19	1.73E-04	8.600E-05	8.600E-01	8.854E-05	8.854E-01	6.468E-12	2.957E-02	2.957E+00
0.0754	0.0949	0.19	1.73E-04	6.000E-05	6.000E-01	5.917E-05	5.917E-01	6.924E-13	1.387E-02	1.387E+00
0.0377	0.1424	0.19	1.73E-04	2.500E-05	2.500E-01	2.519E-05	2.519E-01	3.762E-14	7.758E-03	7.758E-01
Average:								1.180E-11	3.344E-01	4.867E+00

Table J-6: Estimated rate parameters, mean residual sum of squares (MRSS) and standard error of estimation (SEE) from the mechanistic rate model.

Hydroformylation of 1-octene with $\text{HRh}(\text{CO})(\text{PPh}_3)_3 / \text{P}(\text{OPh})_3$ catalyst in TMS-system at temperature of 373 K.

k 1.00E+04
 K1* 2.25E+02
 K2* 9.70E+02
 K3* 9.67E-06
 K4* 7.06E+00

[H ₂]	[CO]	[1-octene]	[catalyst]	R _{expt}	R _{expt} X 10 ⁴	R _{calc}	R _{calc} X 10 ⁴	MRSS	SEE	%SEE
0.0765	0.0990	0.19	8.66E-05	3.700E-05	3.700E-01	3.789E-05	3.7893E-01	7.971E-13	2.413E-02	2.413E+00
0.0765	0.0990	0.19	1.73E-04	7.500E-05	7.500E-01	7.570E-05	7.5698E-01	4.873E-13	9.307E-03	9.307E-01
0.0765	0.0990	0.19	3.46E-04	1.490E-04	1.490E+00	1.514E-04	1.5140E+00	5.741E-12	1.608E-02	1.608E+00
0.0765	0.0990	0.19	6.44E-04	2.820E-04	2.820E+00	2.818E-04	2.8179E+00	4.441E-14	7.473E-04	7.473E-02
0.0765	0.0990	0.1	1.73E-04	4.122E-05	4.122E-01	3.992E-05	3.9917E-01	1.697E-12	3.160E-02	3.160E+00
0.0765	0.0990	0.212	1.73E-04	8.500E-05	8.500E-01	8.442E-05	8.4424E-01	3.322E-13	6.781E-03	6.781E+00
0.0765	0.0990	0.29	1.73E-04	1.200E-04	1.200E+00	1.153E-04	1.1529E+00	2.214E-11	3.922E-02	3.922E+00
0.0765	0.0990	0.34	1.73E-04	1.400E-04	1.400E+00	1.350E-04	1.3503E+00	2.471E-11	3.550E-02	3.550E+00
0.0765	0.0990	0.39	1.73E-04	1.600E-04	1.600E+00	1.547E-04	1.5472E+00	2.785E-11	3.298E-02	3.298E+00
0.1431	0.0132	0.19	1.73E-04	1.500E-04	1.500E+00	1.496E-04	1.4960E+00	1.598E-13	2.665E-03	2.665E-01
0.1148	0.0397	0.19	1.73E-04	1.250E-04	1.250E+00	1.302E-04	1.3024E+00	2.745E-11	4.191E-02	4.191E+00
0.1022	0.0659	0.19	1.73E-04	1.100E-04	1.100E+00	1.101E-04	1.1012E+00	1.324E-14	1.046E-03	1.046E-01
0.0765	0.0990	0.19	1.73E-04	7.500E-05	7.500E-01	7.570E-05	7.5698E-01	4.873E-13	9.307E-03	9.307E-01
0.0382	0.1486	0.19	1.73E-04	3.300E-05	3.300E-01	3.333E-05	3.3335E-01	1.120E-13	1.014E-02	1.014E+00
Average:								1.120E-11	2.614E-01	4.538E+00

Table J-7: Kinetic data, estimated rate parameters, mean residual sum of squares (MRSS) and standard error of estimation (SEE) from the mechanistic rate model.

Hydroformylation of 1-dodecene with HRh(CO)(PPh₃)₃/ P(OPh)₃ catalyst in TMS-system at temperature of 353 K.

k	700.006
K1*	0.986379
K2*	2437.357
K3*	0.624826
K4*	0.996482

[H ₂]	[CO]	[1-octene]	[catalyst]	R _{expt}	R _{expt} X 10 ⁴	R _{calc}	R _{calc} X 10 ⁴	MRSS	SEE	%SEE
0.0748	0.0931	0.5	8.66E-05	9.500E-06	9.500E-02	9.347E-06	9.347E-02	2.340E-14	1.610E-02	1.610E+00
0.0748	0.0931	0.5	1.73E-04	2.000E-05	2.000E-01	1.867E-05	1.867E-01	1.762E-12	6.638E-02	6.638E+00
0.0748	0.0931	0.5	3.46E-04	3.700E-05	3.700E-01	3.734E-05	3.734E-01	1.190E-13	9.323E-03	9.323E-01
0.0748	0.0931	0.2	8.66E-05	3.900E-06	3.900E-02	3.775E-06	3.775E-02	1.568E-14	3.211E-02	3.211E+00
0.0748	0.0931	0.5	8.66E-05	9.200E-06	9.200E-02	9.347E-06	9.347E-02	2.162E-14	1.598E-02	1.598E+00
0.0748	0.0931	0.675	8.66E-05	1.200E-05	1.200E-01	1.255E-05	1.255E-01	3.011E-13	4.573E-02	4.573E+00
0.0499	0.0621	0.5	8.66E-05	8.800E-06	8.800E-02	8.690E-06	8.690E-02	1.219E-14	1.255E-02	1.255E+00
0.1272	0.0621	0.5	8.66E-05	2.200E-05	2.200E-01	2.216E-05	2.216E-01	2.510E-14	7.202E-03	7.202E+00
0.1496	0.0621	0.5	8.66E-05	2.550E-05	2.550E-01	2.607E-05	2.607E-01	3.235E-13	2.230E-02	2.230E+00
0.0499	0.0124	0.5	8.66E-05	1.100E-05	1.100E-01	1.100E-05	1.100E-01	1.545E-37	3.573E-14	3.573E-12
0.0499	0.0248	0.5	8.66E-05	1.300E-05	1.300E-01	1.316E-05	1.316E-01	2.599E-14	1.240E-02	1.240E+00
0.0499	0.0373	0.5	8.66E-05	1.200E-05	1.200E-01	1.185E-05	1.185E-01	2.107E-14	1.210E-02	1.210E+00
0.0499	0.0621	0.5	8.66E-05	8.500E-06	8.500E-02	8.690E-06	8.690E-02	3.594E-14	2.230E-02	2.230E+00
0.0499	0.1242	0.5	8.66E-05	5.000E-06	5.000E-02	4.803E-06	4.803E-02	3.885E-14	3.942E-02	3.942E+00
0.0499	0.1863	0.5	8.66E-05	3.500E-06	3.500E-02	3.268E-06	3.268E-02	5.381E-14	6.628E-02	6.628E+00
Average:								2.527E-13	3.802E-01	3.501E+00

Table J-8: Kinetic data, estimated rate parameters, mean residual sum of squares (MRSS) and standard error of estimation (SEE) from the mechanistic rate model.

Hydroformylation of 1-dodecene with HRh(CO)(PPh₃)₃/ P(OPh)₃ catalyst in TMS-system at temperature of 363 K.

k	1366.306
K1*	2218.616
K2*	0.169272
K3*	0.479424
K4*	5.347078

[H ₂]	[CO]	[1-octene]	[catalyst]	R _{expt}	R _{expt} X 10 ⁴	R _{calc}	R _{calc} X 10 ⁴	MRSS	SEE	%SEE
0.0756	0.0951	0.5	8.66E-05	2.000E-05	2.000E-01	1.961E-05	1.961E-01	1.536E-13	1.960E-02	1.960E+00
0.0756	0.0951	0.5	1.73E-04	3.780E-05	3.780E-01	3.917E-05	3.917E-01	1.879E-12	3.627E-02	3.627E+00
0.0756	0.0951	0.5	3.46E-04	7.650E-05	7.650E-01	7.834E-05	7.834E-01	3.392E-12	2.408E-02	2.408E+00
0.0756	0.0951	0.2	8.66E-05	7.800E-06	7.800E-02	7.867E-06	7.867E-02	4.437E-15	8.540E-03	8.540E-01
0.0756	0.0951	0.5	8.66E-05	2.000E-05	2.000E-01	1.961E-05	1.961E-01	1.536E-13	1.960E-02	1.960E+00
0.0756	0.0951	0.675	8.66E-05	2.600E-05	2.600E-01	2.643E-05	2.643E-01	1.807E-13	1.635E-02	1.635E+00
0.0504	0.0634	0.5	8.66E-05	1.800E-05	1.800E-01	1.824E-05	1.824E-01	5.973E-14	1.358E-02	0.000E+00
0.1285	0.0634	0.5	8.66E-05	4.600E-05	4.600E-01	4.652E-05	4.652E-01	2.737E-13	1.137E-02	1.137E+00
0.1512	0.0634	0.5	8.66E-05	5.350E-05	5.350E-01	5.473E-05	5.473E-01	1.521E-12	2.305E-02	2.305E+00
0.0504	0.0127	0.5	8.66E-05	2.500E-05	2.500E-01	2.500E-05	2.500E-01	2.155E-35	1.857E-13	1.857E+00
0.0504	0.0254	0.5	8.66E-05	2.900E-05	2.900E-01	2.849E-05	2.849E-01	2.577E-13	1.750E-02	1.750E+00
0.0504	0.0381	0.5	8.66E-05	2.450E-05	2.450E-01	2.515E-05	2.515E-01	4.269E-13	2.667E-02	2.667E+00
0.0504	0.0634	0.5	8.66E-05	1.830E-05	1.830E-01	1.824E-05	1.824E-01	3.093E-15	3.039E-03	3.039E-01
0.0504	0.1268	0.5	8.66E-05	9.700E-06	9.700E-02	1.009E-05	1.009E-01	1.493E-13	3.984E-02	3.984E+00
0.0504	0.1903	0.5	8.66E-05	6.800E-06	6.800E-02	6.878E-06	6.878E-02	6.116E-15	1.150E-02	1.150E+00
Average:								7.692E-13	2.574E-01	3.755E+00

Table J-9: Kinetic data, estimated rate parameters, mean residual sum of squares (MRSS) and standard error of estimation (SEE) from the mechanistic rate model.

Kinetic data for the hydroformylation of 1-dodecene with $\text{HRh}(\text{CO})(\text{PPh}_3)_3/\text{P}(\text{OPh})_3$ catalyst in TMS-system at temperature of 373 K.

k	2686.86
K1*	2044.202
K2*	0.019827
K3*	0.101234
K4*	34.81747

[H ₂]	[CO]	[1-octene]	[catalyst]	R _{expt}	R _{expt} X 10 ⁴	R _{calc}	R _{calc} X 10 ⁴	MRSS	SEE	%SEE
0.0766	0.0992	0.5	8.66E-05	3.300E-05	3.300E-01	3.597E-05	3.597E-01	8.819E-12	8.999E-02	8.999E+00
0.0766	0.0992	0.5	1.73E-04	6.500E-05	6.500E-01	7.186E-05	7.186E-01	4.701E-11	1.055E-01	1.055E+01
0.0766	0.0992	0.5	3.46E-04	1.270E-04	1.270E+00	1.437E-04	1.437E+00	2.793E-10	1.316E-01	1.316E+01
0.0766	0.0992	0.2	8.66E-05	1.450E-05	1.450E-01	1.439E-05	1.439E-01	1.143E-14	7.373E-03	7.373E-01
0.0766	0.0992	0.5	8.66E-05	3.800E-05	3.800E-01	3.597E-05	3.597E-01	4.122E-12	5.343E-02	5.343E+00
0.0766	0.0992	0.675	8.66E-05	5.000E-05	5.000E-01	4.855E-05	4.855E-01	2.106E-12	2.903E-02	2.903E+00
0.0511	0.0662	0.5	8.66E-05	3.200E-05	3.200E-01	3.207E-05	3.207E-01	4.707E-15	2.144E-03	2.144E-01
0.1303	0.0662	0.5	8.66E-05	8.500E-05	8.500E-01	8.177E-05	8.177E-01	1.040E-11	3.794E-02	3.794E+00
0.1533	0.0662	0.5	8.66E-05	1.000E-04	1.000E+00	9.621E-05	9.621E-01	1.440E-11	3.794E-02	3.794E+00
0.0511	0.0132	0.5	8.66E-05	4.300E-05	4.300E-01	4.300E-05	4.300E-01	4.284E-29	1.522E-10	1.522E+00
0.0511	0.0265	0.5	8.66E-05	4.700E-05	4.700E-01	4.676E-05	4.676E-01	5.734E-14	5.095E-03	5.095E-01
0.0511	0.0397	0.5	8.66E-05	4.100E-05	4.100E-01	4.202E-05	4.202E-01	1.051E-12	2.500E-02	2.500E+00
0.0511	0.0662	0.5	8.66E-05	3.200E-05	3.200E-01	3.207E-05	3.207E-01	4.707E-15	2.144E-03	2.144E-01
0.0511	0.1323	0.5	8.66E-05	2.000E-05	2.000E-01	1.899E-05	1.899E-01	1.012E-12	5.031E-02	5.031E+00
0.0511	0.1985	0.5	8.66E-05	1.300E-05	1.300E-01	1.334E-05	1.334E-01	1.147E-13	2.605E-02	2.605E+00
Average:								3.339E-11	5.272E-01	3.550E+00

Appendix K

AAS Standard Calibration Curve

This appendix includes the AAS standard calibration curve for the quantitative analysis of rhodium.

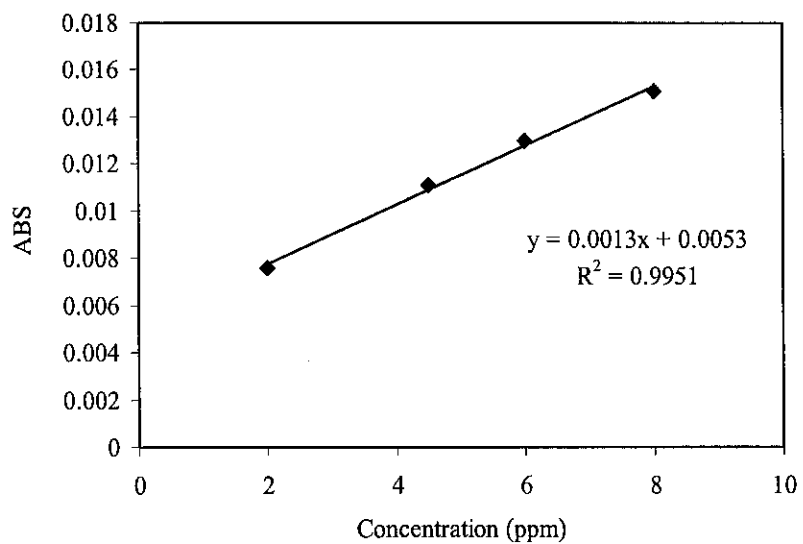


Figure K-1: Rhodium standard curve

APPENDIX L

Experimental Tie-Line Data

Table L-1: Experimental tie-line data for TMS (PC+1,4-dioxane+dodecane)+1-octene system.

Polar-rich phase (weight fraction)				Non-polar rich phase (weight fraction)			
PC	1,4-dioxane	dodecane	1-octene	PC	1,4-dioxane	dodecane	1-octene
298.15 K							
0.1593	0.6596	0.1460	0.0351	0.1174	0.1380	0.2866	0.4580
0.1992	0.6437	0.1202	0.0369	0.1276	0.1509	0.4345	0.2870
0.2303	0.6074	0.1096	0.0527	0.1444	0.1522	0.4864	0.2170
308.15 K							
0.1486	0.6656	0.1344	0.0514	0.2733	0.1480	0.1507	0.4280
0.1935	0.6607	0.1112	0.0346	0.3929	0.1589	0.2045	0.2437
0.1974	0.6459	0.1013	0.0554	0.3887	0.1599	0.2464	0.2050

Table L-2: Experimental tie-line data for TMS (PC+1,4-dioxane+dodecane)+nonanal system.

Polar-rich phase (weight fraction)				Non-polar rich phase (weight fraction)			
PC	1,4-dioxane	dodecane	nonanal	PC	1,4-dioxane	dodecane	nonanal
298.15 K							
0.1489	0.7225	0.1238	0.0048	0.1219	0.4206	0.3475	0.1100
0.1739	0.6646	0.1506	0.0109	0.1253	0.3554	0.3693	0.1500
0.1972	0.6325	0.1578	0.0125	0.0446	0.3405	0.3849	0.2300
308.15 K							
0.1381	0.7300	0.1271	0.0048	0.1333	0.4195	0.3467	0.1006
0.1724	0.6541	0.1649	0.0086	0.1018	0.4380	0.3565	0.1037
0.1862	0.6439	0.1578	0.0121	0.0149	0.3760	0.4052	0.2039

Table L-3. Experimental tie-line data for TMS (PC+1,4-dioxane+dodecane)+1-octene+nonanal system.

Polar-rich phase (weight fraction)					Non-polar rich phase (weight fraction)				
PC	1,4-dioxane	dodecane	1-octene	nonanal	PC	1,4-dioxane	dodecane	1-octene	nonanal
298.15 K									
0.1079	0.7096	0.1460	0.0361	0.0004	0.0104	0.1380	0.3066	0.4580	0.0870
0.0489	0.7837	0.1202	0.0379	0.0093	0.0146	0.1509	0.3045	0.2870	0.2430
0.1563	0.6674	0.1096	0.0537	0.0130	0.0154	0.1522	0.3164	0.2170	0.2990
0.0283	0.7774	0.1317	0.0565	0.0061	0.0629	0.1390	0.3081	0.1310	0.3590
0.0600	0.5485	0.2026	0.0814	0.1075	0.0119	0.1276	0.3199	0.3580	0.1826
308.15 K									
0.0772	0.7356	0.1344	0.0524	0.0004	0.0901	0.1480	0.2507	0.4280	0.0832
0.1059	0.7407	0.1112	0.0356	0.0066	0.0919	0.1589	0.2845	0.2437	0.2210
0.1731	0.6759	0.1013	0.0364	0.0134	0.0707	0.1599	0.2764	0.2050	0.2880
0.1000	0.6947	0.1280	0.0702	0.0071	0.0783	0.1590	0.2958	0.1210	0.3459
0.0822	0.6000	0.2057	0.0608	0.0514	0.1311	0.1386	0.2599	0.3248	0.1456
0.1821	0.5399	0.1289	0.1094	0.0398	0.0996	0.1717	0.3885	0.2115	0.1287

Table L-4: Experimental tie-line data for TMS (PC+1,4-dioxane+dodecane)+P(OPh)₃+HRh(CO)(PPh₃)₃+1-octene+nonanal system.

Polar-rich phase (weight fraction)							Non-polar rich phase (weight fraction)						
PC	1,4-dioxane	dodecane	P(OPh) ₃	catalyst	1-octene	nonanal	PC	1,4-dioxane	dodecane	P(OPh) ₃	catalyst	1-octene	nonanal
298.15 K													
0.0914	0.7300	0.0400	0.0957	0.0073	0.0056	0.0301	0.0080	0.4970	0.3190	0.0055	0.0011	0.1370	0.0324
0.0930	0.7500	0.0166	0.0915	0.0037	0.0361	0.0091	0.0092	0.0830	0.8050	0.0098	0.0001	0.0534	0.0395
0.1343	0.7526	0.0150	0.0109	0.0032	0.0770	0.0070	0.0031	0.1200	0.7520	0.0066	0.0001	0.0856	0.0326
0.2127	0.7210	0.0154	0.0141	0.0053	0.0230	0.0085	0.1146	0.1485	0.5540	0.0020	0.0000	0.1275	0.0534
0.1158	0.6830	0.0157	0.0811	0.0044	0.0610	0.0390	0.0117	0.1010	0.7110	0.0099	0.0001	0.1246	0.0417
0.0419	0.7400	0.0281	0.0925	0.0031	0.0260	0.0684	0.0058	0.6310	0.2060	0.0085	0.0001	0.0740	0.0747
308.15 K													
0.0825	0.6410	0.0376	0.1940	0.0071	0.0055	0.0323	0.0052	0.4759	0.3256	0.0050	0.0001	0.1530	0.0352
0.0502	0.7850	0.0162	0.1000	0.0043	0.0356	0.0087	0.0063	0.0808	0.8146	0.0080	0.0001	0.0528	0.0375
0.1206	0.7689	0.0140	0.0100	0.0026	0.0769	0.0070	0.0029	0.1190	0.7480	0.0060	0.0001	0.0859	0.0381
0.1600	0.7709	0.0153	0.0120	0.0051	0.0287	0.0081	0.0601	0.1419	0.6024	0.0019	0.0003	0.1377	0.0557
0.1302	0.6980	0.0155	0.0521	0.0043	0.0615	0.0385	0.0225	0.1000	0.6980	0.0099	0.0000	0.1246	0.0450
0.0392	0.7387	0.0272	0.0903	0.0033	0.0372	0.0641	0.0058	0.6288	0.2134	0.0108	0.0001	0.0702	0.0710

APPENDIX M

Papers Published/Presented

M-1 Papers Published in International Journal

- i) Shaharun, M.S., Mukhtar, H., Dutta, B.K. (2008). Solubility of carbon monoxide and hydrogen in propylene carbonate and thermomorphic multicomponent hydroformylation solvent. *Chem Eng Sci.* 63, 3024-3035.
- ii) Shaharun, M.S., Mukhtar, H., Dutta, B.K. (2009). Ab Initio Energy Calculations and Macroscopic Rate Modeling of Hydroformylation of Higher Alkenes by Rh-based Catalyst. *AIChE J.* (accepted).
- iii) Shaharun, M.S., Dutta, B.K. Mukhtar, H., Maitra, S. (2009). Hydroformylation of 1-octene using rhodium-phosphite catalyst in a thermomorphic solvent system - *In Press.*

M-2 Papers Presented in Local and International Conference

- i) Shaharun, M.S., Mukhtar, H., Bhatia, S., Dutta, B.K. (2008). Hydroformylation of 1-octene using rhodium-phosphite catalyst in a thermomorphic solvent system. *National Postgraduate Conference (NPC)*, 31st March 2008, Tronoh, Perak.
- ii) Shaharun, M.S., Mukhtar, H., Bhatia, S., Dutta, B.K. (2008). Hydroformylation of 1-octene using rhodium-phosphite catalyst in a thermomorphic solvent system. *20th International Symposium on Chemical Reaction Engineering (ISCRE)*, 7-10th September, 2008, Kyoto, Japan.
- iii) Shaharun, M.S., Mukhtar, H., Bhatia, S., Yusup, S., Dutta, B.K. (2008). Kinetics of hydroformylation of higher olefins using rhodium-phosphite catalyst in a thermomorphic solvent system. *2008 Annual Meeting – AIChE*, 16-21st November, 2008, Philadelphia, USA.